Nanoparticle Bound Nucleic Acid Probes for DNA Detection and Gene Inactivation

UNIVERSITY OF BIRMINGHAM

David Michael Kershaw

A thesis submitted to the University of Birmingham for the degree of Doctor of Philosophy

PSIBS Doctoral Training Centre
School of Chemistry
College of Engineering and Physical Sciences
University of Birmingham
September - 2016

Abstract

In this project, a gold nanoparticle system has been developed that is able to detect SNP variations through a DNA based anthracene probe. A second probe is bound to the gold nanoparticle which allows the fluorescent output of the anthracene probe to be normalized. This allows the detection of SNP variations without the need for an initial reading, opening the possibility for using this system for cellular SNP identification. Through this work a new method for coating gold nanoparticles in oligonucleotides has been developed.

In further work, the use of gold nanoparticles to deliver siRNA into cells and induce gene inactivation was investigated. Efforts to improve the knockdown efficiency of these siRNA-gold nanoparticles were made by integrating a second probe onto the nanoparticle surface, non-specific effects were observed upon addition of this second probe.

Acknowledgements

I would firstly like to thank my supervisors, Professor Jim Tucker, Professor Zoe Pikramenou, Professor Roy Bicknell and Dr Iain Styles, all of whom have provided valuable advice and support throughout my project. Throughout my PhD, I have had help and advice from many people, therefore I thank all members past and present from the Tucker, Pikramenou and Bicknell groups, especially the Tucker group members who gave up their own time to run the DNA synthesiser. Special thanks go to Rosie who helped greatly throughout the PhD. As a chemist working in biology labs, thanks must be given to the Bicknell group for being patient, especially Kab for the time he gave up teaching me new techniques and explaining basic biology to me.

I thank the EPSRC for funding this research.

Thank you to my fellow 2011 PSIBS students, it has been lovely.

Thanks to my parents Tanya and Nick for their help with university and my general upbringing, time and money well spent. My siblings: Rachael (who actually did help), Deborah, Paul and Philly you have all been superb throughout.

Finally, I should thank my dearest Róisín for funding my write up; your feigned interest in my work was greatly appreciated.

1 CONTENTS

1.1 Abbreviations

A	Adenine
APS	Ammonium persulfate
$AuNP$	Gold nanoparticle
BDF	Base discriminating fluorophore
C	Cytosine
CD	Circular dichroism
$CDCl_3$	Deuterated chloroform
CD_3CN	Deuterated acetonitrile
CHO	Chinese hamster ovary
CPG	Controlled pore glass
DCM	Dichloromethane
DEA	Diethylamine
$DIPEA$	N,N-Diisopropylethylamine
DLS	Dynamic light scattering
DMF	Dimethyl formamide
$DMSO$	Dimethyl sulfoxide
DMT	Dimethoxytrityl
DNA	Deoxyribonucleic acid
EDC	1-ethyl-3-(-3-dimethylaminopropyl) carbodiimide
$EDTA$	Ethylenediaminetetraacetic acid
EPR	Enhanced permeability and retention
$EtAc$	Ethyl acetate
$EtOH$	Ethanol
FCS	Foetal calf serum
$FLIM$	Fluorescent lifetime image microscopy
$FRET$	Förster resonance energy transfer
G	Guanine
$HBTU$	1-(1H-benzotriazol-1-yl)-1,1,3,3-tetramethyluronium hexafluorophosphate
$HOBt$	Hydroxybenzotriazole
$HPLC$	High performance liquid chromatography
HRP	Horseradish peroxidase
$HUVEC$	Human umbilical vein endothelial cell

$ICP\text{-}MS$	Inductively coupled plasma mass spectrometry
LC	Ligand charge
LNA	Locked nucleic acid
$MeOH$	Methanol
$MLCT$	Metal ligand charge transfer
$miRNA$	Micro ribonucleic acid
$mRNA$	Messenger ribonucleic acid
NHS	N-Hydroxysuccinimide
NMR	Nuclear magnetic resonance
$MLCT$	Metal ligand charge transfer
PBS	Phosphate buffered saline
$PBS\text{-}T$	Phosphate buffered saline Tween-20
PCR	Polymerase chain reaction
PEG	Polyethylene glycol
PEI	Polyethylene imine
PET	Photoinduced energy transfer
PFA	Paraformaldehyde
PNA	Polymeric nucleic acid
RCA	Rolling circle amplification
$RIPA$	Radioimmunoprecipitation assay
$RISC$	Ribonucleic acid induced silencing complex
RNA	Ribonucleic acid
$RNAi$	Ribonucleic acid interference
$rRNA$	Ribosomal ribonucleic acid
Rt	Room temperature
SDS	Sodium dodecyl sulphate
$siRNA$	Short interfering ribonucleic acid
SNA	Spherical nucleic acid
SNP	Single nucleotide polymorphism
SPR	Surface plasmon resonance
T	Thymine
$TBAF$	Tetra-n-butylammonium fluoride

TEA	Triethylamine
TEM	Transmission electron microscopy
$TEMED$	Tetramethylethylenediamine
THF	Tetrahydrofuran
T_m	Thermal melting
TO	Thiazole orange
$TOF\text{-}MS\text{-}ES^+$	Time of flight mass spectroscopy electrospray positive mode
$TOF\text{-}MS\text{-}ES^-$	Time of flight mass spectroscopy electrospray negative mode
$tRNA$	Transfer ribonucleic acid
U	Uracil
UV	Ultra violet

1.2 List of figures

1.3 List of Tables

2 INTRODUCTION

2.1 DNA

2.1.1 Structure of DNA

The molecule deoxyribonucleic acid (DNA) carries the genetic instructions for the development, function and reproduction of all known living organisms. DNA is a large polymer made up of monomers called nucleotides. Each nucleotide consists of a pentose sugar, a heterocyclic base and a phosphate group. In DNA there are 4 different nucleobases; adenine (A), cytosine (C), guanine (G) and thymine (T). The bases are split into two groups; the purines (A and G) consisting of a five membered ring bound to a six membered ring, and the pyrimidines (C and T) formed of a single six membered ring. Each strand of DNA has directionality which is caused by the position of the two hydroxyl groups on the nucleotides, 3' (secondary hydroxyl) and 5' (primary hydroxyl) (Figure 2.1). Oligomers are formed by covalently binding a phosphate group at the 5' end of a nucleotide to the hydroxyl group at the 3' end of another nucleotide, forming a phosphodiester bond. At physiological pH (7.4), the phosphate groups exist as anions, therefore DNA is a highly negatively charged molecule.

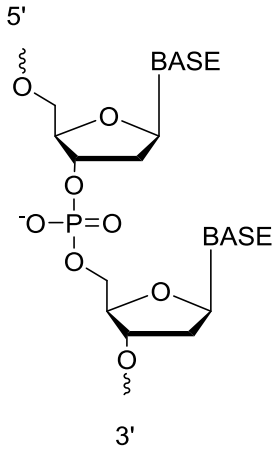

Figure 2.1 Chemical structure of DNA
DNA chain showing 2 nucleotides bound together via a phosphodiester bond.

Franklin and Wilkins established that the common structure of DNA was as a double stranded molecule and Watson and Crick[1] showed that this structure was formed by bases on opposite strands, hydrogen bonding to each other. The purine base A always pairs with the pyrimidine T forming two hydrogen bonds, whilst the purine G always pairs with the pyrimidine C through 3 hydrogen bonds (Figure 2.2).

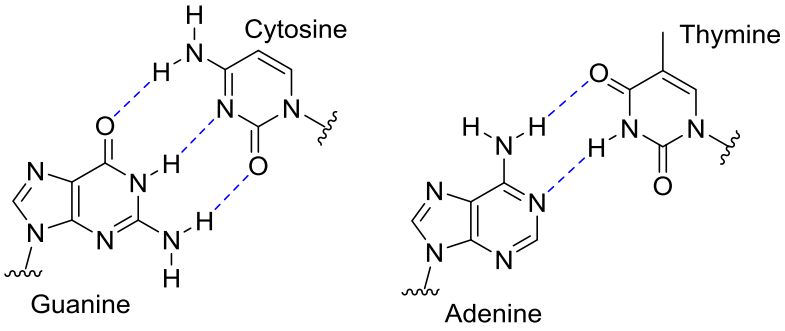

Figure 2.2 Hydrogen bonding between DNA bases
Hydrogen bonding between complementary base pairs in DNA, G-C and A-T (dashed blue lines denote H-bonds)

There are alternative mechanisms of base pairing, such as Hoogsteen pairing; these are less common yet their importance in nature is becoming increasingly apparent.[2] The Watson-Crick binding rules state that one strand of the DNA defines the sequence of the other strand; therefore the strands are complementary to one another. The two strands run anti-parallel to one another with the 5' of one strand opposite the 3' of the other. The two strands wrap around each other forming a right handed double helix; the hydrophobic base pairs in the centre of the duplex, and the charged phosphate groups forming a hydrophilic surround. In the duplex, the bases stack on top of one another in a planar fashion. This base stacking, along with the H-bonding, is what gives the DNA double helix its stability. In the most common form of DNA, B-DNA, the distance between each base is 0.34 nm, whilst one

complete helical turn is made every 10.5 bases. B-DNA contains a large major groove and a narrow minor groove. Other forms of DNA such as A and Z DNA have been discovered (

Figure **2.3**).

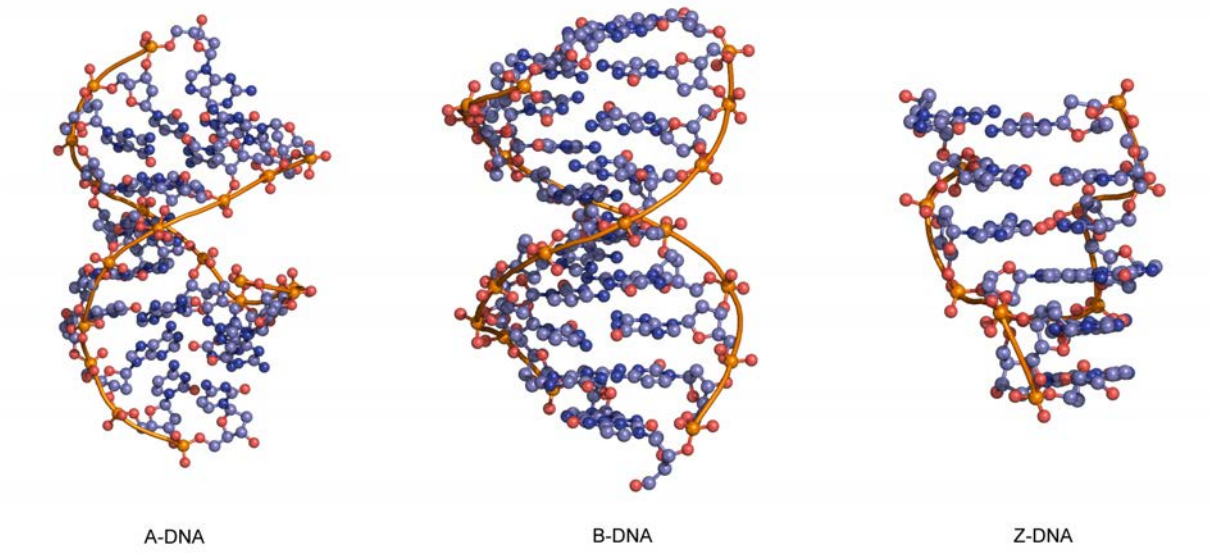

Figure 2.3 The different structures of DNA duplexes.[3]

2.1.2 Ribonucleic Acid

Ribonucleic acid (RNA) transforms the information held within DNA into proteins, within a cell. RNA can take multiple forms, such as messenger RNA (mRNA), transfer RNA (tRNA) and ribosomal RNA (rRNA). In the ribosomes, these RNA molecules are required to bring together specific amino acids, the building blocks of proteins. RNA is very similar in structure to DNA, however there are important differences. In RNA, the base thymine is replaced with uracil which has no methyl group at carbon-5. Also, the sugar ring in RNA contains an additional 2'-OH group (Figure 2.4). RNA mainly exists in single stranded form, however if it forms a duplex it is in the A-form of DNA (Figure 2.3). The A-form duplex has a much deeper

major groove and a shallow minor groove, DNA will only adopt this form under low humidity conditions.

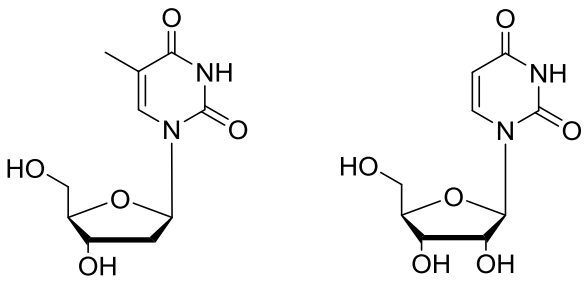

Figure 2.4 A comparison of the structure of deoxythymidine with uridine

2.1.3 Artificial oligonucleotide synthesis

In 1955, Michelson and Todd reacted two deoxythymine nucleosides together to form the first recorded synthesis of a dinucleotide.[2] Khorana developed a phosphodiester method,[3] which enabled the synthesis of much longer oligonucleotides. Letsinger utilised phosphotriester chemistry.[5] Importantly, he synthesised oligonucleotides on solid polystyrene supports;[6] once synthesised, the oligonucleotide could be cleaved from the support. The method used today was developed by a student of Letsinger and Khorana, Marvin Caruthers. Caruthers developed the phosphoramidite chemistry,[7] whilst also discovering controlled pore glass (CPG) as a superior solid support to polystyrene.[8] The phosphoramidite method is outlined in (Scheme 2.1).

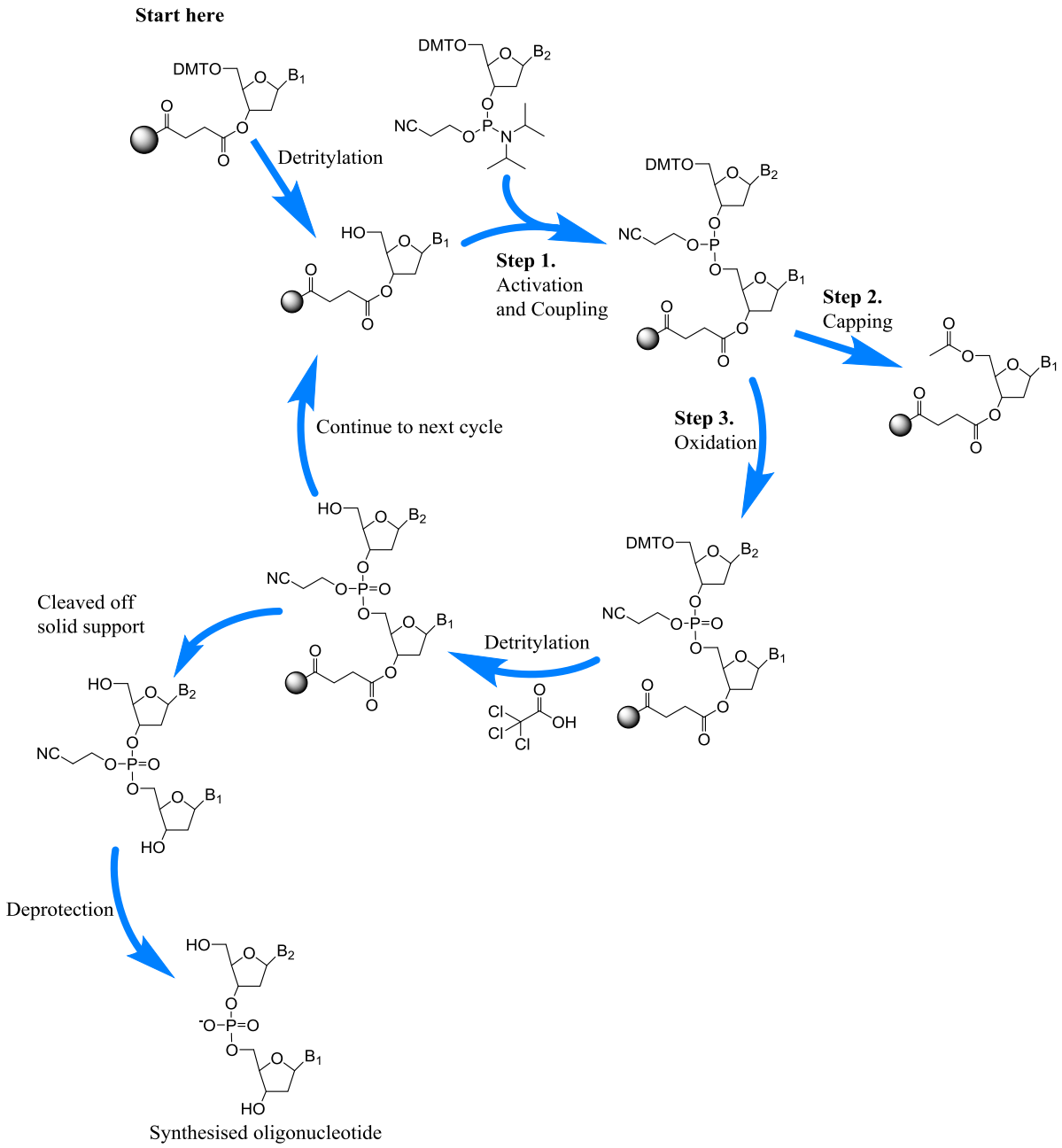

Scheme 2.1 Chemical synthesis of artificial DNA

This method is still widely used today and has allowed for the ready synthesis of oligonucleotides up to 100 bases in length on DNA synthesisers.

2.2 Single Nucleotide Polymorphisms

Upon the completion of the initial phase of the Human Genome Project, many variations in DNA sequence among the population were found, the most common of these variations (~90%) being single nucleotide polymorphisms (SNPs).[9] A SNP is a single nucleotide variation at a specific locus (position of gene in a chromosome) within a sequence giving rise to alleles (different versions of a gene), with the least frequent allele being found in more than 1% of the population. If the frequency of the variation is any less than 1%, then the variation is classed as a mutation.[9] On average, SNPs occur once every 1000-2000 base pairs, although they are not evenly distributed throughout the genome. Most SNPs are found in the non-coding regions of DNA; variations found in the coding region cause alterations to protein structure and therefore affect a protein's function, leading to the possible development of disease. Identifying these SNPs is therefore an area of great interest as they can be used as molecular markers in the field of disease genetics.[10,11] Consequently, there is growing research into techniques that can be used to distinguish the variants at SNP sites. There is also growing interest into the link between SNPs and a patient's response to medicine, with the ultimate goal being personalised medicine.[13] Next generation sequencing is a fast developing technique which allows a whole genome to be sequenced; whilst this will give the identity of SNP sites, it is still expensive and also looks at the whole genome when only a small region (i.e. the SNP site) needs to be observed.[14,15] Therefore, alternative methods for determining the variant of a specific SNP site of interest exist. Present methods for SNP sensing mainly rely upon the difference in hybridization affinity between the SNP site containing DNA strand and a sensing probe. Differences in hybridisation affinity allow the

sensing probe to differentiate between the SNP variants, as one will bind with a higher affinity than the other, various techniques are detailed in the following section.

2.3 Fluorescent DNA detection

2.3.1 Molecular Beacons

Molecular beacons are a commercial example of a DNA sensing technique; it involves oligonucleotide hybridization probes which can sense the presence of specific nucleic acids. These probes are short oligonucleotide sequences held in a hairpin conformation, with a fluorophore and quencher at either end of the sequence. In the hairpin conformation, the fluorophore and quencher are close enough together so that the fluorescence from the fluorophore is quenched. However, upon binding to the complementary target of the sequence, the hairpin unwraps and the fluorophore and quencher dye are no longer held in close proximity, resulting in the restoration of fluorescence from the fluorophore.[16,17]

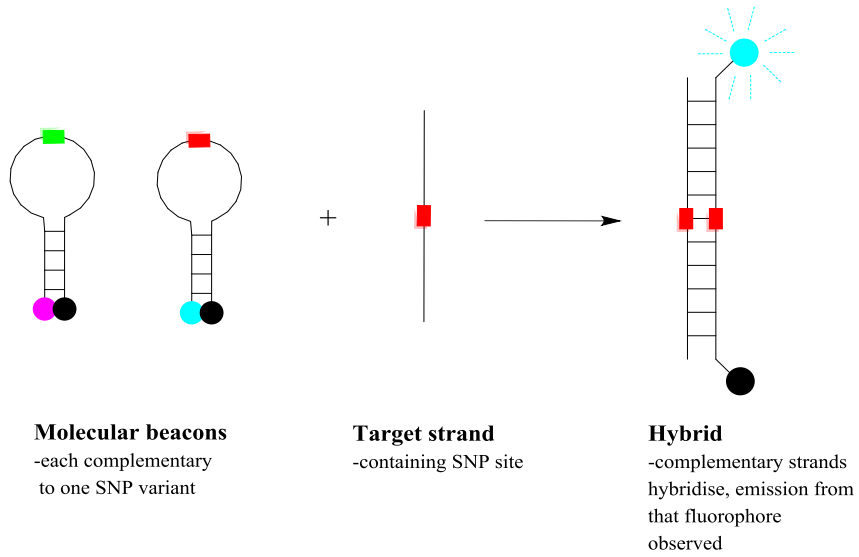

Figure 2.5 Molecular beacon mechanism
Upon hybridisation with target strand, the fluorescent probe moves away from the quencher molecule and its signal increases. Within set temperature windows, only fully complementary probes will hybridise allowing the identity of the SNP to be found.

2.3.2 Taqman™

Taqman™ is a technique which involves two probe strands of DNA that differ only in one base. One probe is fully complementary for one SNP variant, the other complementary to the other variant. Each probe contains a reporter fluorescent dye at the 5'- end (the two probes have a different fluorescent dye attached to them) and a quencher dye at the 3'-end. The dyes are close enough that the reporter dye is quenched by the quencher dye. When the probes find a complementary DNA sequence, the probe with the highest binding affinity will bind preferentially to the target strand (i.e. probe with complete base matching). During the Polymerase Chain Reaction (PCR), Taq DNA polymerase cleaves the probe/target duplex in the 5'→3' direction. The reporter dye will be released from the quencher, leading to an increase in its fluorescence intensity (Figure 2.6). As each probe targeting each SNP variant has a different fluorescent probe bound to it, the SNP site present in the target strand can be identified. Taqman™ has been used for SNP detection by Ralston *et al.*.[18] However one problem with Taqman™ is the requirement for PCR, which is currently difficult to do in cells. Rolling Circle Amplification (RCA) has been developed which could potentially overcome these issues.[19] These problems prevent the use of Taqman™ for cellular SNP detection.

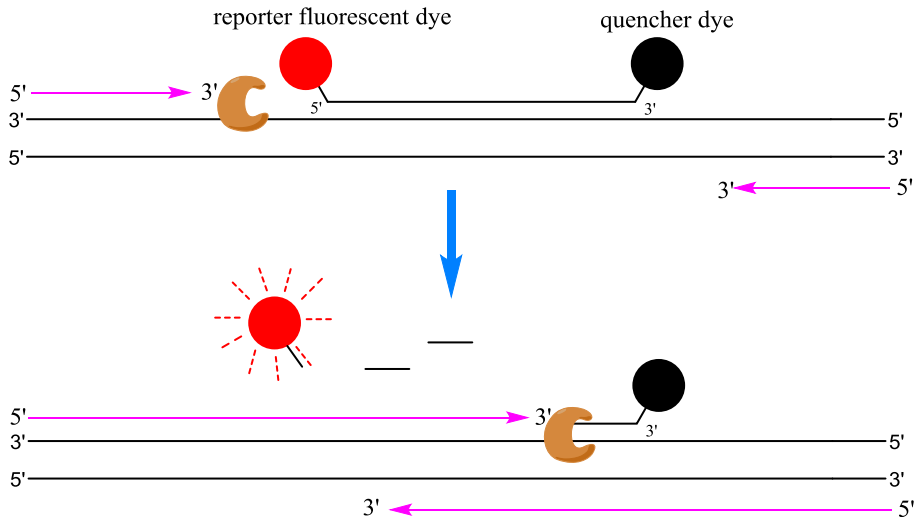

Figure 2.6 Mechanism of Taqman assay
Mechanism of action for Taqman mediated SNP detection. (Top) The probe with highest affinity hybridises to the target site. (Bottom) Taq polymerase chews up double stranded pieces of DNA in the 5'->3' direction, releasing the fluorescent probe from the quencher molecule, leading to an increase in its emission. Careful temperature control results in only probe strands complementary to the SNP site to bind, allowing for SNP detection.

2.3.3 Scorpion Probe

Another SNP sensing method is the scorpion probe, which was initially developed by Little *et al.* as a probe for monitoring the products of PCR.[16] The scorpion probe (Figure 2.7) consists of a specific probe sequence held in a hairpin loop configuration by complementary stem sequences on the 5' and 3' sides of the probe, similar to a molecular beacon. The fluorophore attached to the 5'-end is quenched by a quenching fluorophore at the 3'-end of the loop. The hairpin loop is linked to the 5'-end of a primer via a PCR stopper; the PCR stopper helps to eliminate detection of non-PCR events e.g. primer dimers. After extension of the primer during PCR amplification, the specific probe sequence is able to bind to its complement within the same strand of DNA. This hybridisation event opens the hairpin loop so that fluorescence is no longer quenched and an increase in signal is observed.

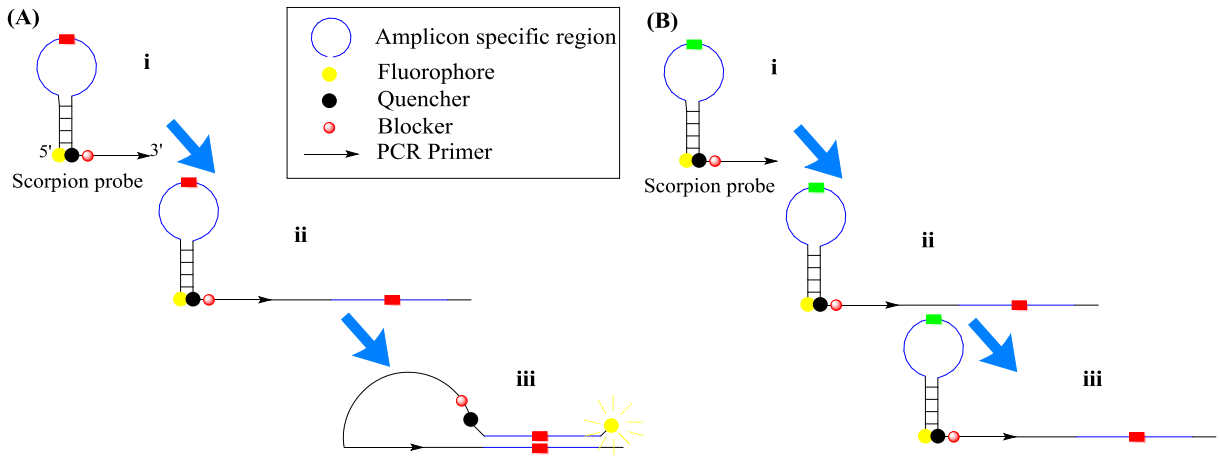

Figure 2.7 Scorpion probe mechanism
*(**A**)**i**) A Scorpions primer carries a 5' extension comprising a probe element, a pair of self-complementary stem sequences, and a fluorophore/quencher pair. The extension is "protected" from copying by a blocking HEG monomer. **ii**) After PCR extension from the primer, a newly synthesized target region is now attached to the same strand as the probe. **iii**) Following a second round of denaturation and annealing, the probe and target hybridize. **(B)** Identical procedure except hybridisation does not occur at iii) due to base mismatch, allowing detection of SNP variant.*[16]

The probe was found to be specific enough to identify single base changes within a sequence and therefore its potential for SNP detection has been investigated, showing it is able to detect heterozygous SNP variants.[17,18] It was found that the Scorpion probe outperformed Taqman and Molecular Beacons, being quicker in identifying the target, which is particularly useful for high through-put screening.

2.3.4 HyBeacon™

Hybridisation beacons (HyBeacon™) are another type of SNP detecting probe developed by French *et al.*.[35,36,37] These probes contain a fluorescent molecule bound to a uracil base within a sequence of DNA. Upon binding to the fully complementary sequence, the emission of the fluorescent molecule increases greatly. The emission is lower when bound to a mismatching sequence and lowest when the probe is single stranded (Figure 2.8).

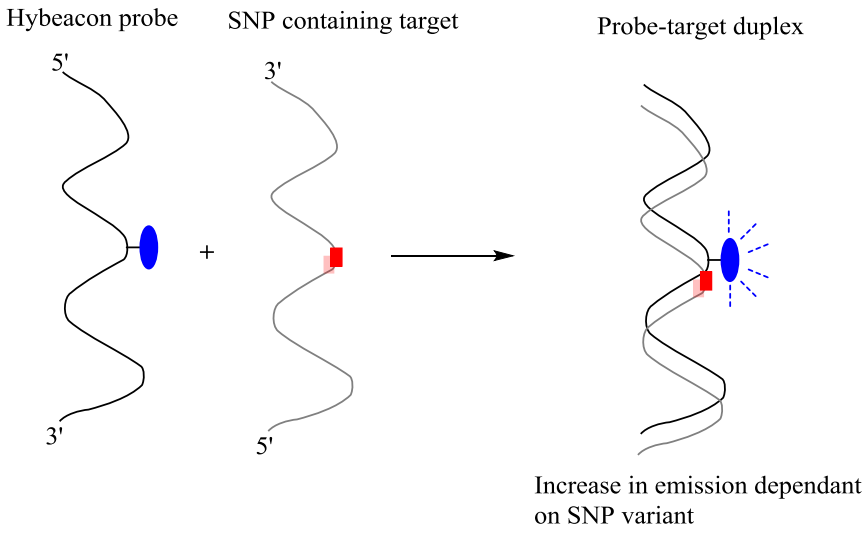

Figure 2.8 Mechanism of action for SNP detection using a Hybeacon™

By using the melting temperature difference between the fully matching and single mismatching targets (i.e. the two SNP variants); they are able to observe the fluorescence change only for the target desired. This not only allows the real time analysis of PCR products, but also real time determination of whether a sample is homozygous or heterozygous.

The two main issues encountered by these hybridisation based methods are the reliance on a significant difference in hybridisation affinity between the two SNP sites and the requirement to heat the samples. The difference in hybridization affinities may be very small as it is only a single base variation within a sequence that is being distinguished. This problem will amplify with increasing sequence length. Heat requirement limits the use of some of these techniques to cuvette studies, as the heat would damage cells, leading to cell stress and therefore unreliable results.

2.3.5 DNA modification

An alternative route for SNP detection is to use a molecular probe that gives a different response for different targets; these systems are often called base discriminating fluorophores (BDF). The change in fluorescent readout is caused by a change in the environment that the fluorophore is held in. The advantage of these systems is that they do not rely on differences in hybridisation binding strength, obviating the need for a temperature window. Saito *et al.* were able to identify the presence of a thymine base at a specific position using a pyrene residue, the pyrene showed significant quenching when hybridised opposite a thymine.[26] They have also modified nucleosides to differentiate between purine bases by fluorescent changes.[27] Tanaka *et al.* integrated an acridine fluorophore into the DNA backbone via a threoninol linker. They found that upon duplex formation, the acridine successfully intercalated into the duplex where a change in its immediate environment resulted in an increase in the acridine emission.[28] The group of Seitz has also worked on base discriminating fluorophores; their work has mainly been based around the use of thiazole orange (TO) (Figure 2.9).

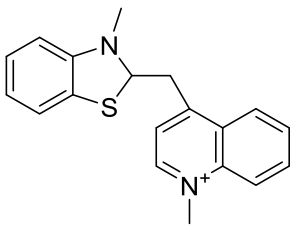

Figure 2.9 Thiazole orange

Initially the TO was integrated into the middle of a strand of Polymeric Nucleic Acid (PNA) (Figure 2.10) and was able to discriminate between bases on a binding DNA strand, showing both an increase and decrease in fluorescence dependent on the base opposite the TO modification.[29,30] More recently the Seitz group has developed DNA based probes.[31] The group have also used the PNA probe to image different targets within cells,[32,33] although not SNP sites.

2.4 Cellular delivery of DNA probes

Two major problems associated with the use of fluorescent DNA probes within cellular systems (*in vitro)* include the stability of the oligonucleotide to enzymatic degradation, and the ability of oligonucleotides to cross the cell membrane. As oligonucleotides are highly negatively charged and large molecules, they do not pass the lipid bilayer easily. The lipid bilayer consists of a charged outer region and a lipophilic core; the lipophilic region does not allow charged molecules to pass through easily. There are a number of methods to internalise oligonucleotides into cells; positively charged transfection agents,[27,28] microinjection [29] or to permeabilise the cell membrane e.g. electroporation.[30] With all these methods requiring an external input to facilitate the uptake. Once delivered into cells, oligonucleotides are quickly broken down by DNA nucleases;[36] this is a significant problem for DNA probes. There have been multiple attempts to chemically modify DNA probes to make them resistant to degradation. Examples include locked nucleic acids (LNA),[31] peptide nucleic acids (PNA)[32] and 2'-OMe modified bases[40] (Figure 2.10).

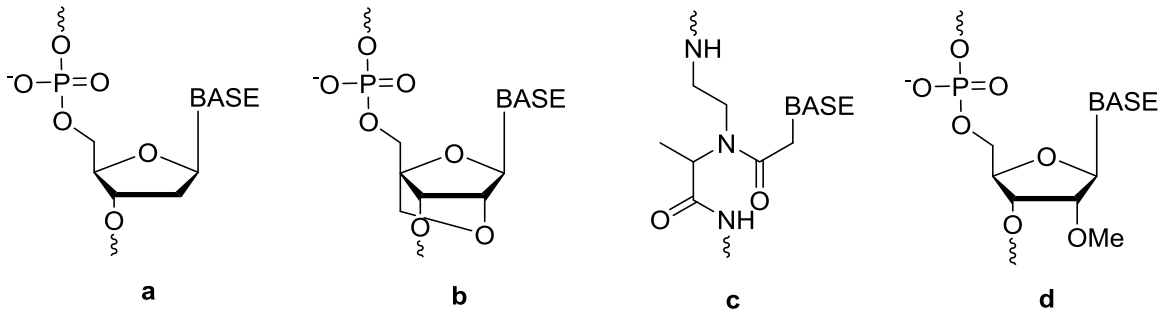

Figure 2.10 DNA chemical modifications to overcome nuclease degradation
(a) Natural phosphodiester linked DNA, (b) LNA, (c) PNA and (d) 2'-OMe modified bases

.

A new variety of nucleic acid established by the Mirkin group has been termed Spherical Nucleic Acids (SNA). These give good cellular stability and are discussed in more detail in Section **2.6**. This variant of nucleic acid constitutes oligonucleotides bound to gold nanoparticles (AuNP), forming a 3D conformation of oligonucleotides which gives the SNA unique properties. SNA have been shown to be readily taken up by cells without the need for chemical transfection agents, whilst also protecting the oligonucleotides from enzymatic degradation. Therefore there is much interest in attaching fluorescent sensors onto AuNPs to form SNA fluorescent sensors.[41]

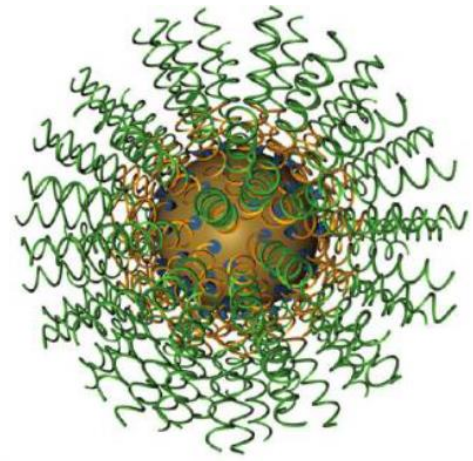

Figure 2.11 Mirkin representation of spherical nucleic acid
Gold nanocore, with oligonucleotide (green) coating. Showing the attachment group (blue) and spacer group (yellow).[42]

2.5 Gold nanoparticles

The optical properties of AuNPs have been of interest to scientists for centuries. The first paper written describing AuNPs was by Faraday in 1857, which explained that their red colour was caused by the colloidal nature of the nanoparticles.[28] The absorption which gives the nanoparticles their characteristic red colour was rationalised by Mie in 1908, using Maxwell's equations. This absorption band at 520 nm (for 13 nm AuNP) is termed the Surface Plasmon Resonance (SPR) which is a specific characteristic of colloidal AuNP. The SPR band is caused by collective oscillation of the conduction band electrons induced by the interacting electromagnetic field (Figure 2.12).[29,30]

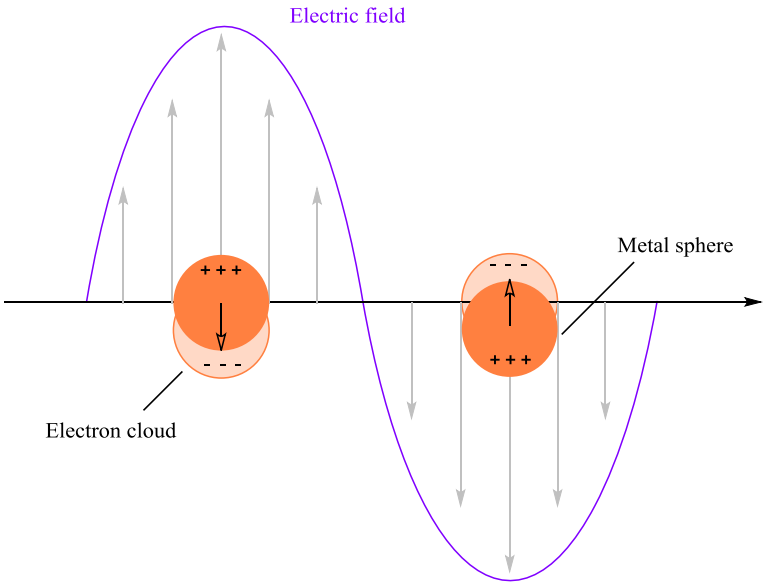

Figure 2.12 The origin of the localised surface plasmon of a gold nanoparticle
Under the influence of an excitation wave with wavelength greater than the dimension of the particle, the electrons oscillate as a whole and the system can be viewed as an oscillating dipole.

Due to the size of AuNPs (1-100nm, between single molecule and bulk metal size) they have specific physical properties which are very dependent on their size, shape, inter-particle distance and surface environment.[31] The SPR peak shifts as the dielectric constant of the

local surrounding medium changes, caused by changes in coating of the AuNP surface.[32] The sensitivity of the SPR can therefore be used to track the coating of a particle surface; when there is no further shift in SPR it is assumed there is no further change in the surface environment of the AuNP, therefore the surface is assumed to be fully coated.

The most common method for synthesising citrate stabilised AuNPs was established by Turkevich *et al.* in 1951.[33] Starting with the commercially available $HAu(III)Cl_4$, the gold is reduced by citrate ions. Dicarboxyacetone (a result of the oxidation of citrate ions) stabilise the AuNP formed, which is formed of aurous salt assembling onto Au(0) atoms.[34] The layers of capping agents (in this case citrate ions) coating the AuNPs cause a coulombic repulsion force which is greater than the Van der Waals interactions between AuNPs, which induces stability that prevents the AuNPs from aggregating. This produces AuNPs coated in citrate ligands, which can be subsequently displaced by a ligand of choice. The Turkevich method has been modified and improved.[35,36] Recently Shulz *et al.*[37] have developed a modified protocol which produces AuNPs (Figure 2.13) with a remarkably narrow size distribution.

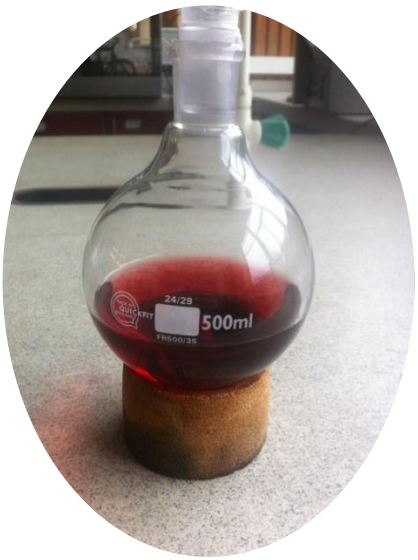

Figure 2.13 13 nm AuNP synthesised using the improved Turkevich method developed by Shulz *et al.*.[37]

There are alternative methods for the synthesis of AuNPs using different stabilising ligands. The Brust-Schiffrin method[38] forms thiolate stabilised AuNP, whilst Schmid's Au_{55} cluster[39] forms phosphine stabilised AuNPs. The coating of these particles cannot be altered once synthesised, however the stabilising groups can be tuned to contain functional groups which can be modified with external molecules to further functionalise the particles.[40]

The advantage of Turkevich's citrate reduction method is that it produces larger particles than the Brust-Schiffrin method, which are more suitable for applications in nanomedicine due to their lower toxicity. In addition, the Au-citrate bond is weak and can therefore be easily displaced post synthetically. Therefore, citrate stabilised AuNPs can be modified easily to form more valuable AuNP materials.[41,42] The most common binding ligand which displaces the citrate ions, is thiol modified ligands; this is because of the formation of the relatively strong S-Au bond, the exact nature of which is an area of great research.[48]

Another property of AuNPs that needs to be considered is their ability to quench fluorescence. At small distances (>10 nm), a quenching efficiency of up to 99% is observed. This is caused by two equally important effects: firstly the AuNPs increase the non-radiative rate of the fluorophore molecules, and secondly the radiative rate of the molecules is decreased due to the molecular dipole and the AuNPs dipole radiating out of phase.[59,60] It is known that the size of the particle greatly affects the amount of quenching.[61]

2.6 Spherical Nucleic Acids

The binding of oligonucleotides to AuNPs was initially driven by the desire to controllably form nanostructures, utilising the specific base pairing of DNA. This was first discovered by the groups of Mirkin[41] and Alvisatos[38] who independently showed that nanostructures could be manipulated based upon the DNA sequences bound to the nanoparticles.

Although DNA is usually modified before binding it to AuNPs, it can also bind in a non-specific manner.[63] Salt is required to overcome the repulsion between the DNA and the gold,[64] resulting in non-specific binding to the gold possibly via the bases.[65] However it has also been shown that un-modified double stranded DNA (i.e. in which the bases are hidden inside the duplex) will also bind to AuNPs.[66] Generally though, it is more common for either the oligonucleotide or the AuNPs to be modified in some way to improve binding, since non-specific binding is fairly weak. The two main routes of chemical modification are to either modify the oligonucleotide with a functional group which can covalently bind to the gold, or to modify the AuNP so it can electrostatically bind to the oligonucleotide. The most common way to covalently attach oligonucleotides to AuNPs is through a thiol modification on the strand of DNA, forming a covalent S-Au bond. However, Dougan *et al.* have developed a thioctic acid binding group, which when bound to AuNPs was found to be much more stable relative to the single thiol bond (Figure 2.14).[67] Another method for binding oligonucleotides to AuNPs is to modify the surface of the AuNPs with a highly cationic compound, such as quaternary ammonium chains. The negatively charged DNA is then bound to the cationic AuNPs through electrostatic interactions (Figure 2.14). This has been used by Sandhu *et al.* to successfully deliver DNA strands into cells.[68]

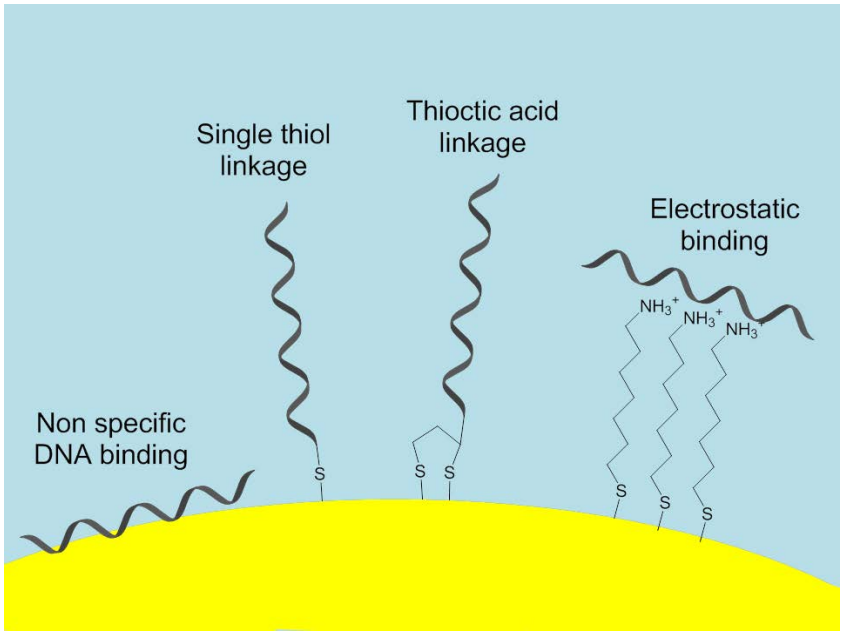

Figure 2.14 Methods for binding oligonucleotides to AuNPs

As discussed earlier (**2.5**), AuNPs quench fluorescence. This property has been used to develop fluorescent probes that increase in fluorescence upon finding their target, as will be discussed later. However, this property also means that there are issues with false positive measurements. If the fluorescent probe is not attached strongly to the AuNPs it can detach and an increase in signal will be seen, which will be interpreted as the target being found. Therefore, for fluorescent sensing technologies, the probe is most commonly attached to the AuNPs surface covalently.

The most widely used method for covalently coating particles with thiol modified DNA is the 'salt ageing' method developed by the Mirkin group.[69] The thiolated oligonucleotides are added to the AuNP in one addition, before the salt concentration is slowly increased. This increase in salt concentration is done over a period of many hours, as adding too much salt at once causes the citrate stabilised AuNP to aggregate. The salt allows maximum coating of the particles as it reduces the repulsion between the negatively charged oligonucleotides

allowing for closer packing on the AuNP surface.[70] Among alternative coating methods, Zhang *et al.* found that lowering the pH of the solution to 3.0 during the DNA attachment step allowed for rapid coverage of AuNPs.[71]

There have been investigations into varying the region between the surface binding group and oligonucleotide, sometimes referred to as the spacer region, and the affect that this has on the SNA properties. Mirkin *et al.* have used a polyethylene glycol (PEG) linker group, and found that it increased the loading of oligonucleotides onto the AuNP surface, when compared to a spacer group consisting of just 10 A bases or 10 T bases.[69] In the same experiments they found that sonication greatly increased the level of DNA coating on AuNP. It was proposed that sonication could reduce the amount of non-specifically bound DNA, exposing more of the AuNP surface for the DNA to bind to.

2.6.1 Cell uptake and stability of SNA

The two major benefits of SNAs are that they are readily taken up by cells,[72] and the oligonucleotides that are bound to the AuNP show a much increased stability to enzymatic degradation.[73,74] The size, shape and functionality of AuNPs have been known to dramatically affect how readily they are taken up by cells,[75] whilst the type of cell being investigated also needs to be taken into account.[75] The Mirkin group have investigated the mechanism of uptake that these SNA particles exhibit. They have shown that they are successfully taken up by over 50 cell types,[76] and the greater density of oligonucleotides on the particle surface, the greater the cellular uptake of SNAs.[72] It is proposed that the SNAs interact with proteins in the cell serum; these positively charged proteins aid the uptake of the particles. Patel *et al.* proposed that the mechanism for uptake was the serum coated

SNAs interacting with class A scavenger receptors in a lipid raft mediated uptake (Figure 2.15).[77] Choi *et al.* showed the mechanism was dependant on the 3-D structure of the SNA; they were able to cross link the oligonucleotides once bound to the AuNP surface, retaining its 3D structure, then dissolve the AuNP.[78] These 'hollow SNAs' still retained the cell uptake properties of the AuNP-containing SNAs.[79]

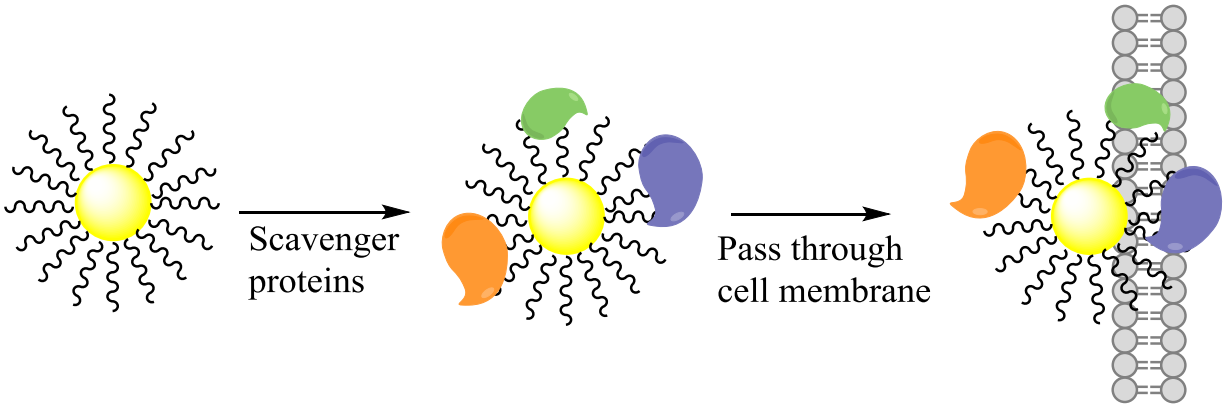

Figure 2.15 SNA interacting with scavenger receptors before passing through the cell membrane

The observed increase in stability that DNA displays in DNA-AuNPs, (it has been shown to have a 4 times longer half-life) has been investigated.[74] The high density of the DNA strands was initially thought to prevent the binding of enzymes to the DNA; however it has been shown that nucleases may in fact show increased binding affinity to SNAs in comparison to single stranded DNA. The major reason for the increased stability has therefore been attributed to the high charge and local salt concentration surrounding the particles.[74]

2.6.2 SNA as fluorescent DNA detection probes

Due to the increased stability and ready uptake by cells, there has been much research in coating AuNPs with fluorescent probes.[80] The group of Libchaber have integrated AuNPs into molecular beacon systems, replacing the quencher dye with a AuNP.[81] They found that small

AuNPs (1.4 nm) showed greater quenching efficiencies in a molecular beacon system than the commonly used quencher, DABCYL. Maxwell *et al.* has also employed AuNPs in a similar fashion, using 2.5 nm particles.[82] However these small AuNPs were found to be not suitable for *in vitro* work due to their cytotoxicity. The scaffold provided by the AuNP allows for multiple different tags to be bound to a single AuNP. Song *et al.* have developed a multicolour system for sensing multiple DNA targets using multiple AuNP bound molecular beacons (Figure 2.16).[83]

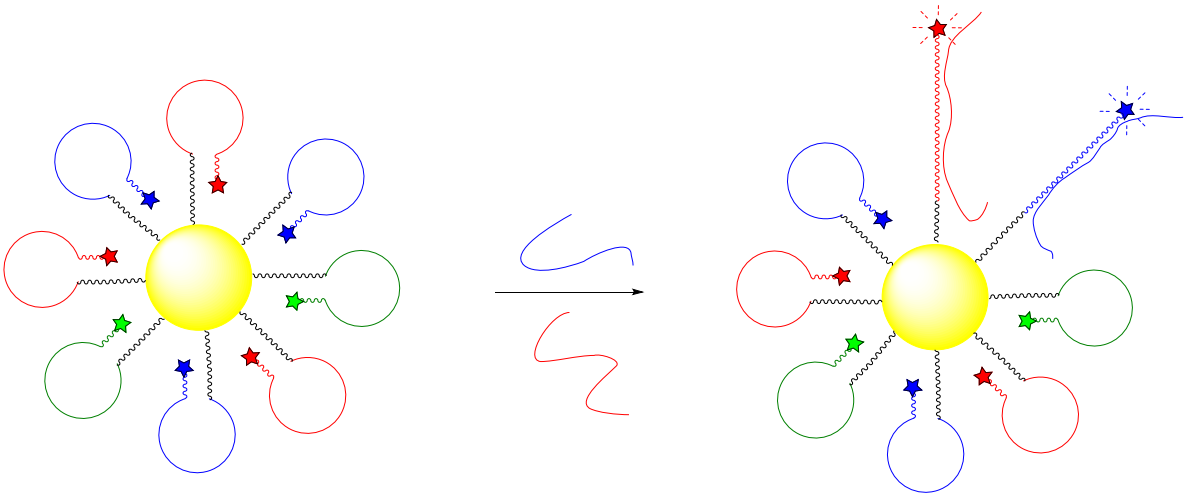

Figure 2.16 Nano molecular beacons[83]
Upon binding to their targets, the fluorophores move away from the quenching nanoparticle.

The Mirkin group have developed a method for gene detection termed 'nanoflares', which utilises the quenching property of AuNP plus the highly specific nature of DNA to elicit a switch ON detector of target DNA.[84] A nanoflare consists of an SNA whose oligonucleotides are complementary to the target DNA to be detected. A short strand of DNA modified with a fluorophore, the flare, is then hybridised to the AuNP bound oligonucleotide. The flare is close enough to the AuNP so that its fluorescence is significantly quenched. Importantly though, the flare is shorter than the AuNP bound DNA. Therefore in the presence of the

target strand, the flare will be displaced by the longer target resulting in an increase in fluorescence (Figure 2.17). This technique has been used for cellular detection of mRNA.[85]

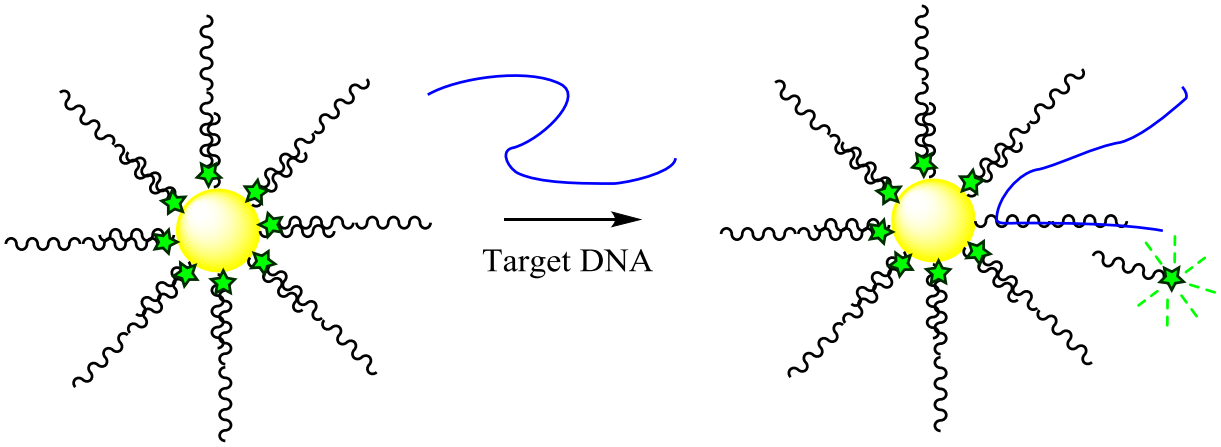

Figure 2.17 Mirkins nanoflare system
Upon addition of larger and more specific target DNA strand, the flare is displaced from the duplex. Once clear of the quenching AuNP the fluorophore increases in fluorescence, indicating the presence of target DNA.

The system was improved to identify multiple targets, by coating the particles with multiple different nanoflares. Each target was identified by the increased fluorescence of its specific fluorophore.[86] Li *et al.* have used this system to identify multiple mRNA tumour markers in cell samples to help identify cancerous cells.[87]

2.7 Luminescent probes

Fluorescence and phosphorescence are photon emission processes that occur during molecular relaxation from electronic excited states. In fluorescence, a photon is absorbed by a molecule, exciting an electron from the ground singlet state into an excited singlet state. The electron quickly relaxes to the lowest vibrational energy state through internal conversion. This relaxation process, in the region of picoseconds, is responsible for the

wavelength of emitted photons being longer than that of the absorbed photons, i.e. the Stokes shift. The length of time the electron remains in the lowest vibrational level of the excited state; is termed the fluorescence lifetime. The electron drops down to an available ground state vibrational level, emitting a photon of light. The photon of light emitted is what is detected in fluorescence studies (Figure 2.18).

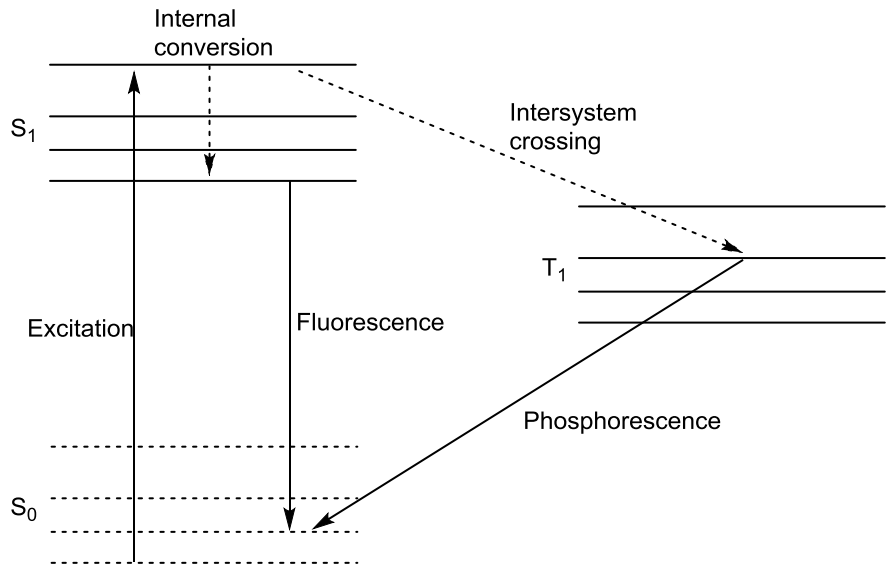

Figure 2.18 Jablonski diagram showing the energy transfer processes involved for fluorescence and phosphorescence.

Phosphorescence is different to fluorescence due to another relaxation process that can occur called intersystem crossing. This involves electrons from the excited singlet state moving to an excited lower energy triplet state. Phosphorescence emission occurs as the excited triplet electron drops to the ground singlet state; this transfer is spin forbidden and therefore takes much longer than internal conversion which leads to an extended lifetime, in the order of micro seconds to seconds. The large energy change between the singlet and triplet state, results in phosphorescence having a larger Stoke shift than fluorescence.

Anthracene is a polyaromatic molecule which upon UV irradiation fluoresces in the region of 390-550 nm; these properties make it a molecule of interest for sensing systems. Anthracene has been used for a variety of sensing applications, such as metal ions[88] and pH.[89] It has been integrated into oligonucleotides as a BDF. Brown and Saito have both used anthracene as a BDF, varying both the binding groups to the anthracene and also the position at which the anthracene was bound (Figure 2.19).[90,91] Both groups found that the anthracene emission increased upon hybridisation.

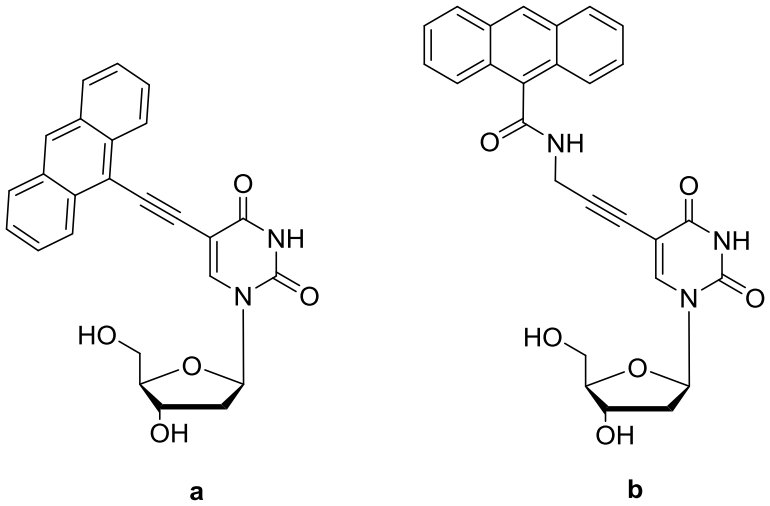

Figure 2.19 ***Anthracene as a BDF***
Examples of anthracene as a BDF, (a) Brown et al.[90] *(b) Saito et al..*[91]

Previous work within the Tucker group has incorporated anthracene tags into the DNA backbone via initially a serinol linker[92] or more recently using a threoninol linker,[93,94] a more in depth introduction to the Tucker group system is found in Section **3.1**.

Owing to its long fluorescence lifetime and large Stoke shift, tris(bipyridine)ruthenium(II) ($Ru(II)(bpy)_3$) complexes have been used widely in imaging.[95,96] They have been used to detect oxygen levels within a cell using Fluorescent Lifetime Imaging Microscopy (FLIM).[97] More recently modification to the ligands has allowed the complexes to be able to bind to

nanoparticles. Zanarani *et al*. modified a bipyridine ligand to contain a trimethoxysilane group, which was then used to bind the ruthenium complex to silica nanoparticles (Figure 2.20).[98] Rogers et al have modified a bipyridine ligand with two thiol terminating "legs" which allows the probe to be bound to AuNP (Figure 2.20).[99]

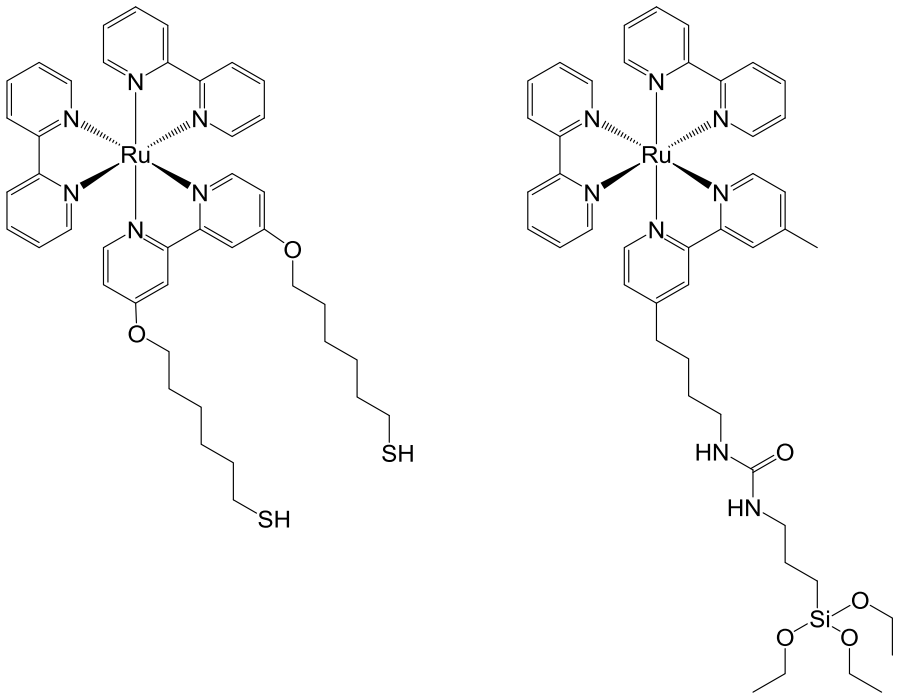

Figure 2.20 Ru(II)(bpy)$_3$ molecule
Ru(II)(bpy)$_3$ complex able to bind to AuNP by Rogers et al.[99] *(b) Ru(II)(bpy)$_3$ complex able to bind to silica nanoparticles by Zanarani et al..*[98]

2.8 References

1. Watson, J. D. & Crick, F. H. C. Molecular Structure of Nucleic Acids. *Nature* **171,** 737–738 (1953).
2. Nikolova, E. N. *et al.* Transient Hoogsteen base pairs in canonical duplex DNA. *Nature* **470,** 498–502 (2011).
3. http://www.atdbio.com/content/5/Nucleic-acid-structure.
4. Michelson. A. A. & Todd, A. R. Nucleotides Part XXXII. Synthesis of a Dithymidine Dinucleotide Containing a 3' : 5' - Internucleotidic Linkage. *J. Chem. Soc.* 2632–2638 (1955).
5. Gilham, P. T. & Khorana, H. G. Studies on Polynucleotides. I. A New and General Method for the Chemical Synthesis of the C 5 ″-C 3 ″ Internucleotidic Linkage. Syntheses of Deoxyribo-dinucleotides 1. *J. Am. Chem. Soc.* **80,** 6212–6222 (1958).
6. Letsinger, R. L. & Ogilvie, K. K. Nucleotide chemistry. XIII. Synthesis of oligothymidylates via phosphotriester intermediates. *J. Am. Chem. Soc.* **91,** 3350–3355 (1969).
7. Letsinger, R. & Mahadevan, V. Oligonucleotide Synthesis on a Polymer Support1, 2. *J. Am. Chem. Soc.* **414,** 3526–3527 (1965).
8. McBride, L. J. & Caruthers, M. H. An investigation of several deoxynucleoside phosphoramidites useful for synthesizing deoxyoligonucleotides. *Tetrahedron Lett.* **24,** 245–248 (1983).
9. Caruthers, M. & Matteucci, M. D. Synthesis of Deoxyoligonucleotides on a Polymer Support. *J. Am. Chem. Soc.* **103,** 3185–3191 (1981).
10. Brookes, a J. The essence of SNPs. *Gene* **234,** 177–86 (1999).
11. Kim, S. & Misra, A. SNP genotyping: technologies and biomedical applications. *Annu. Rev. Biomed. Eng.* **9,** 289–320 (2007).
12. Kathiresan, S. *et al.* Genome-wide association of early-onset myocardial infarction with single nucleotide polymorphisms and copy number variants. *Nat. Genet.* **41,** 334–341 (2009).
13. Ginsburg, G. S. & Willard, H. F. Genomic and personalized medicine: foundations and applications. *Transl. Res.* **154,** 277–287 (2009).
14. Davey, J. W. *et al.* Genome-wide genetic marker discovery and genotyping using next-generation sequencing. *Nat. Rev. Genet.* **12,** 499–510 (2011).
15. DePristo, M. a *et al.* A framework for variation discovery and genotyping using next-generation DNA sequencing data. *Nat. Genet.* **43,** 491–8 (2011).
16. Tan, W., Fang, X., Li, J. & Liu, X. Molecular beacons: a novel DNA probe for nucleic acid and protein studies. *Chemistry* **6,** 1107–11 (2000).
17. Musa. M, M. & Lovisa, M. Using Molecular Beacons to detect Single Nucleotide Polymorphisms using real time PCR. *Methods* **25,** 463–471 (2001).
18. McGuigan, F. E. a & Ralston, S. H. Single nucleotide polymorphism detection: allelic discrimination using TaqMan. *Psychiatr. Genet.* **12,** 133–6 (2002).
19. Larsson, C., Grundberg, I. & Söderberg, O. In situ detection and genotyping of individual mRNA molecules. *Nat. Methods* **7,** 395–397 (2010).
20. Whitcombe, D., Theaker, J., Guy, S. P., Brown, T. & Little, S. Detection of PCR products using self-probing amplicons and fluorescence. *Nat. Biotechnol.* **17,** 804–7 (1999).
21. Thelwell, N., Millington, S., Solinas, a, Booth, J. & Brown, T. Mode of action and application of Scorpion primers to mutation detection. *Nucleic Acids Res.* **28,** 3752–61 (2000).
22. Solinas, A. *et al.* Duplex Scorpion primers in SNP analysis and FRET applications. *Nucleic Acids Res.* **29,** E96 (2001).
23. French, D. J., Archard, C. L., Brown, T. & McDowell, D. G. HyBeacon probes: a new tool for DNA sequence detection and allele discrimination. *Mol. Cell. Probes* **15,** 363–374 (2001).
24. French, D. J., Archard, C. L., Andersen, M. T. & McDowell, D. G. Ultra-rapid DNA analysis using

HyBeacon probes and direct PCR amplification from saliva. *Mol. Cell. Probes* **16,** 319–326 (2002).
25. Ben Gaied, N. *et al.* End-capped HyBeacon probes for the analysis of human genetic polymorphisms related to warfarin metabolism. *Org. Biomol. Chem.* **8,** 2728–34 (2010).
26. Saito, Y., Miyauchi, Y., Okamoto, A. & Saito, I. Base-discriminating fluorescent (BDF) nucleoside: distinction of thymine by fluorescence quenching. *Chem. Commun. (Camb).* 1704–1705 (2004).
27. Okamoto, A., Tainaka, K. & Saito, I. Clear distinction of purine bases on the complementary strand by a fluorescence change of a novel fluorescent nucleoside. *J. Am. Chem. Soc.* **125,** 4972–3 (2003).
28. Fukui, K., Morimoto, M., Segawa, H., Tanaka, K. & Shimidzu, T. Synthesis and properties of an oligonucleotide modified with an acridine derivative at the artificial abasic site. *Bioconjug. Chem.* **7,** 349–55 (1996).
29. Seitz, O., Bergmann, F. & Heindl, D. A convergent strategy for the modification of peptide nucleic acids: Novel mismatch-specific PNA-hybridization probes. *Angew. Chemie - Int. Ed.* **38,** 2203–2206 (1999).
30. Köhler, O., Jarikote, D. V. & Seitz, O. Forced Intercalation Probes (FIT Probes): Thiazole Orange as a Fluorescent Base in Peptide Nucleic Acids for Homogeneous Single-Nucleotide-Polymorphism Detection. *ChemBioChem* **6,** 69–77 (2005).
31. Bethge, L., Singh, I. & Seitz, O. Designed thiazole orange nucleotides for the synthesis of single labelled oligonucleotides that fluoresce upon matched hybridization. *Org. Biomol. Chem.* **8,** 2439–48 (2010).
32. Kummer, S. *et al.* Fluorescence imaging of influenza H1N1 mRNA in living infected cells using single-chromophore FIT-PNA. *Angew. Chemie - Int. Ed.* **50,** 1931–1934 (2011).
33. Kummer, S. *et al.* PNA FIT-probes for the dual color imaging of two viral mRNA targets in influenza H1N1 infected live cells. *Bioconjug. Chem.* **23,** 2051–2060 (2012).
34. Boussif, O. *et al.* A Versatile Vector for Gene and Oligonucleotide Transfer into Cells in Culture and in vivo : Polyethylenimine. *Proc. Natl. Acad. Sci.* **92,** 7297–7301 (1995).
35. Bielinska, A. U., Chen, C., Johnson, J. & Baker, J. R. DNA Complexing with Polyamidoamine Dendrimers : Implications for Transfection. 843–850 (1999).
36. Fisher, T. L., Terhorst, T., Cao, X. & Wagner, R. W. Intracellular disposition and metabolism of fluorescently-labeled unmodified and modified oligonucleotides microinjected into mammalian cells. *Nucleic Acids Res.* **21,** 3857–3865 (1993).
37. Neumann, E., Schaefer-Ridder, M., Wang, Y. & Hofschneider, P. H. Gene transfer into mouse lyoma cells by electroporation in high electric fields. *EMBO J.* **1,** 841–845 (1982).
38. Kumar, R., Meldgaard, M., Olsen, E. & Wengel, J. LNA (Locked Nucleic Acids): Synthesis of the Adenine, Cytosine, Guanine, 5-Methylcytosine, Thymine and Uracil Bicyclonucleoside Monomers, Oligomerisation, and Unprecedented Nucleic Acid Recognition. *Tetrahedron* **54,** 3607–3630 (1998).
39. Egholm, M. *et al.* PNA hybridizes to complementary oligonucleotides obeying the Watson-Crick hydrogen-bonding rules. *Nature* **365,** 566–568 (1993).
40. Sproat, B. S., Beijer, B. & Iribarren, A. New synthetic routes to protected purine 2'-O-Methylriboside-3'-O-phosphoramidites using a novel alkylation procedure. *Nucleic Acids Res.* **18,** 41–49 (1990).
41. Williams, S. C. P. Spherical nucleic acids: A whole new ball game. *Proc. Natl. Acad. Sci.* **110,** 13231–13233 (2013).
42. Cutler, J. I., Auyeung, E. & Mirkin, C. A. Spherical Nucleic Acids. *J. Am. Chem. Soc.* **134,** 1376–1391 (2012).
43. Faraday, M. Experimental Relations of Gold (and other Metals) to Light. *Philos. Trans. R. Soc. London* **147,** 145–181 (1857).

44. Link, S. & El-Sayed, M. a. Spectral Properties and Relaxation Dynamics of Surface Plasmon Electronic Oscillations in Gold and Silver Nanodots and Nanorods. *J. Phys. Chem. B* **103,** 8410–8426 (1999).
45. Louis, C. & Pluchery, O. *Gold Nanoparticles for Physics, Chemistry and Biology*. (2012).
46. Brust, M. & Kiely, C. J. Some recent advances in nanostructure preparation from gold and silver particles: a short topical review. *Colloids Surfaces A Physicochem. Eng. Asp.* **202,** 175–186 (2002).
47. Aslan, K. & Pérez-Luna, V. H. Surface modification of colloidal gold by chemisorption of alkanethiols in the presence of a nonionic surfactant. *Langmuir* **18,** 6059–6065 (2002).
48. Turkevitch, J., Stevenson, P. C. & Hillier, J. . *Discuss. Faraday. Soc* **11,** 55–75 (1951).
49. Kumar, S., Gandhi, K. S. & Kumar, R. Modeling of Formation of Gold Nanoparticles by Citrate Method. *Ind. Eng. Chem. Res.* **46,** 3128–3136 (2007).
50. Kimling, J. *et al.* Turkevich method for gold nanoparticle synthesis revisited. *J. Phys. Chem. B* **110,** 15700–7 (2006).
51. Frens, G. Controlled Nucleation for the Regulation of the Particle Size in Monodisperse Gold Suspensions. *Nat. Phys. Sci.* **241,** 20–22 (1973).
52. Schulz, F. *et al.* Little Adjustments Significantly Improve the Turkevich Synthesis of Gold Nanoparticles. *Langmuir* **30,** 10779–10784 (2014).
53. Brust, M., Walker, M., Bethell, D., Schiffrin, D. J. & Whyman, R. Synthesis of Thiol-derivatised Gold Nanoparticles in a Two-phase Liquid-Liquid System. *J. Chem. Soc. Chem. Commun.* 801–802 (1994).
54. Schrnidet, G. *et al.* Au55[P(C6H5)3]12Cl6 — ein Goldcluster ungewöhnlicher Größe. *Chemishe Berichte* **114,** 3634–3642 (1981).
55. Zubarev, E. R., Xu, J., Sayyad, A. & Gibson, J. D. Amphiphilic gold nanoparticles with V-shaped arms. *J. Am. Chem. Soc.* **128,** 4958–4959 (2006).
56. Mirkin, C., Letsinger, R., Mucic, R. & Storhoff, J. A DNA-based method for rationally assembling nanoparticles into macroscopic materials. *Nature* **382,** 607–609 (1996).
57. Levy, R. *et al.* Rational and combinatorial design of peptide capping ligands for gold nanoparticles. *J. Am. Chem. Soc.* **126,** 10076–10084 (2004).
58. Häkkinen, H. The gold–sulfur interface at the nanoscale. *Nat. Chem.* **4,** 443–455 (2012).
59. Dulkeith, E. *et al.* Gold nanoparticles quench fluorescence by phase induced radiative rate suppression. *Nano Lett.* **5,** 585–9 (2005).
60. Anger, P., Bharadwaj, P. & Novotny, L. Enhancement and quenching of single-molecule fluorescence. *Phys. Rev. Lett.* **96,** 113002 (2006).
61. Dulkeith, E. *et al.* Fluorescence Quenching of Dye Molecules near Gold Nanoparticles: Radiative and Nonradiative Effects. *Phys. Rev. Lett.* **89,** 12–15 (2002).
62. Alvisatos, A. P. *et al.* Organization of 'nanocrystal molecules' using DNA. *Nature* **382,** 609–611 (1996).
63. Zhang, X., Liu, B., Dave, N., Servos, M. R. & Liu, J. Instantaneous Attachment of an Ultrahigh Density of Nonthiolated. *Langmuir* **28,** 17053–17060 (2012).
64. Liu, J. Adsorption of DNA onto gold nanoparticles and graphene oxide: surface science and applications. *Phys. Chem. Chem. Phys.* **14,** 10485–96 (2012).
65. Jiang, H., Materon, E. M., Sotomayor, M. D. P. T. & Liu, J. Fast assembly of non-thiolated DNA on gold surface at lower pH. *J. Colloid Interface Sci.* 1–6 (2013).
66. Sandstrom, P., Boncheva, M. & Akerman, B. Nonspecific and Thiol-Specific Binding of DNA to Gold Nanoparticles. *Langmuir* **19,** 7537–7543 (2003).
67. Dougan, J. a, Karlsson, C., Smith, W. E. & Graham, D. Enhanced oligonucleotide-nanoparticle conjugate stability using thioctic acid modified oligonucleotides. *Nucleic Acids Res.* **35,** 3668–75 (2007).

68. Sandhu, K. K., McIntosh, C. M., Simard, J. M., Smith, S. W. & Rotello, V. M. Gold nanoparticle-mediated transfection of mammalian cells. *Bioconjug. Chem.* **13,** 3–6 (2002).
69. Hurst, S. J., Lytton-Jean, A. K. R. & Mirkin, C. a. Maximizing DNA loading on a range of gold nanoparticle sizes. *Anal. Chem.* **78,** 8313–8 (2006).
70. Hurst, S. J., Lytton-Jean, A. K. R. & Mirkin, C. A. Maximising DNA Loading on a Range of Gold Nanoparticle Sizes. *Anal. Chem.* **78,** 8313–8318 (2006).
71. Zhang, X., Servos, M. R. & Liu, J. Instantaneous and Quantitative Functionalization of Gold Nanoparticles with Thiolated DNA Using a pH-Assisted and Surfactant-Free Route. *J. Am. Chem. Soc.* 7266–7269 (2012).
72. Giljohann, D. a *et al.* Oligonucleotide loading determines cellular uptake of DNA-modified gold nanoparticles. *Nano Lett.* **7,** 3818–21 (2007).
73. Prigodich, A. E., Alhasan, A. H. & Mirkin, C. A. Selective Enhancement of Nucleases by Polyvalent DNA-Functionalized Gold Nanoparticles. *J. Am. Chem. Soc.* **133,** 2120–2123 (2011).
74. Seferos, D. S., Prigodich, A. E., Giljohann, D. A., Patel, P. C. & Mirkin, C. A. Polyvalent DNA Nanoparticle Conjugates Stabilize Nucleic Acids. *Nano Lett.* **9,** 308–311 (2009).
75. Alkilany, A. M. & Murphy, C. J. Toxicity and cellular uptake of gold nanoparticles: What we have learned so far? *J. Nanoparticle Res.* **12,** 2313–2333 (2010).
76. Giljohann, D. a *et al.* Gold nanoparticles for biology and medicine. *Angew. Chem. Int. Ed. Engl.* **49,** 3280–94 (2010).
77. Patel, P. C. *et al.* Scavenger receptors mediate cellular uptake of polyvalent oligonucleotide-functionalized gold nanoparticles. *Bioconjug. Chem.* **21,** 2250–6 (2010).
78. Cutler, J. I. *et al.* Polyvalent Nucleic Acid Nanostructures. *J. Am. Chem. Soc.* **133,** 9254–9257 (2011).
79. Choi, C. H. J., Hao, L., Narayan, S. P., Auyeung, E. & Mirkin, C. a. Mechanism for the endocytosis of spherical nucleic acid nanoparticle conjugates. *Proc. Natl. Acad. Sci. U. S. A.* **110,** 2–7 (2013).
80. Heuer-Jungemann, A., Harimech, P. K., Brown, T. & Kanaras, A. G. Gold nanoparticles and fluorescently-labelled DNA as a platform for biological sensing. *Nanoscale* **5,** 9503–10 (2013).
81. Dubertret, B., Calame, M. & Libchaber, a J. Single-mismatch detection using gold-quenched fluorescent oligonucleotides. *Nat. Biotechnol.* **19,** 365–70 (2001).
82. Maxwell, D. J., Taylor, J. R. & Nie, S. Self-assembled nanoparticle probes for recognition and detection of biomolecules. *J. Am. Chem. Soc.* **124,** 9606–12 (2002).
83. Song, S. *et al.* Gold-Nanoparticle-Based Multicolor Nanobeacons for Sequence-Specific DNA Analysis. *Angew. Chemie* **121,** 8826–8830 (2009).
84. Seferos, D. S., Giljohann, D. a, Hill, H. D., Prigodich, A. E. & Mirkin, C. a. Nano-flares: probes for transfection and mRNA detection in living cells. *J. Am. Chem. Soc.* **129,** 15477–9 (2007).
85. Prigodich, A. E. *et al.* Nano-flares for mRNA regulation and detection. *ACS Nano* **3,** 2147–52 (2009).
86. Prigodich, A. E. *et al.* Multiplexed nanoflares: mRNA detection in live cells. *Anal. Chem.* **84,** 2062–6 (2012).
87. Li, N., Chang, C., Pan, W. & Tang, B. A multicolor nanoprobe for detection and imaging of tumor-related mRNAs in living cells. *Angew. Chem. Int. Ed. Engl.* **51,** 7426–30 (2012).
88. Hager, R. *et al.* An Anthracene-Based Fluorescent Sensor for Transition Metal Ions. *Chem. Commun.* **33,** 1975–1977 (1994).
89. Silva, A. P. De & Rupasinghe, R. A. D. D. A New Class of Fluorescent pH Indicators based on Photo-induced Electron Transfer. *J. Chem. Soc. Chem. Commun.* 1669–1670 (1985).
90. Xiao, Q., Ranasinghe, R. T., Tang, A. M. P. & Brown, T. Naphthalenyl- and anthracenyl-ethynyl dT analogues as base discriminating fluorescent nucleosides and intramolecular energy transfer donors in oligonucleotide probes. *Tetrahedron* **63,** 3483–3490 (2007).

91. Saito, Y., Motegi, K., Bag, S. S. & Saito, I. Anthracene based base-discriminating fluorescent oligonucleotide probes for SNPs typing: synthesis and photophysical properties. *Bioorg. Med. Chem.* **16,** 107–13 (2008).
92. Moran, N. *et al.* Detection of a single DNA base-pair mismatch using an anthracene-tagged fluorescent probe. *Chem. Commun. (Camb).* 5003–5 (2006). doi:10.1039/b611650g
93. Duprey, J.-L. H. a *et al.* Detection of DNA base variation and cytosine methylation at a single nucleotide site using a highly sensitive fluorescent probe. *Chem. Commun. (Camb).* **47,** 6629–31 (2011).
94. Zhao, Z.-Y. *et al.* Detection of single nucleotide polymorphisms within a sequence of a gene associated with prostate cancer using a fluorophore-tagged DNA probe. *Bioorg. Med. Chem. Lett.* **22,** 129–32 (2012).
95. Fernandez-Moreira, V., Thorp-Greenwood, F. L. & Coogan, M. P. Application of d6 transition metal complexes in fluorescence cell imaging. *Chem. Commun.* **46,** 186–202 (2010).
96. Baggaley, E., Weinstein, J. A. & Williams, J. A. G. Lighting the way to see inside the live cell with luminescent transition metal complexes. *Coord. Chem. Rev.* **256,** 1762–1785 (2012).
97. Gerritsen, H. C., Sanders, R., Draaijer, A., Ince, C. & Levine, Y. K. Fluorescence Lifetime Imaging of Oxygen in Living Cells. *J. Fluoresc.* **7,** 11–15 (1997).
98. Zanarini, S. *et al.* Ru (bpy) 3 Covalently Doped Silica Nanoparticles as Multicenter Tunable Structures for Electrochemiluminescence Amplification. *J. Am. Chem. Soc.* **131,** 2260–2267 (2009).
99. Rogers, N. J. *et al.* High coating of Ru(II) complexes on gold nanoparticles for single particle luminescence imaging in cells. *Chem. Commun. (Camb).* **50,** 617–9 (2014).

3 SNP SENSING ON AUNP

3.1 Introduction to SNP sensing anthracene probe

The discovery that our genetic code contains a multitude of information regarding our health and wellbeing has led to the invention of multiple ways to read and understand how variations in this information affect the human body.[1] Single Nucleotide Polymorphisms (SNPs) are single base variations in our genome that are present in more than 1% of the population. It is thought that whilst they may not directly cause diseases, they give an insight into the likelihood of disease development. The ability to detect Single Nucleotide Polymorphisms has therefore become an area of great interest.[2] As discussed earlier in Section **2.3**, current methods include: Taqman, molecular beacons, Hybeacons and Scorpion probes. However, one drawback is that these methods rely upon the difference in hybridisation energies and can therefore only work within narrow temperature windows. As described below, the Tucker group has created an assay which does not rely on the differences in hybridisation energies to identify base changes at a SNP site in a strand of target DNA.

An anthracene tag is integrated into the DNA molecule through a threoninol unit (Figure 3.1) which inserts into the DNA backbone, with the anthracene mimicking a base. The strand then forms a duplex with the target strand of interest. It is designed to be complementary to the target strand, and single base variations are then detected through changes in the emission intensity of the anthracene. The structure of the anthracene probe is crucial to its SNP sensing capabilities. The anthracene probe can be varied through the carbon linker group between the peptide bond and the ether (labelled **n** in Figure 3.1). This linker can be from n = 1 to n = 7 (n = 2 cannot be synthesised). There are also two stereoisomers of the

threoninol unit, l and d (the stereogenic centre is highlighted at ***** position in Figure 3.1). Changing these two variables affects how the anthracene probe reacts to different SNP targets.

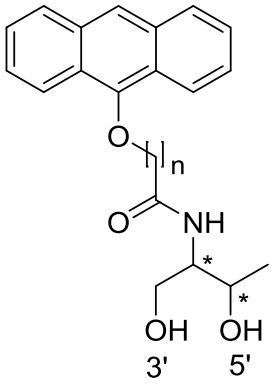

Figure 3.1 Anthracene threoninol unit
*Carbon linker can be varied at n(n = 1-7 n ≠ 2). Stereocentres at *.*

Based upon the structural variations in the anthracene probe, two different systems have been developed for SNP sensing. The first system named *base-adjacent sensing* is used for the majority of this chapter, whilst the second system, *base-opposite sensing*, will be introduced in Section **3.8.4**. The base adjacent system requires a short linker length to the anthracene probe, (*n* = 1) and its synthesis is shown in Scheme 3.3. The probe strand is able to detect base variations in the target strand at the position adjacent, in the 3' position, to the base opposite the anthracene tag (Figure 3.2).

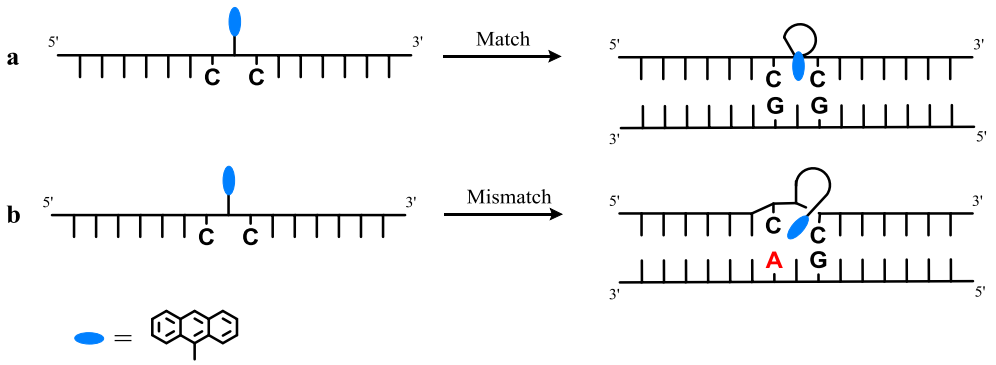

Figure 3.2 Schematic of base adjacent sensing system
The identity of the base opposite adjacent the anthracene tag determines the level of intercalation into the DNA duplex, (red base is variation).

The presence of a mismatch (i.e. indicating the other variant of the SNP site) is detected through a change in emission of the anthracene probe; a completely matching strand leads to a decrease in emission whereas a single base mismatch at the position opposite adjacent the probe leads to an increase in emission (Figure 3.3).

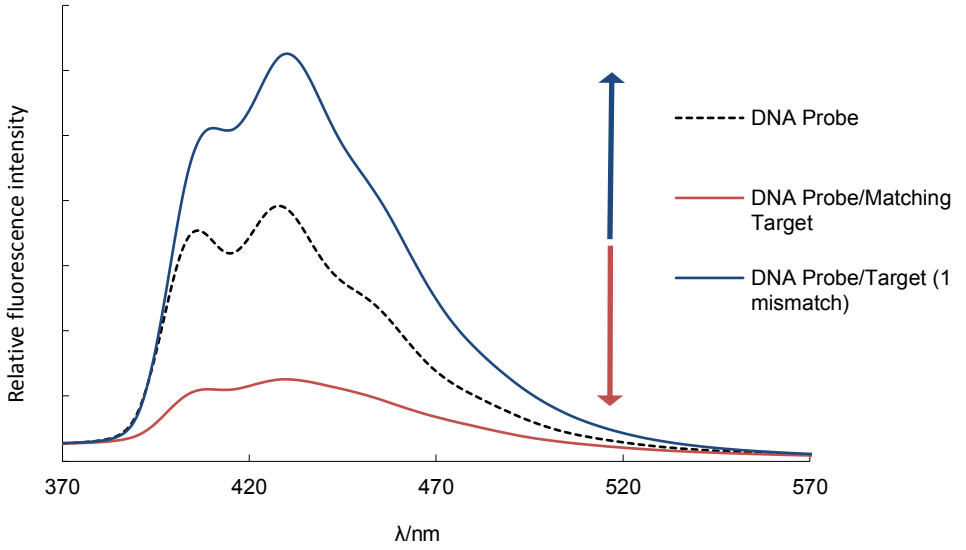

Figure 3.3 Fluorescence response of 1L anthracene probe upon target addition
Upon duplex formation, an increase in anthracene emission intensity is observed for mismatch target and a decrease in emission intensity for fully matching target (pH = 7.0, 10 mM phosphate buffer, 100 mM NaCl, 293 K, λ_{ex} = 350 nm).

These differences in intensity can be explained by the extent to which the anthracene excited state can be quenched, which is linked to the position of the anthracene and in particular the amount of intercalation into the DNA duplex (Figure 3.2). For the fully matched duplex, the anthracene intercalates into the duplex and the anthracene excited state is quenched due to π-stacking interaction with proximate base pairs (Figure 3.2 **a**). Other groups have undertaken studies on this type of system, most notably using pyrene.[3] However, for the mismatch target (containing the other SNP variant) the cavity into which the anthracene intercalates is larger; this is due to the lack of H-bonding between one mismatching base pair next to the anthracene unit. The anthracene is therefore not quenched to the same extent by the nearby base pairs (Figure 3.2 **b**). In fact, as there is more room for it to be intercalated further into the duplex, the anthracene probe is screened from quenching water molecules. This hydrophobic environment leads it to display increased emission relative to the probe alone.

The probe has been tested in cuvettes successfully; however the ultimate goal is for cellular (*in vitro*) SNP detection in RNA and DNA. *In vitro* detection would allow the process of SNP detection to be done quickly and cheaply, as there would be no need for isolation of genetic material before sensing the target of interest. There are, however, multiple problems associated with *in vitro* delivery of oligonucleotides, which include the delivery of nucleic acids into cells, the stability of nucleic acids within a cellular environment and the amount of target material available to bind to the probe.[4]

To start to overcome the problems associated with *in vitro* delivery of oligonucleotides and their stability in cells, a modified anthracene probe that can be bound to gold nanoparticles

(AuNP) has been developed. Attaching oligonucleotides to AuNPs increases the stability of the oligonucleotide to enzyme degradation. Furthermore, these DNA-AuNP particles can be taken up by a variety of cell types without the need for chemical additives. Seferos *et al.* found that by increasing the oligonucleotide density on the surface of the AuNP, nuclease mediated degradation decreased.[5] Originally this increased stability was thought to stem from the densely packed oligonucleotides hindering the enzyme's ability to bind to the oligonucleotides. However, more recent model studies have suggested that increasing the packing of the nanoparticle surface actually results in an enhancement in enzyme binding.[5] However, it was found that the high salt concentration surrounding the DNA coated particles inhibited the enzyme's ability to hydrolyse the DNA. This high salt concentration is a direct result of the densely packed, negatively charged oligonucleotides, which therefore attract a large concentration of monovalent counter cations (e.g. Na^+ and K^+). It has been shown that monovalent cations, such as Na^+ inhibit *DNase I* and other nucleases by displacing Ca^{2+} and Mg^{2+} ions which are bound to enzymes and required for activity. Seferos *et al.* found that the DNA-AuNPs were over four times more stable in salt-dependant conditions compared to free DNA molecules.

Gold nanoparticles have long been used for the delivery of compounds into cells,[6] and investigations into the uptake of DNA-coated AuNPs show that they are readily up-taken into multiple cell types, although the method of cell uptake is still debated (see Section **2.6.1**).[7,8,9]

3.2 Modified DNA synthesis

Non-functionalised DNA can bind to AuNP in a non-specific manner.[10,11,12] It can adsorb on to AuNP through the nitrogen containing groups within the DNA bases.[13] However binding in

this manner does not allow for the controllable binding of DNA to AuNP as the strands can easily detach from the surface of the AuNP. For the purposes of delivering the probe into cells and forming stable particles, DNA has to be covalently bound to the surface; therefore the DNA needs to be modified with a suitable group. Sulphur groups are commonly used for binding molecules to AuNP, as it can form a strong S-Au bond. The nature of the binding mode between the gold and sulphur has been the subject of many studies.[14] Most work with AuNPs has been done using mono-thiolated DNA,[15] but tetrathiolated DNA has also been investigated.[16] Following work by Graham *et al.,*[17] where it was found that a thioctic acid modified DNA strand was more stable once bound to AuNP than a thiolated DNA strand, it was decided to modify the probe strands with a thioctic acid. This forms a bis-thiolated adduct upon reduction of the disulphide which binds to the gold through both sulphur atoms.[18,19]

To modify the DNA, an activated ester form of the thioctic acid was synthesised as per Stokes *et al*.,[20] this could then be coupled to amine terminating DNA forming a thioctic acid modified strand of DNA (Scheme 3.1) for full details see Section **6.1.1.2**.

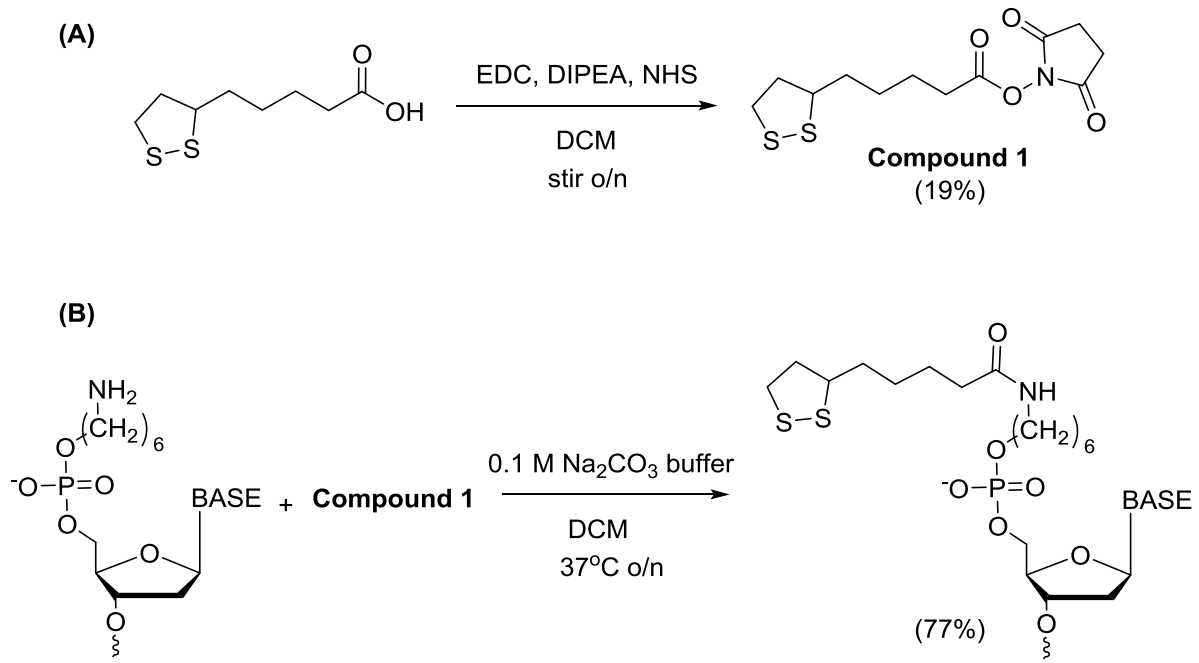

Scheme 3.1 Modifying DNA strand with thioctic acid analogue
*(A) Formation of the activated NHS ester of thioctic acid. (B) Activated NHS ester is coupled to amine modified DNA strand, yield estimated from semi-prep HPLC (**7.4**).*

3.3 Coupling NHS ester to DNA

The DNA was first modified with an amine group to which the activated ester could be coupled. A 5' amine C6 modification was added as the final base on the DNA synthesiser, giving an amine terminated probe strand. Initially, problems were encountered during the deprotection of the amine-modified DNA, with the total mass of the major product after purification being 53 Daltons higher than expected. This increase in molecular weight was ascribed to a side reaction occurring during the removal of the cyanoethyl protection from the phosphate backbone; acrylonitrile is produced once the cyanoethyl is removed (Scheme 3.2 **a**), which then reacts with the unprotected amine group (Scheme 3.1 **b**).

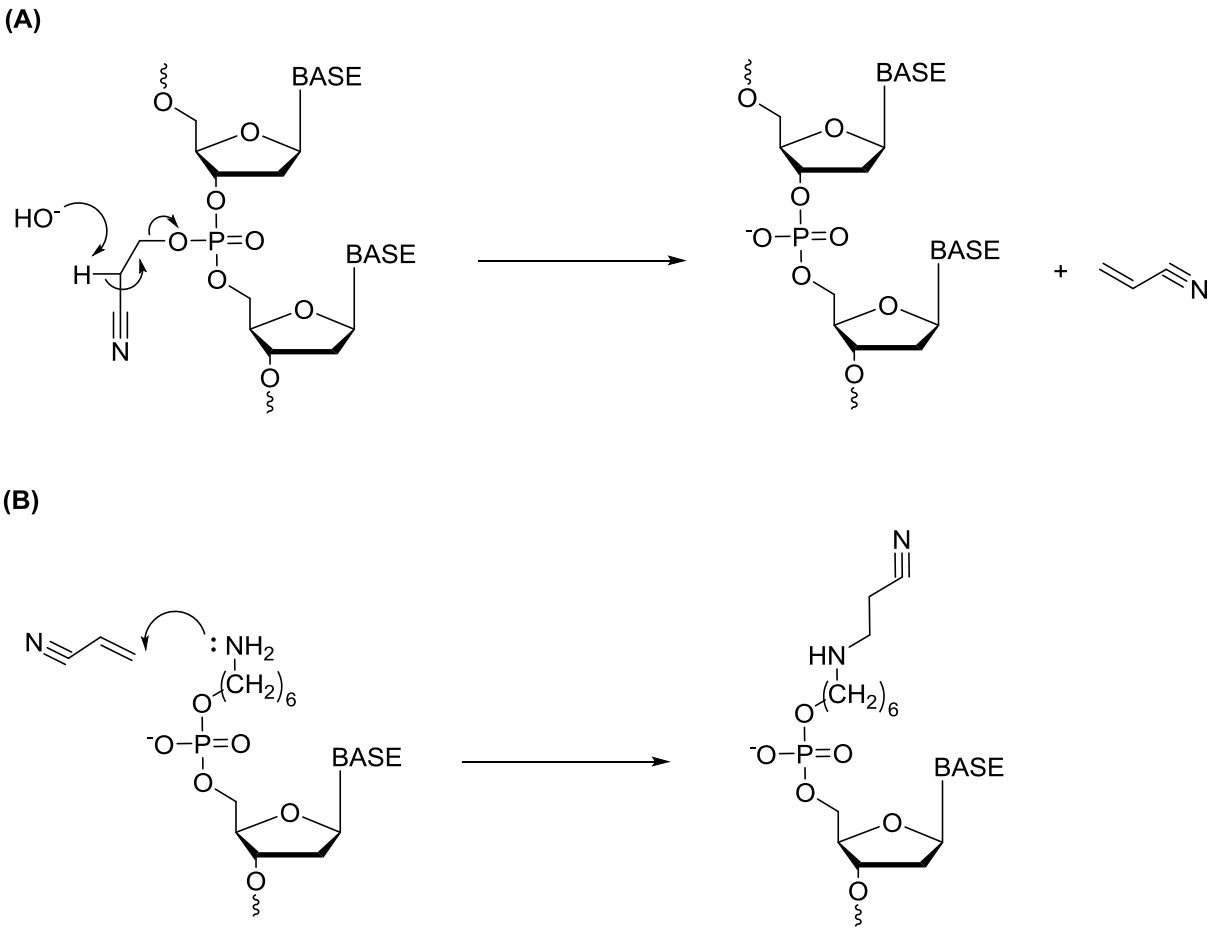

Scheme 3.2 Side reaction forming +53 adduct on amine modified DNA
(a) Formation of acrylonitrile. (b) Acrylonitrile reacting with deprotected 5' amine modification.

To prevent this side reaction, the resin was treated with 20% Diethylamine (DEA) in anhydrous acetonitrile followed by washing with acetonitrile prior to the amine deprotection step. The DEA removed the cyanoethyl group, allowing the reactive acrylonitrile to be washed away before deprotecting the amine. The activated ester was then coupled to the amine modified DNA in an overnight coupling reaction (Scheme 3.1). For full experimental details see Section **6.1.1**.

3.4 Anthracene probe synthesis

The phosphoramidite of the anthracene probe was synthesised following the route shown in Scheme 3.3 and as described previously,[21,22] (full experimental details see Section **6.1.4**) before being inserted into the DNA sequence via standard phosphoramidite chemistry.

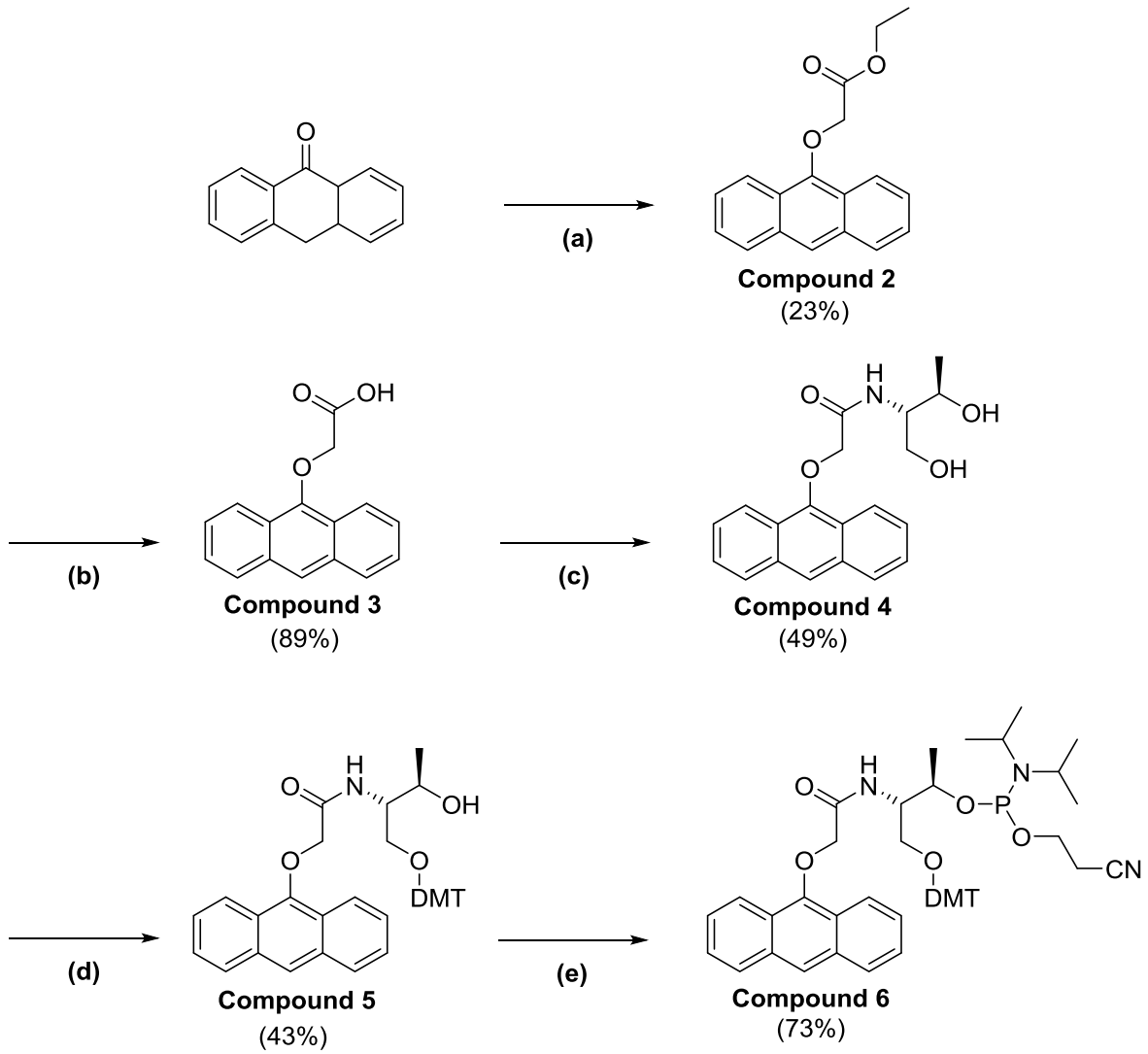

Scheme 3.3 Synthesis for 1L anthracene probe
Reagents and conditions: (a) Ethyl Bromoacetate, K_2CO_3, acetone, reflux o/n. (b) i) 10% NaOH (aq) soln- EtOH (1:1) , reflux, o/n, ii) HCl. (c) L-threoninol, HBTU, DIPEA, DMF, 40°C , 40 hours. (d) DMT-Cl, DMAP, pyridine, rt, o/n. (e) (i-Pr_2N)PClO(CH_2)$_2$CN, DIPEA, DCM, rt, 2 hr.

The anthracene probes synthesised for the first section of work were the 1L and 1D probes. The number 1 refers to the carbon linker length between the anthracene molecule and the threoninol unit. The L and D indicate the isomer of threoninol used in the synthesis.

3.5 Gold Nanoparticle Synthesis

The size of AuNP chosen for this work was 13 nm due to their water solubility, ease to functionalise their surface and also because they are relatively non-toxic to cells. Citrate stabilised particles were chosen as their synthesis is relatively simple and also it is easy to displace the citrate ions to functionalise the AuNP. Initially, citrate stabilised gold nanoparticles were synthesised as per Grabar *et al.*,[23] however it was later found that the particles made when using the new improved Turkevich method were more monodisperse.[24] Details of the Turkevich method for synthesising the particles can be found in Section **6.2**, the calculations for determining the particle concentration are outlined in Section **7.1.1**. The particles synthesised were sized at 12 nm (+/- 3 nm) using DLS (**6.2.1**). The absorption peak for the SPR was 520 nm (Figure 3.4).

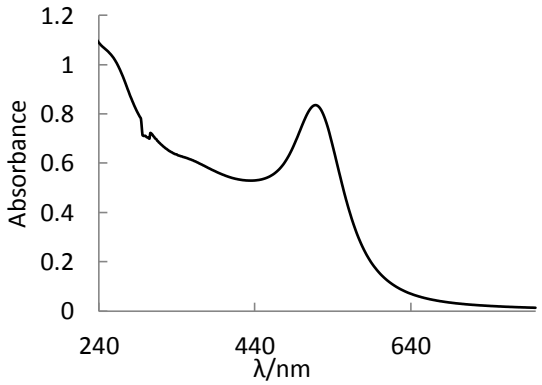

Figure 3.4 UV-vis absorbance spectra of AuNP
UV-vis absorption spectrum of AuNP in deionised H_2O (conc = 3 nM, size = 13 nm).

3.6 Attaching DNA to AuNP

The anthracene probe used for this work is a sequence already investigated by the Tucker group; this sequence is a randomly designed 15-mer which will not display any secondary structure. The strands of DNA synthesised are highlighted in Table 3.1. **P.UM** is probe sequence; **P.AF** is probe sequence with thioctic acid modification. The probe strands (**P.UM**, **P.AF**, **P.1L** and **P.1D**) are the strands that are bound to the gold nanoparticles and used to detect the target strands (**DNA-T.1**, **DNA-T.2**). Each strand was synthesised on an Applied Biosystems 9394 DNA/RNA Synthesizer within the group; for full experimental details of the DNA synthesis see Section **6.1.1**. They were purified by reverse phase HPLC and characterised by mass spectrometry.

Table 3.1 Probe and target strands of DNA synthesised
Oligonucleotide strands synthesised. W = thioctic acid modification. L = 1L anthracene probe. D = 1D anthracene probe.

Strand name	Strand sequence
P.UM	5' TGG ACT CTC TCA ATG 3'
P.AF	5' **W**-TGG ACT CTC TCA ATG 3'
P.1L	5' **W**-TGG ACT C**L**C TCA ATG 3'
P.1D	5' **W**-TGG ACT C**D**C TCA ATG 3'
DNA-T.1	5' CAT TGA GAG AGT CCA 3'
DNA-T.2	5' CAT TGA GAA AGT CCA 3'

The most common method for coating AuNP with DNA uses the salt aging technique developed by Chad Mirkin's group.[25,26] There are alternative coating methods such as the

low pH method used by Liu *et al.*.[27] The salt aging coating technique involves slowly increasing the salt concentration in a solution of AuNP and thiolated DNA; this takes place over many hours. The thiolated DNA will displace the citrate ions which stabilise the particles, whilst the salt allows the DNA to pack together more tightly on the AuNP surface. The salt cannot be added too quickly as the particles would aggregate. Based upon previous work within the Pikramenou group, the aim was to develop a new controlled method of binding DNA to AuNPs. Previous work in the group involved binding pH responsive peptides to AuNP,[28] to aid cell uptake. Davis *et al.* titrated in small amounts of protein whilst tracking the SPR band of the AuNP to monitor the particles coating, it is known that small changes in the environment of the particles' surface causes a shift in its SPR band. When no further change in the SPR is observed, it can be assumed that there is no further change to the properties of the surface and consequently the AuNP surface is saturated. This technique has since been used to coat AuNP with various molecules.[29,30] To coat the AuNP with the anthracene-DNA probe, small amounts of DNA were titrated into a solution of citrate stabilised AuNP, and the UV spectrum taken after each addition. This allows the binding of DNA to be tracked in real time, and a level of control to be exerted.

To track the shift in SPR, a MatLab algorithm was used which was written by Dr Sunil Claire; it involves fitting a Gaussian curve to the UV spectrum from which an accurate value for the SPR maximum can be calculated.[31] The position of the SPR maximum can then be plotted against the concentration of DNA added to allow an easy visualisation of its shift.

3.6.1 Comparing thioctic acid modified DNA vs non-thiolated DNA

As discussed earlier, modifying the DNA strands with sulphur groups was expected to give a level of control with regards to the orientation of the bound probe on the nanoparticle surface. However, given the propensity of unmodified DNA to also bind to gold nanoparticles through non-specific interactions,[11,12] the desired binding mode had to be verified. This was done by comparing the thioctic acid modified DNA (**P.AF**, **P.1L**, **P.1D**) with an identical strand without the thioctic acid modification (**P.UM**). A schematic representation of how the thioctic acid modified DNA binds to AuNP compared to non-modified DNA can be seen in Figure 3.5. The thioctic acid modified DNA binds through the sulphur groups, with the negatively charged DNA repelling strands nearby so that a relatively ordered surface should form with the DNA standing perpendicular to the surface. In contrast, for the non-modified DNA it is hard to envisage any organised structure forming on the particle surface, as bases can bind in a non-specific manner and the strand would be expected to wrap around the particle in a random manner.

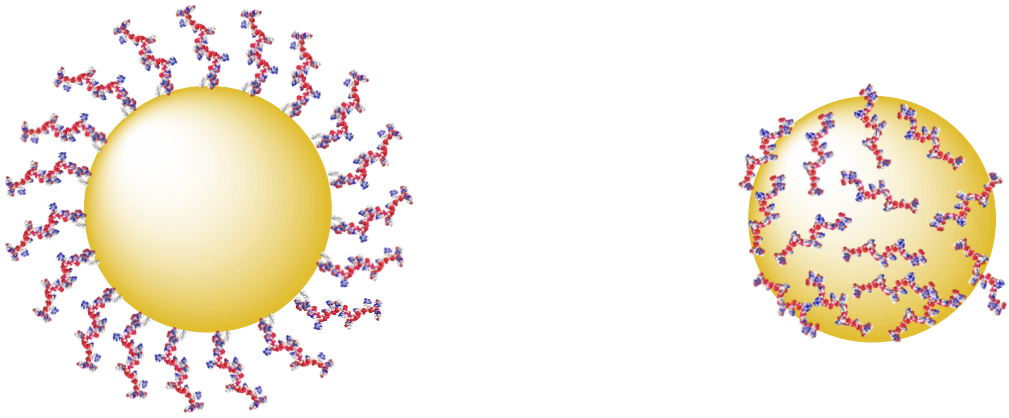

Figure 3.5 Envisaged binding of 13 nm gold nanoparticles coated in thioctic acid modified DNA (left) and non-thiolated DNA (right)

The optimum nanoparticle concentration for coating had to be established, so a range of concentrations were investigated: 3 nM, 6 nM and 9 nM. Higher concentrated particles did not appear to be as stable during coating and did not give as reproducible results when monitoring their SPR shift; therefore it was decided to continue the studies with nanoparticles at 3 nM concentration.

To test whether any differences in binding occurred when the two different probe strands (**P.UM** vs **P.1L**) were added to the particles alone, a UV experiment was set up to track the SPR shift of the particles every 60 minutes over 13 hours. An excess of DNA, 3 μM, was added to 3 nM AuNP in deionised water before commencing the UV experiment.

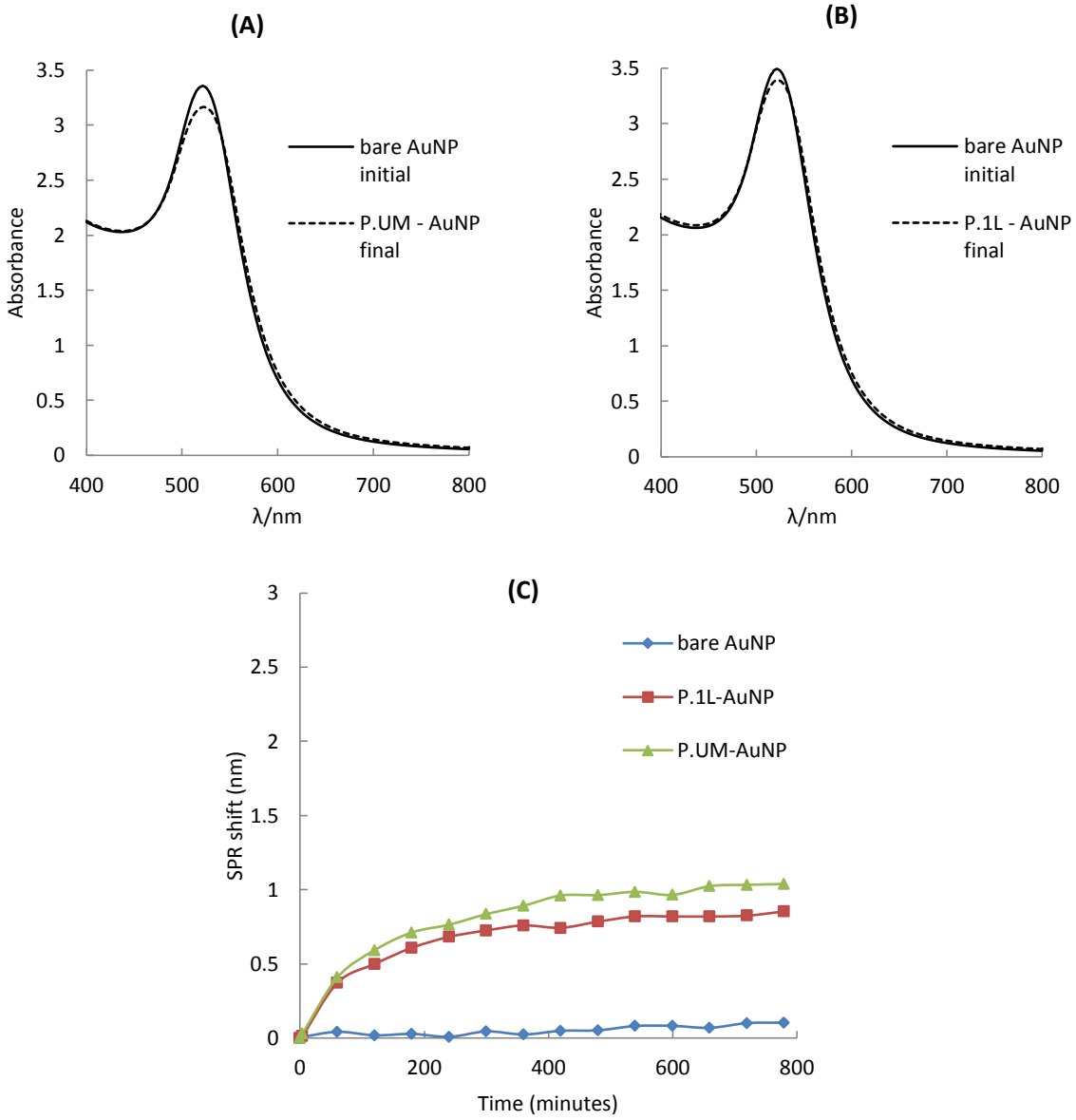

Figure 3.6 UV-vis absorption monitoring SPR band for non-thiolated and disulphide modified DNA binding to AuNP

(A) UV-vis absorption spectra of AuNP (3 nM, 13 nm) in H_2O (line), upon addition of 3 µM non-thiolated DNA (dash). (B) UV-vis absorption spectra of AuNP (3 nM, 13 nm) in H_2O (line), upon addition of 3 µM disulphide modified DNA (dash).(C) SPR band shift for A (green) and (red), control AuNP (3nM, 13nm) in H_2O with titrations of deionised water(blue).

Monitoring the SPR band shifts gives an insight into what is happening on the surface of the nanoparticles. With just the addition of deionised water, there is no variation in the SPR shift over the length of the experiment (**(C)** Figure 3.6). This is expected as there is no change to

the particles surface, it does however inform us that any change in SPR shift, must be due to what is added to the particle and not just as a result of experimental factors. When the DNA strands were added to the nanoparticles, there was a noticeable shift in the particle's SPR band of 1 nm (Figure 3.6). It is interesting to note that the shift appears to be very similar for both the DNA strands added, suggesting that the surface chemistry of the particles is altering in a similar fashion for both particles. This implies that both strands are interacting with the particles through similar surface chemistry and that either the thioctic acid group is not binding directly to the particles under these conditions, or that it is binding yet the strands are still wrapping around the particles in a similar fashion to the non-thiolated DNA strands.

Terne *et al.*[13] found that the presence of a buffer was crucial in coating gold surfaces with thiolated DNA molecules, as they found little difference in coating between non-thiolated and thiolated DNA without the presence of a buffer. It was proposed that intermolecular electrostatic repulsion between strands of DNA is minimised under the high ionic strength conditions, as the charged strands are better electrostatically shielded. This would then allow for a higher surface coverage for the thioctic acid modified DNA strands as they could now begin to extend away from the gold particles surface, the buffer providing counter ions to allow neighbouring DNA strands to pack more densely and allowing a higher surface coverage. Therefore, the effect of buffer on the binding process was then investigated, which involved repeating the same experiments in the presence of 10 mM phosphate buffer.

3.6.1.1 Testing the effects of buffer on DNA binding to AuNP

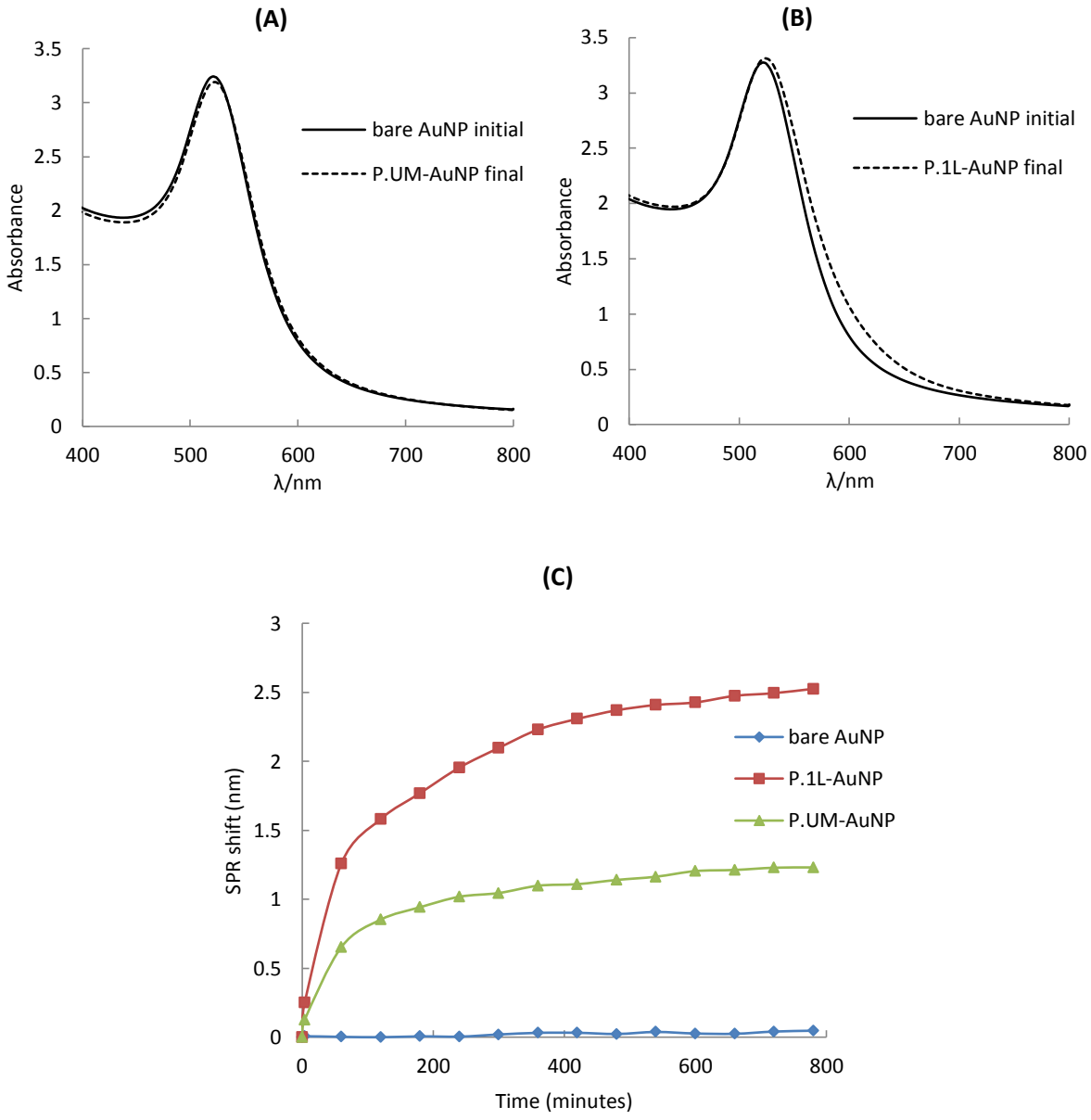

Figure 3.7 UV absorption of SPR band tracking non-thiolated and disulphide modified DNA binding to AuNP in the presence of *10 mM phosphate buffer*

(A) UV-vis absorption spectra of AuNP (3 nM, 13 nm) in H_2O and 10 mM phosphate buffer (line), upon addition of 3 µM non-thiolated DNA (dash). (B) UV-vis absorption spectra of AuNP (3 nM, 13 nm) in H_2O and 10 mM phosphate buffer (line), upon addition of 3 µM disulphide modified DNA (dash).(C) SPR band shift for A (green) and (red), control AuNP (3nM, 13nm) in H_2O and 10 mM phosphate buffer with titrations of deionised water(blue).

As expected, the buffer had no effect on the bare AuNP as the SPR band did not shift throughout the experiment (**(C)** Figure 3.7, and **(C)** Figure 3.6). Additionally, once again only a small SPR shift was observed (*ca.* 1 nm) for the non-thiolated DNA (**(A)** *and* **(C)** Figure 3.7), which was consistent with the non-thiolated DNA strands again adsorbing onto the nanoparticle surface. However, now a more pronounced SPR shift of 2.5 nm was observed for the thioctic acid modified DNA (**(B)** *and* **(C)** Figure 3.7). The difference in SPR shift indicates a different change to the surface environment of the AuNP in comparison to the non-thiolated DNA AuNP; this would indicate a difference in interaction and stabilisation of the final species as a result of the thioctic acid group.

3.6.1.2 Testing the effects of sonication on DNA binding to AuNP

It was suggested in the literature that short periods of sonication could increase the surface coverage of DNA on a nanoparticle surface. Hurst *et al.*[25] found that sonication during the binding process resulted in nearly double the amount of DNA binding to the AuNP than without it. As previously shown in Figure 3.7, when the thioctic acid modified DNA (3 µM) was left to bind to AuNP (3 nM) in a cuvette with only initial stirring, the process took nearly 8 hours. As it was possible to track the degree of DNA binding, it was thought that a short period of sonication may speed up the binding process. The DNA was added in small titrations (2.0 µL, 100 µM) to amplify the predicted effects of sonication, subjecting the AuNP/DNA solution to a short 20 seconds of sonication after each titration.

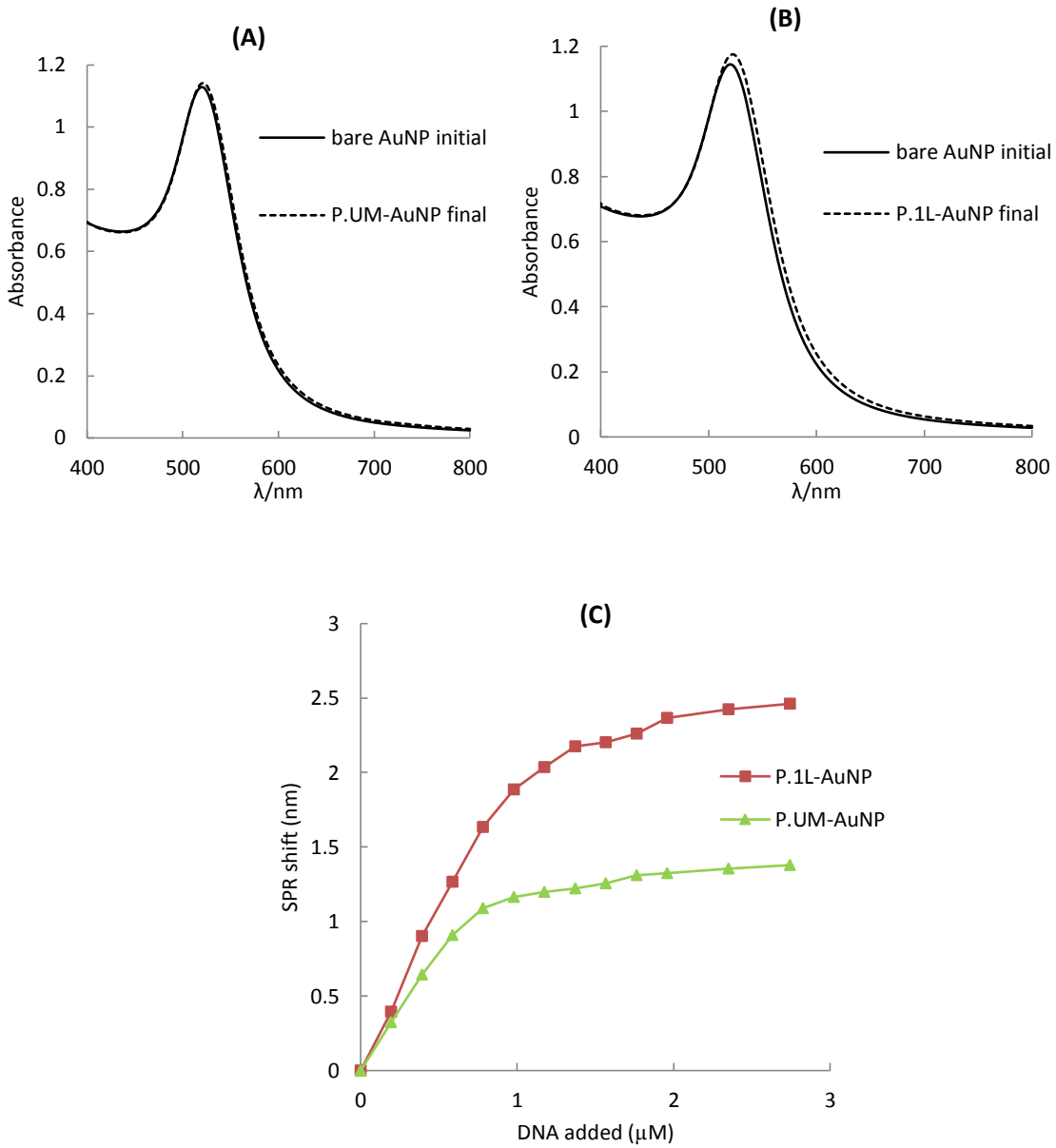

Figure 3.8 UV absorption of SPR band tracking non-thiolated and disulphide modified DNA binding to AuNP in the presence of *10 mM phosphate buffer* with 20 seconds sonication after each addition
(A) UV-vis absorption spectra of AuNP (3 nM, 13 nm) in H_2O and 10 mM phosphate buffer (line), upon titration of non-thiolated DNA with 20 seconds titration between each titration (dash). (B) UV-vis absorption spectra of AuNP (3 nM, 13 nm) in H_2O and 10 mM phosphate buffer (line), upon titration of disulphide modified DNA with 20 seconds sonication between each titration(dash).(C) SPR band shift for A (green) and (red).

The total time required for the SPR maximum to be reached was just 30 minutes, which included the time taken for all of the additions (additions done at 3 minute intervals). Comparing the total time taken to reach the SPR max for the sonicated binding (30 minutes)

to the non-sonicated binding (8 hours, Figure 3.7), it is clear that the sonication is having an effect on the rate that DNA is binding to the AuNP. The effect of sonication is to break off parts of the weakly adsorbed DNA, allowing for more space on the particle surface for disulphide groups on other DNA strands to bind. Binding through the disulphide bond is both entropically favourable (more degrees of movement when strand bound through a single group) and enthalpically favourable (strong Au-S bond), sonication appears to speed this process up.

The number of additions required to still coat the particles in a reduced amount of time was then investigated, as the speed at which the particles could be covered may also have been hindered by the large number of small additions used in the previous experiment (Figure 3.8). The amount of DNA coating the AuNP surface was established by titrating in known amounts of target until no further change in anthracene emission was observed (discussed in **3.8.1**). It was found there were about 360 strands of anthracene probe per AuNP, however to increase the rate of binding, an excess of DNA was added to help drive the equilibrium to completion. Therefore, fewer larger additions were tried, culminating in the final protocol of three equal additions of DNA to 3 nM AuNPs, with a final total DNA concentration of 2.97 µM. After each DNA addition, the AuNP-DNA solution was stirred for 2 minutes with a magnetic stirrer and then sonicated for 20 seconds. After the DNA had been added to the particles, the particles were passed through a Sephadex G-50 column to remove any excess unbound DNA (for full experimental see **6.2.4.1**). This is confirmed by assessing the UV spectra of DNA-AuNPs before and after they have been purified. A clear decrease in the DNA peak (260 nm) can be observed (Figure 3.9), normalising the graphs at

the SPR peak (523 nm) which is an indication of the AuNP concentration, shows the decrease in DNA concentration is greater than a dilution effect.

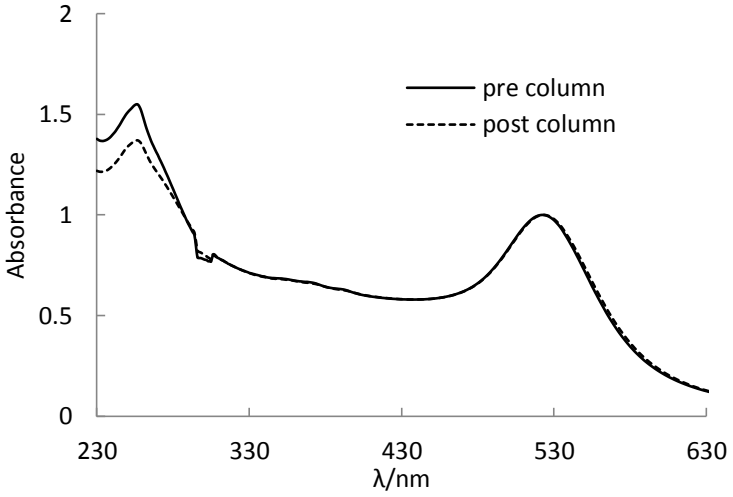

Figure 3.9 UV-vis absorption spectra of DNA coated AuNP before and after Sephadex G-50 column
*(line) UV-vis absorption of **P.1L-AuNP** before column (3 nM, 13 nm). (dash) UV-vis absorption spectrum of **P.1L-AuNP** once passed through Sephadex G-50 column using H_2O as eluent. Both graphs are normalised by their SPR peak to correct for dilution.*

An estimate of the DNA coverage can be found using the differences in the before and after values at 260 nm. Knowing the total amount of DNA added, the difference can be subtracted and the final concentration of DNA calculated; this gave values in the region of 4-600 strands of DNA per AuNPs, across a range of samples. However, it should be stressed that this remains an estimate as the absorption spectra of the particles does change once it is passed through the sephadex column, resulting in a decrease in the absorption at wavelengths lower than 220 nm which may affect the accuracy of these calculations.

3.6.2 Experiments to prove disulphide modification is binding to the AuNP

To provide further evidence that thioctic acid modified DNA was bound to the particles through its disulphide group, a series of studies were devised to compare the modified particles with those treated with non-thiolated DNA. It was immediately apparent in the purification process that the thioctic acid modified DNA AuNPs were more stable than their non-thiolated DNA counterparts through a G-50 Sephadex column; this traps any unbound DNA, whilst the large coated particles pass straight through the column. It was found that bare citrate coated nanoparticles could not pass through the Sephadex column, remaining stuck at the top, this was also observed for the particles which were coated in the non-thiolated DNA (Figure 3.10).

Figure 3.10 Sephadex size exclusion column showing the non-thiolated DNA coated particles are unable to pass though the column

In contrast, the thioctic acid modified AuNPs travelled through the column under the same conditions which provided good evidence that these DNA functionalised particles were more

stable, again indicating that the DNA was binding to the particles through the thioctic acid group.

3.6.2.1 Salt stability studies

Bare AuNPs are not stable in salty conditions, a fact observed by the need for slow increases in salt concentration in Mirkin's salt aging method.[15] In citrate coated particles an increase in salt concentration causes aggregation as the salt allows the AuNPs to approach each other very closely, upon which van der Waals force dominates, inducing aggregation.[32] However, when the particles are coated, they are much more stable to salty conditions. Therefore, to ensure that the new DNA coating method established was coating particles through the thioctic acid modification and creating stable particles, a simple experiment was set up which would test the particles' relative stabilities to increasing salt concentration. As previously described, the non-thiolated DNA coated AuNP could not be purified by passing through a Sephadex column (Figure 3.10). Therefore an alternative method for particle purification had to be used. The particles were centrifuged at 13000 rpm for 30 minutes and the supernatant removed, removing any excess unbound DNA, before re-dispersing them in de-ionised water. To ensure consistency, this method of purification was used for both the thioctic acid modified DNA and also the non-thiolated DNA coated particles during this experiment. Once purified, titrations of NaCl (2 µL, 5 M NaCl per titration) were added to the particles (1 mL, 2 nM) whilst monitoring their UV spectrum (Figure 3.11).

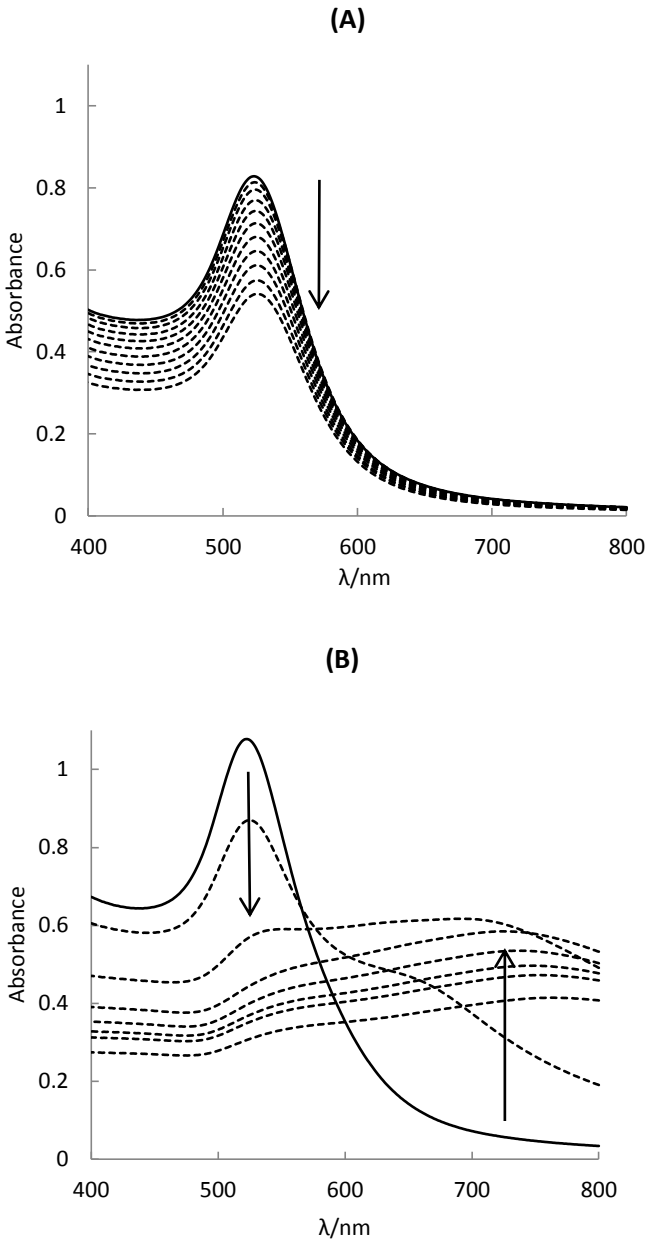

Figure 3.11 Comparing salt stability of DNA coated AuNP by UV-vis absorption
(A) UV-vis absorption spectrum of disulphide modified DNA coated 13 nm AuNP in H_2O (1mL, 2 nM)(line), upon subsequent titrations of NaCl (2 µL, 5 M)(dash). (B) UV-vis absorption spectrum of non-thiolated DNA coated AuNP in H_2O (1 mL, 2 nM)(line), upon subsequent titrations of NaCl (2 µL, 5 M)(dash). Progression of graphs indicated by arrows.

From their UV spectra (Figure 3.11) it is clear that the thioctic acid modified DNA coated particles are much more stable to the presence of salt than the non-thiolated DNA coated

particles. The UV spectrum of the latter shows a large growth of an absorption band at 720 nm, which is an indication of plasmon coupling between agglomerating nanoparticles. [33] There is also a rapid loss of the 520 nm SPR band, indicating a loss in small 13 nm particles. These observations become apparent at a salt concentration of just 0.01 M. Visible observation of the particles show the non-thiolated particle solution becoming clear and small black aggregates forming with increasing salt concentration.

The thioctic acid DNA coated AuNP remained stable to salt up to the final concentration of 0.1 M NaCl, this is biologically relevant as the NaCl concentration within a cell is no higher than 0.015 M[34] therefore proving these particles will remain stable in cells. There was no evidence of any 720 nm band growth and only a slight decrease in the 520 nm band. This decrease in the 520 nm band was shown to be only a dilution factor.

It can be hypothesised that the non-thiolated DNA is displaced from the surface of the nanoparticles upon the addition of salt, allowing the particles to approach each other and aggregate. In contrast, the thioctic acid modified DNA is more strongly bound to the AuNP surface, therefore the negatively charged DNA molecules will not allow the particles to approach each other and aggregate, even in the presence of salt. This experiment proved that this new rapid method for coating AuNP in DNA produced particles which are stable to very high salt concentrations.

3.7 Characterising particles

3.7.1 Dynamic Light Scattering

Dynamic Light Scattering (DLS) was used to determine the size of the AuNP particles with and without coating, and also to measure the zeta potential of the particles.

Particles suspended in liquid are in Brownian motion due to random collisions with solvent molecules. This motion causes the particles to diffuse through the medium; the diffusion coefficient (D) is inversely proportional to the particle size according to the Stokes-Einstein equation:

$$D = \frac{k_B T}{3\pi\eta_0 \mathrm{d}}$$

Equation 3.1 Stokes-Einstein Equation
D = diffusion coefficient, k_B = Boltzmann's constant, absolute temperature, η_0 = viscosity, d= hydrodynamic diameter

From this equation (Equation 3.1), it is clear that larger molecules will have a smaller diffusion coefficient and move more slowly than smaller particles; therefore the size of a particle can be deduced from the speed that the particles diffuse in a given media. Dynamic Light Scattering (DLS) measures the scattering of laser light; this random scattering is caused by the particles and its intensity at any one point depends upon the relative positions of the particles. As the particles are in motion, their relative position changes and therefore the scattering intensity changes. The speed of these scattering fluctuations can then be used to define the speed at which the particles are moving, and therefore the size of the particles.

The particles sized were: bare citrate coated AuNP, non-thiolated DNA-AuNP and thioctic acid modified DNA-AuNP. Throughout this chapter, different types of the anthracene probe are bound to AuNP, so for completeness, the sizing of them all is displayed in Table 3.2.

Table 3.2 DLS sizing and zeta potential of particles coated with DNA
Sized using a Malvern Zeta sizer nano ZEN5600, particles at 2 nM in deionised water.

	Bare AuNP	**P.UM-AuNP**	**P.AF-AuNP**	**P.1L-AuNP**	**P.1D-AuNP**
Number distribution (nm)	12 (± 3)	13 (± 4)	14 (± 4)	14 (± 4)	14 (± 4)
Intensity distribution (nm)	21 (± 6) (100%)	48 (± 34) (96%)	48 (± 32) (96%)	34 (± 17) (96%)	30 (± 11) *96%*
Zeta potential	-35 mV (100%) (± 10 mV)	-32 mV (57%) (± 10 mV) 7 mV (42%) (± 8 mV)	-37 mV (97%) (± 12 mV)	-23 mV (99%) (± 8 mV)	-26 mV (96%) (± 7 mV)

The sizing of the particles shows that there is not much change in the size of the particles once coated with DNA; all the measured sizes are within error of each other. An increase in size would be expected due to the addition of an estimated 3 nm long strand surrounding the particles, for the full extension of the DNA, additional salt or buffer may be required. It has been shown in the literature that the increase in size expected does not necessarily correlate with the size observed when measured by DLS, for example a 19 base pair DNA strand bound to a 13 nm AuNP increased in size by only 3 nm.[35,11] Other papers have reported much larger increases in particle size upon the addition of DNA strands, however these were measured in phosphate buffered saline (PBS) solution.[8]

The zeta potentials also give an interesting insight into the coating of the particles. Zeta potential is a measure of the magnitude of charge repulsion/attraction between particles, and is therefore a very useful tool in determining the stability of particles. The greater the zeta potential of a colloidal solution the more repulsion between the particles there is and therefore the particles are less likely to aggregate. Once coated in the DNA the particles remain relatively stable, with a high zeta potential, except for the **P.UM-AuNP**. The particles coated in the non thiolated DNA have a large proportion (42%) with a small zeta potential, indicating that many of these particles are not stable. This again reiterates the requirement of the disulphide modification to form stable particles.

3.7.2 Transmission electron microscopy

Transmission electron microscopy (TEM) images confirmed the mono dispersity of the DNA coated AuNPs, whilst the sizing corresponds with the DLS measurements (Figure 3.12).

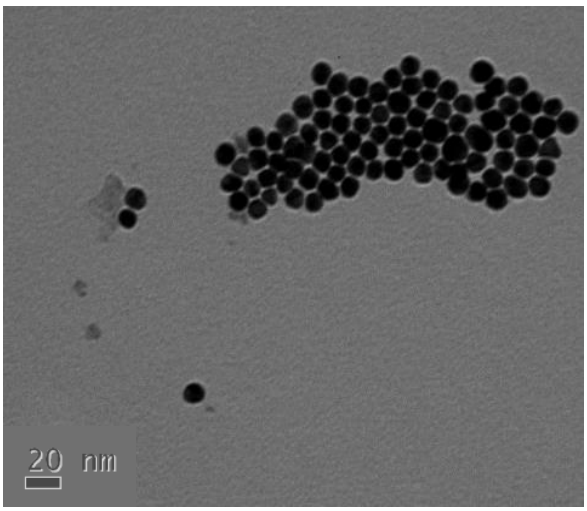

Figure 3.12 TEM image of P.1L-AuNP
Imaged using a JEOL 1200 TEM.

3.7.3 ICP-MS data

In Section **3.8.1**, the SNP sensing probe is used to estimate the number of DNA strands bound to each AuNP. Initially however, ICP-MS was used to quantify the number of DNA strands that were bound to the AuNP. Dr Lijiang Song at the University of Warwick is acknowledged for running the samples. From ICP-MS the gold: phosphorus ratio was obtained, from this the number of DNA strands bound to each AuNP could be calculated (Table 3.3), for calculations see Section **7.1.2**.

Table 3.3 ICP-MS data giving approximate number of DNA strands per AuNP
Values given assume particles are 13 nm in size, containing 100082 gold atoms. 3 mL of 1 nM AuNP dissolved in 5% aqua regia.

	P.AF-AuNP	P.1L-AuNP
Strands of DNA per particle	1042	1570

The values obtained were much larger than expected, literature values vary from 150 strands per particle[26] to the maximum level of particle coating reported as 250 strands per AuNP.[15] The maximum coating was observed for 15-mer oligonucleotides, the same length used in these studies; however the oligonucleotides were modified with a thiol terminating PEG spacer group. Whilst ICP-MS will give a large error as it is a coating average, with a large variation in coating as well as particle size, the much larger than expected value would indicate that there is an issue using this method. There is the potential for false positives when detecting phosphorus caused by $[^{15}N\ ^{16}O]^+$ and $[^{14}N\ ^{16}O\ ^{1}H]^+$ at m/z 31, which may contribute to this high value.[36] The coating process was done in the presence of phosphate buffer and whilst the particles were columned in deionised water to remove larger molecules such as DNA, some phosphate buffer will inevitably be carried through. The presence of the phosphate buffer will lead to false positive counts for phosphorus, giving a

much greater phosphorus ratio being counted. To overcome this problem, attempts to coat the particles in the presence of an alternative buffer, Tris (2-Amino-2-hydroxymethyl-propane-1,3-diol), were made. However they proved unsuccessful as the particles aggregated upon addition of the buffer. Therefore, it was established that ICP-MS is not the best method for calculating the DNA coverage of AuNPs.

3.7.4 Duplex formation: Variable Temperature UV spectroscopy

Once the particles were coated in single stranded DNA, it was crucial to this work that the strands were still available for hybridisation with a target strand. Mirkin *et al.* showed that they were able to monitor duplex formation on particles through variable temperature UV spectroscopy, monitoring the 260 nm band.[37] The absorption at 260 nm is caused by the DNA bases and is at its maximum when strands are un-hybridised. Upon duplex formation the absorption of the bases decreases due to the stacking of the DNA once it forms the helical structure.[38] The melting temperature given as the T_m value is the temperature at which 50% of the duplex is dissociated and gives an indication of a duplex's stability.[39]

Table 3.4 Duplex melting temperatures comparing free DNA with DNA bound to AuNP
Experiments run at 1μM of DNA samples in 10 mM Phosphate Buffer, 100 mM NaCl. ***DNA-T.1*** *is the fully matching target, whilst* ***DNA-T.2*** *contains a single base mis-match.* T_m *values are given in °C.*

Probe	**DNA-T.1**	**DNA-T.2**
P.AF	54	40
P.1L	47	40
P.1D	45	34
P.AF-AuNP	53	39
P.1L-AuNP	49	38
P.1D-AuNP	46	37

When a random target is added to the DNA-AuNP, no T_m value is observed indicating that the observed values are a consequence of duplex formation only. The T_m values of the AuNP bound DNA are similar to the values obtained from the duplexes alone. The similarity in T_m values between AuNP bound DNA and free DNA is also seen in the literature for DNA coated AuNP when the DNA is bound via a thiol modification.[40]

3.7.5 Duplex formation: CD spectroscopy

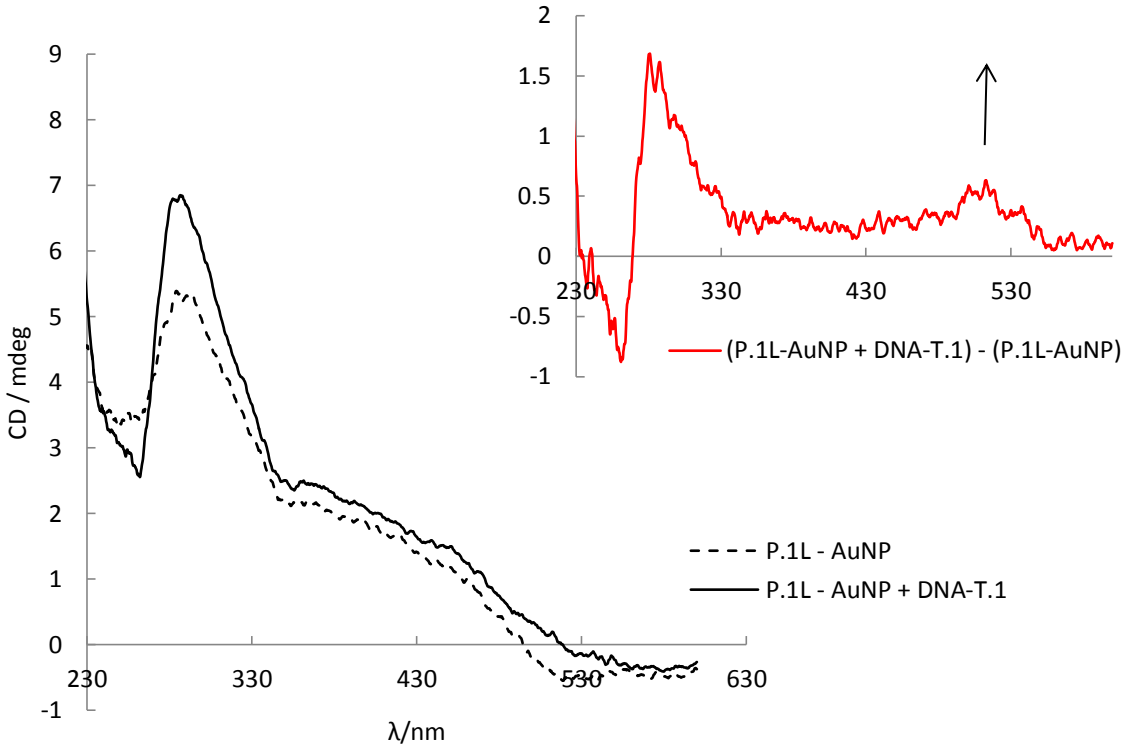

Figure 3.13 CD spectrum indicating duplex formation for DNA-AuNP
*(main) CD spectrum of **P.1L-AuNP** (dashed black) and after addition of complementary target (solid black). (inset) Difference between the two spectra (red). **P.1L-AuNP** at 2 nM in 10 mM Phosphate Buffer, 100 mM NaCl, room temperature.*

CD studies were performed for DNA coated AuNPs with the intention of observing an induced dipole where the AuNPs absorb as an indication that the DNA had bound to the particles. According to the literature, an induced dipole would only be observed if the DNA was covalently bound to the particles.[41] The CD spectrum (Main, Figure 3.13) of purified DNA

coated AuNP was ran; with a single stranded probe, there is an observable B-DNA structure (peaks 265 and 285 nm). This would indicate that once bound to the particles, the DNA adopts a fairly helical structure. However, once the complementary target strand is added, an increase in intensity of the bands at 285 and 265 nm is observed, indicating a tighter packed B-DNA structure, as expected. Subtracting the final spectra from the initial spectra shows the differences in the spectra (Figure 3.13, inset); the increase in these B-DNA bands can be clearly seen. A broad band can also be observed at 520 nm; correlating with the SPR band of the AuNPs and would suggest that the particles have some induced chirality, which indicates that the particles are indeed coated and interacting with the target DNA. The increases in these bands do not occur upon addition of a non-complementary target. The exact reason why this induced CD peak appears at the AuNP SPR band, and in this case why it is only apparent for duplex DNA, is unclear. Some reports suggest it is caused by the chiral adsorbate (i.e. chiral DNA molecules attached to the metal surface) influencing the electronic states of the metal nanoparticle.[42] Theoretical models predict that the mechanism may be due to optical absorption of the nanocrystal-molecule complex due to the chiral currents inside the metal nanocrystal induced by the dipole of the chiral molecule.[41] The observation of the band does however confirm there is an interaction between the AuNP and DNA, which is more pronounced in duplex DNA.

3.7.6 Anthracene excitation and emission

It is known that the emission of an organic fluorophore when placed near a metallic nanoparticle is greatly reduced, up to 99.8%.[43] This quenching is caused by two factors; the first is that AuNPs increase the non-radiative rate of decay of the molecules due to energy transfer. The second factor, is the radiative rate of the molecules is decreased, this is due to the molecular dipole of the dye and the dipole induced on the AuNP radiating out of phase if the molecules are oriented tangiently to the AuNPs surface.[44,43] Once the particles had been coated in the anthracene probe, an excitation and emission spectrum was taken (Figure 3.14). The spectra observed confirmed the presence of the anthracene probe on the particles once they had been purified. To measure the level of quenching caused by the nanoparticles, the emission of the unbound probe was collected for a comparison. Problems in calculating the exact number of probe molecules in a solution of DNA-AuNP caused by a lack of knowing the exact concentration of nanoparticles once synthesised means this comparison contains errors; efforts to minimise this concentration problem are explained in Section **7.1.3**. However it does indicate that there is a large amount of quenching of the anthracene probe once bound to the AuNP (Figure 3.14).

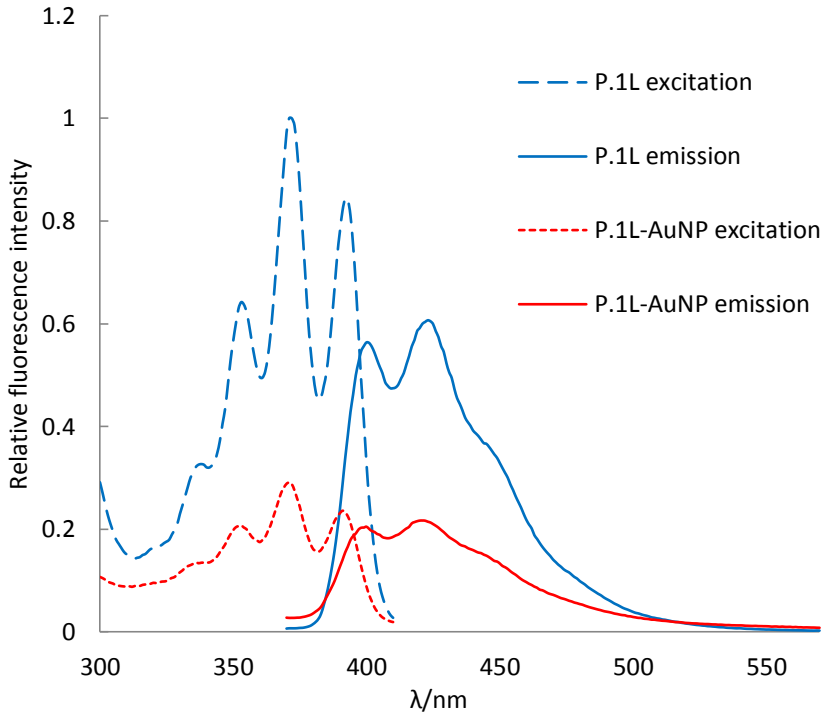

Figure 3.14 Excitation and emission scans of 1L probe when free and bound to AuNP
*Excitation scan of free **P.1L** at 1 µM (dashed red) and when bound to AuNP, **P.1L-AuNP** (dashed blue) Emission scan of free **P.1L** at 1 µM (solid red) and when bound to AuNP, **P.1L-AuNP** (solid blue), (pH = 7.0, 10 mM phosphate buffer, 100 mM NaCl, 293 K, λ_{ex} = 350 nm, λ_{em} = 426 nm.).*

3.8 SNP sensing on particles

Once it had been shown that the SNP sensing probe was available for hybridisation and its emission could be observed once it was bound to AuNPs, the project moved on to testing the SNP sensing ability of the AuNP bound probe.

3.8.1 Base adjacent sensing

For the base adjacent SNP sensing system, the SNP target site is adjacent to and on the 3' side of the base that is opposite the anthracene tag (Figure 3.2). The particles were coated with the **P.1L** probe as described in Section **3.6.1.2,** purified by passing through a sephadex column. The coated particles solution was made up with 10 mM phosphate buffer (pH 7) and

100 mM NaCl as standard duplex forming conditions. To test whether the SNP sensing would work, initially a large excess (20 µL, 175 µM) of DNA target (**DNA-T.1**, **DNA-T.2**) was added to ensure that all of the probe would be bound.

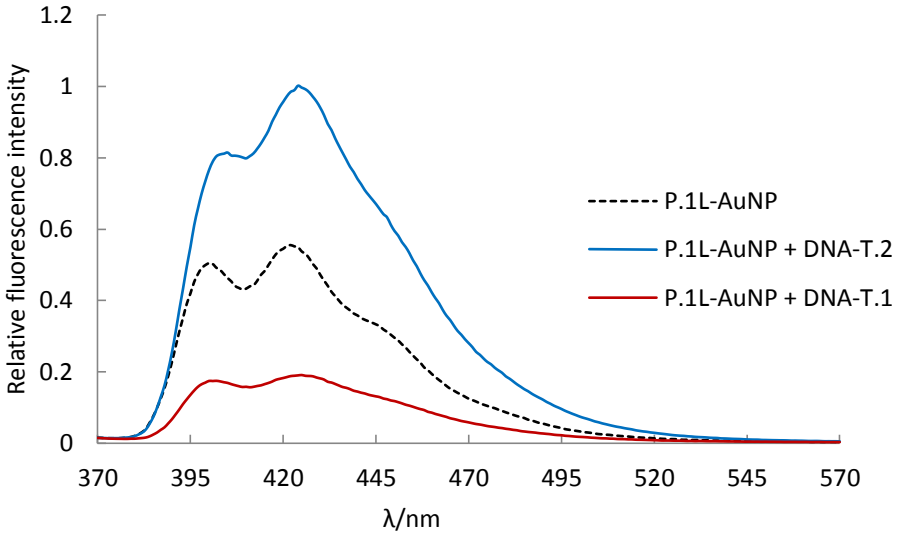

Figure 3.15 Emission for P.1L-AuNP upon target addition
*Anthracene emission for **P.1L-AuNP** 1 mL, 3 nM (dashed black), after addition of excess complementary target **DNA-T.1** (red) and after addition of excess single base mis-match target **DNA-T.2** (blue) both 20 µL, 175 µM, (pH = 7.0, 10 mM phosphate buffer, 100 mM NaCl, 293 K, λ_{ex} = 350 nm, λ_{em} = 370-570 nm).*

Gratifyingly when AuNP-bound, the probe was still able to differentiate between the two SNP targets, as clearly shown in Figure 3.15. Furthermore, the percentage changes in emission of the anthracene probe upon binding two different targets (Table 3.5) were similar to those obtained when not bound to AuNP. This is interesting as it indicates that the degree to which the anthracene signal is quenched by the AuNP is similar, regardless of whether the anthracene moiety is duplex intercalated (upon addition of target) or not (no target added). Duplex DNA is more rigid in its structure compared to single stranded DNA, so it was thought that the quenching may be more pronounced for the single stranded DNA when compared to the duplex form, as the tag may be able to approach nearer to the AuNP surface as a

single strand due to its increased flexibility. This consistent quenching has two explanations; the first is that the anthracene tag is so close to the AuNP surface that any difference in proximity is negligible. Another explanation is that the probe is so tightly packed onto the AuNP that it is in a fairly rigid duplex-like structure when it is single stranded. This would agree with the small changes in CD signal for the single stranded AuNP when compared to duplex coated AuNP (Section **3.7.5**).

As the binding stoichiometry of the target strands to the probe strands is 1:1 then this SNP sensing system can be used to determine the amount of DNA coating the AuNP. Titrating in known amounts of target to a sample of probe coated AuNPs allows an estimate of the surface coverage to be obtained. It remains an estimate as the concentration of the AuNP is difficult to monitor. Whilst the initial concentration of AuNP synthesised can be identified by sizing the particles and knowing the amount of gold used whilst making them (Section **7.1.1**), the AuNP concentration can only be estimated from then on, using the intensity of the SPR band. However, Mie theory indicates there is a scattering contribution to the absorption spectra which does not involve electron transfer, therefore the Beer-Lambert law cannot be used to determine the AuNP concentration. Nevertheless, the intensity of the SPR band can be used to monitor the dilution of the particles from their initial known concentration (Section **7.1.3**). For a 2.5 nM solution of **P.1L-AuNP**, plateauing of the anthracene signal was seen after 900 nM (final concentration) of target strand was added. After each addition of target, the solution was left for 10 minutes before the measurement being taken to ensure duplex formation. This plateau point suggested that the total amount of DNA bound to each AuNP was 360 strands of probe; this is greater than the level of particle coverage seen in the literature (~150 strands per particle), however it is consistently seen with all probes bound

to the AuNP (Figure 3.18) and also agrees with the estimates from the UV-vis subtraction in Figure 3.9.

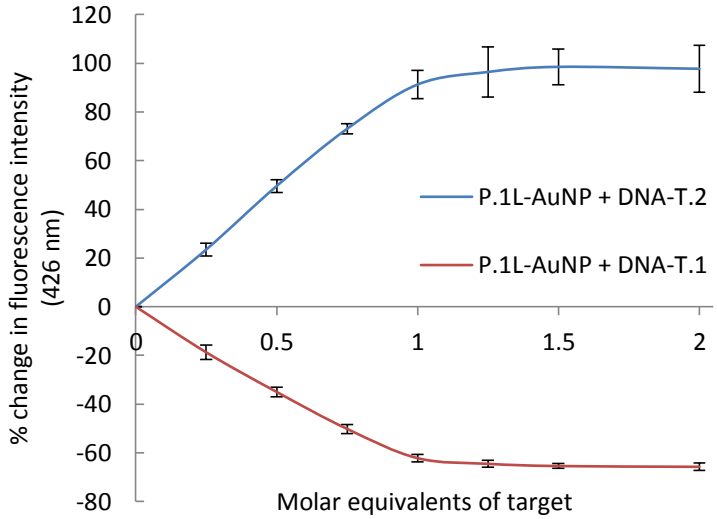

Figure 3.16 Monitoring percentage change in anthracene upon target titrations
*Percentage change of anthracene emission intensity at 426 nm calculated relative to initial emission level of **P.1L-AuNP**. Change in anthracene upon addition of fully matching target (red) and single base mis-match target (blue). Each point represents an addition of target, error bars indicate the standard deviation of three repeats using three different **P.1L-AuNP** syntheses (AuNP at 2 nM, pH = 7.0, 10 mM phosphate buffer, 100 mM NaCl, 293 K, λ_{ex} = 350 nm, λ_{em} = 370-570 nm).*

The small standard deviation seen in Figure 3.16 for three separate repeats of probe coated nanoparticles suggests that using the intensity of the SPR band is an accurate way of monitoring the nanoparticle concentration. The envisaged tightly packed surface of the nanoparticle does not appear to affect the binding of the target DNA. The linearity of the titration graph would suggest that there are no steric effects preventing the probe and target binding when the particle is covered in mostly duplex DNA. Importantly, upon the addition of a random DNA target sequence, no change in anthracene emission is observed.

It is known that the **P.1L** probe binds less strongly to the target **DNA-T.2** than **DNA-T.1** from their respective T_m values (**DNA-T.2** = 38°C **DNA-T.1** = 49°C). Consequently, these fluorimetry experiments were all done at 20°C, which ensured that all strands are fully hybridised.

However, the weaker binding for the DNA-T.2 system may explain the increased error seen in the curve for the **P.1L-AuNP** - **DNA-T.2** binding profile.

Varying the SNP sensing probe to the **P.1D** variant, in which the stereochemistry of the threoninol unit to the anthracene tag is switched from l to d, again gives results which are comparable to the free probe in solution, with the anthracene emission decreasing for both variations of the SNP targets. The initial emission of the anthracene probe is higher for the **P.1D-AuNP** when compared to the **P.1L-AuNP**, this was again expected as the 1D anthracene probe has a higher quantum yield than the 1L probe.[22] As for the 1L system, it can be seen that there is larger error for the **DNA-T.2** target compared to the **DNA-T.1** target, and again this is probably due to the lower T_m of the **P.1D** - **DNA-T.2** duplex.

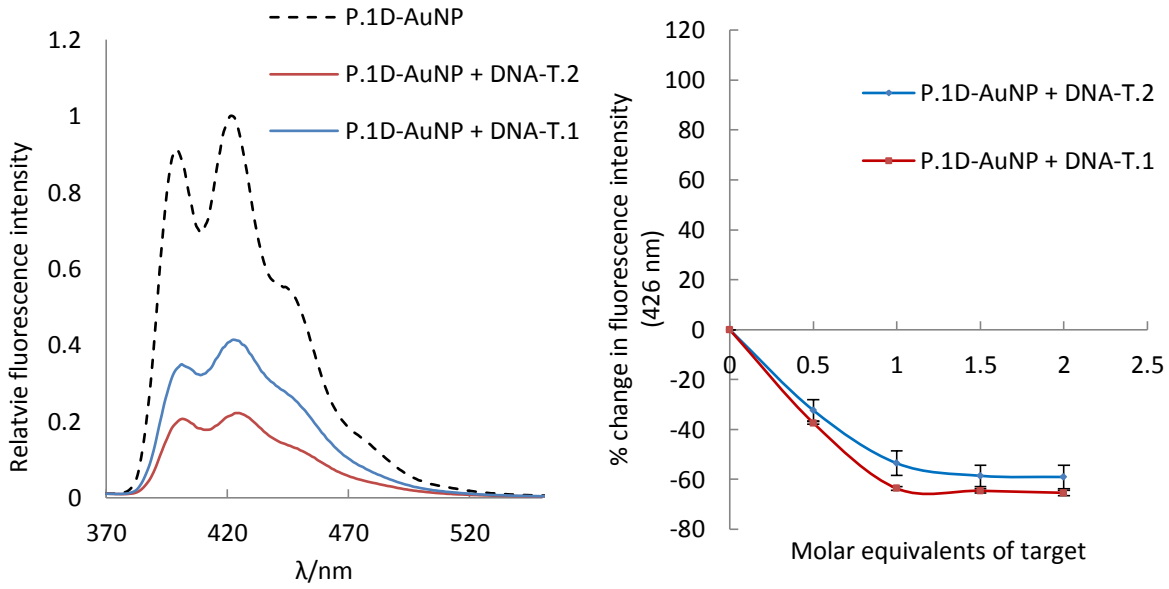

Figure 3.17 1D-AuNP emission response to target addition
*(Left) Anthracene emission for **P.1D-AuNP** (dashed black), after addition of complementary target **DNA-T.1** (red) and after addition of single base mis-match target **DNA-T.2** (blue).(Right) Percentage change in anthracene emission at 426 nm calculated relative to initial emission level of **P.1D-AuNP**. Each point represents an addition of target, error bars indicate the standard deviation of three repeats using three different preps of P.1D-AuNP. (AuNP at 2 nM, pH = 7.0, 10 mM phosphate buffer, 100 mM NaCl, 293 K, λ_{ex} = 350 nm, λ_{em} = 370-570 nm).*

Table 3.5 Percentage change in anthracene emission once probe strand is fully hybridised to different DNA target strands

*Percentage change in anthracene emission upon the addition of fully matching target (**DNA.T-1**), single base mismatch (**DNA.T-2**) and random target. λ_{ex} = 350 nm, λ_{em} = 426 nm. AuNP at 2 nM, 10 mM pH 7.0 phosphate buffer, 100 mM NaCl, 293 K.*

PARTICLE	DNA-T.1	DNA-T.2	RANDOM
P.1L-AUNP	- 66%	+ 98%	- 3%
P.1D-AUNP	- 65%	- 59%	- 4%
P.1L	-77%	+89%	- 2%
P.1D	-72%	-61%	- 3%

3.8.2 Varying distance of anthracene probe from AuNP surface

As a potential imaging probe in biological media, the emission from the anthracene tag needs to be as high as possible to overcome background fluorescence. As previously described, anthracene is not an ideal fluorophore for imaging *in vivo* due to its excitation and emission wavelengths being similar to natural compounds found in the cell, e.g. tryptophan. As discussed earlier in Section **3.7.6**, gold nanoparticles are known to quench the emission of fluorophores bound near to the surface. As there is a distance-dependent relationship for the quenching mechanism, varying the distance between the anthracene probe and the AuNP surface was considered to be an effective way to minimise the quenching and ultimately lead to a more emissive and more sensitive imaging probe. Increasing the number of bases between the thioctic acid modification and the sequence of interest allowed the distance between the tag and the surface to be controlled in a precise manner. The probes

subsequently synthesised are shown in Table 3.6 with the number of additional bases 0, 5 and 10 for **P.1L**, **m.P.1L** and **l.P.1L** respectively.

Table 3.6 Probe strands used to investigate how distance from the particle surface affects the anthracene probe emission
X = 1L anthracene probe, W = thioctic acid modification.

Strand name	Strand sequence
P.1L	5' **W**-TGG ACT C**X**C TCA ATG 3'
m.P.1L	5' **W**-AAAAA TGG ACT C**X**C TCA ATG 3'
l.P.1L	5' **W**-AAAAAAAAAA TGG ACT C**X**C TCA ATG 3'

The number of bases was not increased too greatly due to concerns about how this may alter the loading onto the AuNP. It has been widely reported that varying the spacer group has a large effect on the loading of DNA onto nanoparticles.[25,45,46]

Table 3.7 Duplex melting temperatures of varied length anthracene probe free DNA and varied length probe DNA bound to AuNP
Experiments run at 1µM of DNA, 2 nM AuNP. Samples in 10 mM Phosphate Buffer, 100 mM NaCl. ***DNA-T.1*** *is the fully matching target,* ***DNA-T.2*** *contains a single base mis-match.* T_m *values are given in °C.*

Target	P.1L	m.P.1L	l.P.1L	P.1L-AuNP	l.P.1L-AuNP
DNA.T-1	47	45.5	46.5	49	47
DNA.T-2	40	38.5	37.5	38	37.5

The T_m values for **m.P.1L** and **l.P.1L** showed a slight decrease in stability of the duplexes for the longer strands (Table 3.7). To begin with, the variation in the anthracene emission and SNP sensing of the probes alone (not bound to AuNP) was tested (Figure 3.18) by tracking

the change in anthracene emission upon addition of aliquots of each target strand (**DNA-T.1** and **DNA-T.2**).

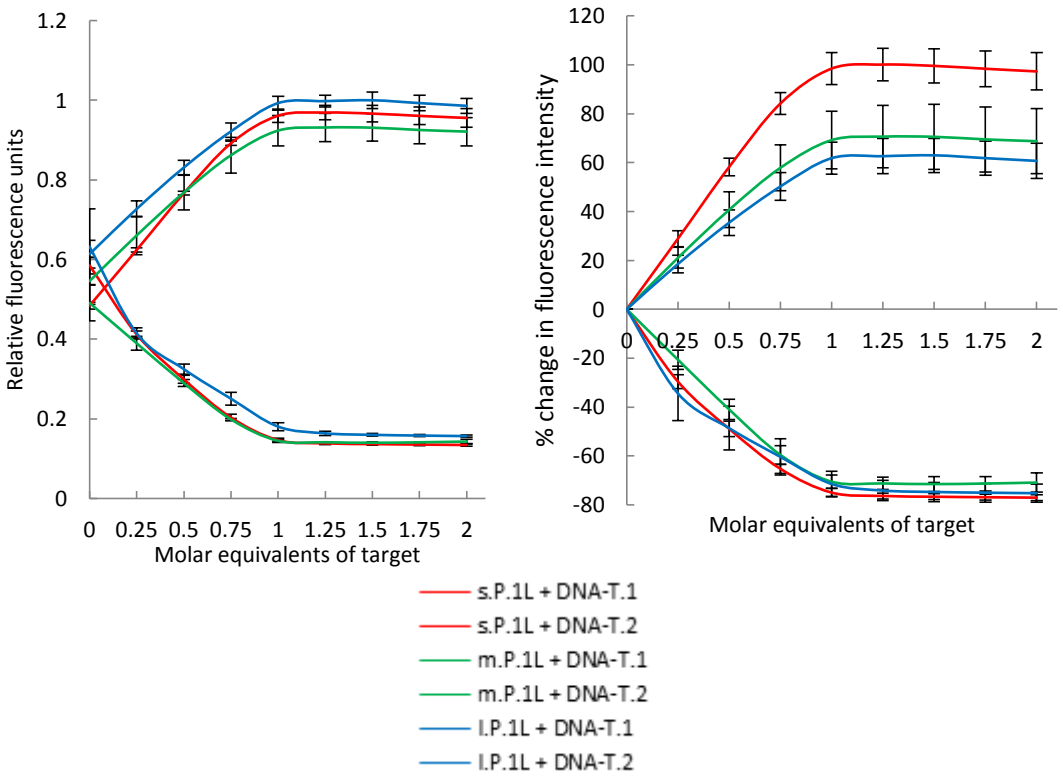

Figure 3.18 Varied length anthracene probe emission response
Variation in anthracene emission of probe alone after addition of target DNA. Red = P.1L, Green = m.P.1L, Blue = l.P.1L. Error bars are standard error of the mean of 3 repeats. λ_{ex} = 350 nm, λ_{em} = 426 nm. AuNP at 2 nM, 10 mM pH 7.0 phosphate buffer, 100 mM NaCl, 293 K.

All probes were able to detect the different SNP targets, with the single mismatch target resulting in an increase in anthracene emission, and the fully matching target resulting in a decrease in anthracene emission. The percentage anthracene emission increase appears to be greater for the shorter **P.1L**, this is not unexpected when we consider the higher T_m value that the **P.1L** has over the **m.P.1L** and **l.P.1L**. The higher T_m indicates a tighter duplex forming; therefore the intercalated anthracene tag may have increased shielding from the

surrounding quenching molecules, resulting in a greater increase in emission for the anthracene.

Once the strands were fully characterised, they were bound to the nanoparticles in the same method as explained earlier (Section **3.5**). The SPR bands were tracked for each set of AuNP and compared against one another, as expected, all the strands gave a very similar shift (Section **7.1.4**), (**P.1L-AuNP** SPR = 522 nm, **m.P.1L-AuNP** SPR = 522 nm, **l.P.1L-AuNP** SPR = 522 nm) which would indicate that the coating coverages are similar. Once purified, the particles were sized by DLS and the resulting data are displayed in Table 3.8.

Table 3.8 DLS sizing of varied length 1L probes on AuNP
DLS sizing data (number intensity) of AuNPs (2 nM in deionised water) with varied length DNA probes bound.

DNA-AuNP	Size (nm) Number distribution	Size (nm) Intensity distribution
P.1L – AuNP	13 (± 4)	34 (± 17) (96%)
m.P.1L – AuNP	14 (± 3)	24 (± 12) (96%)
l.P.1L – AuNP	15 (± 4)	39 (± 21) (97%)

Whilst they are all within error, and the differences in size are very small (Table 3.8), it is interesting to note that the increase in sizing corresponds to the increased length of anthracene probe bound to the particle. This again indicates that the DNA strands on the AuNP surface are extended away from the surface.

The emission spectra of the different probes on AuNPs were then investigated, again using the intensity of the SPR band as a measure of the particles concentration. As expected, the

emission increased and decreased for mismatched and matched duplexes as shown in Figure 3.19.

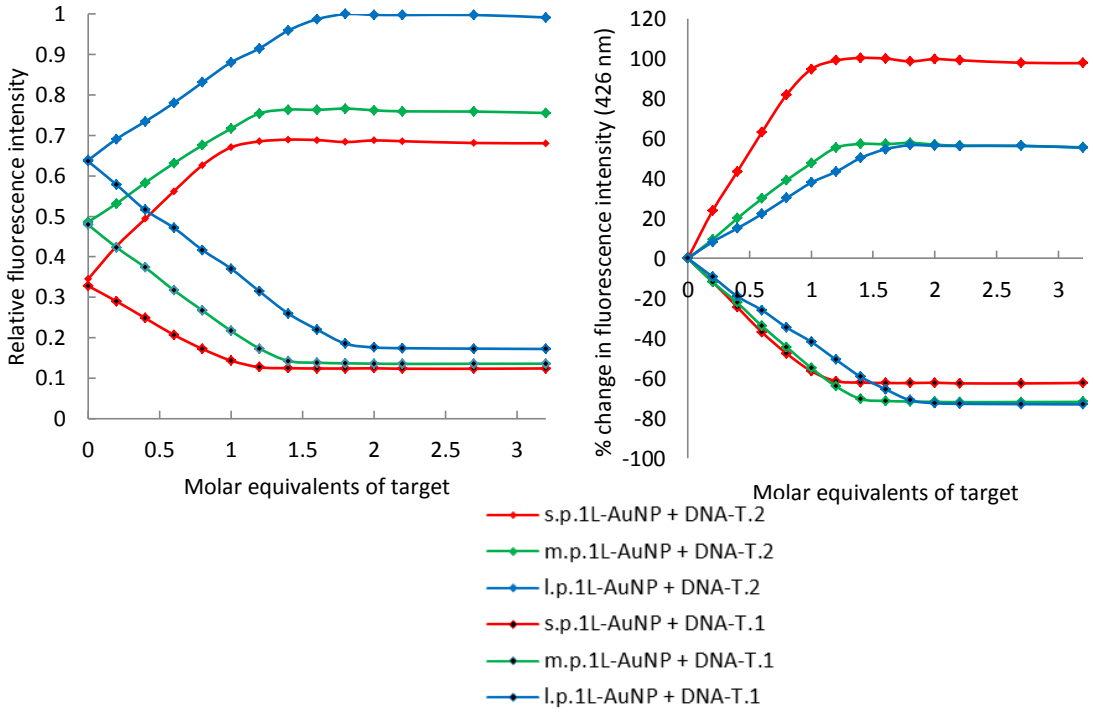

Figure 3.19 Comparing anthracene emission response for varied length 1L probes on AuNP
*(Left) SNP sensing titrations showing fluorescent emission of short (red), medium (green) and long (blue) anthracene probes when bound to AuNP. (Right) SNP sensing titrations showing percentage change in anthracene emission when fully matching target (**DNA-T.1**) and single mis-match containing target (**DNA-T.2**) added to short (red), medium (green) and long (blue) anthracene probes when bound to AuNP. λ_{ex} = 350 nm, λ_{em} = 370-550 nm. AuNP at 2 nM, 10 mM pH 7.0 phosphate buffer, 100 mM NaCl, rt.*

The emission intensity of the anthracene for the varied length probes shows the effect of varying the distance between the anthracene and the AuNP surface (left Figure 3.19). The initial emission of each probe increases with the increased distance the anthracene is from the surface, **P.1L** < **m.P.1L** < **l.P.1L**, with the **l.P.1L-AuNP** having almost double the emission intensity of the **P.1L-AuNP** before target is added. However, when the SNP sensing of the two particles is observed it is clear that more target is required to form the fully duplexed

anthracene probe (indicated by plateau of anthracene signal). The best explanation for this is that the loading on the AuNPs is higher for the longer anthracene probes. Another reason could be that the particle concentration is underestimated; however this was checked by SPR measurements multiple times, and has been shown throughout this project to be an appropriately accurate way to determine the AuNP concentration. As the amount of target added is known, along with the concentration of AuNP, the coating on each particle could be calculated. The increased emission counts observed were shown to correlate to with the increased level of loading (Section **7.1.5**). A possible reason for this is that the packing density is higher through better alignment of longer strands.

Of greater interest are the percentage changes in emission (Right, Figure 3.19), with the anthracene probes acting in much the same way as they do when not bound to particles. It is apparent that the **P.1L** anthracene probe has a much greater increase in emission when compared to the **m.P.1L** and **l.P.1L** once it is bound to AuNPs, a similar trend to that seen when the probes are free in solution (Figure 3.18). The distance the anthracene is away from the AuNP is roughly 4 nm for the **P.1L-AuNP** and 7 nm for **l.P.1L-AuNP** in duplex form**;** this may not be a great enough difference in length to investigate the effect of distance.

3.8.3 Sensing RNA

Although the sensing of DNA is in itself of interest; for *in vitro* imaging of SNPs, it is more useful to sense RNA. There are a number of reasons for this; the first is because within a cellular environment the vast majority of available nucleic acid information is in the form of RNA. The information within DNA is mainly super-coiled in the nucleus and relatively inaccessible for a probe. There are however available RNA strands within the cytoplasm of

the cell, in the form of mRNA. This single stranded RNA is much shorter than genomic DNA, making finding the target easier. Also there are multiple identical RNA strands made from the same gene, this is due to there being only a single copy of a gene in a cell within the DNA. Having multiple identical copies of RNA enables the cell to synthesise the required amount of a protein much more rapidly than if the DNA alone were used as the direct template.[47] Due to the need for the anthracene probe to be fully hybridised with its target, the amount of probe added cannot outnumber the amount of target present. Therefore targeting RNA, which is more abundant in the cell, allows for a greater amount of probe to be used; resulting in a stronger signal to analyse over background.

The ability of the probe to detect RNA SNP targets was tested. The only chemical difference between RNA and DNA is the presence of the 2'OH on the phosphate sugar and uracil bases instead of thymine. The RNA sequences are shown in (Table 3.9); and synthesised using phosphoramidite chemistry (Section **6.1.1.3**).

Table 3.9 RNA target strands synthesised

Strand name	Strand sequence
RNA-T.1	5' CAU UGA GAG AGU CCA 3'
RNA-T.2	5' CAU UGA GAA AGU CCA 3'

Duplex melting temperature experiments confirmed that the RNA targets were still able to form duplexes with the **P.1L-AuNP**, binding with a similar strength to the free probe (Table 3.10).

Table 3.10 Duplex melting temperatures for anthracene probe with RNA targets
Duplex melting temperatures for 1μM RNA, 2 nM AuNP. Experiments run in 10 mM Phosphate Buffer, 100 mM NaCl. RNA-T.1 is the fully matching target, whilst RNA-T.2 contains a single base mis-match.

Probe	RNA-T.1	RNA-T.2	DNA-T.1	DNA-T.2
P.AF	58	44	54	40
P.1L	46	37	48	40

The T_m values show that the DNA-RNA duplexes are stronger than the DNA-DNA duplexes for the unmodified probe. However in the presence of the anthracene probe, the duplexes formed are not as strong which is thought to result in less intercalation of the anthracene probe.

3.8.3.1 SNP sensing of RNA

The RNA targets were then sensed using the **P.1L – AuNP** probe in the same way as described previously (Section **3.8.1**).

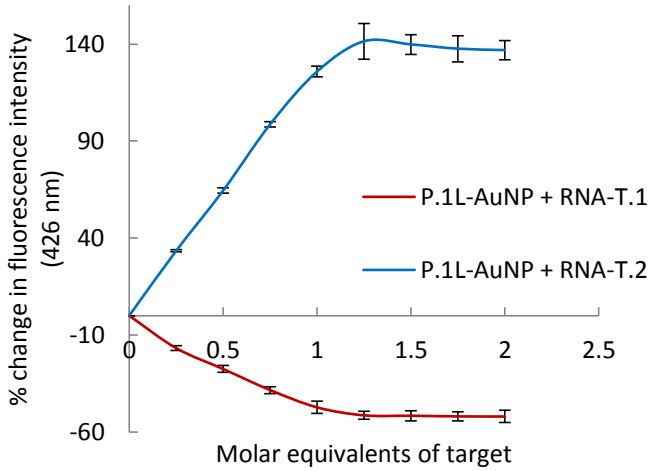

	RNA-T.1	RNA-T.2
P.1L	-55%	+115%
P.1L-AuNP	- 52%	+ 137%

Figure 3.20 Anthracene probe response for 1L-AuNP upon RNA target addition
(left) Percentage change in anthracene emission after each titration of target. Error bars indicate the standard deviation of three repeats using three different preps of probe coated AuNP. (right) Percentage change in anthracene emission once probe is fully hybridised to target. λ_{ex} = 350 nm, λ_{em} = 426 nm. AuNP at 2 nM, 10 mM pH 7.0 phosphate buffer, 100 mM NaCl, rt.

In Figure 3.20 it is shown clearly that the anthracene probe when bound to AuNPs is still able to detect the two different RNA SNP variants. The SNP sensing results are again very similar to the free probe with RNA (Figure 3.20). The difference in percentage emission change between fully bound AAG compared to the fully bound GAG is very similar to the DNA sensing. However, each individual SNP targets percentage change has been shifted more positive by around 20 %, this has been previously observed with the free probe and may be due to differences in the conformation of the duplexes formed as a result of the differences in T_m, and levels of anthracene intercalation.[48]

3.8.4 Base opposite sensing

Another reason for targeting RNA *in vitro* is because of the interest in detecting the transcription of heterozygous DNA for SNP sites of interest. As our genome is made up of pairs of chromosomes, one from each parent, a person can have three possible combinations of the SNP site of interest, depending on the SNP variant their parents have. Either both their chromosomes will contain one of the SNP variants, or they could have one chromosome with one version of the SNP and the other chromosome containing the other SNP variant as shown in Figure 3.21. If a person has two different bases at the SNP site in question, then they are described as having heterozygous DNA at that SNP site.

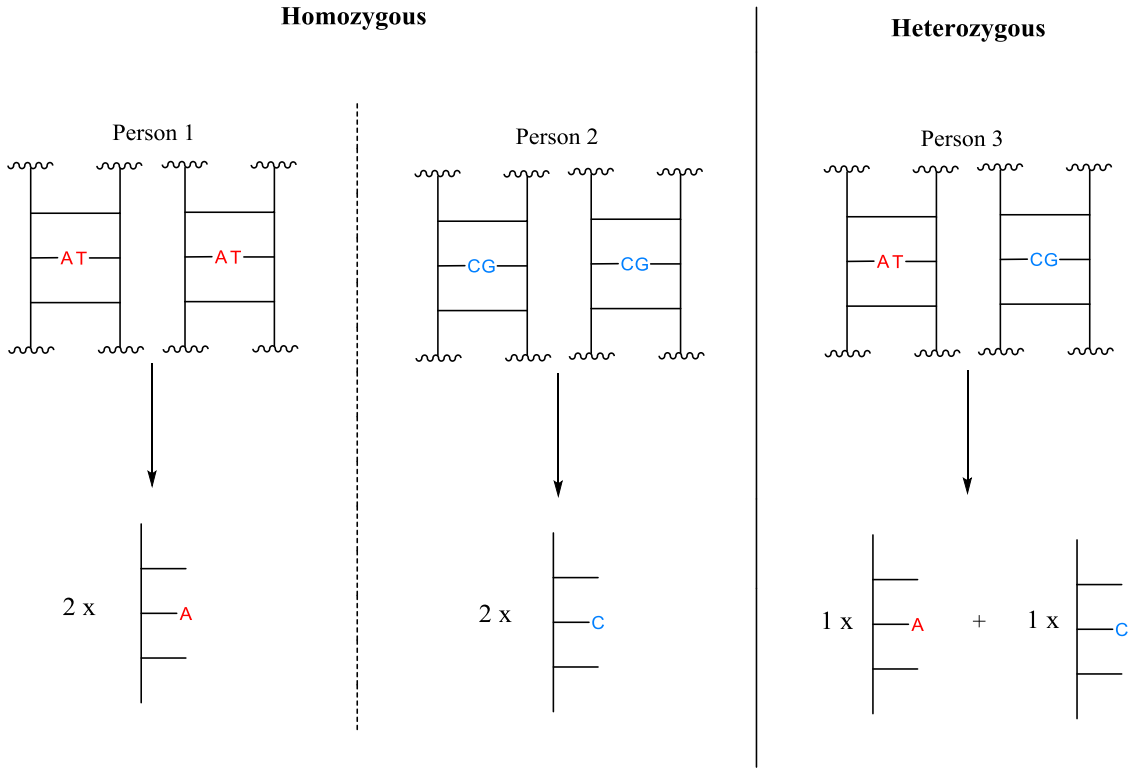

Figure 3.21 Homozygous vs heterozygous SNP sites
Possible chromosome combinations for a SNP site with two variations.

The level that each of the two SNP variants is produced is of growing importance in the prediction of disease, and also with regards to personalised medicine.[49] The Tucker group has developed a technique which is able to discern the percentage of each SNP in a mixture of two SNP samples. This is done using the base opposite method for SNP sensing, using a different anthracene probe. This method uses the same anthracene probe synthesised in Scheme 3.3 only the linker length between the threoninol and the anthracene is 5 carbon bases (in the synthesis replace Ethyl Bromoacetae with Ethyl Bromohexanoate, Section **3.4**). Thanks have to be given to Jonathan Hays for the synthesis of the 5L anthracene linker. This system is able to determine base variations opposite the position of the anthracene probe (Figure 3.22).

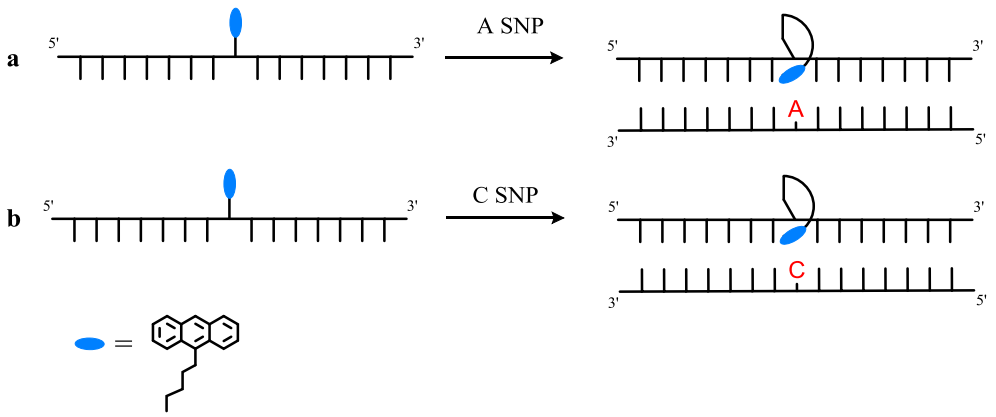

Figure 3.22 Base opposite SNP sensing system
Typically seen when n > 1 for anthracene probe.

The SNP site investigated is a biological SNP site that affects the onset of Alzheimer's disease, it has two variants an A base and a C base. The sequences synthesised are shown in Table 3.11. The anthracene emission intensity increases when bound to the A SNP, but decreases when it binds to the C SNP. This system is able to differentiate between two SNPs in a mixture; because the T_m of the **P.5L** probe with both targets is very similar, see Table 3.12; therefore neither target will bind preferentially. It was found that the anthracene emission could be tracked in a linear fashion when plotted against the percentage of each SNP target. This calibration curve allows the percentage of each SNP variant in a sample to be determined. This method of percentage SNP sensing is novel and would be of great benefit were it possible for it to be done *in vitro*, as real time variations in SNP transcription could be monitored in response to experimental changes to a cell. As described previously (Section **3.1**), using the anthracene probe bound to AuNP will enable cellular delivery of the probe whilst maintaining its stability.

Table 3.11 Strands synthesised for base opposite system
Oligonucleotide strands synthesised for base opposite system W = thioctic acid modification. X = 5L anthracene probe modification.

Strand name	Strand sequence
UM.P1	5' AGT CGC G**X**C TCA GCT 3'
P.5L	5' **W**- AGT CGC G**X**C TCA GCT 3'
DNA.T3	5' AGC TGA GAC GCG ACT 3'
DNA.T4	5' AGC TGA GCC GCG ACT 3'

The **P.5L** probe was bound to the AuNP in the same manner as the **P.1L** probe (Section **6.2.4.1**), the **P.5L-AuNP** was characterised: number distribution = 15 nm (± 4 nm), intensity distribution = 32 nm (± 16 nm) (97%) SPR = 522 nm. Once bound to AuNP the T_m of the probe with both targets remained similar so the probe could be used for the base opposite method percentage SNP sensing.

Table 3.12 Duplex melting temperature comparing free 5L probe with 5L-AuNP
1µM DNA compared to DNA bound to AuNP 2 nM. Tm's run in 10 mM Phosphate Buffer, 100 mM NaCl.

Probe	C SNP	A SNP
P.5L	58.5	58
P.5L-AuNP	59	57.5

A mixture of targets was then added to the **P.5L-AuNP** probe and after 10 minutes, the anthracene emission level was recorded. The linear response of varying the percentage of each SNP in a mixture shows that the probe is still able to work for the base opposite sensing.

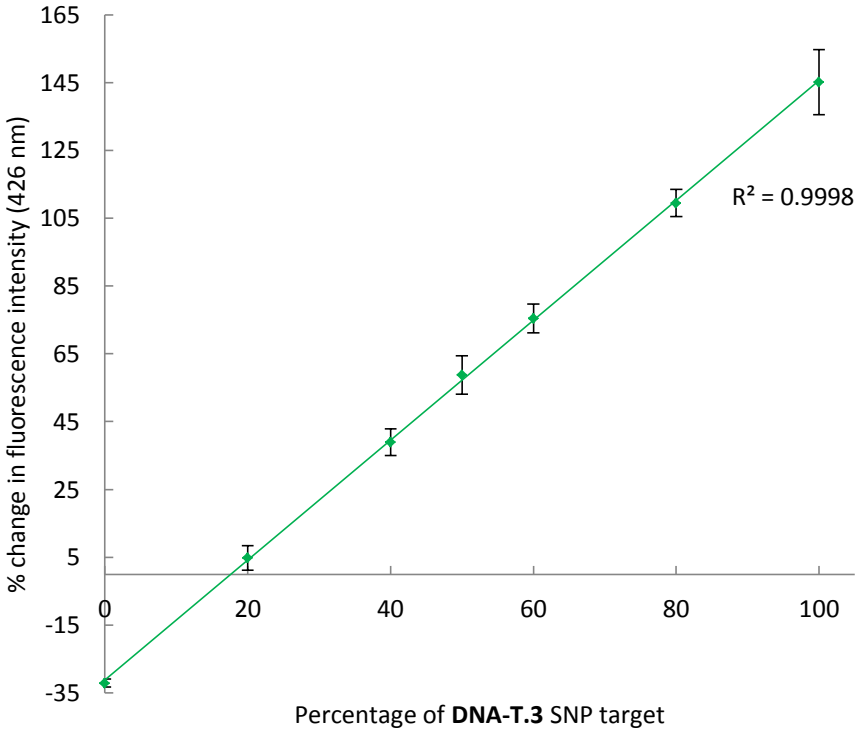

Figure 3.23 Percentage change in anthracene emission for 5L-AuNP upon addition of varied mixtures of SNP targets

*Emission measured at 426 nm after probe is fully hybridised with target. Percentage of target that contains the A SNP variant (**DNA.T3**) or the C SNP variant (**DNA.T4**) SNP on x-axis. Error bars are standard deviation of three repeats with three separate AuNP syntheses.* λ_{ex} *= 350 nm,* λ_{em} *= 426 nm. Samples 2 nM modified AuNP, 10 mM pH 7.0 phosphate buffer, 100 mM NaCl, rt.*

3.9 Cell uptake studies

Binding the anthracene probe to AuNPs was done for stability and cell uptake with no need for any chemical transfection agents. It was also proposed that concentrating the anthracene probe around a single scaffold unit (the AuNP) would aid imaging as a stronger signal would be observed, compared to the disperse probe. This would help overcome the anthracene probes emission limitations, the fact it coincides with autofluorescence, by giving small concentrated regions of signal that could be easily observed and quantified from an image.

Initially it had to be determined whether the particles were taken up by cells when coated in the anthracene probe. Due to the difficulties envisioned with the anthracene probes emission, it was decided to use 100 nm AuNP for these initial experiments. Using these larger DNA coated AuNPs will indicate whether the DNA coating prevents cellular uptake, for the UV-vis binding of DNA to 100 nm AuNP see section **7.1.6**. The benefit of using larger particles is that they can be observed using reflectance microscopy, this has been done before to confirm smaller particle uptake.[29] Reflectance microscopy is similar technique to confocal fluorescence microscopy; however the excitation and detection wavelengths of light are the same, therefore only light that has been reflected back through the objective lens is measured (Figure 3.24).

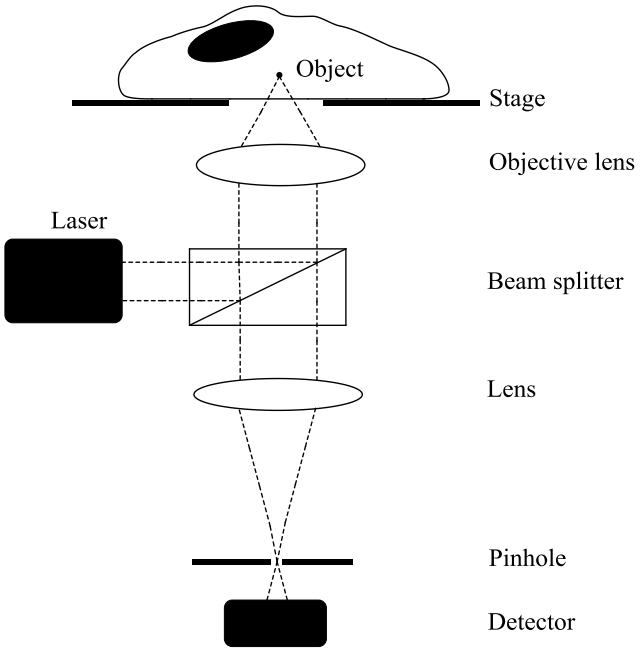

Figure 3.24 Confocal reflectance microscope set up
Fluorescence microscope set up is the same.

In vitro work has been done using the anthracene probe previously within the group,[48] this has worked on Chinese Hamster Ovary cells (CHO). DNA coated particles have been shown to be taken up by CHO cells, work with this cell line was continued. Details of cell culture,

freezing and seeding can be found in experimental (**6.3.2** - **6.3.4**). This work concentrated on investigating the uptake of the **P.1L-AuNP** probe.

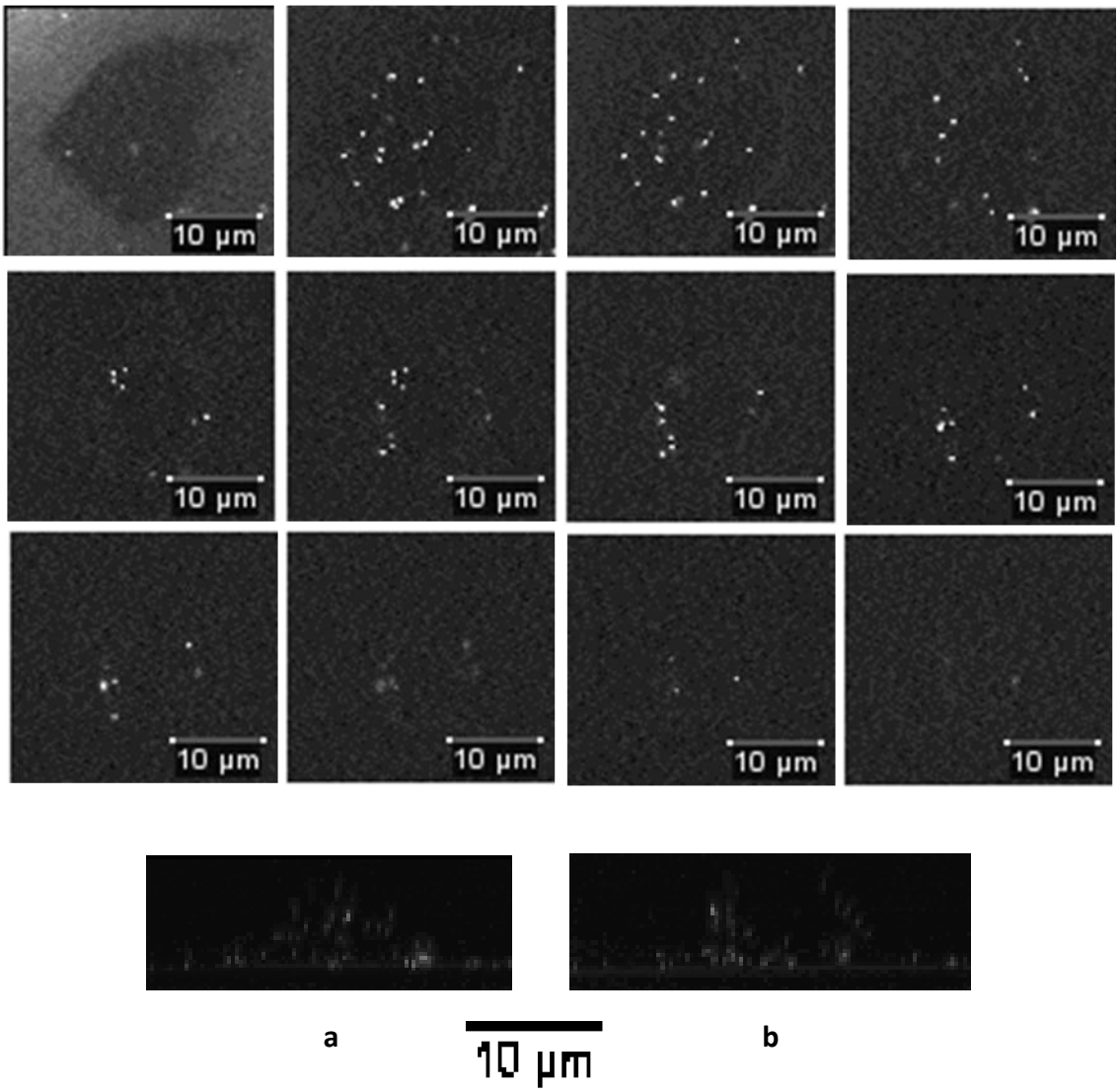

Image 3.1 Reflectance microscopy images of 100 nm 1L-AuNP uptake into CHO cells
(Top) Z-stack of Reflectance microscopy images showing slices of CHO cell treated with 4 pM P.1L-100 nm AuNP. Images taken after cells treated for 2 hours. Slices taken at 0.24 µM intervals. (Bottom) 3D projection of Z-stack showing distribution of particles throughout cell in yz (a) and xz (b) dimensions. Images taken on a Leica SP2 inverted confocal microscope using a 100 x objective lens.

From Image 3.1 it is clear that the particles are readily taken up into cells within 2 hours, which coincides with previous work which suggested that most uptake of particles occurs within 2 hours before plateauing after 4 hours.[50,51] The 3D projections show the particles

within the cell, there is also a notable region in the middle where there are no particles present (Image 3.1 (**b**)), this corresponds to the nuclear region. Overlaying the reflectance and transmission images (Image 3.2) show the particles do not enter the nucleus, they only overlay on the nucleus above or below it (brightfield image **7.1.7**).

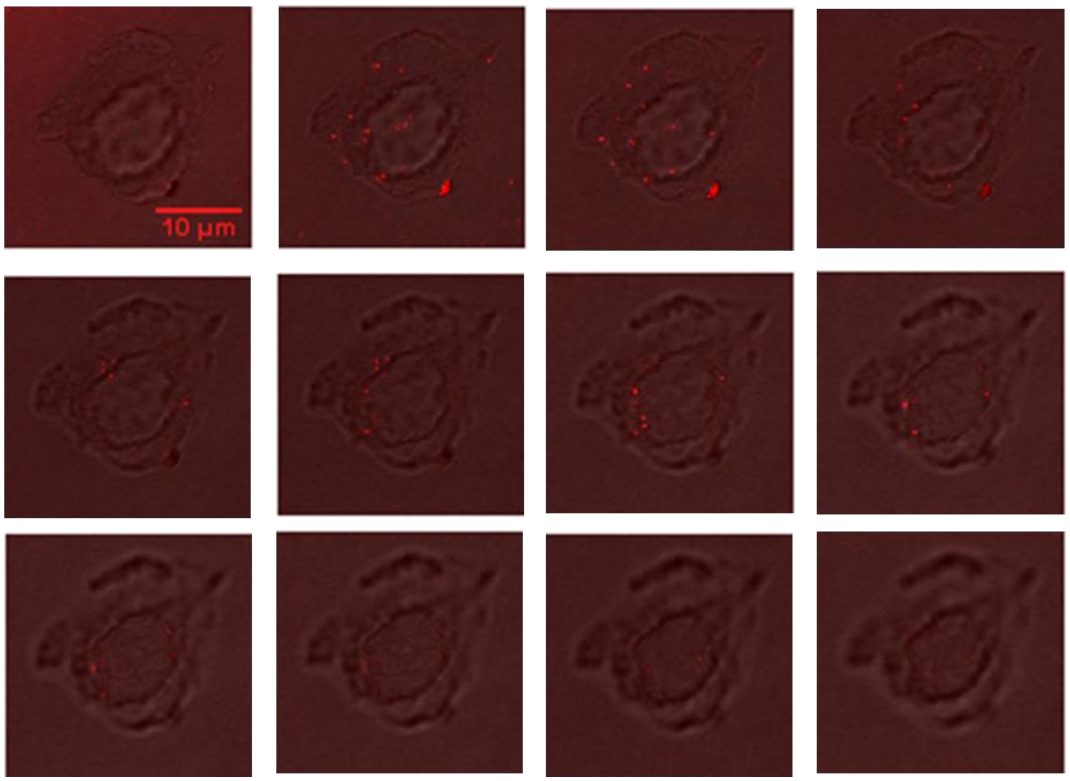

Image 3.2 Overlaying reflectance and transmission microscopy images for 100 nm 1L-AuNP cell uptake

Z-stack overlaying reflectance and transmission microscopy images showing slices of CHO cell treated with 4 pM P.1L-100 nm AuNP. Images taken after cells treated for 2 hours. Slices taken at 0.24 µM intervals. Red spots indicate reflectance from particles. Images taken on a Leica SP2 inverted confocal microscope using a 100 x objective lens

3.10 Conclusions and future work

In this chapter, a SNP sensing DNA probe has been successfully modified so that it can be attached to AuNPs. To bind the probe to AuNPs a new method was developed, this method is both much quicker than previously published methods, whist also allowing for the coating process to be monitored. Once bound to the AuNP the SNP sensing probe retains its SNP sensing capabilities, for both DNA and RNA, giving similar percentage emission changes as seen for the free probe. The particles themselves were stable to large changes in temperature (15-85°C) and also stable in much higher salt concentrations (0.1 M) than those observed *in vitro*. It was shown that the probe coated AuNP were readily taken up by cells without the need for chemical transfection. However there were problems in attempting to image the anthracene probes emission; this is due to a number of factors including quenching of anthracene emission by the AuNP, access to suitable excitation lasers and also cell autofluorescence.

Due to the problems encountered attempting to image the anthracene probe *in vitro*, the work in varying the length of the anthracene probe should be further investigated. It has been shown that the distance a fluorophore is from the surface of AuNPs greatly affects its emission intensity. Fluorophores which are held within 10 nm of the AuNP surface are significantly quenched, however the fluorescence of fluorophores beyond this range can be enhanced.[52] Therefore probe strands should be synthesised containing spacer groups which will extend the distance of the anthracene probe to >10 nm from the AuNP surface. If fluorescence enhancement is observed, this may allow for the probe to be imaged within a cellular environment, leading to *in vitro* SNP detection.

The particles must be free to bind to the target strands once inside the cell, therefore the localisation of the probe coated particles once inside a cell needs to be established. It has been shown that upon uptake, functionalised AuNPs are often internalised into endosomes,[6] if the probe coated AuNP are retained inside these, they will not be able to bind to the target. Uptake studies should therefore be done, whereby the destination of the particles at different time points can be accurately determined by TEM. TEM studies have been used to investigate the uptake mechanism of DNA coated AuNP,[7] however there has been no study of their distribution once inside the cell. If the particles are retained in endosomes upon uptake, then further modification of the surface to include groups which may aid the particles release from endosomes should be investigated.[53]

3.11 References

1. Brookes, a J. The essence of SNPs. *Gene* **234,** 177–86 (1999).
2. Kim, S. & Misra, A. SNP genotyping: technologies and biomedical applications. *Annu. Rev. Biomed. Eng.* **9,** 289–320 (2007).
3. Saito, Y., Miyauchi, Y., Okamoto, A. & Saito, I. Base-discriminating fluorescent (BDF) nucleoside: distinction of thymine by fluorescence quenching. *Chem. Commun. (Camb).* 1704–1705 (2004).
4. Fisher, T. L., Terhorst, T., Cao, X. & Wagner, R. W. Intracellular disposition and metabolism of fluorescently-labeled unmodified and modified oligonucleotides microinjected into mammalian cells. *Nucleic Acids Res.* **21,** 3857–3865 (1993).
5. Seferos, D. S., Prigodich, A. E., Giljohann, D. A., Patel, P. C. & Mirkin, C. A. Polyvalent DNA Nanoparticle Conjugates Stabilize Nucleic Acids. *Nano Lett.* **9,** 308–311 (2009).
6. Nativo, P., Prior, I. a & Brust, M. Uptake and intracellular fate of surface-modified gold nanoparticles. *ACS Nano* **2,** 1639–44 (2008).
7. Choi, C. H. J., Hao, L., Narayan, S. P., Auyeung, E. & Mirkin, C. a. Mechanism for the endocytosis of spherical nucleic acid nanoparticle conjugates. *Proc. Natl. Acad. Sci. U. S. A.* **110,** 2–7 (2013).
8. Giljohann, D. a *et al.* Oligonucleotide loading determines cellular uptake of DNA-modified gold nanoparticles. *Nano Lett.* **7,** 3818–21 (2007).
9. Patel, P. C. *et al.* Scavenger receptors mediate cellular uptake of polyvalent oligonucleotide-functionalized gold nanoparticles. *Bioconjug. Chem.* **21,** 2250–6 (2010).
10. Zhang, X., Servos, M. R. & Liu, J. Surface science of DNA adsorption onto citrate-capped gold nanoparticles. *Langmuir* **28,** 3896–902 (2012).
11. Cárdenas, M. *et al.* Thiol-specific and nonspecific interactions between DNA and gold nanoparticles. *Langmuir* **22,** 3294–9 (2006).
12. Sandstrom, P., Boncheva, M. & Akerman, B. Nonspecific and Thiol-Specific Binding of DNA to Gold Nanoparticles. *Langmuir* **19,** 7537–7543 (2003).
13. Herne, T. M. & Tarlov, M. J. Characterization of DNA probes immobilized on gold surfaces. *J. Am. Chem. Soc.* **119,** 8916–8920 (1997).
14. Häkkinen, H. The gold–sulfur interface at the nanoscale. *Nat. Chem.* **4,** 443–455 (2012).
15. Hurst, S. J., Lytton-Jean, A. K. R. & Mirkin, C. a. Maximizing DNA loading on a range of gold nanoparticle sizes. *Anal. Chem.* **78,** 8313–8 (2006).
16. Rosi, N. L. *et al.* Oligonucleotide-modified gold nanoparticles for intracellular gene regulation. *Science* **312,** 1027–30 (2006).
17. Dougan, J. a, Karlsson, C., Smith, W. E. & Graham, D. Enhanced oligonucleotide-nanoparticle conjugate stability using thioctic acid modified oligonucleotides. *Nucleic Acids Res.* **35,** 3668–75 (2007).
18. Garcia, B. *et al.* Sulfur K-edge XANES study of dihydrolipoic acid capped gold nanoparticles: dihydrolipoic acid is bound by both sulfur ends. *Chem. Commun. (Camb).* 369–71 (2005).
19. Adams, S. J., Lewis, D. J., Preece, J. a. & Pikramenou, Z. Luminescent gold surfaces for sensing and imaging: Patterning of transition metal probes. *ACS Appl. Mater. Interfaces* **6,** 11598–11608 (2014).
20. Stokes, R. J. *et al.* Highly sensitive detection of dye-labelled DNA using nanostructured gold surfaces. *Chem. Commun. (Camb).* 2811–2813 (2007).
21. Duprey, J.-L. H. a *et al.* Detection of DNA base variation and cytosine methylation at a single nucleotide site using a highly sensitive fluorescent probe. *Chem. Commun. (Camb).* **47,** 6629–31 (2011).
22. Duprey, J.-L. H. a. Studies On Anthracene Tagged Oligonucleotides. (2010).

23. Grabar, K. C., Freeman, R. G., Hommer, M. B. & Natan, M. J. Preparation and Characterization of Au Colloid Monolayers. *Anal. Chem.* **67,** 735–743 (1995).
24. Schulz, F. *et al.* Little Adjustments Significantly Improve the Turkevich Synthesis of Gold Nanoparticles. *Langmuir* **30,** 10779–10784 (2014).
25. Hurst, S. J., Lytton-Jean, A. K. R. & Mirkin, C. A. Maximising DNA Loading on a Range of Gold Nanoparticle Sizes. *Anal. Chem.* **78,** 8313–8318 (2006).
26. Demers, L. M. *et al.* A fluorescence-based method for determining the surface coverage and hybridization efficiency of thiol-capped oligonucleotides bound to gold thin films and nanoparticles. *Anal. Chem.* **72,** 5535–41 (2000).
27. Zhang, X., Servos, M. R. & Liu, J. Instantaneous and Quantitative Functionalization of Gold Nanoparticles with Thiolated DNA Using a pH-Assisted and Surfactant-Free Route. *J. Am. Chem. Soc.* 7266–7269 (2012).
28. Davies, A., Lewis, D. J., Watson, S. P., Thomas, S. G. & Pikramenou, Z. pH-controlled delivery of luminescent europium coated nanoparticles into platelets. *Proc. Natl. Acad. Sci. U. S. A.* **109,** 1862–7 (2012).
29. Rogers, N. J. *et al.* High coating of Ru(II) complexes on gold nanoparticles for single particle luminescence imaging in cells. *Chem. Commun. (Camb).* **50,** 617–9 (2014).
30. Osborne, S. A. M. & Pikramenou, Z. Highly luminescent gold nanoparticles: effect of ruthenium distance for nanoprobes with enhanced lifetimes. *Faraday Discuss.* **00,** 1–13 (2015).
31. Claire, S. Development of Nanoparticles for Imaging Applications. (2016).
32. Zhang, X. *et al.* Toward Fast and Quantitative Modification of Large Gold Nanoparticles by Thiolated DNA: Scaling of Nanoscale Forces, Kinetics, and the Need for Thiol Reduction. *J. Phys. Chem. C* **117,** 15677–15684 (2013).
33. Quinten, M. & Kreibig, U. Optical properties of aggregates of small metal particles. *Surf. Sci.* **172,** 557–577 (1986).
34. Lodish, H., Berk, A. & Zipursky, S. *Molecular Cell Biology*. (W. H. Freeman, 2000).
35. Witten, K. G., Bretschneider, J. C., Eckert, T., Richtering, W. & Simon, U. Assembly of DNA-functionalized gold nanoparticles studied by UV/Vis-spectroscopy and dynamic light scattering. *Phys. Chem. Chem. Phys.* **10,** 1870–1875 (2008).
36. Bandura, D. R., Baranov, V. I. & Tanner, S. D. Detection of Ultratrace Phosphorus and Sulfur by Quadrupole ICPMS with Dynamic Reaction Cell. *Anal. Chem.* **74,** 1497–1502 (2002).
37. Mirkin, C., Letsinger, R., Mucic, R. & Storhoff, J. A DNA-based method for rationally assembling nanoparticles into macroscopic materials. *Nature* **382,** 607–609 (1996).
38. Chimiche, T., Roma, U., Vergata, T. & Scientifica, R. On the Nature of DNA Hyperchromic Effect. *J. Phys. Chem. B* **117,** 8697–8704 (2013).
39. Yakovchuk, P., Protozanova, E. & Frank-Kamenetskii, M. D. Base-stacking and base-pairing contributions into thermal stability of the DNA double helix. *Nucleic Acids Res.* **34,** 564–574 (2006).
40. Elghanian, R., Storhoff, J., Mucic, R. C., Letsinger, R. L. & Mirkin, C. Selective Colorimetric Detection of Polynucleotides Based on the Distance-Dependent Optical Properties of Gold Nanoparticles. *Science (80-.).* **277,** 1078–1081 (1997).
41. Govorov, A. O., Fan, Z., Hernandez, P., Slocik, J. M. & Naik, R. R. Theory of Circular Dichroism of Nanomaterials Comprising Chiral Molecules and Nanocrystals: Plasmon Enhancement, Dipole Interactions, and Dielectric Effects. *Nano Lett.* **10,** 1374–1382 (2010).
42. Ha, J.-M., Solovyov, A. & Katz, A. Postsynthetic modification of gold nanoparticles with calix[4]arene enantiomers: origin of chiral surface plasmon resonance. *Langmuir* **25,** 153–8 (2009).

43. Dulkeith, E. *et al.* Gold nanoparticles quench fluorescence by phase induced radiative rate suppression. *Nano Lett.* **5,** 585–9 (2005).
44. Dulkeith, E. *et al.* Fluorescence Quenching of Dye Molecules near Gold Nanoparticles: Radiative and Nonradiative Effects. *Phys. Rev. Lett.* **89,** 12–15 (2002).
45. Milton, J. a *et al.* Efficient self-assembly of DNA-functionalized fluorophores and gold nanoparticles with DNA functionalized silicon surfaces: the effect of oligomer spacers. *Nucleic Acids Res.* **41,** e80 (2013).
46. Zu, Y. & Gao, Z. Facile and controllable loading of single-stranded DNA on gold nanoparticles. *Anal. Chem.* **81,** 8523–8 (2009).
47. Alberts, B. *et al. Cell book.pdf*. *Essential Cell Biology: An introduction to the Molecular Biology of the Cell* (Garland, 1998).
48. Bamford, R. a. Development of fluorophore-tagged DNA probes for cellular imaging applications. (2015).
49. Ginsburg, G. S. & Willard, H. F. Genomic and personalized medicine: foundations and applications. *Transl. Res.* **154,** 277–287 (2009).
50. Chithrani, B. D., Ghazani, A. a & Chan, W. C. W. Determining the size and shape dependence of gold nanoparticle uptake into mammalian cells. *Nano Lett.* **6,** 662–8 (2006).
51. Desai, M. P., Labhasetwar, V., Walter, E., Levy, R. J. & Amidon, G. L. The Mechanism of Uptake of Biodegradable Microparticles in Caco-2 Cells Is Size Dependent. *Pharm. Res.* **14,** 1568–1573 (1997).
52. Anger, P., Bharadwaj, P. & Novotny, L. Enhancement and quenching of single-molecule fluorescence. *Phys. Rev. Lett.* **96,** 113002 (2006).
53. Ma, D. Enhancing endosomal escape for nanoparticle mediated siRNA delivery. *Nanoscale* **6,** 6415–6425 (2014).

4 RATIOMETRIC SNP SENSING AuNPs CONTAINING A SELF-STANDARDISING RUTHENIUM PROBE

4.1 Introduction

Quantification of *in vitro* fluorescent signals is difficult to achieve with single fluorophore probes; this is due to the variation in cell uptake of foreign molecules across a cell population. This variation is due to a cell population not being uniform; each cell is unique and its decisions are affected by both single molecule interactions and also larger scale interactions with nearby neighbours. This is a significant issue for nanoparticles; especially given that the exact method of their uptake is not fully understood.[1–4] The variation in cellular uptake of AuNPs can be as large as 10 fold across a population;[5] in viral particles this variation has been attributed to the cell size, local cell density and receptor molecule distributions.[6] For AuNPs, the local aggregation level of the particles has been shown to be a significant factor.[7]

The variation in uptake of the probe will therefore lead to a variation in the initial fluorescence intensity, making quantification of a change in fluorescence difficult. As the SNP detection of the anthracene probe is based upon a percentage change in emission from a baseline value, an initial emission intensity of the anthracene probe is required. This is simple to do in cuvette studies, where an initial intensity value of the probe can be taken before adding the target strand. However for *in vitro* work, it is not possible to take an initial emission level as the uptake of probe into each cell will not be consistent. Therefore the samples can only be analysed once the probes have entered the cells. Upon entering the cell, the probes will bind to their target before an initial intensity level can be recorded; this makes it difficult to establish whether the emission has increased or decreased upon hybridisation.

The variation in cell uptake and an inability to establish an initial intensity reading leads to a further problem in determining the SNP variant present. Not knowing the concentration of anthracene probe in a cell, means that two cells containing the same anthracene probe and giving an identical emission intensity reading could actually be detecting two different SNP targets. One cell could contain a target that causes a decrease in the anthracene emission but has many probes present, whilst the other cell could contain a target that causes an increase in emission but has fewer probes present. The final result of this would be two cells with very similar emission intensities, yet two different targets.

To overcome these problems, it was proposed to utilise the scaffold nature of AuNPs and attach a second fluorescent probe onto the AuNP surface; this second probe would act as an internal standard for the anthracene probes emission to be normalised to (Figure 4.1). Ideally, this second fluorophore would not interact with the anthracene probe and thus not fluctuate in emission upon the anthracene probe hybridising with the different targets. The ratio of the anthracene signal relative to the standard could then be used give a concentration-independent emission level of the anthracene.

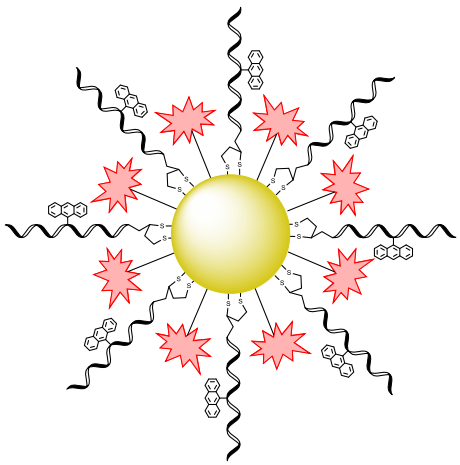

Figure 4.1 AuNP coated in both the anthracene probe and an additional fluorophore.

The idea of an internal standard for the anthracene probe has previously been considered within the group; a second fluorophore was attached to the end of the anthracene probe, although the emission of the second fluorophore fluctuated considerably upon binding to the targets.[8]

There are previous literature examples of the use of ratiometric fluorophore systems to overcome the problems of variable cell concentrations; the main requirement is that both fluorophores must be delivered together, with no possibility of any differences in their relative concentrations. Woodroofe *et al*. used a single molecule, which upon entering the cell was cleaved into two separate fluorophores by esterase enzymes. One of the fluorophores quantified zinc ion concentration, whilst the other quantified the concentration of probe within the cell.[9] Quantum dots have also been used to form ratiometric sensors capable of detecting a variety of molecules; here the studies utilise the inherent fluorescence of quantum dots to determine the concentration of probe delivered into the cell.[10,11] Prigodich *et al.* used multiple fluorophores to integrate an internal standard into their nanoflare gene detection system (Figure 4.2).[12] Two different flares were bound to AuNPs, with one detecting the gene of interest and the second flare specific for a gene which was assumed to be at constant expression level across a cell population, therefore giving a standard level of fluorescence, indicating the relative concentration of the nanoflare within a cell.

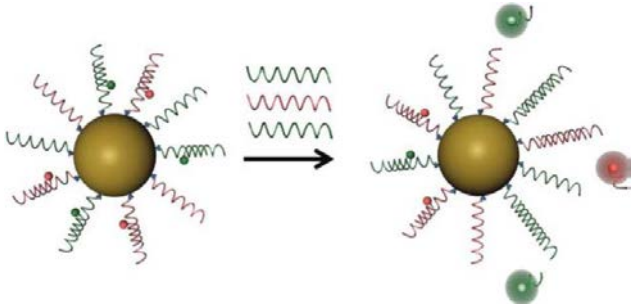

Figure 4.2 Nanoflare probe
Prigoditch et al. nanoflare probe.[12] *The two different flares are specific for different nucleic acid targets. Upon binding to the target, a flare is released and is no longer quenched by AuNP. Using two different fluorophores allows a ratio of two targets to be found.*

To decide upon a suitable probe to act as an internal standard, a number of factors needed to be considered: firstly the anthracene probe excitation and emission profiles should not overlap with the internal standard probe as this would introduce errors such as fluorescence bleed through when exciting each probe. Secondly, the probe had to be sufficiently modified so that it could be bound to AuNP in a manner which would not disrupt the DNA binding to the AuNP.

The probe chosen for this work to act as the internal standard is a ruthenium based probe developed within the group, ruthenium-4,4'-Di(5-lipoamido-1-pentoxy)-2,2'-bi-pyridine (RubpySS) (Figure 4.3). The probe was initially synthesised by Adams *et al.* for the use of metal imprinting onto gold surfaces.[13] The reason for using this RubpySS probe is because of the attractive properties that photoactive transition metal complexes possess, particularly for imaging applications.[14,15] These properties include photostability, excitation and emission profiles within the visible region (more compatible with conventional imaging techniques) and large Stokes shifts. The RubpySS probe excitation (465 nm, MLCT band) and emission (550-800 nm) bands are red shifted when compared to the anthracene probe (λ_{ex} = 350 nm,

λ_{em} = 370-570 nm), and are therefore much removed from the anthracene signal and also, importantly with regards to imaging, away from autofluorescence excitation wavelengths.

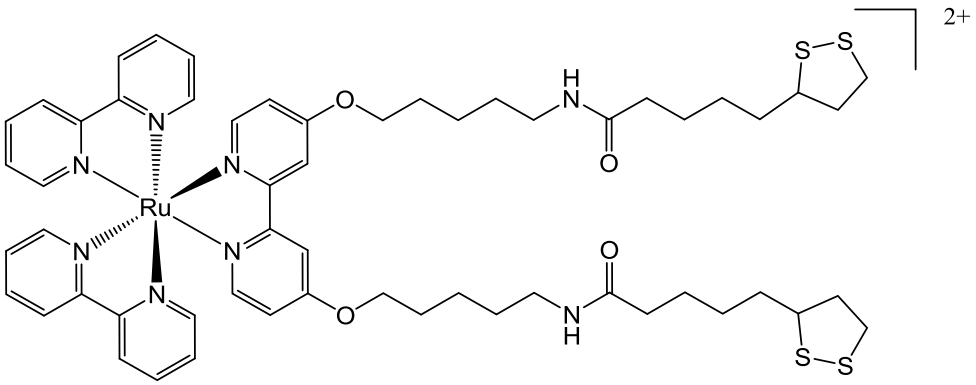

Figure 4.3 RubpySS probe

Dr Sam Adams is acknowledged for providing the RubpySS as its $[PF_6]^-$ salt. However, with a $[PF_6]^-$ counter ion, the probe was not water soluble, and was therefore not suitable for binding to the citrate/DNA stabilised AuNPs. This was converted to the $[Cl]^-$ salt using Dowex beads to give a water soluble complex (section **6.1.2**).

As described below, the RubpySS probe was bound to gold nanoparticles alongside the anthracene probe. The presence of the two disulphide terminating legs on the ruthenium probe allowed it to bind to the gold nanoparticles in a similar fashion to the anthracene probe as previously described (section **3.6**). Investigations into how well the RubpySS works as an internal standard are made and whether it has any effects on the anthracene SNP sensing.

4.2 Binding of DNA and RubpySS to AuNP

Previous work in the Pikramenou group showed that a surfactant layer was required on the AuNP surface before a ruthenium probe, similar to the RubpySS complex used here, could be added.[16] This surfactant layer helped prevent the particles from aggregating once the positively charged ruthenium probes were added. It was proposed that the DNA molecules once bound to the gold nanoparticles, may act as a surfactant themselves, with their negatively charged phosphate groups providing enough repulsion between particles to restrict particle aggregation.

Table 4.1 DNA probe and target strands synthesised
Strands synthesised. W = thioctic acid modification. X = 1L anthracene probe. Y = 1D anthracene probe.

Strand name	Strand sequence
P.1L	5' **W**-TGG ACT C**X**C TCA ATG 3'
P.1D	5' **W**-TGG ACT C**Y**C TCA ATG 3'
l.P.1L	5' **W**-AAAAAAAAAA TGG ACT C**X**C TCA ATG 3'
P.AF	5' **W**-TGG ACT CTC TCA ATG 3'
DNA-T.1	5' CAT TGA GAG AGT CCA 3'
DNA-T.2	5' CAT TGA GAA AGT CCA 3'

The DNA strands used to coat the AuNPs were the same as those used in Chapter 1, and are shown in Table 4.1. It was envisaged that upon coating the particles in DNA, the RubpySS would then be added and, as they are significantly smaller and oppositely charged to the

DNA, bind to the particles in the gaps between DNA strands. The DNA would be bound to the particles in the same way as described previously in Chapter 1.

To test whether the DNA would indeed act as a protective surfactant layer and stabilise the particles from aggregating upon addition of RubpySS, two samples of AuNPs were synthesised, one that was not coated in DNA (i.e. citrate stabilised AuNP) and one that was fully coated in DNA (**P.1L-AuNP**). To these particles, RubpySS was titrated in, with 20 minutes stirring between each addition (each addition = 1.33 µM RubpySS probe, 3 nM AuNP), after which an UV/Vis absorption scan of the particles was taken (Figure 4.4). The SPR band was then used to monitor the binding of the RubpySS and also the stability of the AuNPs.

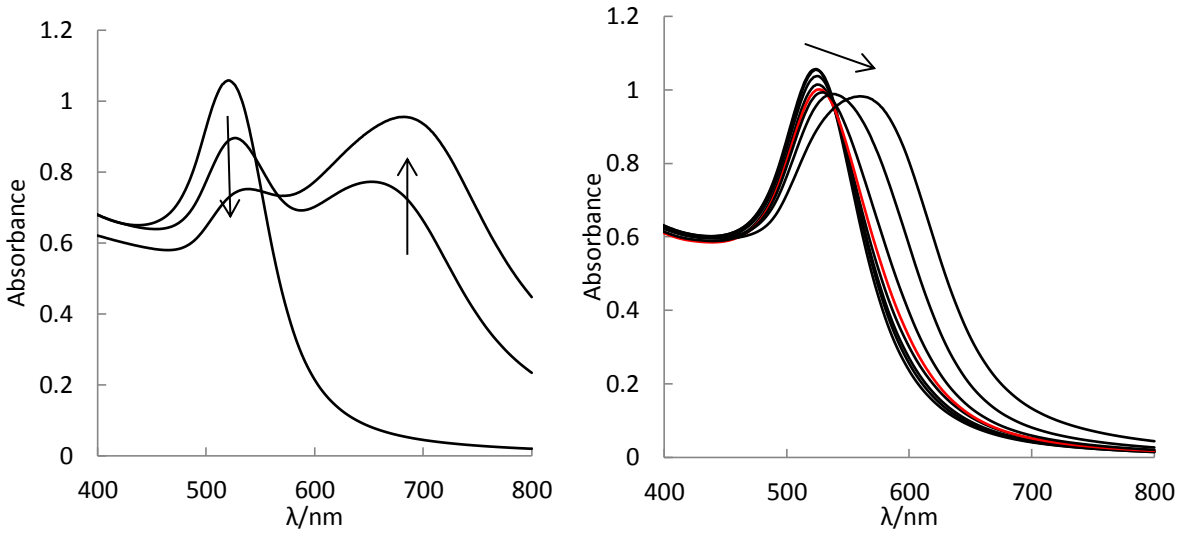

Figure 4.4 UV absorption upon addition of RubpySS probe to bare AuNP and P.1L-AuNP
*(Left) UV-vis absorption spectrum of bare AuNP with titrations of ruthenium probe added in aliquots of 1.33 µM. Arrows denote the decrease in 520 nm band and increase in band at 700 nm. (Right) UV-vis absorption spectrum of DNA coated AuNP (**P.1L-AuNP**) monitoring the addition of ruthenium probe. Arrow denotes the direction of graph movement upon increasing additions (not all additions shown). Samples of 3 nM AuNP in deionised water and 10 mM pH 7.0 phosphate buffer at room temperature.*

As can be seen in Figure 4.4 (left), uncoated AuNPs begin to aggregate immediately with the first addition of RubpySS, indicated by the appearance of an absorption band at ~700 nm

and the decrease in the SPR band at 520 nm, which is why a surfactant is usually used to stabilise the AuNPs prior to coating.[16] On the other hand, the DNA coated particles (**P.1L-AuNP**) appear to be stabilised, with no sudden appearance of the 700 nm absorption band. However, for the DNA coated AuNPs, there is no point at which the SPR band stops shifting to indicate total coverage of the surface of the AuNP. As previously discussed, the SPR band shifting is indicative of further changes to the surface of the AuNP and once it stops shifting, the surface environment of the AuNP is assumed to be constant, i.e. fully coated. It appeared then that although the DNA coating stabilises the particles compared to the citrate stabilised AuNPs, upon the addition of too much RubpySS, aggregation occurs, as indicated by the large red shifting of the SPR band (up to 560 nm) and observable colour change from red to blue.

By analysing the UV-Vis scan, it was established that the **P.1L-AuNPs** were beginning to aggregate after the addition of 8 µM of RubpySS (indicated as red coloured spectrum in Figure 4.4). Therefore 6.67 µM of RubpySS was added to the DNA coated AuNPs (in 10 mM pH 7.0 phosphate buffer) before passing these newly formed **P.1L-AuNP-Ru** particles through a Sephadex G-50 size exclusion column to remove any unbound molecules. Upon testing the ruthenium emission levels however, it was found that the ruthenium emission was very low. Therefore the amount of DNA initially coating the particles was investigated. Reducing the amount of DNA bound to the AuNP surface would allow more space for the RubpySS to bind to each particle, resulting in a greater ruthenium emission intensity being observed.

By analysing the SPR shift of the particles during DNA coating (Figure 4.5), the amount of DNA required to not quite fully saturate the surface was established as being the point just before the SPR band stopped shifting, 0.98 μM of DNA (a third of the total DNA used when fully coating the particles). Reducing the DNA content further was investigated, however this resulted in particle aggregation upon addition of RubpySS.

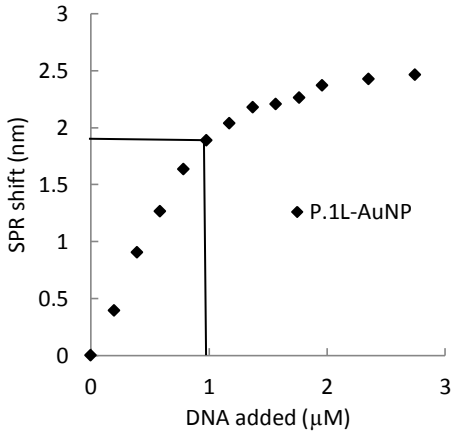

Figure 4.5 SPR shift for P.1L binding to AuNP to identify concentration required for partial coverage
SPR shift tracking aliquots of P.1L binding to AuNP, lines indicate concentration chosen for partial surface coverage. Samples of 3 nM AuNP in deionised water and 10 mM pH 7.0 phosphate buffer at room temperature.

Once the particles were coated in the lower concentration of DNA, the amount of ruthenium probe that could be added was established. From previous work in the group, it was known that when coating zonyl stabilised AuNPs with a similar ruthenium probe the coating levels were of the order 10^3 probes per AuNP.[16] Similar additions of RubpySS were tested and it was found that a 4.5 μM concentration of RubpySS (1500 probes per particle) could be added to a 3 nM **P.1LAuNP** solution before aggregation occurred.

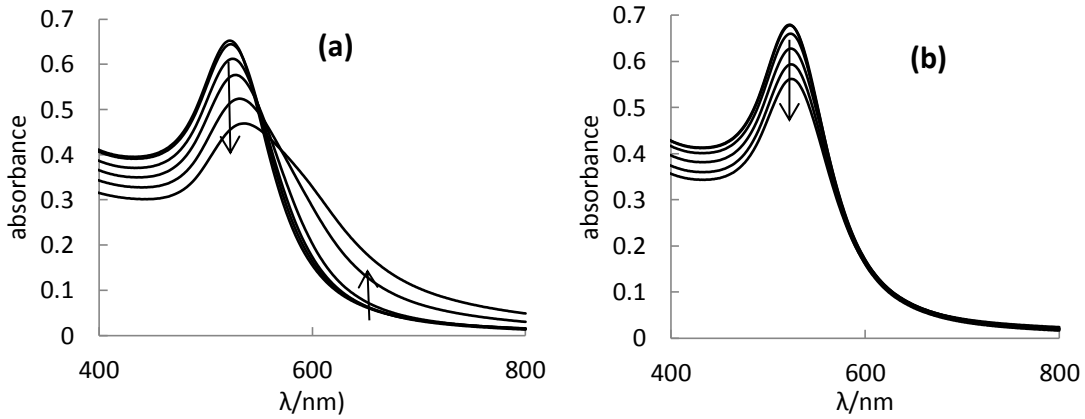

Figure 4.6 Comparing relative salt stabilities of P.1L-AuNP coated in various amounts of RubpySS
UV-vis spectrum tracking the stability of partially coated 1L-AuNPs (1 mL 2 nM) coated with (a) 4.5 µM of ruthenium probe (b) 3.0 µM of ruthenium probe. Each scan is titration of NaCl (2 µL, 5 M NaCl) up to 100 mM (not all peaks shown). Arrows represent trend of peaks. Samples of 2 nM AuNP in deionised water and 10 mM pH 7.0 phosphate buffer at room temperature.

With this information, salt was added to the purified particles because the particles needed to be stable at 100 mM NaCl for *in vitro* work. However, it was found that upon addition of aliquots of NaCl (each aliquot = 10 mM NaCl) it was evident that particles coated at 4.5 µM of ruthenium were unstable and aggregated (Figure 4.6, **(a)**). Reducing the amount of RubpySS added to 3.0 µM gave **P.1L-AuNP-Ru** particles that were stable at the required salt concentrations (Figure 4.6, **(b)**).

4.2.1 Characterisation of AuNPs coated with DNA plus RubpySS

The final protocol for the synthesis of the **P.1L-AuNP-Ru** particles was therefore established. Citrate coated AuNPs (13 nm, 3 nM) are made up in 10 mM pH 7.0 phosphate buffer, coated initially in 0.98 µM of DNA (in 3 equivalents) with 2 minutes stirring and 20 seconds sonication between each addition. To these particles, 3.0 µM of RubpySS is added (in 2 additions) with 20 minutes of stirring in between each addition, after which the particles are passed through a Sephadex G-50 column to purify (for full experimental see **6.2.4.2**). The

SPR shift for the AuNP is 2.5 nm upon DNA addition and then a further 1.5 nm once the RubpySS has been added, Figure 4.7.

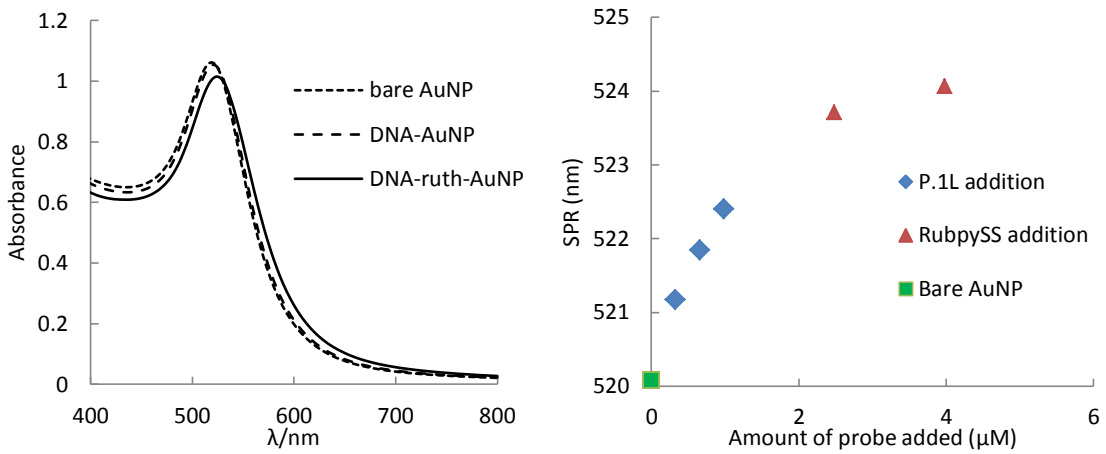

Figure 4.7 Tracking SPR peak through binding of P.1L and RubpySS to AuNP
(Left) UV spectrum of each stage of the coating process. (Right) Tracking the shifting of the SPR peak throughout the coating process. Samples of 3 nM AuNP in deionised water and 10 mM pH 7.0 phosphate buffer at room temperature.

The particles were sized by DLS (Table 4.2), with TEM images confirming the majority of particles are mono-disperse (Figure 4.8). Some larger particles are seen by TEM, these may explain the error seen in the DLS sizing data.

Table 4.2 DLS sizing of all particles coated with DNA and RubpySS used within chapter.
Sizing done on a Malvern Zeta sizer nano ZEN5600 at 2 nM in deionised water.

	Bare AuNP	**P.AF-AuNP-Ru**	**P.1L-AuNP-Ru**	**P.1D- AuNP-Ru**	**l.P.1L-AuNP-Ru**	**P.5L-AuNP-Ru**
Number distribution	12 nm ± 3 nm	14 nm ± 4 nm	14 nm ± 4 nm	14 nm ± 4 nm	16 nm ± 5 nm	15 nm ± 4 nm
Intensity distribution	21 nm ± 6 nm *100%*	40 nm ± 19 nm *97%*	34 nm ± 17 nm *96%*	23 nm ± 9 nm *87%* 286 nm ± 97 nm *10%*	36 nm ± 6 nm *96%*	35 nm ± 16 nm *96%*

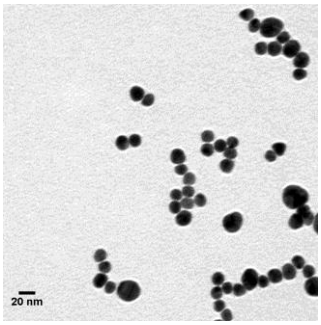

Figure 4.8 TEM image of P.1L-AuNP-Ru.
Imaged using a JEOL 1200 TEM.

Once the particles were purified, it was clear from the UV-vis scan that the anthracene probe and ruthenium probe were present on the particles (Figure 4.9). Again, the relative intensities of the UV scan for the particles cannot be used for accurate concentration calculations; as mentioned in section **3.6.2**.

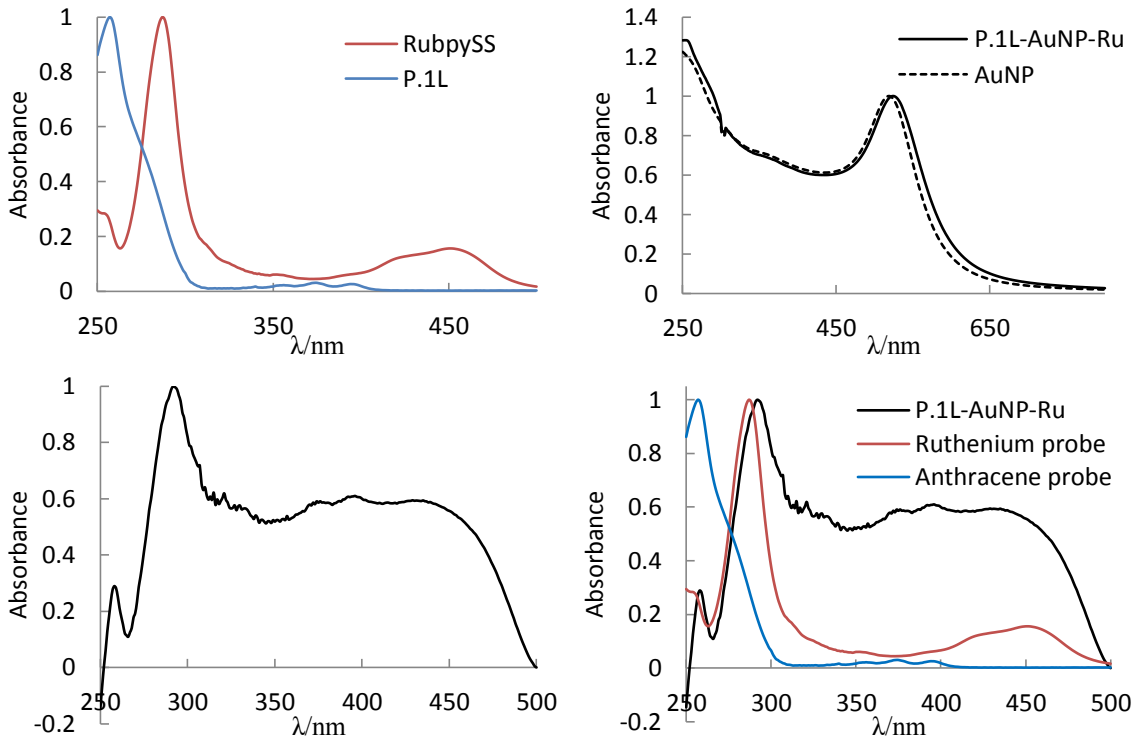

Figure 4.9 UV-vis absorption scan of P.1L-AuNP-Ru showing presence of fluorophores
(a) *UV-vis absorbance spectra for RubpySS (red) and P.1L (blue) in deionised H_2O.* ***(b)*** *UV-vis absorption scan of 2nMcitrate coated AuNP (dashed) and 2 nM* ***P.1L-AuNP-Ru*** *after purified through Sephadex G-50 column (line).* ***(c)*** *UV-vis absorption spectrum of* ***P.1L-AuNP-Ru*** *once a scan of 2 nM citrate coated AuNP is subtracted from it, showing the presence of both P.1L and RubpySS probes.* ***(d)*** *Overlay of graph (a) and graph (c) showing presence of fluorophores.*

The MLCT absorption band appears slightly distorted, although this can be attributed to the shift in the SPR of the particles when they are coated affecting the background subtraction, however it is clearly present in the excitation scan of the isolated particles (Figure 4.10).

The emission of the **P.1L-AuNP-Ru** particles was assessed by inspecting both the anthracene and ruthenium emission (Figure 4.10). Comparing their emission intensities, the anthracene was much more emissive than the ruthenium probe. ICP-MS showed that the number of ruthenium complexes coating the particles was of the order of 100's (150-400) (section **7.2**) which is ten times lower than was found for previous ruthenium coatings,[16] although this might be expected as only a 1000 times excess could be added to the particles, which also explains the relatively low emission counts for the ruthenium.

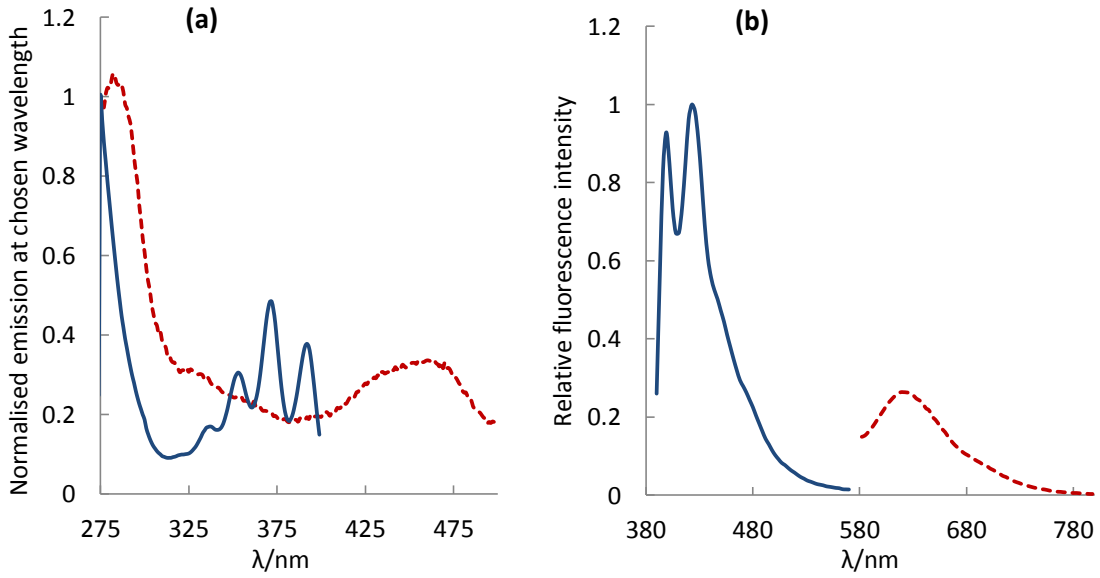

Figure 4.10 Excitation and emission spectrum for P.1L-AuNP-Ru
(a) *Excitation spectrum of* ***P.1L-AuNP-Ru,*** *(Blue, full) Anthracene probe excitation spectrum, λ_{em} = 426 nm (Red, dash) RubpySS probe, λ_{em} = 630 nm.* ***(b)*** *Emission spectrum of* ***P.1L-AuNP-Ru****. (Blue, full) anthracene probe, λ_{ex} = 350 nm. (Red, dash) RubpySS probe, λ_{ex} = 465 nm. 2 nM* ***P.1L-AuNP-Ru*** *in deionised water with 10 mM pH 7.0 phosphate buffer, 100 mM NaCl at room temperature. Slit widths for anthracene: excitation = 5 nm, emission = 10 nm. Slit widths for RubpySS: excitation = 15 nm, emission = 15 nm.*

4.3 SNP sensing AuNPs containing RubpySS

Initially, it had to be established whether the anthracene probe was still able to detect SNPs when the ruthenium probe was also bound to the AuNP. The SNP sensing was tested using the **P.1L** probe and also the **P.1D** probe (Table 4.1), when bound to AuNPs with the RubpySS also attached to the particles. The variation in the anthracene emission upon the addition of **DNA-T.1** and **DNA-T.2** was then plotted as a percentage change in

Figure **4.11**.

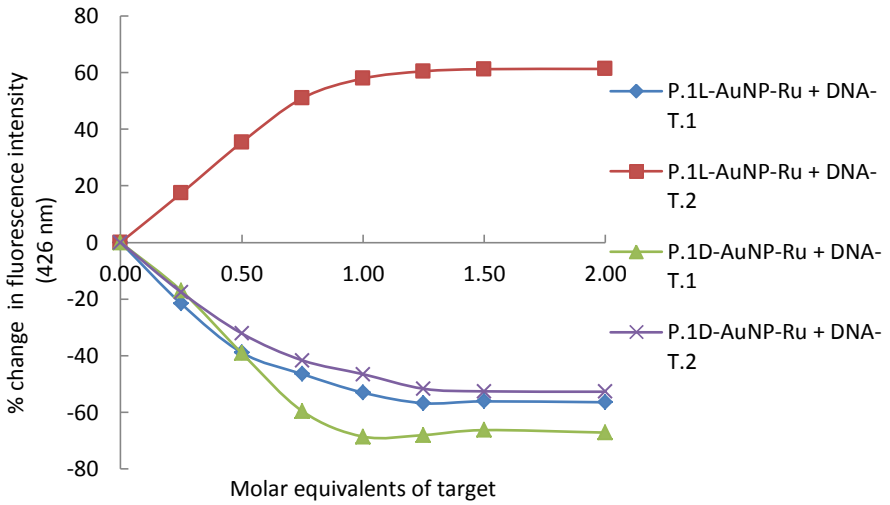

	P.1L-AuNP-Ru	P.1D-AuNP-Ru	P.1L-AuNP	P.1D-AuNP
DNA-T.1	-66	-71	-66	-65
DNA-T.2	+65	-63	+98	-59

Figure 4.11 SNP sensing for 1L-AuNP-Ru and 1D-AuNP-Ru
*Percentage change in anthracene emission for AuNP coated with anthracene probe and also ruthenium probe (**P.1L-AuNP-Ru/ P.1D-AuNP-Ru**). **DNA-T.1** is fully complementary target, whilst **DNA-T.2** contains single base mismatch. Each point indicates the addition of target. 2 nM AuNP sample in deionised water with 10 mM pH 7.0 phosphate buffer, 100 mM NaCl at room temperature. Table of percentage change in anthracene emission at 426 nm upon addition of target.*

It was clear that the anthracene probe was still able to detect SNP targets; with the response of the anthracene emission being the same as previously seen in Section **3.8.1**. The anthracene emission intensity increases for 1L + mismatch whilst all other combinations show a decrease. However, the percentage increase in anthracene emission for the **P.1L** + **DNA-T.2** duplex was lower than expected. Previously (Section **3.8.1**), it was found that the **P.1L-AuNP** + **DNA-T.2** duplex showed an increase of 98%. However, the result of the **P.1L-AuNP-Ru** + **DNA-T.2** duplex only showed a 65% increase in anthracene emission at 426 nm. Comparing the variation in emission intensity of the anthracene probe for the probe alone (**P.1L** = +89%), the probe bound to AuNPs (**P.1L-AuNP** = +98%) and the probe bound to AuNPs with RubpySS (**P.1L-AuNP-Ru** = +67%) it is evident that the 1L mismatch duplex (**1L + DNA-T.2**) is sensitive to its environment. We know that the anthracene probe once in duplex form, is still a dynamic system, shown by the anthracene having 3 lifetimes.[17] The **1L + DNA-T.2** duplex has the lowest T_m of the tested strands; therefore it will be most susceptible to a change in the surrounding environment. The number of anthracene probes bound to the AuNP was calculated once more from the titration experiments, giving 230 anthracene probes bound to each AuNP, which is lower than the 360 anthracene probes per AuNP calculated previously (section **3.8.1**).

Once it was established that the anthracene probe was still able to differentiate between the two SNP variants, the response of the RubpySS was investigated.

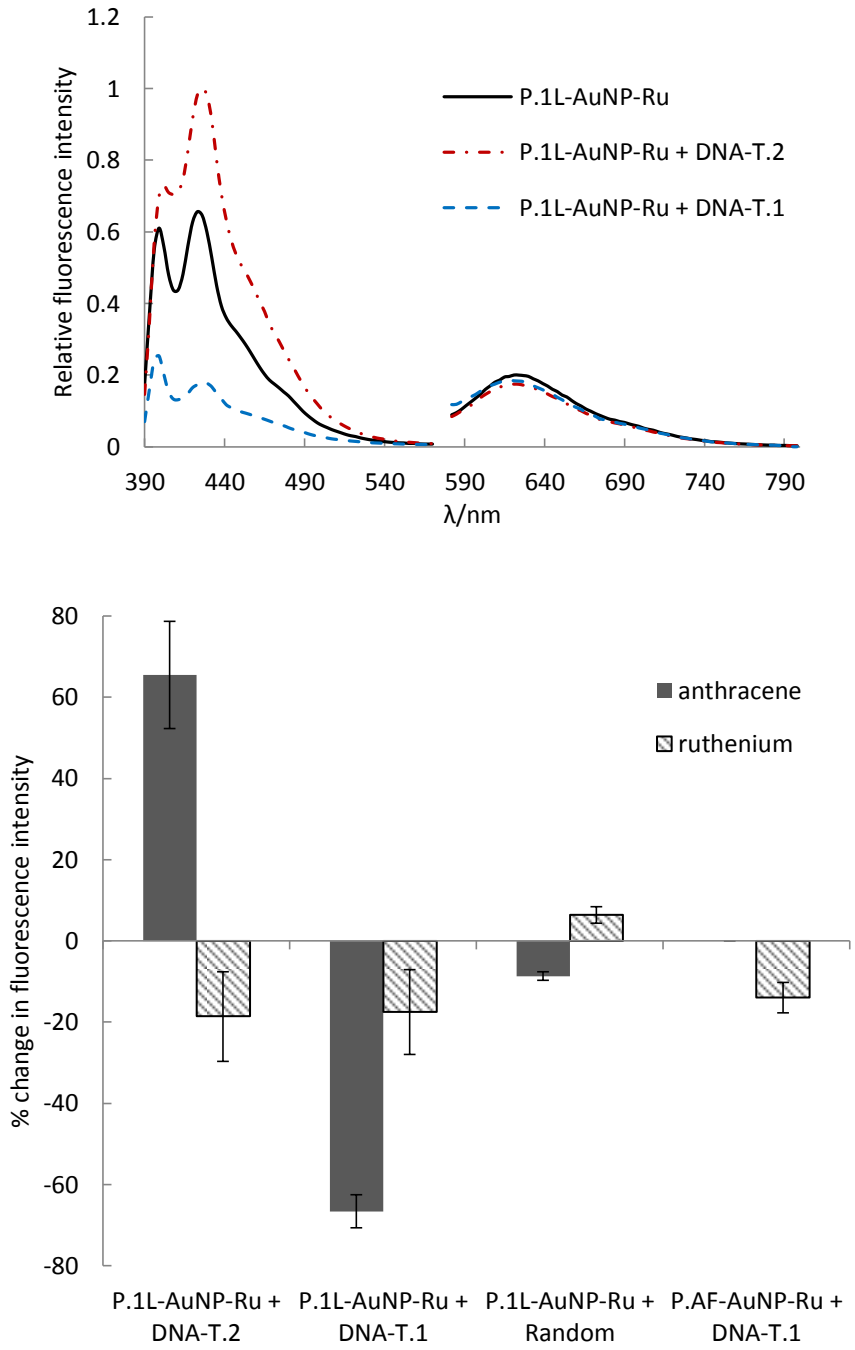

Figure 4.12 Anthracene and ruthenium emission response upon duplex formation for P.1L-AuNP-Ru and P.NA-AuNP-Ru.

*(Top) Emission of **P.1L-AuNP-Ru** probe before (dashed black) and after addition of **DNA-T.1** (blue) and **DNA-T.2** (red).(Below) Percentage change in emission for anthracene (grey) and ruthenium (dashed line) probes after the addition of SNP targets: fully complementary **DNA-T.1** and single mismatch **DNA-T.2**, and also random target. Error bars indicate the standard deviation of three independent repeats. All AuNP samples ran at 2 nM in deionised water with 10 mM pH 7.0 phosphate buffer, 100 mM NaCl at room temperature. Anthracene signal (λ_{ex} = 350 nm λ_{em} = 426 nm, slit widths excitation = 5 nm, emission = 10 nm), ruthenium signal (λ_{ex} = 465 nm λ_{em} = 630 nm, slit widths excitation = 15 nm, emission = 15 nm).*

The addition of target strands induced a decrease in the RubpySS emission centred at 630 nm. Figure 4.12 shows the percentage change in emission for the RubpySS (dashed bar) alongside the anthracene change in emission (grey bar), a table of the values is found in **7.2.1**. However, whilst there is a decrease in emission, it appears to be a constant decrease. Upon duplex formation, regardless of SNP target, the RubpySS emission decreases by 20%. This ruthenium decrease trend was also seen for the **P.1D-AuNP-Ru** (shown in **7.2.2**). It appears that the decrease in emission is not a result of any interference between the anthracene and the ruthenium probes, as the drop in ruthenium emission is still seen when the particles are coated in anthracene free probe strand (far right, **P.AF-AuNP-Ru** + **DNA-T.1**, Figure 4.12).

Investigating the effect of adding a random DNA target to **P.1L-AuNP-Ru** gives an insight into what may be causing the reduction in ruthenium emission. The random target does not bind to the SNP sensing probe, as evidenced by the lack of a T_m and there being no change in anthracene emission upon its addition, except for dilution effect (section **3.8.1**). For the addition of this strand, the ruthenium emission does not decrease (giving in fact a slight increase of 6%); this would suggest that the formation of a duplex upon the surface of the AuNP may be causing this reduction in ruthenium emission. This in itself is an interesting result as it appears that the ruthenium is able to sense the presence of target DNA binding to the anthracene probe. This would be a very useful property for detecting the presence of a particular DNA strand *in vitro* regardless of its SNP identity, and would be especially useful for the base opposite SNP sensing system (discussed later in section **4.3.3**).

The reason for this observed decrease in ruthenium emission is thought to be due to a change in the environment surrounding the RubpySS upon duplex formation. This could be a consequence of duplex DNA having a more rod-like structure than the more flexible single stranded form. When the AuNP surface is less densely coated with DNA (**P.1L-AuNP-Ru** coated in less DNA than **P.1L-AuNP**) in its single stranded form, the anthracene has more flexibility and may therefore partially conceal the ruthenium from quenching molecules from the medium. The decrease in emission of the RubpySS upon duplex formation, was consistent for all targets making it relatively straightforward to standardise the emission of the anthracene probe. This was done by dividing the anthracene signal at 426 nm by the ruthenium signal at 630 nm, giving a ratio which would then indicate the identity of the base in the SNP (Figure 4.13).

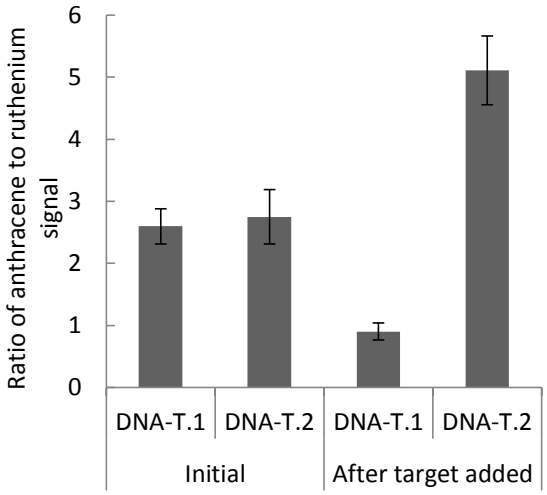

Figure 4.13 Ratio of anthracene to ruthenium signal upon target addition to P.1L-AuNP-Ru
*Ratio of anthracene to ruthenium emission for the **P.1L-AuNP-Ru** before (left) and after (right) the addition of the SNP targets: fully complementary **DNA-T.1** and single mismatch **DNA-T.2**. Error bars are the standard deviation of 6 independent repeats. 2 nM AuNP samples in deionised water with 10 mM pH 7.0 phosphate buffer, 100 mM NaCl at room temperature. Anthracene signal (λ_{ex} = 350 nm λ_{em} = 426 nm, slit widths excitation = 5 nm, emission = 10 nm), ruthenium signal (λ_{ex} = 465 nm λ_{em} = 630 nm, slit widths excitation = 15 nm, emission = 15 nm).*

There are errors in the initial ratio which then continue into the final ratio; these are associated with variations in coating of the particles and with the concentration of the particles, as discussed earlier in Section **3.6**. With each new batch of **P.1L-AuNP-Ru** synthesised, a slightly different ratio of anthracene: ruthenium signal is observed, caused by variation in coating levels as experimental error (error bars on the initial readings for Figure 4.13). However, the error in the final ratio measurement can be reduced by normalising each new batch of synthesised **P.1L-AuNP-Ru** to its own initial anthracene: ruthenium emission ratio. The result of this approach using six separate and freshly prepared samples is shown in Figure 4.14.

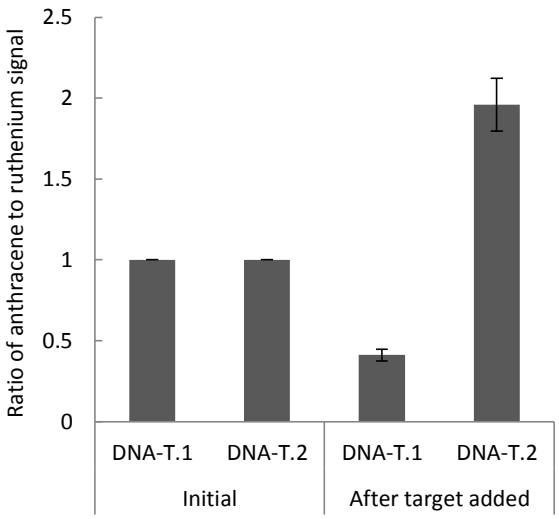

Figure 4.14 Normalised ratio of anthracene to ruthenium emission upon target addition
*Ratio of anthracene to ruthenium emission for the **P.1L-AuNP-Ru** before (left) and after (right) the addition of the SNP targets: fully complementary **DNA-T.1** and single mismatch **DNA-T.2**. Each measurement is normalised to the initial anthracene: ruthenium ratio for the batch of particles made. Error bars are the standard deviation of 6 independent repeats. 2 nM **P.1L-AuNP-Ru** in deionised water with 10 mM pH 7.0 phosphate buffer, 100 mM NaCl at room temperature. Anthracene signal (λ_{ex} = 350 nm λ_{em} = 426 nm, slit widths excitation = 5 nm, emission = 10 nm), ruthenium signal (λ_{ex} = 465 nm λ_{em} = 630 nm, slit widths excitation = 15 nm, emission = 15 nm).*

It is clear that using this ratiometric system allows the detection of different SNP variants without the requirement for a baseline emission level for each experiment. Upon

synthesising a new batch of anthracene/RubpySS coated AuNP, a ratio of the anthracene to RubpySS signal can be measured, this ratio can then be used for all subsequent experiments using this batch. If the ratio when normalised doubles then the mismatching CA base pair is present; however if the ratio halves, then the matching CG base pair is present. Not requiring a baseline emission level for each experiment overcomes the problem of being able to only take a single measurement of the anthracene emission when detecting SNP targets within cells. To overcome this previously,[8] the anthracene probe was inserted into cells that did not contain any of the target sequence; this emission could then be taken as the baseline level. However for real targets, the cells treated will all contain the target sequence, with the only difference being which SNP variant is produced. The ratiometric sensing also overcomes the problem of the variation in cell uptake of the probe. As long as there is surplus target to probe, the ratio of the anthracene to ruthenium signal measured will give an accurate reading for what SNP is present in each cell.

4.3.1 Comparing P.1L-AuNP-Ru and l.P.1L-AuNP-Ru

Notwithstanding the evidence that variations in the surrounding environment led to the decrease in the ruthenium emission, the potential for additional processes was investigated. Excited state processes such as Förster Resonance Energy Transfer (FRET) and Photoinduced Electron Transfer (PET) could also contribute to the decrease in emission of the ruthenium probe and the slight difference in the anthracene response in its presence.[18] Initial fluorescence studies confirmed that there was no emission of the ruthenium probe upon anthracene excitation (350 nm), indicating no FRET. To investigate if any other energy transfer was occurring, differences in the emission properties of **P.1L-AuNP-Ru** compared to

l.P.1L-AuNP-Ru were investigated. The difference in distance between the anthracene and the ruthenium with the **l.P.1L-AuNP-Ru** and the **P.1L-AuNP-Ru** is 10 bases, equating to 3.4 nm, if the DNA is assumed to be fully extended (Figure 4.15). This increased distance between the ruthenium and anthracene probe should greatly reduce any energy transfer effects, as these are highly distance dependent.[19]

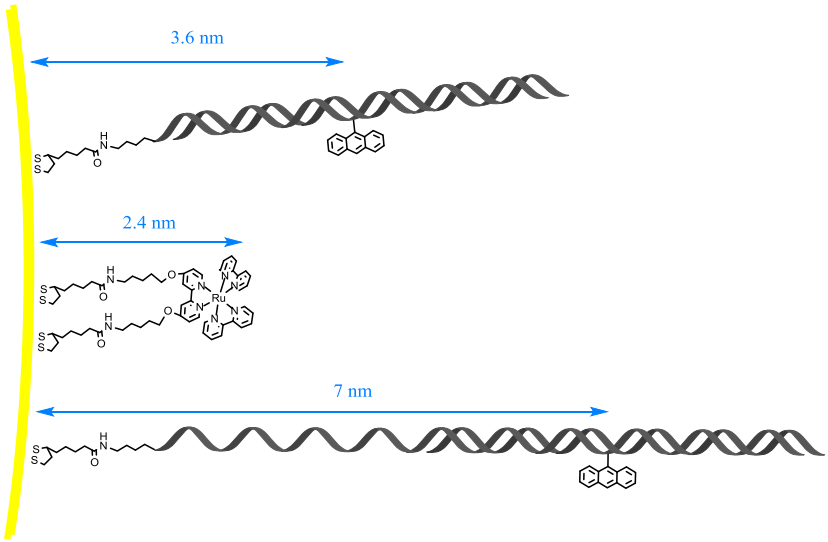

Figure 4.15 Estimated distances from AuNP surface of P.1L, l.P.1L and the RubpySS probe.

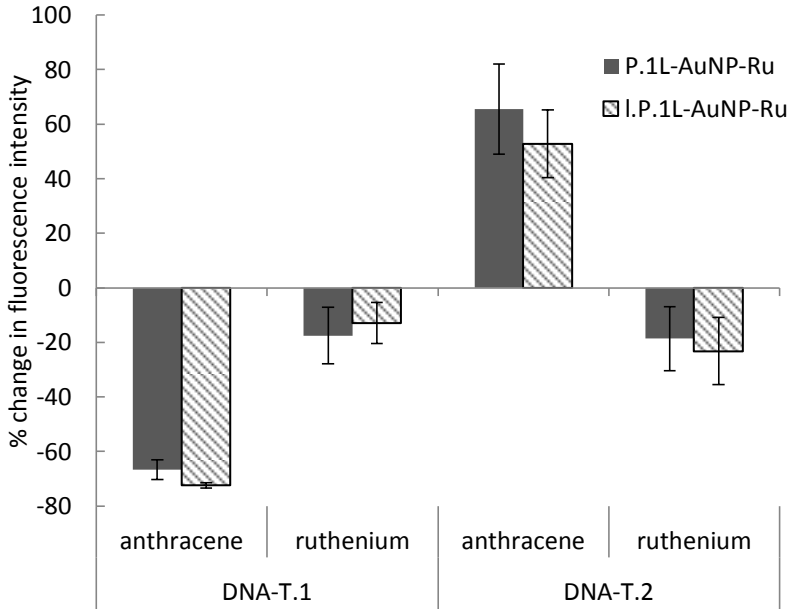

Figure 4.16 Comparing anthracene and ruthenium emission response upon target addition for P.1L-AuNP-Ru and l.P.1L-AuNP

*Chart showing the percentage change in emission for anthracene and ruthenium emission for the **P.1L-AuNP-Ru** (dark grey) and the **l.P.1L-AuNP-Ru** (dashed line) after the addition of the SNP targets: fully complementary **DNA-T.1** and single mismatch **DNA-T.2**. Error bars are the standard deviation of 3 repeats, each repeat is with a fresh preparation of particles. 2 nM AuNP in deionised water with 10 mM pH 7.0 phosphate buffer, 100 mM NaCl at room temperature. Anthracene signal (λ_{ex} = 350 nm λ_{em} = 426 nm, slit widths excitation = 5 nm, emission = 10 nm), ruthenium signal (λ_{ex} = 465 nm λ_{em} = 630 nm, slit widths excitation = 15 nm, emission = 15 nm)*

Plotting the percentage change in emission for both the anthracene and ruthenium probes suggests that there is no significant difference in percentage emission change between the longer **l.P.1L-AuNP-Ru** and the shorter **P.1L-AuNP-Ru** upon duplex formation (Figure 4.16), a t-test confirms this (**7.2.3**). Results when integrating the emission of both fluorophores gave similar results see Section **7.2.4**. This would suggest that there is no energy transfer between the two fluorophores, as the differences in distance between the two fluorophores has little effect on their relative emission intensities. Comparing the ratio of anthracene to ruthenium signal also indicates there is no difference in emission levels between the longer and shorter anthracene probes (Figure 4.17).

The errors for the anthracene probe emission changes when binding to **DNA-T.1** are consistently smaller than for the **DNA-T.2** target, regardless of the distance the anthracene probe is from the AuNP surface. This is apparent in the data for Figure 4.17 and Section **7.2.2**. This could be attributed to differences in T_m with the anthracene tag more dynamic and more sensitive to subtle environmental changes in the mismatched complex.

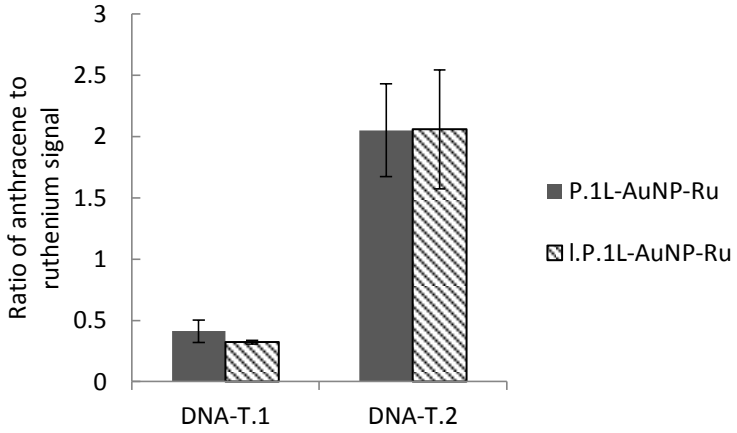

Figure 4.17 Comparing the ratio of anthracene to ruthenium signals for P.1L-AuNP-Ru and l.P.1L-AuNP-Ru

*Chart showing the ratio of anthracene to ruthenium signals for the **P.1L-AuNP-Ru** (dark) and **l.P.1L-AuNP-Ru** (dashed fill) after the addition of the fully complementary target **DNA-T.1** (left) and the single mismatch target **DNA-T.2** (right). Each measurement is normalised to the initial anthracene: ruthenium ratio for the corresponding batch of particles made. Error bars are the standard deviation of 6 repeats for **P.1L-AuNP-Ru** and 3 repeats for **l.P.1L-AuNP-Ru**, each repeat is with a fresh preparation of particles. 2 nM AuNP in deionised water with 10 mM pH 7.0 phosphate buffer, 100 mM NaCl at room temperature. Anthracene signal (λ_{ex} = 350 nm λ_{em} = 426 nm, slit widths excitation = 5 nm, emission = 10 nm), ruthenium signal (λ_{ex} = 465 nm λ_{em} = 630 nm, slit widths excitation = 15 nm, emission = 15 nm)*

4.3.2 Single wavelength excitation of both anthracene and RubpySS

As the SNP sensing probe was developed to improve cell-based DNA detection, consideration had to be given for its use as a cell sensing probe. It was proposed that to further improve the usability of the probe *in vitro*, it would be useful if both fluorophores could be excited with the same wavelength of light to speed up and simplify sample analysis.

The ruthenium probe has another absorption band at 290 nm, which is assigned to the LC π → π* transition[20] (Figure 4.9). The excitation scan of anthracene confirmed it could be excited at 290 nm (Figure 4.10). Therefore the SNP sensing was repeated by exciting at this wavelength (Figure 4.18).

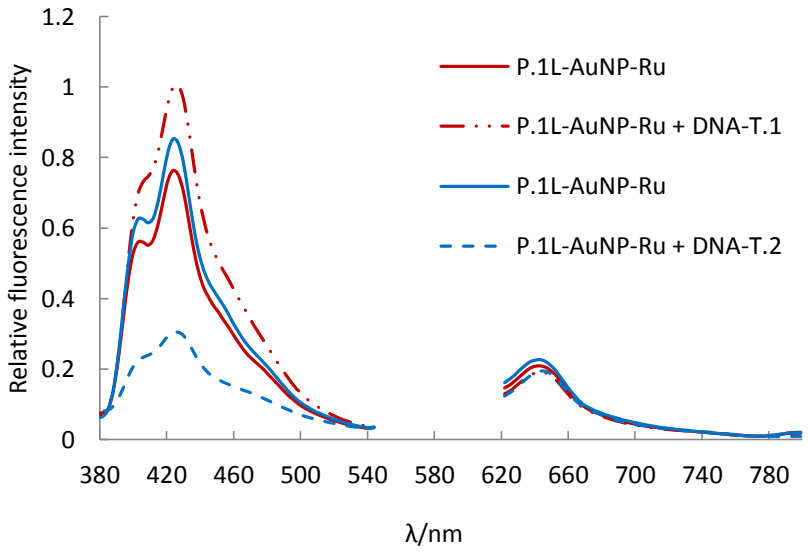

Figure 4.18 Anthracene and ruthenium emission response upon addition of SNP targets for P.1L-AuNP-Ru when excited at 290 nm

Emission scans for anthracene probe and ruthenium when excited at 290 nm. Dashed lines indicate initial emission levels before addition of targets. Blue line is ***P.1L-AuNP-Ru*** *+ fully complementary* ***DNA-T.1*** *whilst redline is* ***P.1L-AuNP-Ru*** *+ single mismatch* ***DNA-T.2****. 2 nM AuNP in deionised water with 10 mM pH 7.0 phosphate buffer, 100 mM NaCl at room temperature. Anthracene signal (λ_{ex} = 290 nm λ_{em} = 380-550 nm, slit widths excitation = 10 nm, emission = 10 nm), ruthenium signal (λ_{ex} = 290 nm λ_{em} = 620-800 nm, slit widths excitation = 10 nm, emission = 10 nm).*

A problem which was immediately obvious was the appearance of a major peak at 580 nm. This peak is a result of the highly scattering nature of AuNP samples,[21] some of the excitation wavelength (290 nm) is scattered at 90° and appears as second order diffraction on the detector at 580 nm. The scan therefore had to be done in two separate collections, 380-540 nm then 620-800 nm.

Table 4.3 Percentage change for P.1L-AuNP-Ru upon addition of target when excited at 290 nm
Percentage change for probes upon excitation at 290 nm. 2 nM AuNP in deionised water with 10 mM pH 7.0 phosphate buffer, 100 mM NaCl at room temperature.

	% anthracene emission change		% ruthenium emission change		Ratiometric sensing	
	DNA-T.1	**DNA-T.2**	**DNA-T.1**	**DNA-T.2**	**DNA-T.1**	**DNA-T.2**
P.1L-AuNP-Ru	- 65	+ 30	- 16	- 15	0.42	1.52

Whilst the anthracene probe retains the ability to distinguish between the two targets, the percentage increase with the mismatch target (**DNA.T-2**) is not as great as previously seen. This may be due to photoexcitation in a region where the DNA molecules absorb; therefore alternative photo-processes may be occurring. However, this is only a preliminary result and further investigation is required.

Whilst the wavelength used (290 nm) is not well suited for cell imaging due to auto fluorescence and possible damage to other biomolecules including DNA, it does however provide a proof of concept that a single excitation could reveal the SNP identity and standardise it. The use of only one wavelength of light is also beneficial for use in cuvette samples as this would speed up throughput.

4.3.3 Base opposite SNP sensing plus ruthenium

It was decided to investigate whether the ratiometric SNP sensing set up could be applied to the base-opposite SNP sensing system. An additional incentive was that the response of the ruthenium probe could provide a useful tool for detecting duplex formation. An issue with the base opposite SNP sensing system, as described in Section **3.8.4**, is that the linear plot crosses the x-axis. At this point, the percentage change in anthracene emission is zero. This

means that in an unknown sample, an alternative explanation to the identification of this particular SNP ratio would be that no target was present at all. However, the observed independent decrease in ruthenium emission upon duplex formation as shown in Section **4.3**, would in principle indicate that the anthracene probe was indeed hybridised to a target. It does however need to be noted that this would still require an initial reading of the ruthenium signal, therefore making this a solution only for cuvette studies of unknown samples in which probe uptake by the cell is not an issue.

Table 4.4 Strands synthesised for base opposite system
W = thioctic acid modification. X = 5L anthracene probe modification.

Strand name	Strand sequence
UM.P	5' AGT CGC G**X**C TCA GCT 3'
P.5L	5' **W**- AGT CGC G**X**C TCA GCT 3'
DNA-T.3	5' AGC TGA GAC GCG ACT 3'
DNA-T.4	5' AGC TGA G**C**C GCG ACT 3'

The particles were coated with the **P.5L** probe (the strands used are repeated in Table 4.4; (**UM.P** probe strand without disulphide modification, **P.5L** = probe strand containing 5L anthracene unit with disulphide modification, **DNA-T.3** = Target containing A base opposite, **DNA-T.4** = Target containing C base opposite) before adding the ruthenium probe in the same way as described in Section **4.2**. The particles were again purified through a Sephadex G-50 column, eluting with deionised water. They were then tested to show that the presence of the ruthenium probe did not affect the linear response of the anthracene probe for the base opposite system.

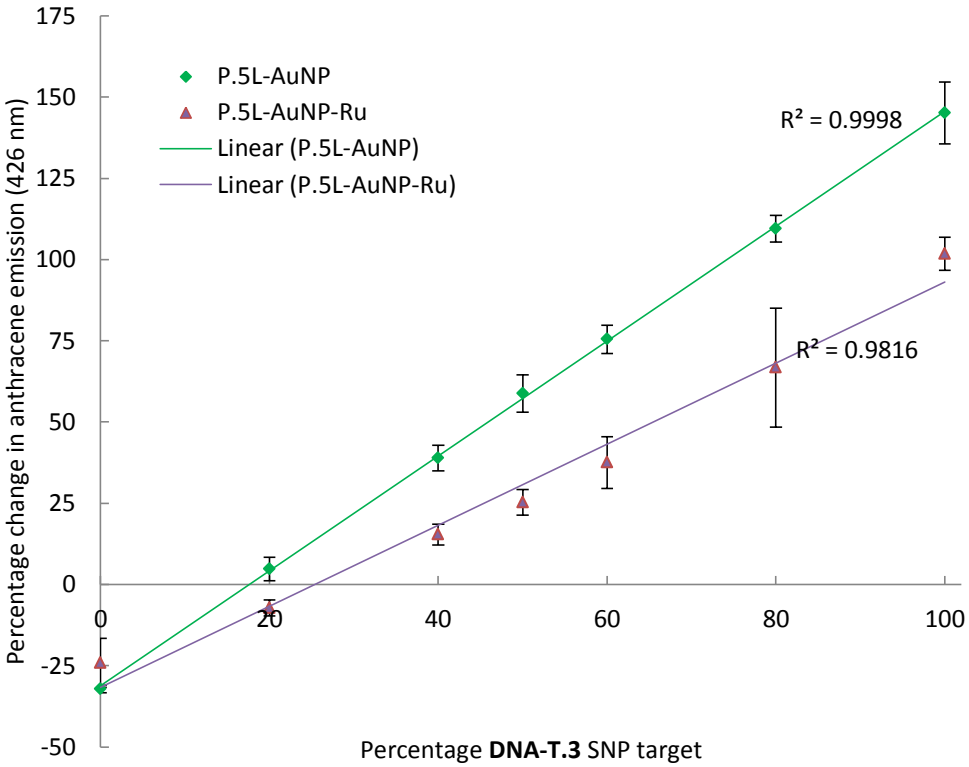

Figure 4.19 Overlaying response of P.5L-AuNP-Ru and P.5L-AuNP upon duplex formation when percentage make up of SNP targets is varied
*(Purple diamonds) Percentage variation in anthracene signal (426 nm) for **P.5L-AuNP-Ru** particles once probe is fully hybridised with target. (Green diamonds) For comparison, percentage variation in anthracene signal (426 nm) for **P.5L-AuNP** particles once probe is fully hybridised with target. Percentage of the targets containing A (**DNA-T.3**) or C (**DNA-T.4**) SNP variant on x-axis. Error bars are standard deviation of three repeats.2 nM AuNP in deionised water with 10 mM pH 7.0 phosphate buffer, 100 mM NaCl at room temperature.*

Figure 4.19 clearly shows that the emission of the anthracene probe still displays the linear relationship when exposed to different percentages of the A and C SNP targets for the **P.5L-AuNP-Ru**. When comparing the anthracene response for particles with (purple, Figure 4.19) and without (green, Figure 4.19) the ruthenium probe, there are evident differences. For the **P.5L-AuNP-Ru** the change in emission of the anthracene is again diminished when compared to **P.5L-AuNP** (for integrated emission see Section **7.2.4**). With 100% **DNA-T.3** SNP variant, the anthracene emission increases by 102%, compared to an increase of 145% seen for the

same target when the particles are coated in solely anthracene probe. This is also lower than the percentage increase seen for the **P.5L** probe alone of 140%.[22] Again this may be explained as discussed earlier (section **4.3.1**) by changes in the surrounding environment of the anthracene probe caused by the presence of the ruthenium complex or by changes in distance between neighbouring probes.

The emission of the ruthenium probe in **P.5L-AuNP-Ru** however, does not have the same response as it does for **P.1L-AuNP-Ru**. As described earlier (section **4.3.1**) the response of the ruthenium probe to duplex formation for **P.1L-AuNP-Ru** was a consistent decrease in emission of 20%. For the **P.5L-AuNP-Ru** however, there appears to be no consistent response of the ruthenium (Figure 4.20). In fact within error, there is no difference in ruthenium emission upon duplex formation.

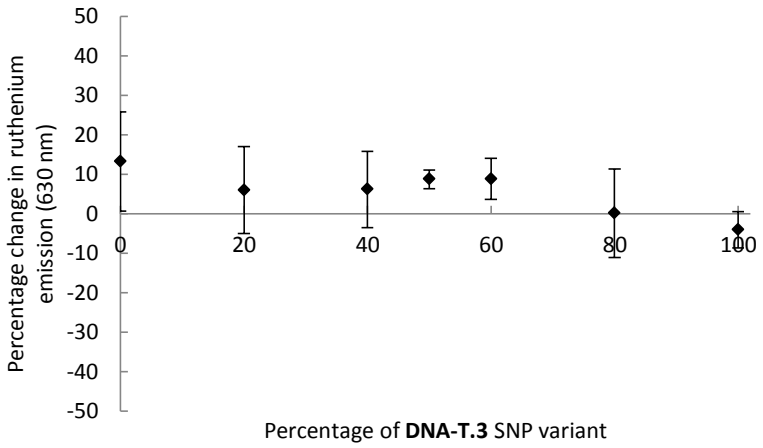

Figure 4.20 Ruthenium emission response upon duplex formation in base opposite system
*Percentage variation in ruthenium emission for **P.5L-AuNP-Ru** particles once probe is fully hybridised with target. Percentage of the target containing A (**DNA-T.3**) or C (**DNA-T.4**) SNP variant on x-axis. Error bars are 1 standard deviation of three repeats.2 nM AuNP in deionised water with 10 mM pH 7.0 phosphate buffer, 100 mM NaCl at room temperature. λ_{ex} = 465 nm λ_{em} = 630 nm, slit widths excitation = 15 nm, emission = 15 nm.*

The reason for this lack of response from the ruthenium complex upon duplex formation may be associated with the reason why a response is seen for the **P.1L-AuNP-Ru** system. In this case, there may be no change in the surrounding environment of the RubpySS upon duplex formation; therefore its emission intensity is retained. There are two major differences between the **P.5L-AuNP-Ru** and the **P.1L-AuNP-Ru** which may help with this explanation; the first is that the anthracene tag in the probe is different, 5L vs 1L, the 5L probe having more flexibility compared to the 1L probe due to its longer carbon linker (Section **6.1.4**). However, the distances between the anthracene tag and the ruthenium complex means that it is unlikely that a relatively small change in the linker length would affect the environment surrounding the ruthenium. The other difference between the **P.5L-AuNP-Ru** and **P.1L-AuNP-Ru** is the DNA sequences of the probes and their targets. The difference in the environment of the ruthenium complex going from the single stranded form to the duplex form must be more marked for **P.1L-AuNP-Ru** than **P.5L-AuNP-Ru.** Further investigations need to be done; if the effects are still observed when the anthracene linkers are changed in each sequence, then any potential effects caused by variations in the linker length can be dismissed.

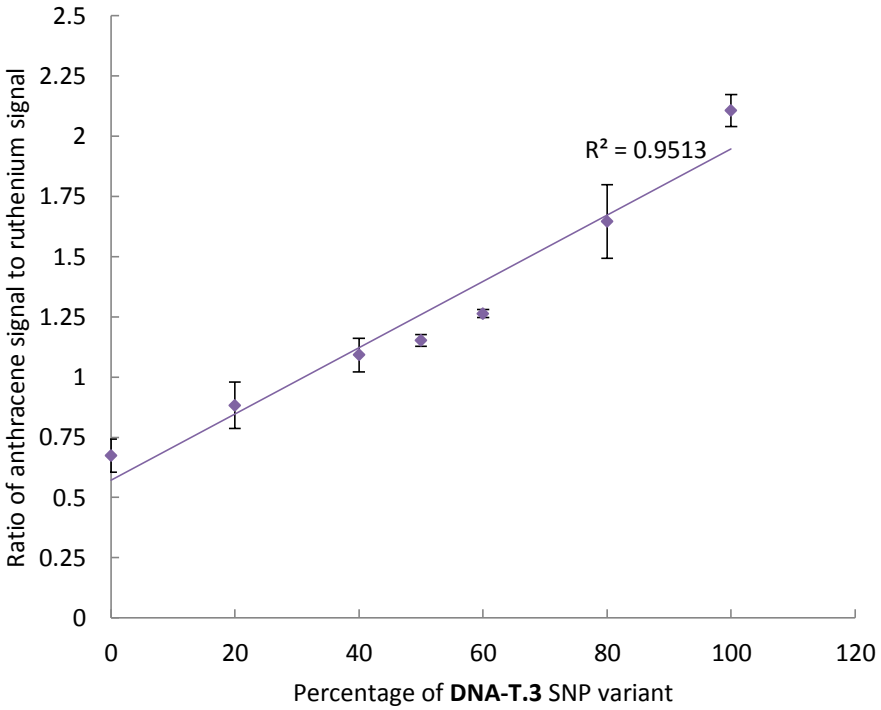

Figure 4.21 Ratiometric sensing for base opposite system
*Ratio of anthracene signal (λ_{ex} = 350 nm λ_{em} = 426 nm, slit widths excitation = 5 nm, emission = 10 nm)/ruthenium signal (λ_{ex} = 465 nm λ_{em} = 630 nm, slit widths excitation = 15 nm, emission = 15 nm) for **P.5L-AuNP-Ru** particles once probe is fully hybridised with target. Percentage of the targets containing A (**DNA-T.3**) or C (**DNA-T.4**) SNP variant on x-axis. Error bars are 1 standard deviation of three repeats. 2 nM AuNP in deionised water with 10 mM pH 7.0 phosphate buffer, 100 mM NaCl at room temperature.*

Plotting the ratio of the anthracene signal against the ruthenium signal showed that the linear relationship was still present when using the ratiometric method for signal output (Figure 4.21). This indicates that this **5L-AuNP-Ru** probe could be suitable for sensing the percentage transcription of two SNP variants within a cell, whilst overcoming the problem of variations in cell uptake. However due to the lack of RubpySS response, it does not overcome the problem regarding the 0% anthracene emission response.

4.4 Cell uptake of DNA-Ru-AuNP

It had to be assessed whether the presence of the ruthenium probe inhibited the ability of a cell to take up these particles. Following the same protocol as for the **P.1L-AuNP** particles, 100 nm particles were coated in the anthracene and ruthenium probes. They were then purified by spinning down and redispersing in MilliQ water. The particles were added to the cells at a concentration of 4 pM in 10 mM phosphate buffer and 100 mM NaCl at pH 7.0. The cells were treated for 2 hours with the 100 nm **P.1L-AuNP-Ru** before washing, fixing and then imaged by reflectance confocal microspcopy. Imaging cross sectional slices of the cells allows it to be established whether the particles are uptaken by the cell or stick to the outer membrane.

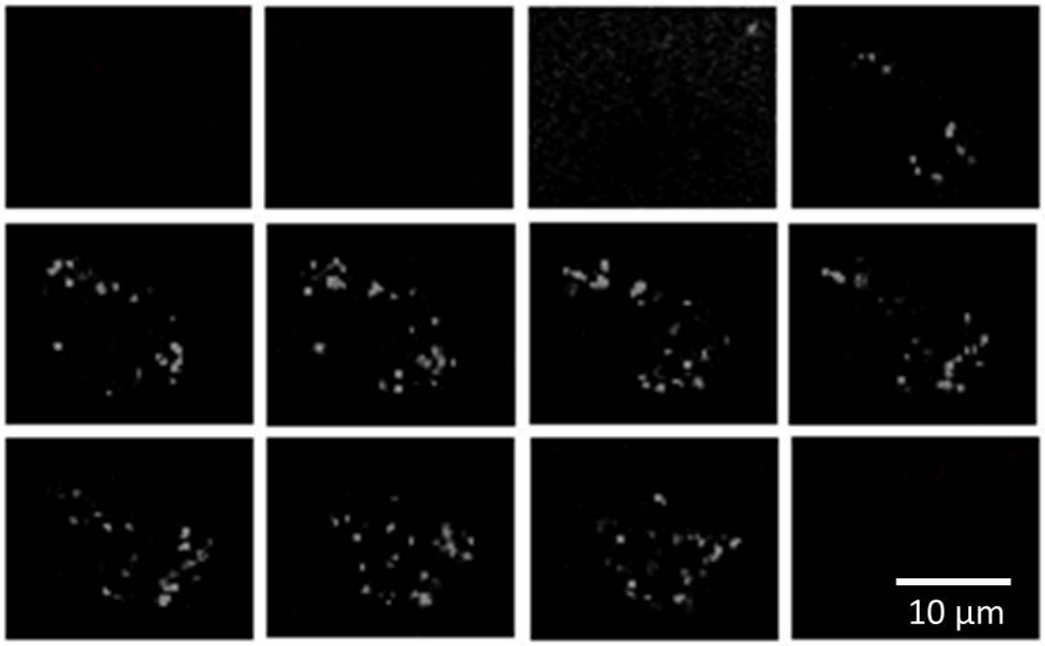

Figure 4.22 Reflectance microscopy images of 100 nm 1L-AuNP-Ru uptake by CHO cells
*Z-stack of reflectance microscopy images showing slices of CHO cell treated with 4 pM **P.1L-AuNP-Ru** 100 nm. Images taken after cells treated for 2 hours. Slices taken at 0.24 µM intervals. Red spots indicate reflectance from particles. Images taken on a Leica SP2 inverted confocal microscope using a 100 x objective lens.*

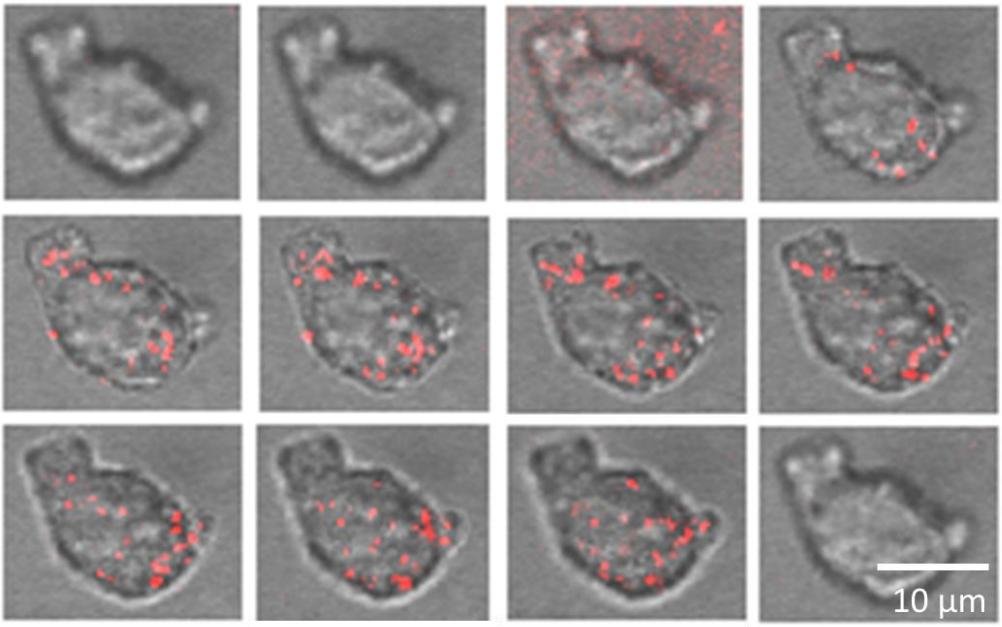

Figure 4.23 Overlaying reflectance and transmission images to show cell uptake of 100 nm 1L-AuNP-Ru

*Z-stack overlaying reflectance and transmission microscopy images showing slices of CHO cell treated with 4 pM **P.1L-AuNP-Ru** 100 nm. Images taken after cells treated for 2 hours. Slices taken at 0.24 µM intervals. Red spots indicate reflectance from particles. Images taken on a Leica SP2 inverted confocal microscope using a 100 x objective lens.*

As was found earlier with the **P.1L-AuNP** (Section **3.9**) the particles appear to be up taken by the CHO cells, indicating that the presence of the ruthenium does not inhibit the particles

uptake (for bright field images see Section **7.2.8**). In

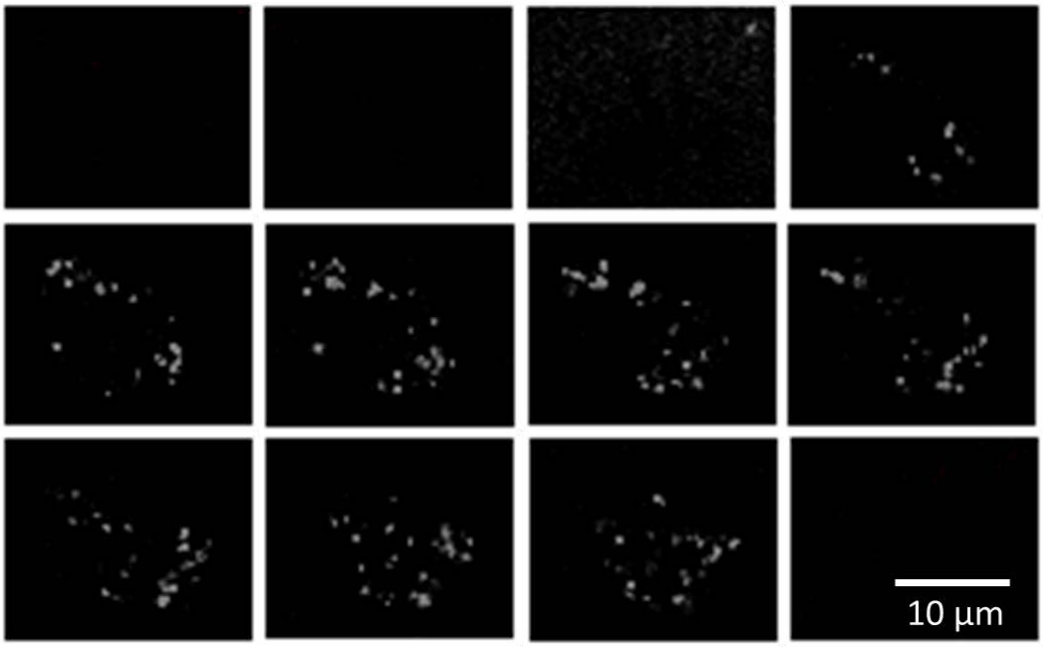

Figure 4.22 Figure 4.22 the white dots are the 100 nm particles, imaging above and below the cell shows that they are within the cell. Figure 4.23 confirms that the cells are within the boundaries of the cell. Imaging the uptake of 13 nm particles was attempted; however the ruthenium probe was not emissive enough to be observed within the cell. This is expected when the low emission counts from the ruthenium on **P.1L-AuNP-Ru** (Figure 4.10) are considered. To overcome this, a zonyl surfactant layer could be used to coat the AuNP, which has been previously shown to enhance the emission of a similar ruthenium probe.[13]

4.5 Conclusions and future work

The work has shown that a ruthenium probe can be bound alongside the anthracene probe onto a AuNP surface. For the base-adjacent and base opposite systems respectively, the probe reacts in a consistent manner upon duplex hybridisation. This has allowed for the major issues regarding the anthracene probe to be overcome. It is now possible for the

percentage variation of the anthracene probe to be calculated when the initial emission level is unknown, i.e. when variation in the uptake of the probe into a cell. Calculating the initial fluorescence ratio of the anthracene and ruthenium probes for a batch of coated AuNPs before adding them into a sample, allows the percentage change in anthracene emission to be calculated by the ratio of the two fluorophores after they have interacted with the targets.

Future work needs to concentrate on increasing the emission of the probes once bound to AuNPs. This could be investigated in a number of ways; the use of a surfactant coating the particles which may lead to an enhancement in the emission of both probes. The use of surfactants have proven to increase the emission of the AuNP bound ruthenium probes,[16] however this has only been done when the particles were used solely as imaging probes, therefore the effects that the surfactant coating may have on sensing is unknown. Also the reaction of the ruthenium probe to hybridisation when a surfactant coating is present may be interesting, considering that the initial hypothesis on its reaction to hybridisation is based upon changes in its surrounding environment.

The ultimate goal is to detect SNPs *in vitro*, this will most probably involve detection of RNA (as discussed in Section **3.8.3**), therefore the SNP sensing of RNA targets should be fully characterised to investigate the response of the ruthenium probe. With probes that have increased emission, the particles could then be used to detect SNPs *in vitro.* If this is possible then it is feasible that real time SNP detection could be attempted, such a process could give an insight into the rate of hybridisation once inside the cell as well as the effect of various triggers on transcription. During this project, plasmids which transcribed the targets for

DNA.T-1 and **DNA.T-2** were integrated into cell lines. These cell lines produce the targets themselves, which would allow the sensing of targets within a cell that are produced by the cell itself.

Regarding the base opposite system discussed in Section **4.3.3**, the differences in the surface environment of the **5L-AuNP-Ru** and the **1L-AuNP-Ru** should be investigated to determine why the RubpySS responds differently upon duplex formation. Investigating different DNA sequences of the probe strands, may also give further insight into the causes of the observed effects.

4.6 References

1. Giljohann, D. a *et al.* Oligonucleotide loading determines cellular uptake of DNA-modified gold nanoparticles. *Nano Lett.* **7,** 3818–21 (2007).
2. Chithrani, B. D., Ghazani, A. a & Chan, W. C. W. Determining the size and shape dependence of gold nanoparticle uptake into mammalian cells. *Nano Lett.* **6,** 662–8 (2006).
3. Patel, P. C. *et al.* Scavenger receptors mediate cellular uptake of polyvalent oligonucleotide-functionalized gold nanoparticles. *Bioconjug. Chem.* **21,** 2250–6 (2010).
4. Hao, Y. *et al.* Exploring the cell uptake mechanism of phospholipid and polyethylene glycol coated gold nanoparticles. *Nanotechnology* **23,** 045103 (2012).
5. Jeynes, J. C. G., Jeynes, C., Merchant, M. J. & Kirkby, K. J. Measuring and modelling cell-to-cell

variation in uptake of gold nanoparticles. *Analyst* 7070–7074 (2013).
6. Snijder, B. & Pelkmans, L. Origins of regulated cell-to-cell variability. *Nat. Rev. Mol. Cell Biol.* **12,** 119–125 (2011).
7. Albanese, A. & Chan, W. C. W. Effect of gold nanoparticle aggregation on cell uptake and toxicity. *ACS Nano* **5,** 5478–89 (2011).
8. Bamford, R. a. Development of fluorophore-tagged DNA probes for cellular imaging applications. (2015).
9. Woodroofe, C. C., Won, A. C. & Lippard, S. J. Esterase-Activated Two-Fluorophore System for Ratiometric Sensing of Biological Zinc (II). *Inorg. Chem.* **44,** 3112–3120 (2005).
10. Zhang, K. *et al.* Instant Visual Detection of Trinitrotoluene Particulates on Various Hybrid Surfaces by Ratiometric Fluorescence of Dual-Emission Quantum Dots Hybrid. *J. Am. Chem. Soc.* **133,** 8424–8427 (2011).
11. Zhu, A., Qu, Q., Shao, X., Kong, B. & Tian, Y. Carbon-dot-based dual-emission nanohybrid produces a ratiometric fluorescent sensor for in vivo imaging of cellular copper ions. *Angew. Chem. Int. Ed. Engl.* **51,** 7185–9 (2012).
12. Prigodich, A. E. *et al.* Multiplexed nanoflares: mRNA detection in live cells. *Anal. Chem.* **84,** 2062–6 (2012).
13. Adams, S. J., Lewis, D. J., Preece, J. a. & Pikramenou, Z. Luminescent gold surfaces for sensing and imaging: Patterning of transition metal probes. *ACS Appl. Mater. Interfaces* **6,** 11598–11608 (2014).
14. Fernandez-Moreira, V., Thorp-Greenwood, F. L. & Coogan, M. P. Application of d6 transition metal complexes in fluorescence cell imaging. *Chem. Commun.* **46,** 186–202 (2010).
15. Baggaley, E., Weinstein, J. A. & Williams, J. A. G. Lighting the way to see inside the live cell with luminescent transition metal complexes. *Coord. Chem. Rev.* **256,** 1762–1785 (2012).
16. Rogers, N. J. *et al.* High coating of Ru(II) complexes on gold nanoparticles for single particle luminescence imaging in cells. *Chem. Commun. (Camb).* **50,** 617–9 (2014).
17. Duprey, J.-L. H. a. Studies On Anthracene Tagged Oligonucleotides. (2010).
18. Clegg, R. M. Fluorescence resonance energy transfer. *Curr. Opin. Biotechnol.* **6,** 103–110 (1995).
19. Turro, N. J., Ramamurthy, V. & Scaiano, J. C. *Principles of Molecular Photochemistry: An Introduction*. (University Science Books, 2009).
20. Juris, A. *et al.* Ru(II) polypyridine complexes: photophysics, photochemistry, eletrochemistry, and chemiluminescence. *Coord. Chem. Rev.* **84,** 85–277 (1988).
21. Jain, P. K., Lee, K. S., El-Sayed, I. H. & El-Sayed, M. a. Calculated absorption and scattering properties of gold nanoparticles of different size, shape, and composition: applications in biological imaging and biomedicine. *J. Phys. Chem. B* **110,** 7238–48 (2006).
22. Bullen, G. A. Anthracene Tagged Biomolecules for DNA Binding. (2016).

5 SHORT INTERFERING RNA COATED AuNP

5.1 The discovery of siRNA

It was as recent as 1986, that Walter Gilbert put forward the idea of the 'RNA world'.[1] Previously, RNA was seen as just a carrier molecule which passed information from DNA to proteins. Since then, RNA has become a pivotal part of cellular biology. In 1998, Fire and Mello showed that double stranded RNA could induce gene silencing in the nematode

worm,[2] this was termed RNA interference (RNAi). Soon after the discovery of RNAi, it was found that artificial double stranded pieces of RNA could induce gene silencing, these small artificial duplexes were called short interfering RNA (siRNA).[3] The siRNA did not, in most cases, initiate an innate immune response, which is unusual as mammalian cells normally recognise RNAs as part of an antiviral defence mechanism. There is therefore great interest in siRNA delivery to discover the roles of genes and also its potential as a gene therapy technique.[4,5]

5.1.1 siRNA mechanism for gene knockdown

The understanding of the mechanism for siRNA mediated gene knockdown allows the pathway to be hijacked for our benefit. It begins with the insertion of a piece of double stranded RNA into the cell cytoplasm; consisting of a sense and antisense strand for the mRNA target of interest. The double stranded RNA interacts with a protein complex named DICER, which cleaves the ends of the RNA duplex; this clipped RNA duplex is the siRNA.[6] siRNA molecules are short double strands of RNA, ~22 base pairs in length with a 2 base overhang at the 3' end of each strand. In the next step of the mechanism, the siRNA forms a ribonulecleoprotein complex called RISC (RNA induced silencing complex). This complex contains an unidentified nuclease named SLICER; RISC mediates the unwinding of the double stranded RNA. The now single stranded RNA, which is coupled to RISC, binds to the complementary sequence of mRNA in the cytoplasm. The binding mediates the cleavage of the mRNA by the nuclease SLICER, cutting the mRNA strand in the centre. These newly formed mRNA fragments are recognised as aberrant by the cell, and therefore broken down.

This stops translation of the peptide from occurring and ultimately silences the gene that the mRNA was transcribed from (Scheme 5.1).[7,8]

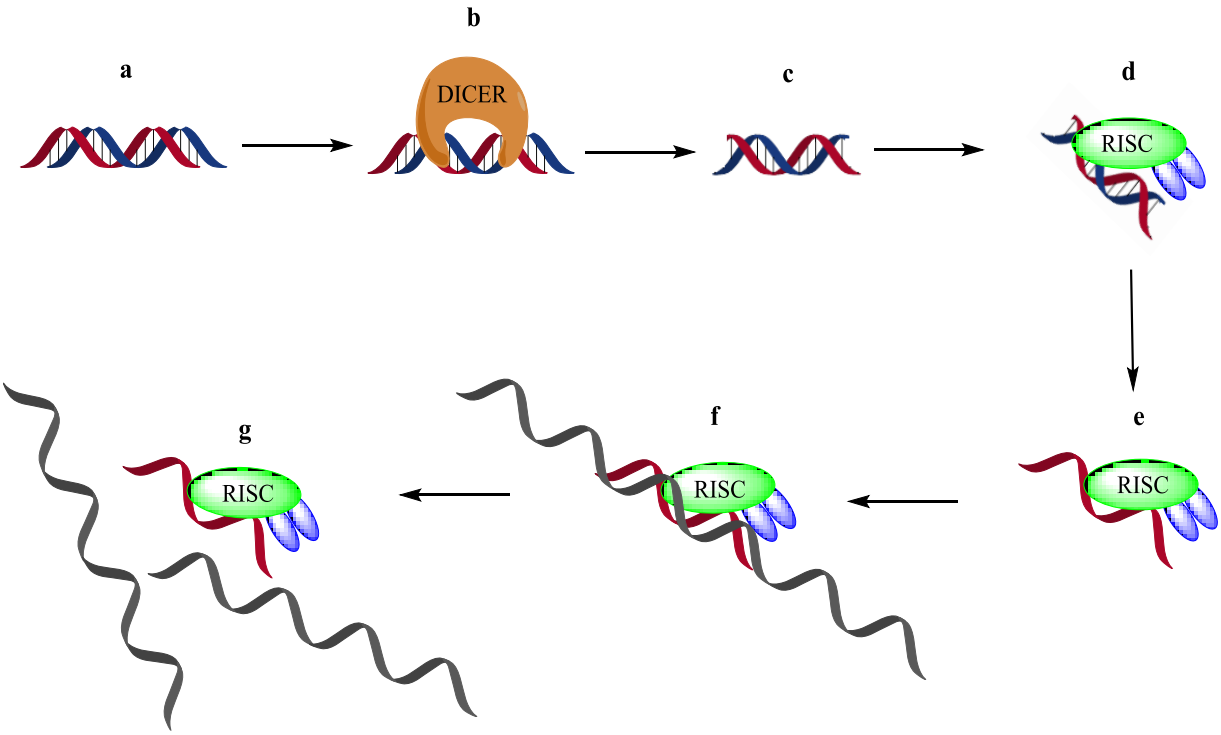

Scheme 5.1 Pathway for siRNA mechanism
a) Double stranded RNA inserted into cytoplasm. b) DICER cleaves end two bases of each RNA strand. c) Formed siRNA. d) RISC complex binds to siRNA e) unravels double stranded siRNA. f) Single stranded RNA binds to complementary mRNA sequence. g) RISC complex cleaves complementary mRNA strand in the centre, forming 'nonsense' strands of RNA and stopping translation of protein.

5.2 siRNA delivery into cells

There are currently a number of problems regarding siRNA as a therapy treatment, which include off target effects, cross reactions with the miRNA mechanism (micro RNA) and the targeted delivery of the siRNA into the body without degrading.[4,9] Sequence-specific off

target effects are caused by partial complementarity with regions of mRNA that are not being targeted, leading to the down regulation of genes that are not targeted.[10] The discovery of seeding regions in siRNA (bases 2-8 in antisense strand) showed they were the main cause of this effect and modifying the bases in this region can reduce the off-target silencing.[11] The miRNA process is involved in monitoring the correct expression levels of genes within a cell, and disruption of this can lead to unwanted side effects. The siRNA pathway can interfere with the miRNA mechanism by using cellular machinery which is required for miRNA.[12] These two problems associated with siRNA treatment can be readily solved by lowering the concentration of the siRNA dose; however the targeted delivery of intact siRNA into cells is the current major problem and an area of great research. The targeted delivery is especially important because siRNA can act in a catalytic manner. During the siRNA mechanism (Scheme 5.1) the RISC complex retains its silencing abilities once it has degraded an mRNA strand. Therefore a small concentration of siRNA can give a large knockdown affect. Currently the delivery of siRNA into cells is broadly split into two methods; the first using a non-viral vector to deliver chemically synthesised siRNA, the other approach is to use a viral infection which will retain the siRNA for longer term treatment. In this project, the non-viral method is being investigated and so the background to these methods is discussed. The delivery of chemically synthesised siRNA suffers from the same problems that were associated with DNA (Section **2.4**), these are degradation and cell uptake, however as siRNA is used in whole animal systems i.e. *in vivo,* cell targeting also needs to be considered. Interestingly, it has been shown that siRNA can be up-taken spontaneously by a cell; however this is only possible when the siRNA is locally delivered, such as intranasal.[13] Local application of siRNA, however, leads to a high concentration of

siRNA in a restricted area and is therefore beset by the problems mentioned previously associated with a high concentration of siRNA. To overcome the problems regarding degradation, many of the same methods used for stabilising DNA *in vitro/vivo*, have been replicated for siRNA. These include LNA, 2'F and 2'OMe. For the 2'F modification it is interesting that even though the modifications had a dramatic effect on siRNAs stability in serum, the effect on gene knockdown *in vivo* was not so dramatic, indicating that the stability of the siRNA may not be the most important factor.[14] As described above, the potential for off target gene silencing means that targeted delivery of siRNA is of great importance. There have been multiple different methods used for the improving the uptake of siRNA into cells; these include modifying the siRNA (such as with cholesterol to increase the siRNAs lipophilicity), encapsulating the siRNA in a liposome or using cationic lipids to carry the siRNA through the cell membrane (Figure 5.1).

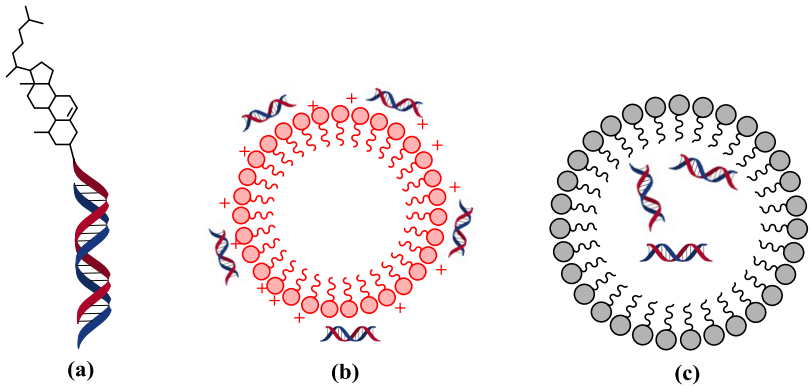

Figure 5.1 Different methods for non-viral delivery of siRNA
(a) cholesterol modified siRNA (b) electrostatically bound siRNA to cationic lipids (c) siRNA encased in a liposome.

5.2.1 Gold nanoparticles for siRNA delivery

AuNPs provide a suitable scaffold for the delivery of siRNA into cells. The surface of a AuNP can be readily functionalised with a wide variety of molecules, which allows for extra targeting/tracking molecules to be bound alongside the siRNA relatively easily. Also, the bio-inertness of the particles makes them an ideal candidate for *in vivo* work.

5.2.1.1 Electrostatically bound siRNA-AuNP

Once inside the cell the siRNA bound to AuNP needs to be either released from the particles or accessible enough so that it can be clipped off the particle by the DICER complex. Therefore there are more examples of electrostatic binding of siRNA to AuNP than seen for fluorescence sensors (Section **2.6.2**). Binding the siRNA less tightly to the particle allows for easier release once inside the cell. However, there remains the issue of loss of siRNA during delivery, which, due to the catalytic nature of siRNA, has the potential for causing noticeable off target knockdown.

Park *et al.* were able to develop an siRNA delivery system using AuNPs which were co-coated with siRNA and polyethyleneimine (PEI).[15] PEI was used to form self-assembled polyelectrolyte complexes with siRNA, providing them protection from enzymatic degradation, enhanced cellular uptake, and endosome escape. However there have been issues regarding cell toxicity and instability *in vivo*.[16] Rotello *et al.* have used AuNPs coated in positively charged polymers, which are able to carry the negatively charged siRNA into cells.[17] These polymer coated particles have an added advantage of being able to force the proton sponge affect to aid their release from endosomes. Once internalised into a cell, particles are often trapped inside highly acidic endosomes. The release of the siRNA from these endosomes is a problem which is often difficult to overcome. The amine groups on the

positively charged polymers release H^+ once inside the acidic endosome, resulting in a Cl^- and H_2O molecule being internalised for each H^+. This causes the endosome to swell and eventually burst, releasing the siRNA into the cytoplasm.[18,19] Elbakry *et al.* have extended the use of electrostatic binding of siRNA to AuNP by creating a layer by layer system.[20] Initially coating the particles in positively charged PEI, the siRNA was then added to coat the positively charged particles. A final layer of PEI was added, to aid the uptake of the particles whilst also reducing the amount of siRNA lost in delivery.

5.2.1.2 Covalently bound siRNA-AuNP

Covalently binding siRNA to AuNP minimises the issues regarding off target knockdown, whilst also allowing greater control of siRNA attachment onto the surface. It has been reported that electrostatically coated gold nanoparticles are prone to aggregation due to cross linking of the coating, or loss of coating from the surface.[21] A potential issue with covalently binding the siRNA to AuNPs is that the siRNA may not be released from the AuNP surface and interact in the siRNA pathway.

Conde *et al.* compared ionically bound siRNA-AuNP to covalently bound siRNA-AuNP for *in vivo* systems. They found that the covalently bound siRNA had nearly double the knockdown efficiency of the ionically bound siRNA.[22] The Mirkin group have bound siRNA molecules onto AuNPs, modifying the sense strand of the siRNA with a thiolated PEG. They were able to coat the particle in the sense strand initially, and then hybridise the anti-sense strand post synthesis.[23] The use of these covalently modified siRNA-AuNP *in vivo* has been demonstrated by Zheng *et al.,* using the siRNA-AuNP for the topical delivery of siRNA.[24] They have also

demonstrated that the siRNA-AuNP conjugates show a six times greater half-life and prolonged gene knock down compared to free RNA duplexes.[25]

To increase the amount of available siRNA in the cell, cleavable linkage groups have been investigated. Lee *et al.* bound an amine terminating PEG chain to AuNP, and conjugated the siRNA to the PEG chain through a biodegradable disulphide bond.[26] This disulphide bond would be cleaved upon entering the cells, due to the increased reducing conditions within a cell.

5.3 Chapter aims

The ability to switch off a gene which is known to cause or facilitate disease progression has exciting potential as a drug therapy. The concept that this could be targeted to specific diseased cells makes siRNA as a treatment extremely appealing and has led to a remarkable amount of research.[5,27,28] There are other techniques which utilise a similar approach most notably CRISPR, which consists of a short strand of RNA which complexes with a specific protein and can alter or slice target strands of DNA.[29,30]

Currently, the major problem in the development of siRNA as a medical treatment is the delivery of the siRNA duplex into the body and cells in a targeted manner. As described

previously in Section **2.4**, oligonucleotides are notoriously difficult to deliver into cells without chemical transfection, and are prone to degradation once inside the body, reducing their effectiveness, also the siRNA process is catalytic in its nature. This is a result of the RISC-RNA complex remaining intact once a single target RNA has been destroyed, and can therefore bind to more target strands (see part **g** of Scheme 5.1). This catalytic nature means that any non-specific delivery of siRNA must be kept to a minimum.

AuNPs are an appropriate solution to the associated problems of *in vitro* use of siRNA. As previously discussed in section **2.6.1**, oligonucleotide coated AuNPs are readily taken up by cells, and are stable to nuclease degradation. Also, the AuNP provides a scaffold to which additional targeting molecules can be attached. Research into the use of nanoparticles to deliver siRNA into cells has been fairly extensive utilising a wide variety of nanoparticles, including; magnetic,[31] gold and polymer.[32] The use of gold nanoparticles for the delivery of siRNA has been studied due to their well understood surface chemistry and relative inertness within the body.[18]

The aim of the work described in this chapter was to create siRNA coated nanoparticles that could begin to overcome the problems associated with degradation and duplex loss. In particular, controllably coating AuNPs with siRNA through a bis-thiolate attachment would ensure as much of the siRNA as possible would reach the target area. Firstly a modified siRNA is synthesised to include a bis-thiolate modification, this is then tested to ensure the modification does not affect the siRNA mechanism. Secondly, the modified siRNA is bound to the AuNP, before testing whether these siRNA-AuNP are able to induce gene silencing (Figure 5.2).

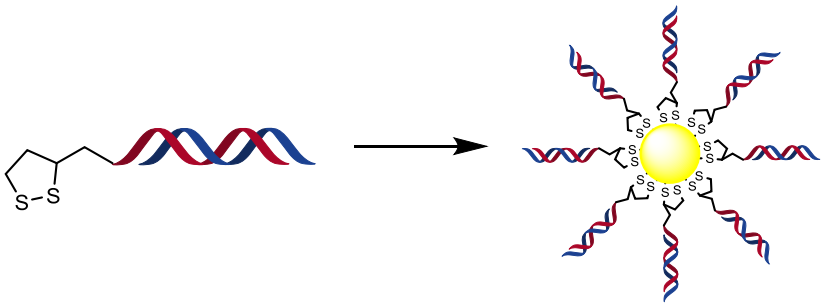

Figure 5.2 Proposed modification of siRNA, leading to coating of AuNP

5.3.1 Target protein to test gene knockdown, CLEC-14A

To monitor the knockdown efficiency of the siRNA-AuNP, the expression level of the targeted gene needs to be quantified. The easiest method for this is to target a gene which codes for a protein that is easily identifiable; the expression level of the protein is more easily determined and will correlate to the level of gene knockdown. For this project the gene targeted for knockdown was the gene coding for the protein CLEC-14A. This was chosen due to the expertise within the Bicknell group working with this protein, including an established method for monitoring the expression of CLEC-14A.

The protein CLEC-14A is a recently discovered novel endothelial marker and is strongly expressed in tumour vasculature when compared to healthy vasculature. It induces filopodia and facilitates endothelial migration, tube formation and vascular development in zebra fish. The knocking down of CLEC-14A results in anti-angiogenic activity by inhibiting cell migration and tube formation.[9]

Anti-angiogenic treatment is a method for inhibiting the growth of a cancerous tumour. Restricting a tumour's ability to establish a blood supply limits the growth of a tumour. The siRNA-AuNPs therefore will ultimately need to target tumours once inside the body. This

may be achieved by further modifying the surface of the particles with tumour specific molecules; however the use of nanoparticles themselves introduces a level of tumour targeting. The enhanced permeability and retention effect (EPR),[34,35] aids the targeting of the siRNA-AuNP to tumours within the body. Around areas of fresh tumour growth, the vessels are rapidly forming and therefore contain imperfections resulting in leaky vessels. Particles sized 10-100 nm are retained in the blood stream, however upon entering a tumours vessels they will leak into the surrounding tissue. Also, tumours do not develop a lymph system and so they cannot clear out chemical build up surrounding the vessels. This leads to a build-up of particles in tumours as they are pumped around the circulatory system.

5.4 siRNA modification

5.4.1 Amine modified RNA coupling to NHS ester

To attach the siRNA to AuNPs, the siRNA itself must be modified to incorporate a binding group onto it. As described previously (Section **5.2.1.2**) only one strand of the duplex has to be modified to bind it to the AuNP. The first strand is bound to the AuNP, with the complementary strand hybridised to form the completed siRNA duplex. It has been shown that the orientation of the siRNA when bound to nanoparticles has no effect on its ability to silence genes,[10] therefore either strand can be modified for binding to the particle surface. The binding group chosen was again a cyclic disulphide group as used for binding the anthracene probe to AuNP (Section **3.3**). The cyclic disulphide was chosen due to the

increased strength of the bis-thiolate bonds compared to a single thiol bond. This ensures as much of the siRNA remains bound to the AuNP as possible before reaching its target.

Initially, the 5' terminus of one of the strands of the siRNA was modified with an amine linker group on column as previously done with DNA (Section **3.2**). This was then reacted with the NHS ester form of thioctic acid once the RNA was cleaved off the column (Scheme 5.2).

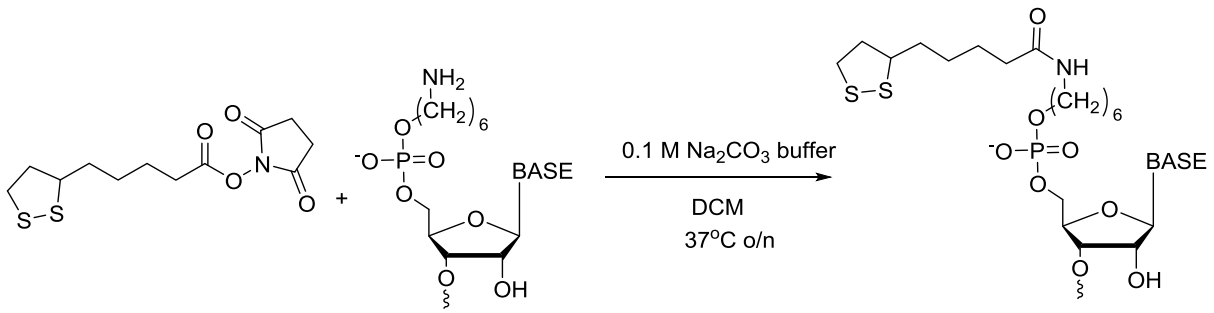

Scheme 5.2 Reaction to form thioctic acid modified RNA using NHS ester route
Conditions: 0.1 M sodium carbonate buffer, heated at 37°C overnight.

Although this reaction was successful when modifying DNA, when modifying RNA it did not work so efficiently. Despite multiple attempts, the product could not be obtained in a pure or large enough yield. By HPLC analysis, it was evident that there was degradation of the RNA during the coupling reaction. Efforts to obtain enough modified RNA resulted in mixtures of either unreacted amine or various degradation products. By MS analysis, it was evident that the desired product was formed, but only in very small amounts. The increased instability of RNA is attributed to the 2'-OH. If deprotonated (e.g. in alkaline conditions) the 2'-O^- can attack the phosphorus in the phosphodiester bond; resulting in the loss of the next nucleotide in the sequence, forming fragments of the RNA sequence (Scheme 5.3). This may

explain the observed degradation of the RNA strands during the coupling reaction, as the coupling reaction is done in alkaline 0.1 M sodium carbonate buffer.

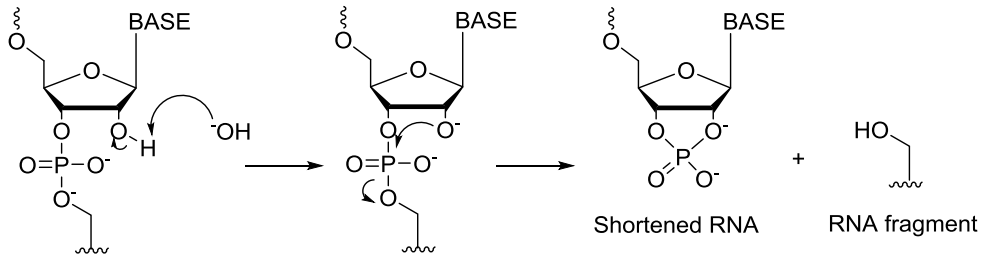

Scheme 5.3 RNA degradation in alkaline conditions

5.4.2 Disulphide phosphoramidite modification

Modification of the RNA using an NHS ester of thioctic acid was unsuccessful, therefore an alternative method for modifying the RNA was required. Synthesising a phosphoramidite of the thioctic acid (Figure 5.3) would allow the RNA sequence to be modified on column using the DNA synthesiser; and the coupling step could then be done under mild RNA coupling conditions.

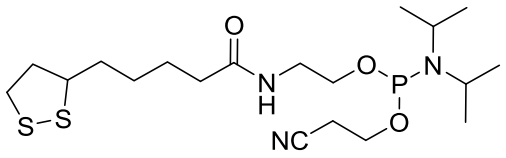

Figure 5.3 Phosphoramidite of thioctic acid

This thioctic acid phosphoramidite could then be coupled to the RNA sequence using the DNA synthesiser, minimising the amount of off-column modification of the RNA strands. Therefore maximising the amount of product obtained, whilst also removing any side products that may be being formed during the off-column coupling.

The literature gives conflicting information about the synthesis of a phosphoramidite from thioctic acid. Dougan *et al.*[12] reported difficulty in synthesising the phosphoramidite. They found the thioctic acid phosphoramidite was unstable, (suggesting this may be due to the ring strain within the cyclic disulphide group) with the sulphur atoms in the cyclic disulphide possibly reacting with the P(III) centre, allowing for a number of side reactions. Therefore they developed a method for the synthesis of an H-phosphonate form of a thioctic acid derivative (Figure 5.4).

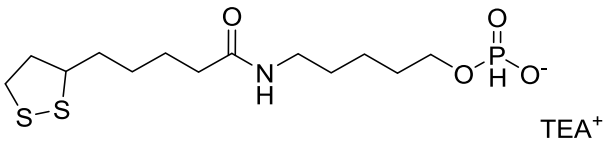

Figure 5.4 H-phosphonate of a derivative of thioctic acid synthesised by Dougan et al.[12]

However, contrary to the findings of Dougan *et al.*, there are reports of the target phosphoramidite as well as other derivatives of thioctic acid. Seliger *et al.*[13] originally

patented the synthesis of a phosphoramidite derivative of thioctic acid, noting its importance in immobilising organo/biochemical molecules on noble metals, noble metal alloys or semiconductors. Interestingly, Srivastava *et al.*[14] recently patented another synthesis of a thioctic acid phosphoramidite to modify oligonucleotides at any point within a sequence. They remarked that the synthesis put forward by Seliger *et al.* was inconsistent and only worked for compounds with short carbon chains between the peptide and phosphodiester bonds.

The work in this project was done before the patent by Srivastava *et al.* was released and proposes a slightly different procedure. Initially the thioctic acid was reacted with 2-amineethan-1-ol to give an available alcohol group. This alcohol group could then be phosphitylated to give the target phosphoramidite (Figure 5.5) which was successfully characterised in the usual manner (Section **6.1.5**).

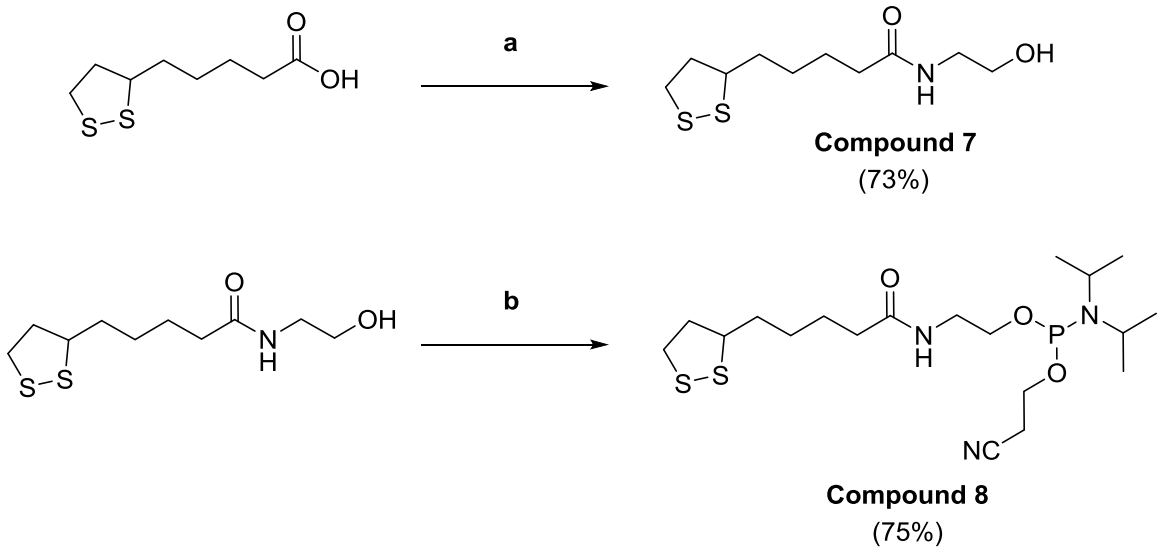

Figure 5.5 Synthesis of phosphoramidite form of thioctic acid derivative.

Reagents and conditions: (a)(i)HOBt, DMF,0°C, EDC, 1 hr (ii) $H_2N(CH_2)_2OH$, 4-ethymorpholine, rt, o/n, 73% yield. (b) $(i\text{-}Pr_2N)PClO(CH_2)_2CN$, DIPEA, DCM, rt, 2 hr, 75% yield.

5.4.3 Characterisation of the modified siRNA

The RNA was synthesised on an Applied Biosystems 394 DNA/RNA synthesizer as per standard RNA oligo synthesis (Section **6.1.1.3**). The strands synthesised are shown in Table 5.1.

Table 5.1 RNA sequences synthesised
(top) RNA sequences synthesised. (bottom) Duplex siRNA when RNA.3 and RNA.4 hybridised. Q = ***Compound 8*** *modification.*

Strand name	Strand sequence
RNA.3	5' **Q**-CAA UCA GGG UCG ACG AGA A 3'
RNA.4	5' UUC UCG UCG ACC CUG AUU G 3'

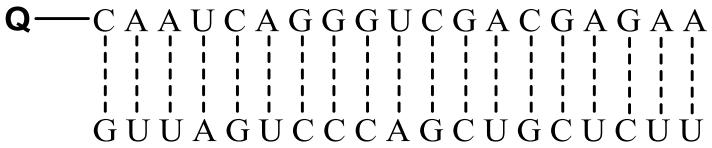

siRNA.1

(siRNA.1 = RNA.3 + RNA.4)

All strands were purified by reverse phase HPLC and characterised by Mass Spectrometry (Section **6.1.1.4**). The synthesis of the modified RNA (**RNA.3**) proved problematic and was produced in lower yield than the unmodified RNA (**RNA.4**). The presence of the thioctic acid modification was confirmed by MS but it should be noted that the reaction was not always successful, often resulting in only the unmodified **RNA.3** being isolated. When the reaction did occur, the yields of **RNA.3** were low e.g. 500µL at 35 µM, compared to **RNA.4** which

yielded 500µL at 80 µM. A T_m of the **siRNA.1** duplex of 63°C confirmed the formation of the duplex.

5.5 CLEC-14A knockdown

5.5.1 Western Blot introduction

To monitor siRNA knockdown efficiency, the expression levels of the protein formed from the silenced genes needed to be quantified. This is done using a technique called a Western Blot. This involves treating cells with a siRNA duplex before lysing the cells. A gel of the cell lysate is run to separate the proteins present in the lysate based upon their size. The proteins are then transferred onto a membrane which can be treated with protein specific antibodies. The primary antibody will bind to the protein of interest, photoactive secondary antibodies are then added and bind to the primary antibodies. The photoactive antibodies can then be seen using photoactive film, allowing the proteins to be identified (Figure 5.6).

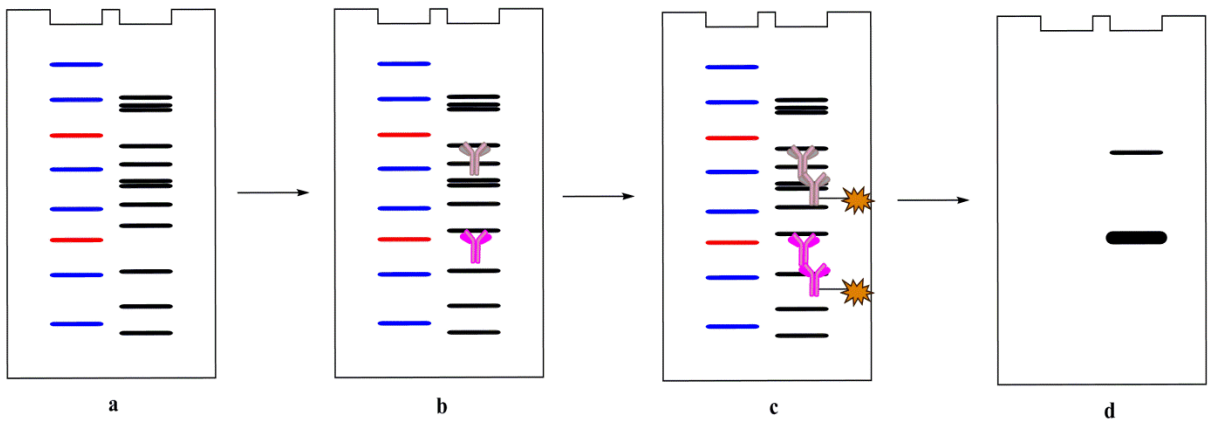

Figure 5.6 Developing a Western Blot.
Protein size marker (blue/red dashes) runs alongside proteins (black dashes) from cell lysate. (a) Proteins from cell lysate run on gel and transferred to membrane. (b) Membrane treated with primary antibodies for CLEC-14A (purple) and tubulin (pink). (c) Membrane treated with horseradish peroxidase (yellow star) containing secondary antibodies. (d) Membrane developed on photoactive film and observing relative expression of proteins observed.

The proteins analysed were the gene being targeted CLEC-14A, and also Tubulin. Tubulin is a protein highly expressed in cells, it polymerises to form microtubules which serve as a skeletal system for cells.[15] The expression of Tubulin should not be affected by the siRNA treatment; therefore it can be used as a control to reference the CLEC-14A expression levels against.

5.5.2 Knockdown using modified siRNA alone

Before testing how effective siRNA coated AuNP would be, it first had to be established whether the disulphide modification on **RNA.1** affected the knockdown capability of the siRNA duplex. Therefore, the **siRNA.1** duplex was tested alongside the standard bought CLEC-14A siRNA used within the lab (**labsiRNA**), to compare their relative knockdown efficiencies. A random duplex of RNA is used as a control for each experiment run; the control shows the normal level of protein expression, from which the knockdown efficiency is calculated from.

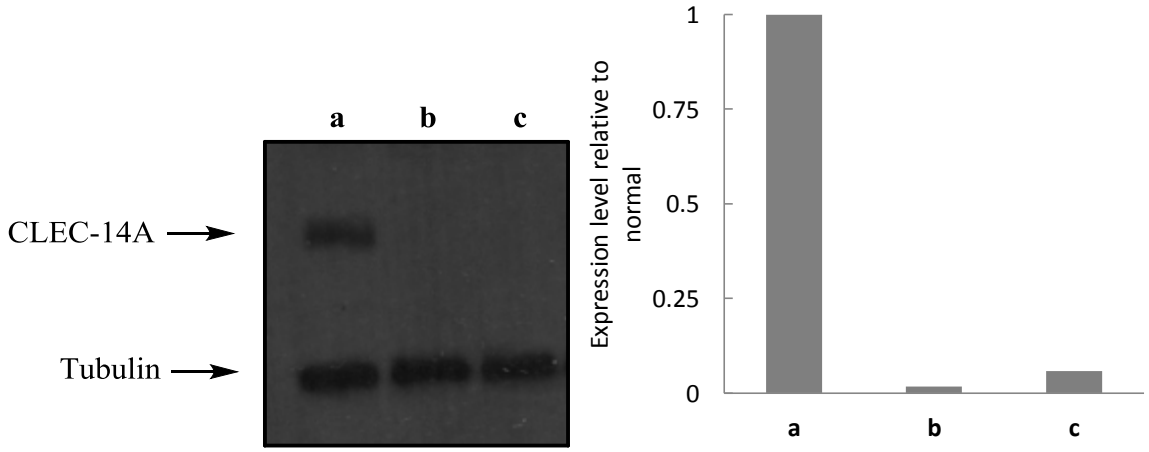

Figure 5.7 Western blot for CLEC14A knockdown using modified siRNA.1
(*Left) Developed film showing relative expression levels of target protein CLEC-14A and reference protein, Tubulin. (a) Negative control experiment showing normal expression levels of both proteins. (b) Knockdown with CLEC-14A* ***labsiRNA*** *(c) Knockdown using synthesised* ***siRNA.1****. (Right) Percentage*

knockdown of CLEC-14A compared to the negative control, each experiment normalised to its own tubulin expression.

The darkness of the band is proportional to the amount of protein expressed. A darker band indicates a higher concentration of photoactive secondary antibody, a direct result of higher protein concentration. The percentage knockdown efficiency of the **siRNA.1** can be found by using ImageJ software[41] to analyse the average pixel value for each protein band. Normalising each experiment to its internal control, tubulin, the relative percentage knockdown of CLEC-14A can be found by comparing it to the negative control (Figure 5.7, right). The experiments confirmed that the disulphide modification did not affect the siRNA's ability to induce protein knockdown (Figure 5.7).

5.6 Binding siRNA to AuNP

5.6.1 Track UV binding upon siRNA addition

Once it was proven that the presence of the disulphide modification did not affect the siRNAs knockdown efficiency, the siRNA was bound to 13 nm AuNP. From previous work with DNA-AuNP (Section **3.6.2.1**), it was known that the AuNP could not be exposed to salty conditions until coated in DNA; as the particles would aggregate. Therefore, RNA could not be bound to the particles as a duplex since the salt required to form the duplex would cause the particles to aggregate. Consequently, the particles would be initially coated with a single strand of modified RNA forming particles that are stable to salt addition. The second strand of RNA could then be added along with salt allowing the duplexes to form.

To coat the AuNP with RNA the same procedure was employed as used previously (Section **3.6**). To 13 nm AuNP (1 mL, 3 nM) in 10mM phosphate buffer, the **RNA.3** was titrated in three equal additions (28 µL, 35 µM). After each RNA addition the AuNP-RNA solution is

stirred for 2 minutes with a magnetic stirrer and then sonicated for 20 seconds. The binding was monitored by UV-vis absorption tracking the shift of the SPR band of the AuNP (Figure 5.8). For full experimental details see Section **6.2.4.5**.

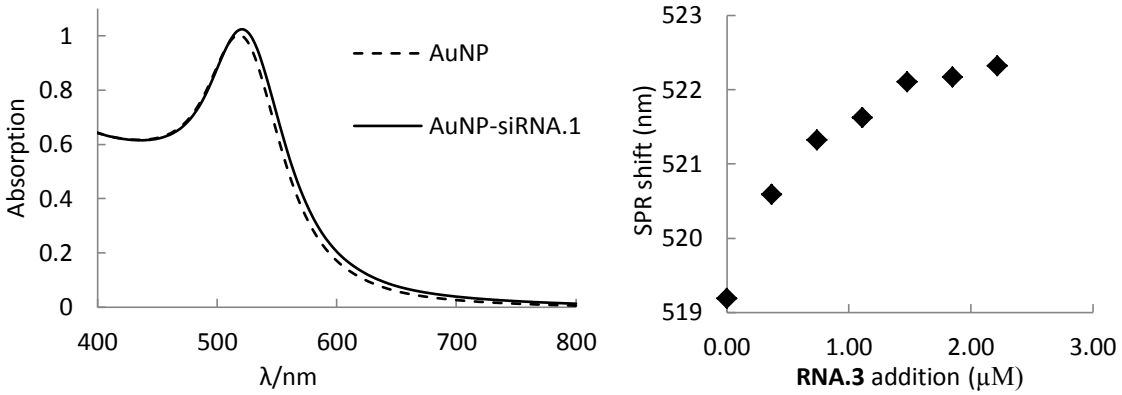

Figure 5.8 Tracking RNA binding to AuNP
*(left) UV absorption of SPR band showing before and after addition of siRNA.1. (right) Graph plotting the shift in SPR band upon titration of **RNA.3** (9 µL, 35 µM) to 1 mL of 3 nM AuNP in 10 mM Phosphate buffer.*

The SPR shift observed was very similar to the SPR shift seen when DNA was bound to the AuNP using a thioctic acid modification. This was expected as the SPR band is sensitive to changes of the surface environment of the AuNP where the binding takes place. The surface environment of the RNA coated particles will be similar to the DNA coated particles as they bind through the same thioctic acid modification (Section **3.6**). Also, the number of RNA molecules coating the particles is assumed to be similar to that of DNA as the presence of the 2'-OH groups in RNA should not affect the packing level to any great extent.

Once the AuNPs were coated with **RNA.3**, they were passed through a Sephadex G-50 size exclusion column to remove any unbound RNA. Once purified the second strand of RNA (**RNA.4**) was added to the particles along with buffer and salt to ensure duplex formation. No further purification was done after the second strand of RNA was added as passing the

hybridised particles through a size exclusion column would greatly reduce the salt concentration, causing the siRNA duplexes to fall apart. Any single stranded **RNA.3** in solution would be readily degraded inside the cell, if it was taken up at all. Therefore if any single stranded RNA was carried through into cells it would not affect the knockdown experiments. The particles were sized at 14 nm ± 3 nm by DLS, as described previously (Section **3.7.1**).

5.6.2 Cell uptake

It had to be established that the particles, once coated in siRNA, were taken up by Human Umbilical Vein Endothelial Cells (HUVECs). HUVECs are often used to analyse endothelial cells for angiogenesis, as they retain the features of native vascular endothelial cells such as endothelial cell specific markers.[42] The method for extracting the cells from the umbilical vein using collagenase is shown in experimental Section **6.4**. As previously discussed, the 13 nm **siRNA.1-AuNP** could not be imaged via reflectance as they are too small. Therefore to image cell uptake, 100 nm AuNPs were coated in siRNA (Section **6.2.4.7**). These particles are large enough to be imaged by reflectance microscopy. After purifying the 100 nm siRNA coated particles by spinning down, HUVEC cells were dosed at 4 pM of 100 nm for 4 hours. This time period corresponds to the time allowed for chemical transfection of siRNA duplexes.

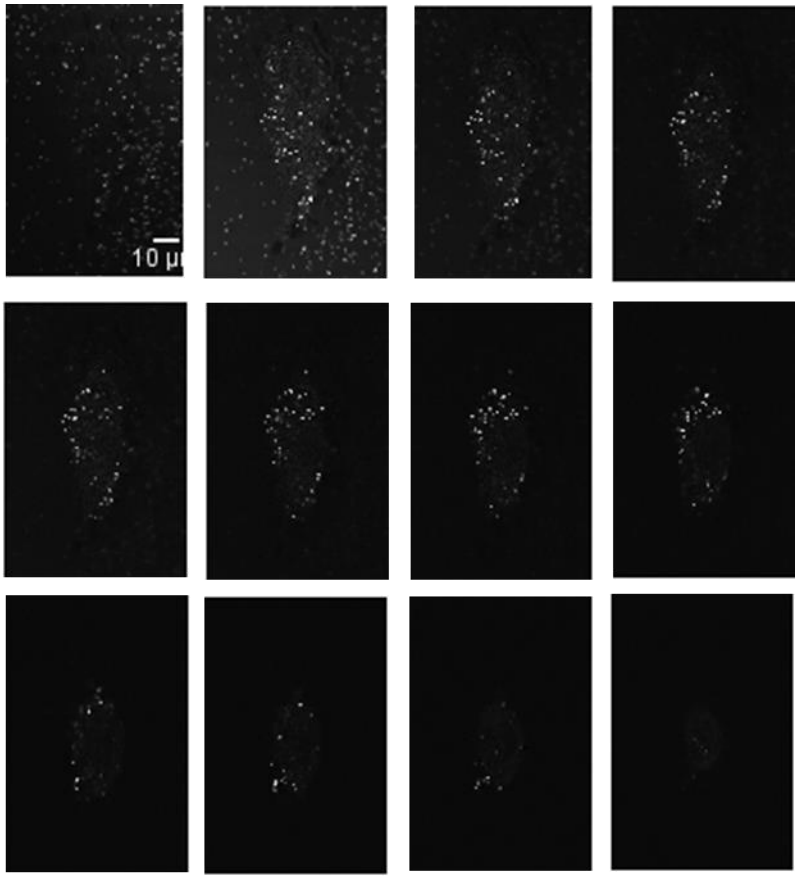

Image 5.1 HUVEC uptake of 100 nm siRNA.1-AuNP
Z stack of images taken by reflectance confocal microscopy of HUVECs treated with 100 nm siRNA.1-AuNP for 4 hours. Each slice is an increment of 0.45 µM. Particles added at 4 pM in deionised water with 100 mM NaCl and 10 mM phosphate buffer.

The uptake of the particles was then imaged by reflectance microscopy (Image 5.1), which confirmed the particles were taken up within the same time period used in standard siRNA treatment. Therefore direct comparisons could be made between transfection mediated siRNA and siRNA-AuNP knockdown.

5.6.3 Knockdown using siRNA-AuNPs

Once it was shown that the **siRNA.1-AuNPs** were taken up by HUVECs without the need for chemical transfection agents, the knockdown capabilities of the **siRNA.1-AuNP** was tested. The method followed was the same as standard siRNA treatment as already described but

without lipofectamine. The **siRNA.1-AuNPs** (0.25 nM) were added to the cells in deionised water with 100 mM NaCl and 10 mM phosphate buffer at pH 7.0. This gave a total concentration of siRNA added ≈ 100 nM (assuming around 400 strands per particle as per DNA), which was higher than the minimum amount of siRNA shown to induce CLEC-14A knockdown under standard treatment (50 nM).[33] However, not all particles would be taken up by cells and the availability of the siRNA bound to the AuNP was unknown, therefore it was decided that concentrations surrounding 0.25 nM of **siRNA.1-AuNP** were tested. ImageJ was again used to analyse the relative expression levels of the proteins of interest. To monitor whether the particles induced a protein expression response from the cell themselves, an initial control experiment confirmed no effect was exhibited by DNA-AuNP.

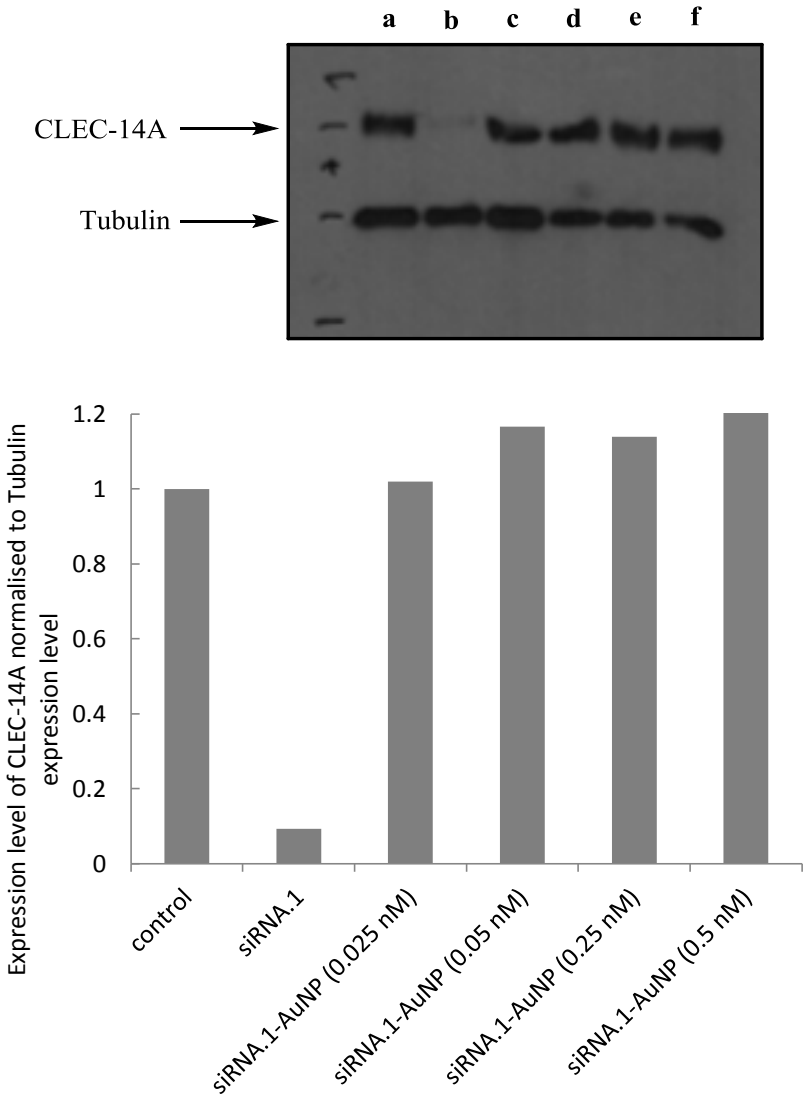

Figure 5.9 Western blot of CLEC14A knockdown using siRNA.1-AuNP
(Top) Developed film for a single experiment indicating relative expression levels of target protein CLEC-14 and reference protein, Tubulin. (a) Control experiment showing normal expression levels of both proteins. (b) ***siRNA.1*** *(c)* ***siRNA.1-AuNP*** *(0.025 nM) (d)* ***siRNA.1-AuNP*** *(0.05 nM) (e)* ***siRNA.1-AuNP*** *(0.25 nM) (f)* ***siRNA.1-AuNP*** *(0.5 nM) (Right) Percentage knockdown of CLEC-14A compared to the negative control, each experiment normalised to its own tubulin expression. Average of two independent repeats.*

The results in Figure 5.9 indicate that the **siRNA.1-AuNPs** are not able to induce protein knockdown. There was no observable decrease in the CLEC-14A protein expression for the cells that were treated with siRNA coated AuNPs when they were compared to the control cells. Variations in the concentration of **siRNA.1-AuNPs** did not seem to have an effect on

the levels of CLEC-14A knockdown (Figure 5.9). Extending the time the cells were treated with **siRNA.1-AuNP** from 4 hours to 24 hours showed no difference in the expression levels of CLEC-14A, indicating that the lack of gene silencing was not due to the siRNA mechanism taking longer as a result of the siRNA being bound to AuNP. It therefore appeared that the reason for the inactivity was the siRNAs inability to be cleaved from the AuNP surface. The observed increased stability of oligonucleotides when bound to AuNPs has been discussed previously (Section **2.6.1**); the tight packing of the oligonucleotides and high local salt concentration makes the strands stable to enzyme degradation.

In the first step of the siRNA mechanism, the DICER enzyme clips the double stranded RNA into the siRNA form. This step may be being inhibited by the aforementioned tight packing and high local salt concentration properties that the **siRNA.1-AuNP** has. To overcome these issues, it was proposed to bind a second molecule to the AuNPs alongside the siRNA. This second molecule would act firstly as a spacer molecule, in effect forcing the strands of RNA apart from each other and making it more available for the DICER enzyme. Also, it was proposed that the second molecule should be positively charged as this would help decrease the overall negative charge surrounding the AuNPs, again making the immediate environment surrounding the siRNA more accessible (Figure 5.10). The RubpySS probe used in chapter 4 was deemed suitable (Figure 4.3). The ruthenium complex can bind to the AuNPs through its disulphide terminating legs, forcing the strands of siRNA apart, whilst its overall 2+ charge will neutralise the negative charge of the RNA. The ruthenium probe also has the additional benefit of being a luminescent probe. The ability to track the siRNA-AuNPs probes once inside a cell or animal is of great interest, as the localisation of siRNA-AuNPs once administered needs to be investigated.

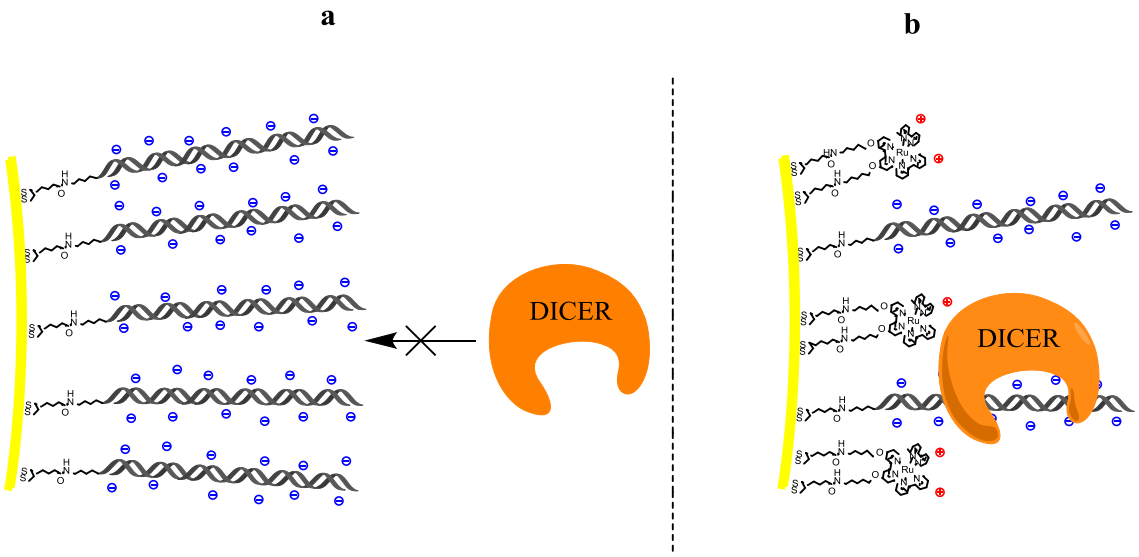

Figure 5.10 Proposed reasoning behind attachment of second probe to AuNP
(a) DICER enzyme unable to bind to RNA strands due to high surface density and high negative charge (b) DICER complex is able to interact with RNA strands due to lower density and lower negative charge due to presence of ***RubpySS****.*

5.7 Binding siRNA and ruthenium probe to AuNP

To coat the AuNPs with both RNA and RubpySS, the procedure for binding the anthracene probe alongside the RubpySS was carried out as described previously in Section **4.2**. The bare AuNPs are made up in 10 mM pH 7.0 phosphate buffer, coated initially in 0.98 µM of DNA (three additions of 9 µL, 35 µM **RNA.3**) with 2 minutes stirring and 20 seconds sonication between each addition. To these particles, RubpySS is added (two additions of 15 µL, 20 mM with 20 minutes of stirring between each addition). The SPR was tracked by UV (Figure 5.11) to monitor the binding. The particles were then passed through a Sephadex G-50 column to remove any unbound molecules. After purification, the particles were made up in 100 mM NaCl, 10 mM phosphate buffer (pH 7.0) and then the second strand of RNA was added to the coated particles, forming **siRNA.1-AuNP-Ru** particles. These were sized at 15 nm ± 3 nm by DLS.

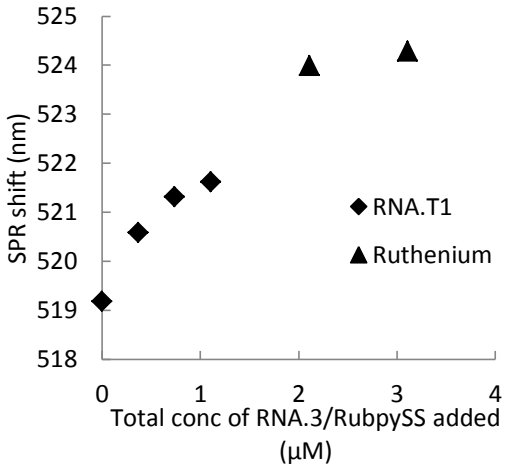

Figure 5.11 SPR shift for siRNA.1-AuNP-Ru coating
*Binding initially with **RNA.3** (9 µL, 35 µM) (diamond) and then **RubpySS** (15 µL, 20 mM)(triangle). 1 mL of AuNP at 3 nM in 10 mM phosphate buffer, pH 7.0.*

5.7.1 Knockdown using siRNA.1-AuNP-Ru

Upon testing the knockdown efficiency of the **siRNA.1-AuNP-Ru** particles, there was a clear decrease in the production of CLEC-14A (Figure 5.12).

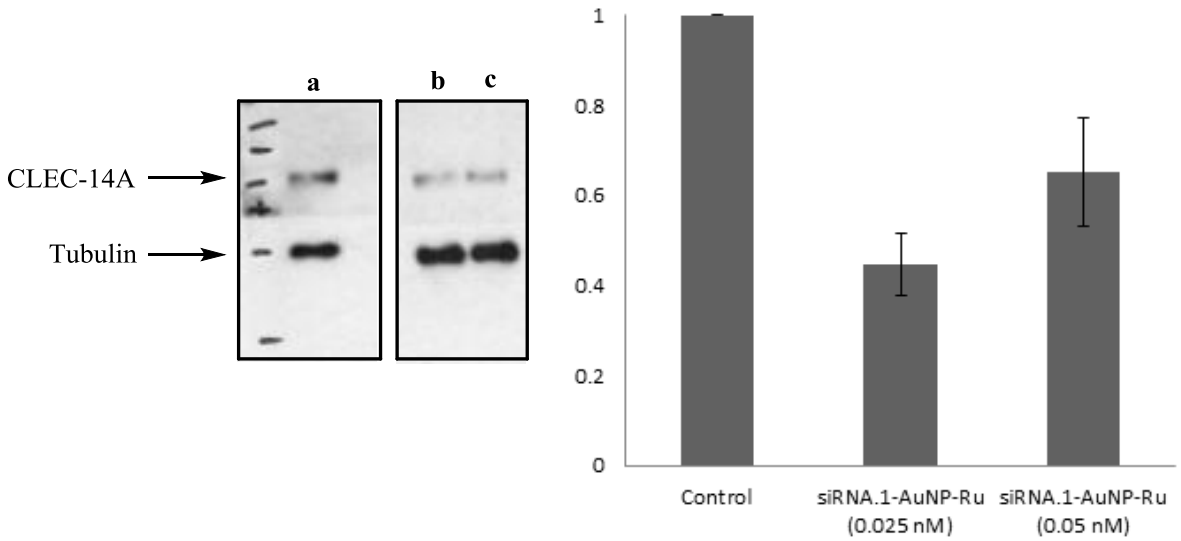

Figure 5.12 Western blot for CLEC14A knockdown using siRNA.1-AuNP-Ru
*(Left) Developed film for a single **siRNA.1-AuNP-Ru** experiment indicating relative expression levels of target protein CLEC-14 and reference protein, Tubulin. (a) Control experiment showing normal expression levels of both proteins. (b) **siRNA.1-AuNP-Ru** at 0.025 nM (c) **siRNA.1-AuNP-Ru** at 0.05 nM (Right) Percentage knockdown of CLEC-14A compared to the negative control, each experiment normalised to its own tubulin expression. Error bars are standard deviation of 3 independent repeats.*

It therefore appeared that the ruthenium probe had delivered the desired affects with regards to the siRNA knockdown mechanism, and the siRNA could be successfully cleaved off the AuNP surface and induce gene silencing.

Although these results were extremely encouraging, it had to be determined that the effects observed were a direct result of the siRNA being cleaved and inducing knockdown through the siRNA mechanism, or whether the ruthenium probe was having some effect on the cell causing a decrease in CLEC-14A production.

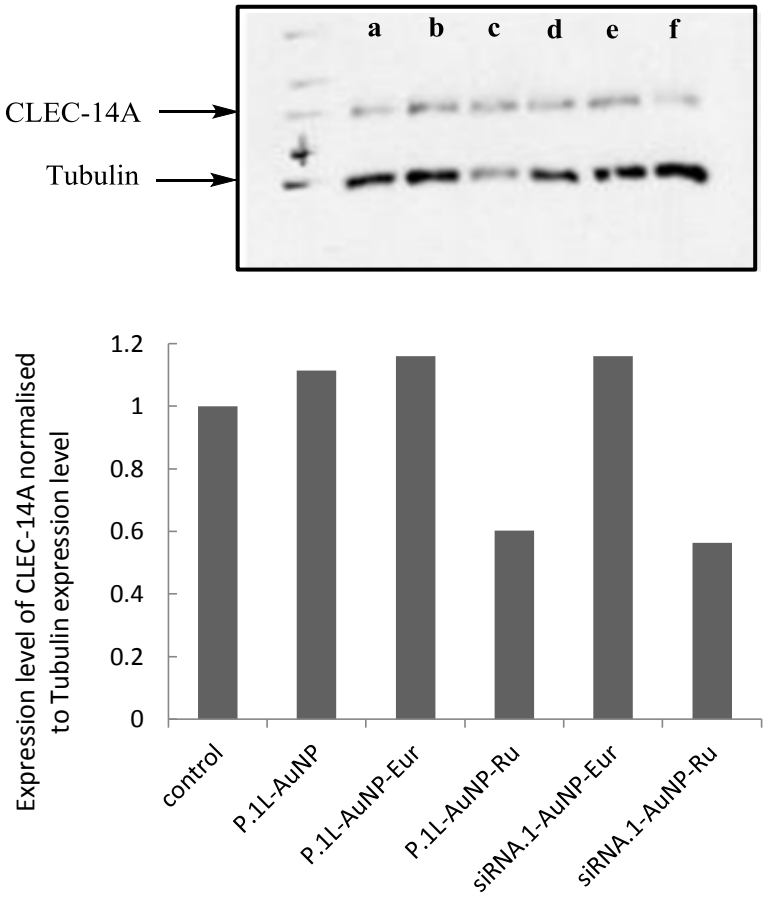

Figure 5.13 Western blot for CLEC14A using various standards
(Top) Developed film indicating relative expression levels of target protein CLEC-14 and reference protein, Tubulin. (a) Negative control (b) ***P.1L-AuNP*** *(c)* ***P.1L-AuNP-Eur*** *(d)* ***P.1L-AuNP-Ru*** *(e)* ***siRNA.1-AuNP-Eur*** *(f)* ***siRNA.1-AuNP-Ru****. (Bottom) Percentage knockdown of CLEC-14A compared to the negative control, each experiment normalised to its own tubulin expression. Results are average of two independent repeats.*

Therefore two control experiments were done; firstly the siRNA was replaced with the anthracene probe used previously, which should result in no knockdown of CLEC-14A. Whilst in the second experiment, the ruthenium probe was replaced by a neutral Europium probe (**Eur**; provided by Johnathon Lilley) which will show whether the effects observed were caused by co-coating the particles with a second probe, or whether they are directly caused by the ruthenium probe. The effect these changes had on the levels of CLEC-14A were then tested (Figure 5.13).

It is apparent from the results of the control experiments that the reason for the observed knockdown in **siRNA.1-AuNP-Ru** is the presence of the ruthenium probe. It appears that the siRNA pathway is not the route that leads to the decrease in CLEC-14A production, as the reduction in CLEC-14A is still observed for the ruthenium probe coated AuNP even when no siRNA is bound to the AuNP. Also, when the ruthenium probe is replaced by a Europium probe, the knockdown is not observed, indicating the ruthenium is causing the knockdown of CLEC-14A.

These results suggest that the ruthenium probe alone causes the cell to produce less CLEC-14A. It is difficult to envisage how this could be a specific interaction with CLEC-14A, and it is more likely that it is some non-specific anti-angiogenic effect being observed. The mechanism of which is caused by the presence of the ruthenium probe. The deduction of this mechanism which leads to the knockdown of CLEC-14A is outside the scope of this project. However, from literature, it is seen that ruthenium (II) based compounds have been found to display anti-angiogenic properties.[43,44,45]

5.8 Conclusions and future Work

In this work a new method for modifying RNA so that it is able to bind to AuNP has been developed. This modified siRNA still retains its ability to induce gene silencing at a similar level to non-modified siRNA. A method for controllably binding the modified siRNA onto AuNP in a covalent manner has been developed. These particles were able to be taken up by HUVECs, however no gene silencing was observed. Further modifying these particles with a ruthenium probe gave interesting, if ultimately unsuitable, results, causing the down regulation of the protein of interest even when no siRNA was present. Investigating these anti-angiogenic properties of the ruthenium probe would be interesting future work.

The observed lack of activity of the siRNA strands once bound to the AuNPs, could be caused by a number of factors which should be further investigated. The use of a cleavable linker group to the AuNPs has been investigated by some groups,[26] where a cleavable disulphide group was placed between the siRNA AuNP (Figure 5.14). The siRNA was released once the particle entered the reducing environment of the cytoplasm. However, this has not yet been done when using the disulphide attachment site.

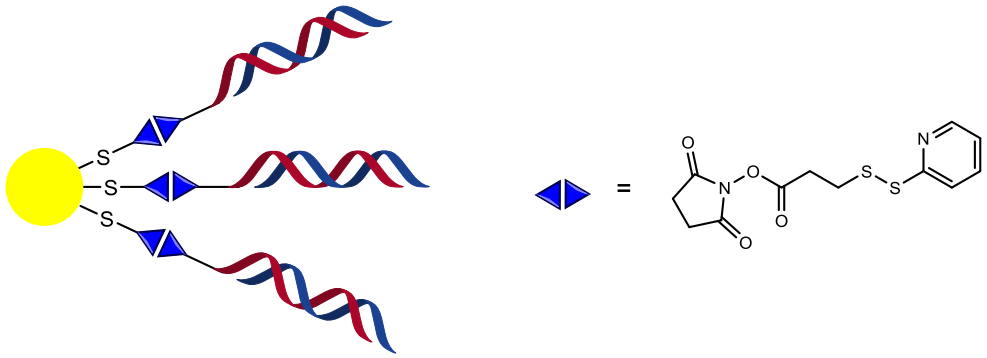

Figure 5.14 Incorporation of a cleavable linker to aid siRNA release from AuNP by Lee *et al.*.[26]

As the aim of the project was to attempt to track the delivery of siRNA to cells, alternative fluorophores need to be investigated. The observed activity caused by the ruthenium probe makes this unsuitable, especially for tracking the CLEC-14A protein knockdown. Alternative AuNP binding dyes have been developed within the Pikramenou group, such as Europium and Iridium metal based dyes.

A route which may prove interesting would be to tag one of the strands of the siRNA duplex with an organic dye. These can be readily purchased and coupled to oligonucleotides during DNA synthesis. This has already been explored with DNA within the Tucker group, to prove duplex formation in cells.[46] This would determine whether the siRNA is cleaved from the AuNP surface, as the emission of the dye would increase upon removal from the quenching AuNP.

Alternative nanoparticles to gold could also be investigated; this work has already started within the group using silica nanoparticles. The siRNA does not bind to these silica particles covalently but through electrostatic interactions; therefore they may suffer from the already discussed problems of loss of sample. However it may provide a means to successfully release the siRNA into the cells cytoplasm, whilst it has already been shown within the group that the silica particles are able to be modified with fluorophores for tracking within cells.[47]

5.9 References

1. Gilbert, W. The RNA world. *Nature* **319**, 618 (1986).
2. Fire, A. *et al.* Potent and specific genetic interference by double-stranded RNA in Caenorhabditis elegans. *Nature* **391**, 806–811 (1998).
3. Hamilton, a. J. A Species of Small Antisense RNA in Posttranscriptional Gene Silencing in Plants. *Science* **286**, 950–952 (1999).
4. Castanotto, D. & Rossi, J. J. The promises and pitfalls of RNA-interference-based therapeutics. *Nature* **457**, 426–33 (2009).
5. Fougerolles, A. De, Vornlocher, H., Maraganore, J. & Lieberman, J. Interfering with disease : a progress report on siRNA-based therapeutics. *Nature Reviews: Drug Delivery* **6**, 443–453 (2007).
6. Bernstein, E., Caudy, a a, Hammond, S. M. & Hannon, G. J. Role for a bidentate ribonuclease in the initiation step of RNA interference. *Nature* **409**, 363–6 (2001).
7. Liu, J. *et al.* Argonaute2 is the catalytic engine of mammalian RNAi. *Science (New York, N.Y.)* **305**, 1437–41 (2004).
8. Hammond, S. M. Dicing and slicing: the core machinery of the RNA interference pathway. *FEBS letters* **579**, 5822–9 (2005).
9. Kurreck, J. RNA interference: from basic research to therapeutic applications. *Angewandte Chemie (International ed. in English)* **48**, 1378–98 (2009).
10. Jackson, A. L. *et al.* Expression profiling reveals off-target gene regulation by RNAi. *Nature biotechnology* **21**, 635–637 (2003).
11. Jackson, A. L. *et al.* Position-specific chemical modification of siRNAs reduces “off-target” transcript silencing. *RNA (New York, N.Y.)* **12**, 1197–1205 (2006).
12. Grimm, D. *et al.* Fatality in mice due to oversaturation of cellular microRNA/short hairpin RNA pathways. *Nature* **441**, 537–541 (2006).
13. Bitko, V., Musiyenko, A., Shulyayeva, O. & Barik, S. Inhibition of respiratory viruses by nasally administered siRNA. *Nature Medicine* **11**, 50–55 (2005).
14. Layzer, J. M., Mccaffrey, A. P., Tanner, A. K., Huang, Z. a N. & Kay, M. a In vivo activity of nuclease-resistant siRNAs In vivo activity of nuclease-resistant siRNAs. *RNA* **10**, 766–771 (2004).
15. Lee, Y. *et al.* Controlled synthesis of PEI-coated gold nanoparticles using reductive catechol chemistry for siRNA delivery. *Journal of controlled release : official journal of the Controlled Release Society* **155**, 3–10 (2011).
16. Neu, M., Fischer, D. & Kissel, T. Recent advances in rational gene transfer vector design based on poly(ethylene imine) and its derivatives. *The journal of gene medicine* **7**, 992–1009 (2005).
17. Kim, S. T. *et al.* Dendronized Gold Nanoparticles for siRNA Delivery. *Small (Weinheim an der Bergstrasse, Germany)* **8**, 3253–6 (2012).
18. Ding, Y. *et al.* Gold nanoparticles for nucleic acid delivery. *Molecular therapy : the journal of the American Society of Gene Therapy* **22**, 1075–83 (2014).
19. Guo, S. *et al.* Enhanced Gene Delivery and siRNA Silencing by Gold Nanoparticles Coated with Charge-Reversal Polyelectrolyte. *ACS Nano* **4**, 5505–5511 (2010).
20. Elbakry, A. *et al.* Layer-by-layer assembled gold nanoparticles for siRNA delivery. *Nano letters* **9**, 2059–64 (2009).
21. Schneider, G. & Decher, G. Functional core/shell nanoparticles via layer-by-layer assembly. Investigation of the experimental parameters for controlling particle aggregation and for enhancing dispersion stability. *Langmuir* **24**, 1778–1789 (2008).
22. Conde, J. *et al.* Design of Multifunctional Gold Nanoparticles for In Vitro and In Vivo Gene Silencing. *ACS nano* **6**, 8316–8324 (2012).

23. Giljohann, D., Seferos, D. S., Prigodich, A. E., Patel, P. C. & Mirkin, C. a Gene Regulation with Polyvalent siRNA-Nanoparticle Conjugates. *Journal of American Chemical Society* **131**, 2072–2073 (2009).
24. Zheng, D. *et al.* Topical delivery of siRNA-based spherical nucleic acid nanoparticle conjugates for gene regulation. *Proceedings of the National Academy of Sciences of the United States of America* **109**, 11975–80 (2012).
25. Barnaby, S. N., Lee, A. & Mirkin, C. a Probing the inherent stability of siRNA immobilized on nanoparticle constructs. *Proceedings of the National Academy of Sciences of the United States of America* **111**, 9739–44 (2014).
26. Lee, J. *et al.* Gold , Poly (-amino ester) Nanoparticles for Small Interfering RNA Delivery. *Nano letters* **9**, 2402–2406 (2009).
27. Resnier, P., Montier, T., Mathieu, V., Benoit, J. P. & Passirani, C. A review of the current status of siRNA nanomedicines in the treatment of cancer. *Biomaterials* **34**, 6429–6443 (2013).
28. Wittrup, A. & Lieberman, J. Knocking down disease: a progress report on siRNA therapeutics. *Nat Rev Genet* **16**, 543–552 (2015).
29. Cong, L. *et al.* Multiplex Genome Engineering Using CRISPR/Cas Systems. *Science* **339**, 819–823 (2013).
30. Doudna, J. A. & Charpentier, E. The new frontier of genome engineering with CRISPR-Cas9. *Science* **346**, 1258096–1258096 (2014).
31. Qi, L. *et al.* Cell-Penetrating Magnetic Nanoparticles for Highly Efficient Delivery and Intracellular Imaging of siRNA. (2012).
32. Davis, M. E. *et al.* Evidence of RNAi in humans from systemically administered siRNA via targeted nanoparticles. *Nature* **464**, 1067–70 (2010).
33. Mura, M. *et al.* Identification and angiogenic role of the novel tumor endothelial marker CLEC14A. *Oncogene* **31**, 293–305 (2012).
34. Maeda, H. The enhanced permeability and retention (EPR) effect in tumor vasculature: The key role of tumor-selective macromolecular drug targeting. *Advances in Enzyme Regulation* **41**, 189–207 (2001).
35. Iyer, A. K., Khaled, G., Fang, J. & Maeda, H. Exploiting the enhanced permeability and retention effect for tumor targeting. *Drug Discovery Today* **11**, 812–818 (2006).
36. Singh, N., Agrawal, A., Leung, A. K. L., Sharp, P. a & Bhatia, S. N. Effect of nanoparticle conjugation on gene silencing by RNA interference. *Journal of the American Chemical Society* **132**, 8241–3 (2010).
37. Dougan, J. a., Reid, A. K. & Graham, D. Thioctic acid modification of oligonucleotides using an H-phosphonate. *Tetrahedron Letters* **51**, 5787–5790 (2010).
38. Ave, H. ODMT phosphine S _ S. **1**, (2005).
39. Thatikonda, S. K., Srivastav, S. K. & Praveen, K. (19) United States. **1**, (2014).
40. Hammond, J., Cai, D. & Verhey, K. J. Tubulin modicfications and their cellular functions. *Current Opinion in Cell Biology* **20**, 71–76 (2008).
41. Schneider, C. a, Rasband, W. S. & Eliceiri, K. W. NIH Image to ImageJ: 25 years of image analysis. *Nature Methods* **9**, 671–675 (2012).
42. Park, H.-J. *et al.* Human umbilical vein endothelial cells and human dermal microvascular endothelial cells offer new insights into the relationship between lipid metabolism and angiogenesis. *Stem cell reviews* **2**, 93–102 (2006).
43. Nowak-Sliwinska, P. *et al.* Antiangiogenic and Anticancer Properties of Bifunctional Ruthenium(II)-p-Cymene Complexes: Influence of Pendant Perfluorous Chains. *Molecular Pharmaceutics* **12**, 3089–3096 (2015).
44. Nowak-Sliwinska, P. *et al.* Organometallic ruthenium(II) arene compounds with antiangiogenic activity. *Journal of Medicinal Chemistry* **54**, 3895–3902 (2011).

45. Sun, D. *et al.* The effects of luminescent ruthenium(II) polypyridyl functionalized selenium nanoparticles on bFGF-induced angiogenesis and AKT/ERK signaling. *Biomaterials* **34**, 171–180 (2013).
46. Bamford, R. a *et al.* Electroporation and Microinjection Successfully Deliver Single-Stranded and Duplex DNA into Live Cells as Detected by FRET Measurements. *PloS one* **9**, e95097 (2014).
47. Claire, S. *et al.* The deposition and imaging of silica sub-micron particles in dentine. *Journal of dentistry* **43**, 1242–8 (2015).

6 EXPERIMENTAL

6.1 Chemical Synthesis

6.1.1 Oligonucleotide Synthesis

6.1.1.1 DNA synthesis

Sequences were synthesised on an Applied Biosystems 394 DNA/RNA synthesizer as per normal oligo synthesis, using standard Syn Base CPG 1 µM (Link Technologies). Base de-protection was performed off column, in 1 M ammonia heated to 55°C for 6 hours using a heating block (Grant Instruments). The ammonia is removed under reduced pressure, before the sequences were purified by semi-prep HPLC (Dionex UVD 1705) using a Clarity 5µ Oligo-RP 150x4.6 mm (Phenomenex) column. After collecting the purified peak, the solvent is removed in vacuo (Thermo Scientific SAVANT SPD 131 DDA) before dissolving in water and passing through a NAP-10 column (GE Healthcare). The samples were then characterised by Mass Spectrometry and analytical HPLC (Shimadzu UFLC) on a Clarity 5µ Oligo-RP 150x4.6 mm 5 micron (Phenomenex) column.

6.1.1.2 NHS ester coupling reaction

Amine modified oligonucleotide was dissolved in sodium carbonate buffer (100 µL, 0.1 M). A 5 molar excess of the thioctic acid NHS ester was added dissolved in DMSO (5 µL). The reaction was vortexed and heated overnight at 37°C. The reaction was then passed through a NAP-5 column (GE Healthcare) using TEAA buffer (0.1 M) as eluent. The modified oligonucleotide was then purified by HPLC and characterised by Mass Spectrometry.

6.1.1.3 RNA synthesis

Sequences were synthesised on an Applied Biosystems 394 DNA/RNA synthesizer as per standard RNA oligo synthesis, using standard RNA bases (Link Technologies). The sequences were left on column after the synthesis; columns were then removed from the synthesiser and washed with 2.5 mL ammonia: ethanol (3:1) using syringes, washing through every 30 minutes for 2 hours. The mixture was then poured into a vial, washing the column once more with 1 mL ammonia: ethanol (3:1). The solution was then heated for 6 hours at 55°C. Once cooled, the solution was dried on a rotor evaporator. The dry sample was vortexed in 0.5 mL of TBAF (1 M in THF) and left overnight. The samples were then passed through a NAP-10 column (GE Healthcare) using water as eluent. The solution was then concentrated, 375 mL of sample was placed into a 2 mL Eppendorf, to this 0.2 mL of Sodium acetate (0.1 M) and 1.4 mL of iso-propanol were added. The mixture was centrifuged in a refrigerated centrifuge at 15000 rpm at 4 °C for 15 minutes. The supernatant was removed in a speed vac, the pellets were recombined in 1 mL water, vortexing to re-dissolve them. The samples were then purified by semi-prep HPLC using a Clarity 5µ Oligo-RP 150x4.6 mm column. The solvent was then removed and the samples passed through a NAP-10 column to desalt. The samples were then characterised by Mass Spectrometry and analytical HPLC on a Clarity 5µ Oligo-RP 150x4.6 mm 5 micron column.

6.1.1.4 Oligonucleotide purification

Probe	Sequence	Mass Spec ES+
P.UM	TGG ACT CTC TCA ATG	4696 $[M+H]^+$

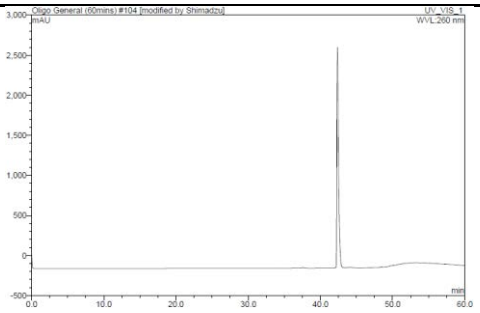

Analytical HPLC UV absorption at 260 nm

Probe	Sequence	Mass Spec ES+
P.AF	W-TGG ACT CTC TCA ATG	4911 $[M]^+$

W = thioctic acid modification

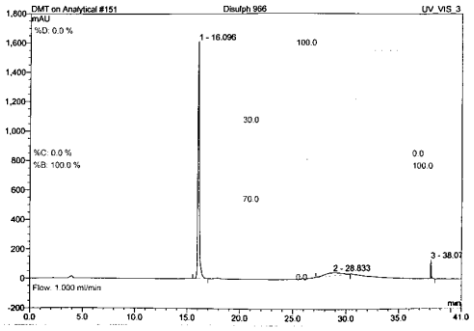

Analytical HPLC UV absorption at 260 nm

Probe	Sequence	Mass Spec ES+
P.1L	W-TGG ACT CLC TCA ATG	5008 $[M]^+$

W = thioctic acid modification **L** = 1L anthracene probe

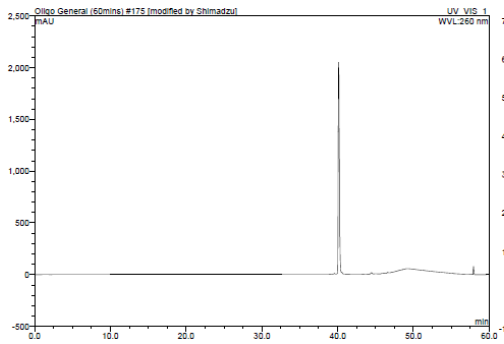

Analytical HPLC UV absorption at 260 nm

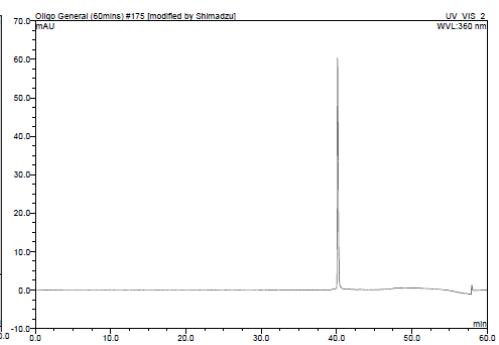

Analytical HPLC λ_{ex} 350 nm λ_{em} 426 nm

Probe	Sequence	Mass Spec ES+
P.1D	**W**-TGG ACT C**D**C TCA ATG	5008 $[M]^+$

W = thioctic acid modification **D** = 1D anthracene probe

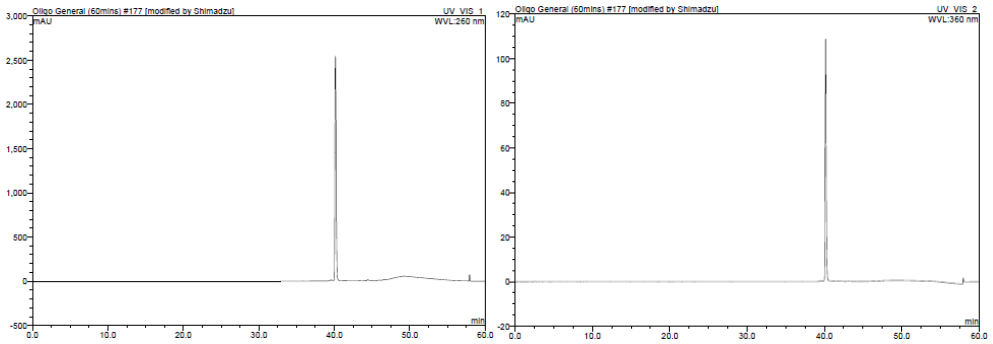

Analytical HPLC UV absorption at 260 nm Analytical HPLC λ_{ex} 350 nm λ_{em} 426 nm

Probe	Sequence	Mass Spec ES+
P.5L	**W**-CAU UGA G**X**G AGU CCA	5065 $[M]^+$

W = thioctic acid modification **X** = 5L anthracene probe

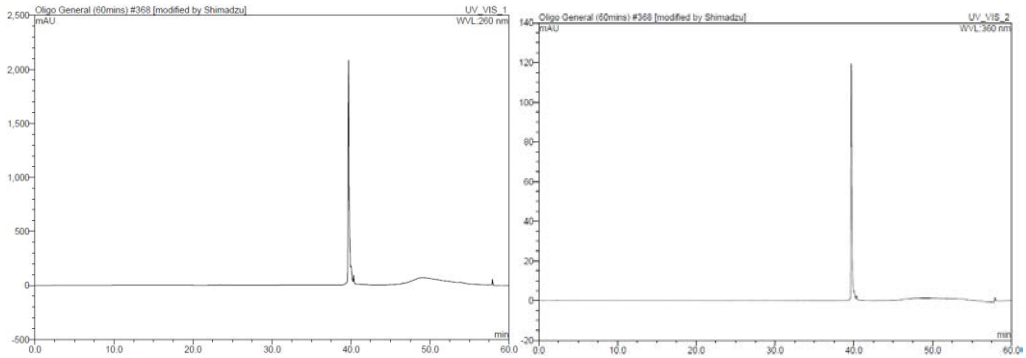

Analytical HPLC UV absorption at 260 nm Analytical HPLC λ_{ex} 350 nm λ_{em} 426 nm

Probe	Sequence	Mass Spec ES+
m.P.1L	**W**-AAAAA TGG ACT C**L**C TCA ATG	6573 $[M-H]^-$

W = thioctic acid modification **L** = 1L anthracene probe

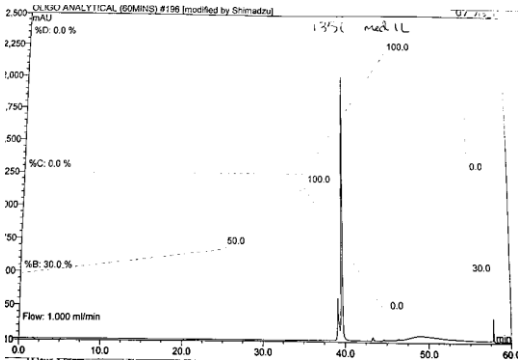

Analytical HPLC UV absorption at 260 nm

Probe	Sequence	Mass Spec ES-
l.P.1L	**W**-AAAAA AAAAA TGG ACT C**L**C TCA ATG	8139 $[M-H]^-$

W = thioctic acid modification **L** = 1L anthracene probe

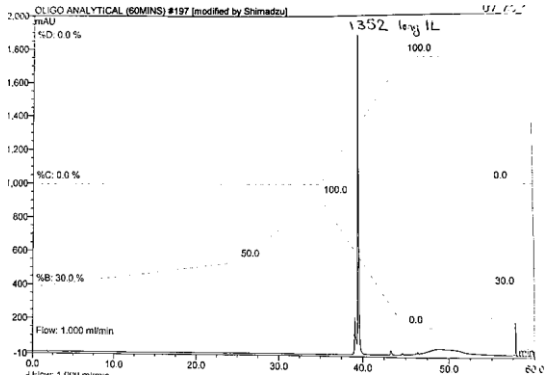

Analytical HPLC UV absorption at 260 nm

Probe	Sequence	Mass Spec ES+
DNA-T.1	CAT TGA GAG AGT CCA	4601 $[M+H]^+$

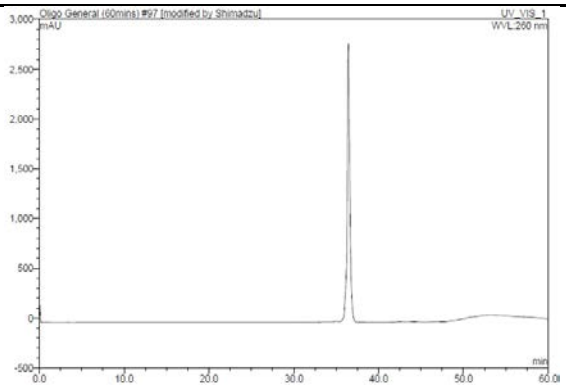

Analytical HPLC UV absorption at 260 nm

Probe	Sequence	Mass Spec ES-
DNA-T.2	CAT TGA GAA AGT CCA	4585 [M]

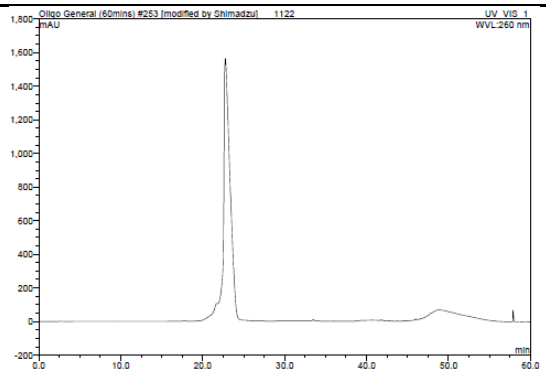

Analytical HPLC UV absorption at 260 nm

Probe	Sequence	Mass Spec ES-
RNA-T.1	CAU UGA GAG AGU CCA	4798 $[M-H]^-$

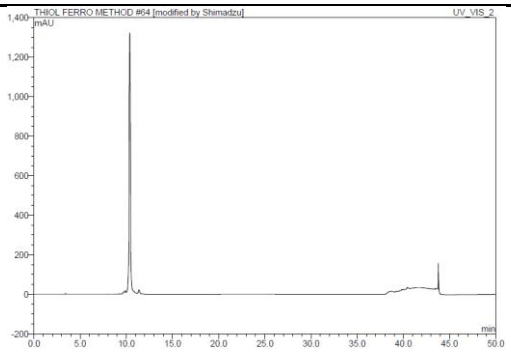

Analytical HPLC UV absorption at 260 nm

Probe	Sequence	Mass Spec ES-
RNA-T.2	CAU UGA GAA AGU CCA	4782 $[M-H]^-$

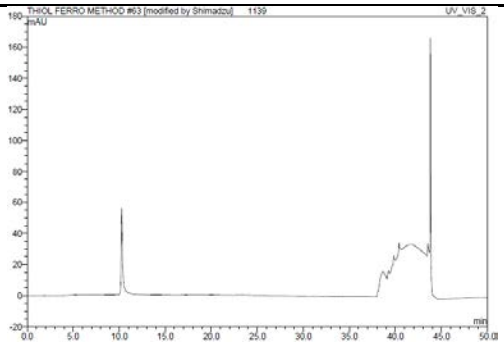

Analytical HPLC UV absorption at 260 nm

Probe	Sequence	Mass Spec ES-
DNA-T.3	AGC TGA GAC GCG ACT	4602 [M]

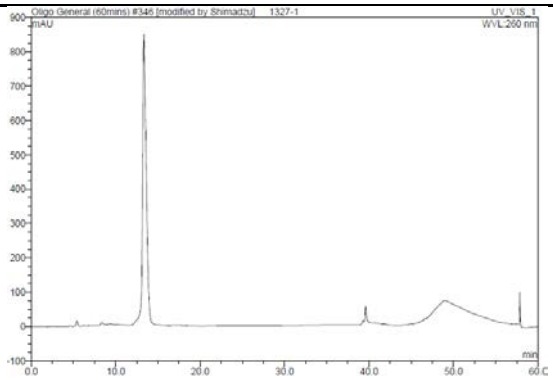

Analytical HPLC UV absorption at 260 nm

Probe	Sequence	Mass Spec ES-
DNA-T.4	AGC TGA GCC GCG ACT	4577 $[M-H]^-$

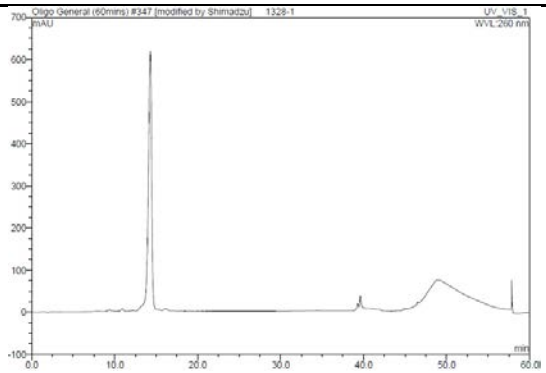

Analytical HPLC UV absorption at 260 nm

Probe	Sequence	Mass Spec ES+
RNA.1	**Q**-CAA UCA GGG UCG ACG AGA A	6458 [M]

Q = Compound **8** modification

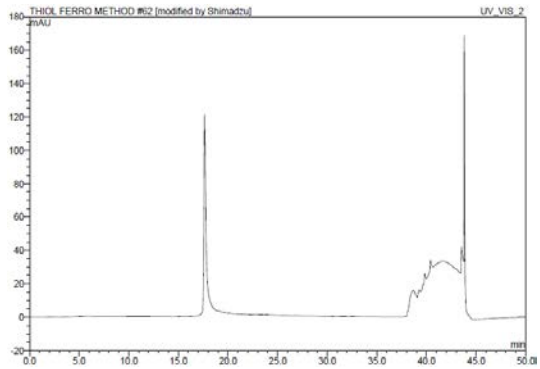

Analytical HPLC UV absorption at 260 nm

Probe	Sequence	Mass Spec ES-
RNA.2	UUC UCG UCG ACC CUG AUU G	5952 [M]

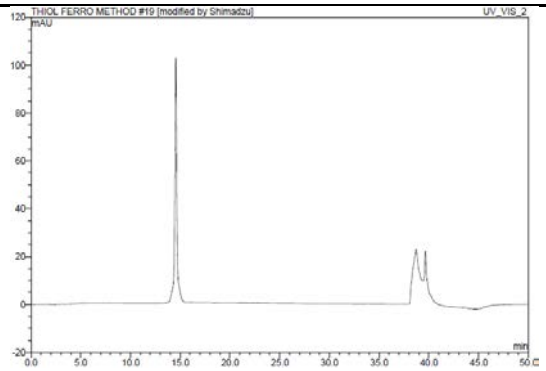

Analytical HPLC UV absorption at 260 nm

6.1.1.5 UV-Vis concentration

Concentration of DNA strands calculated using a Shimadzu UV-1800 UV Spectrophotometer, placing 10 µL of sample into a UV cuvette before making up to 1000 µL with MilliQ water (MilliQ water as blank). Entering the sequence onto the website http://biophysics.idtdna.com/UVSpectrum.html allowed the absorption coefficient of the strand to be determined. The Beer-Lambert law is then used to calculate the concentration of the DNA sample using the absorption value at 260 nm.

6.1.1.6 Duplex melting temperature

A 1 µM solution of the duplex DNA was made up with 10 mM phosphate buffer (pH 7.0) and 100 mM NaCl, the solution is thoroughly mixed using a pipette, the sample is placed in a T_m cuvette and made up to 1000 µL using deionised water. A sample made up of 10 mM phosphate buffer (pH 7.0) and 100 mM NaCl was used for blank correction. The samples were run on a Cary-5000 UV-Vis-NIR Spectrophotometer fitted with a Cary Temperature Controller. The absorption at 260 nm was monitored at a temperature range of 15°C-85°C. Measurements were taken every 0.5°C, with a heating rate of 0.5°C per minute, each temperature was held for 3 minutes before the reading is taken.

6.1.1.7 Fluorescence spectroscopy

A 1 µM solution of the duplex DNA was made up with 10 mM phosphate buffer (pH 7.0) and 100 mM NaCl, the solution is thoroughly mixed using a pipette. For DNA-AuNP samples, 2.5 nM AuNP sample was made up with 10 mM phosphate buffer (pH 7.0) and 100 mM NaCl, the solution is thoroughly mixed using a pipette. For samples run on Shimadzu RF-5301 PC

Spectrofluorophotometer, anthracene λ_{ex} = 350 nm λ_{em} = 370-550 nm, slit widths for excitation were 5 nm and emission 10 nm. Each run dwell time 1.0 second, 1 nm bandwidth 1 accumulation. For samples run on FLSP920 Times Resolved Spectrometer (Edinburgh), anthracene λ_{ex} = 350 nm λ_{em} = 390-550 nm, slit widths for excitation 5 nm and emission 10 nm. Each run dwell time 1.0 second, 1 nm bandwidth 1 accumulation. For the ruthenium probe, λ_{ex} = 465 nm λ_{em} = 580-800 nm, slit widths for excitation 15 nm and emission 15 nm. Each run dwell time 1.0 second, 3 nm bandwidth 3 accumulations.

6.1.1.8 Circular Dichroism

9 nM AuNP sample was made up with 10 mM phosphate buffer (pH 7.0) and 100 mM NaCl, the solution is thoroughly mixed using a pipette. A sample made up of 10 mM phosphate buffer (pH 7.0) and 100 mM NaCl was used for blank correction. The samples were run on a JASCO J-810 Spectropolarimeter. 10 scan accumulations were made at a data pitch of 0.2 nm at 200 nm/min.

6.1.2 Ion exchange for RubpySS

Two spatulas (1 x 2 cm) of Dowex beads (Dowex 1 x 8 200-400 MESH Cl) were placed in a 100 mL beaker containing 50 mL deionised H_2O. The pH of the H_2O was lowered to pH 5.0 using concentrated hydrochloric acid and allowed to stir for 1 hour before the beads are removed using filter paper. The Dowex beads are rediluted in MeOH (50 mL) to which the RubpySS is added (2 mL, 200 µM). The solution is allowed to stir vigorously for 4 hours before removing the Dowex beads by filtration taking care to rinse the beads with plenty of MeOH. The MeOH is then removed under reduced pressure.

6.1.3 2,5-dioxopyrrolidin-1-yl 5-(1,2-dithiolan-3-yl)pentanoate (Compound 1)

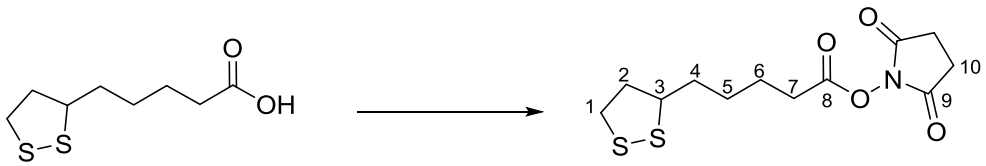

In a round bottomed flask 1.84 g N-(3-Dimethylaminopropyl)-N'- ethylcarbodiimide hydrochloride was dissolved in anhydrous DCM (20 mL). 1.7 mL of N,N-Diisopropylethlyamine (DIPEA) was added the reaction and the reaction was allowed to stir for 10 minutes. The reaction vessel was placed in an ice bath before 1.29 g of N-Hydroxy succinimide (NHS) was added to the mixture and allowed to stir. 1.643 g of thioctic acid was firstly dissolved in 10 mL of anhydrous DCM, then added to the reaction over 5 minutes. The reaction was then left to stir overnight at room temperature. The reaction was washed with HCl (aq) (5% [v/v], 50 mL) twice and then with 50 mL water. The organic layer was dried over Na_2SO_4 and then solvents concentrated in vacuo. The residue was dry loaded onto Na_2SO_4 and purified by column chromatography (50% EtAc : 50% Hexane) giving the purified product (compound 1) as a yellow powder (0.451g, 1.49 mmol, 19%).

Rf = 0.57 in EtAc: Hexane 50:50; ^{1}HNMR (300 MHz, DMSO) δ 3.56–3.65 (1H, m, H_3), 3.12–3.21 (2H, m, H_1), 2.81 (4H, s, H_{10}), 2.69 (2H, t, J 7.1, H_7), 2.38–2.46 (1H, m, H_2), 1.84–1.93 (1H, m, H_2), 1.4–1.7 (6H, m, H_4 H_5 H_6); ^{13}CNMR (100 MHz, DMSO) δ 170.2 (*2 x* C_9), 168.9 (C_8), 55.9 (C_3), 40.1 (C_2), 38.1 (C_1), 33.8 (C_4), 30.0 (C_7), 27.6 (C_5), 25.4 (*2 x* C_{10}), 24.0 (C_6),

TOF MS EI$^+$ $[M]^+$ 303.09

6.1.4 Anthracene probe synthesis

6.1.4.1 Synthesis of acetate (Compound 2)

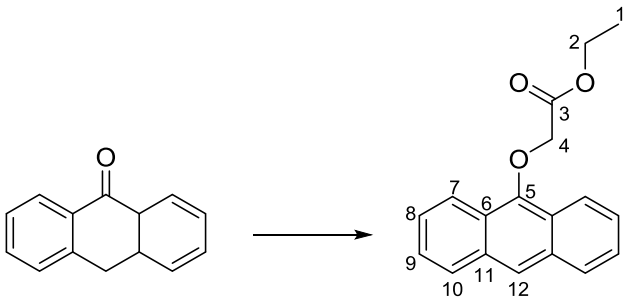

In a round bottomed flask anthrone (5.83 g) and K_2CO_3 (4.15 g) were dissolved in degassed acetone (200 mL) and stirred for 15 minutes in the dark. Ethyl Bromoacetae (3.3 mL) was then syringed into the flask and the reaction refluxed under N_2 overnight in the dark. The solution was filtered to remove the K_2CO_3 and the solvent removed *in vacuo*. The solid was re-dissolved in DCM (100 mL) and washed with water (50 mL) before drying with $MgSO_4$. The solvent was removed by reduced pressure and the solid (compound 2) purified by column chromatography (10% hexane: DCM) giving a yellow solid (1.91 g, 23%).

Rf = 0.54 in 10% hexane: DCM; ^{1}HNMR (300 MHz, $CDCl_3$) δ 8.23 (2H, d, J 8.5, H_7), 8.09 (1H, s, H_{12}), 7.84 (2H, d, J 8.1, H_{10}), 7.28-7.44 (4H, m, H_8 H_9), 4.66 (2H, s, H_4), 4.24 (2H, q, J 7.1, H_2), 1.23 (3H, t, J 7.1, H_1);

TOF-MS-ES$^+$ $[M+H]^+$ 281.12 $[M+Na]^+$ 303.09

6.1.4.2 Synthesis of Carboxylic acid (Compound 3)

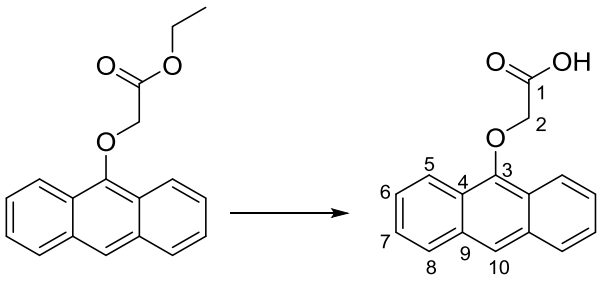

In a round bottomed flask, 1 g of 2-(anthracen-9-yloxy) acetate was dissolved in 10% NaOH in EtOH 1:1 (200 mL), this was refluxed overnight in the absence of light under N_2. The EtOH was removed *in vacuo* and water was added (400 mL), conc HCl was then added dropwise whilst swirling the solution until a creamy precipitate appears and does not disappear upon mixing, to give a cream solid (800 mg, 89%).

^{1}HNMR (300 MHz, $CDCl_3$) δ 8.34 (1H, s, H_{10}), 8.31 (2H, d, J 8.3, 2 x H_5), 8.06 (2H, d, J 8.0, 2 x H_8), 7.49-7.60 (4H, m, 2 x H_6,H_7), 4.91 (2H, s, H_2); ^{13}CNMR (100 MHz, $CDCl_2$) 172.1 (C_1), 149.5 (C_3), 132.6 (2 x C_9), 128.9 (2 x C_8), 127.2 (2 x C_6), 126.1 (2 x C_7), 125.7 (2 x C_6), 123.6 (C_{10}), 121.6 (2 x C_5), 71.2 (C_2);

TOF-MS-ES$^-$ $[M-H]^-$ 251.06

6.1.4.3 Synthesis with L-threoninol (Compound 4)

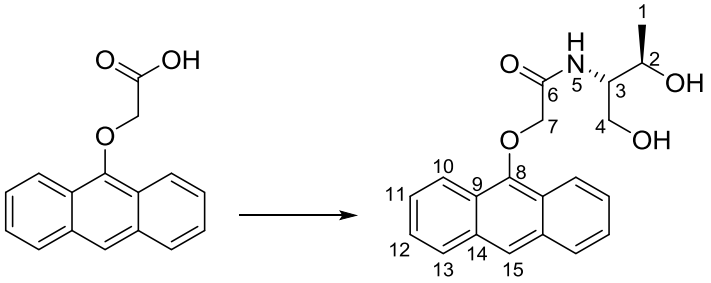

In a round bottomed flask the 2-(anthracen-9-ylox) acetic acid (300 mg) was dissolved in dry DMF (20 mL) under inert conditions. 2-(1H-benzotriazol-1-yl)-1,1,3,3-tetramethyluronium hexafluorophosphate (HBTU) (0.455 g) was added and the solution stirred for 15 minutes in the dark. L-threoninol (0.126 g) and DIPEA (0.21 mL) were added and the solution stirred at 40°C for 40 hours. The solvent was removed *in vacuo* the product was then purified by column chromatography (5% MeOH: DCM) giving a pale yellow solid (203 mg, 49%).

Rf = 0.27 in DCM : 5% MeOH; ^{1}HNMR (300 MHz, $CDCl_3$) δ 8.38 (1H, s, H_{15}), 8.30-8.35 (2H, m, H_{10}), 8.06-8.11 (2H, dd J 8.4 & 2.0, H_{13}), 7.49-7.60 (4H, m, H_{11} ,H_{12}), 4.74 (2H, d, J 5.8, H_7), 4.15-4.23 (1H, m, H_2), 4.07-4.14 (1H, m, H_3), 3.83 (2H, m, H_4), 1.35 (3H, d, J 6.4, H_1); ^{13}CNMR (100 MHz, $CDCl_3$) δ 132.1 (C_{14}), 128.3 (C_{13}), 125.7 (C_{11}), 125.3 (C_{12}), 124.0 (C_9), 122.9 (C_{15}), 121.1 (C_{10}), 73.2 (C_7), 65.6 (C_2), 61.6 (C_4), 55.8 (C_3), 19.3 (C_1);

TOF-MS-ES$^+$ $[M+Na]^+$ 362.1

6.1.4.4 DMT protection of primary alcohol (Compound 5)

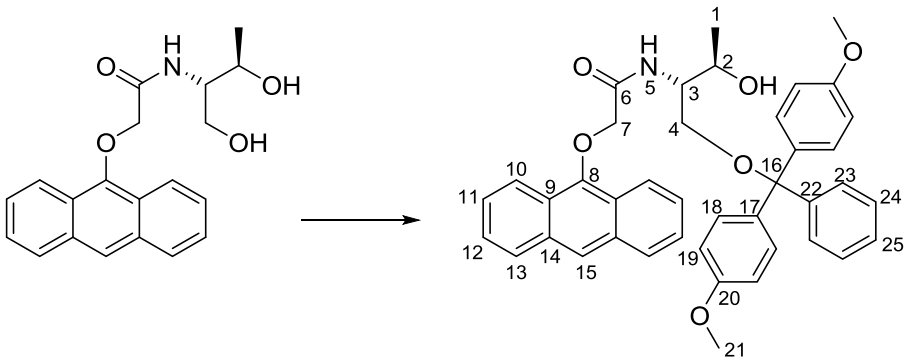

In a round bottomed flask 2-(anthracen-9-yloxy)-N-((2S,3S)-1,3-dihydroxybutan-2-yl)acetamide (200 mg) was dissolved in pyridine (30 mL) under an inert atmosphere. To this 4,4'-Dimethoxytrityl chloride (0.20 g) and 4-(Dimethylamino)pyridine (0.01g) were added and the solution was stirred for 24 hours under N_2. The solvent was removed under reduced pressure and the product was then purified by column chromatography (EtAc: Hexane: TEA, 49: 50: 1) giving a yellow crystalline solid (151 mg, 43%).

Rf ; 0.52; ^{1}HNMR (300 MHz, CD_3CN) δ 8.21 (1H, s, H_{15}), 8.12 (2H, d, J 8.3, H_{10}), 7.91 (2H, d, J 8.3, H_{13}), 7.48 (1H, d, J 9.0, H_5), 7.32-7.42 (4H, m, H_{12} H_{23}) 7.24-7.31 (6H, m, H_{11} H_{18}) 7.17 (2H, m, H_{24}) 7.06-7.12 (1H, m, H_{25}), 6.71 (4H, d, J 8.9, H_{19}), 4.57 (2H, s, H_7), 3.98-4.13 (2H, m, H_3, H_2), 3.59 (6H, s, H_{21}), 3.06-3.29 (2H, m, H_4), 1.10 (3H, d, J 6.3, H_1); ^{13}CNMR (100 MHz, CD_3CN) δ 168.8 (C_6), 159.2 (C_{20}), 149.7 (C_8), 145.8 (C_{22}), 136.7 (C_{17}), 132.8 (C_{14}), 130.5 (C_{18}), 129.1 (C_{13}), 128.6 (C_{23}), 128.4 (C_{24}), 127.4 (C_{25}), 126.5 (C_{11}), 126.3 (C_{12}), 124.7 (C_9), 123.7 (C_{15}), 122.1 (C_{10}), 113.6 (C_{19}), 86.5 (C_{16}), 74.3 (C_7), 66.7 (C_2), 63.9 (C_4), 55.4 (C_{21}), 54.9 (C_3), 20.4 (C_1);

TOF-MS-ES$^+$ $[M+Na]^+$ 692.3

6.1.4.5 Reaction forming phosphoramidite (Compound 6)

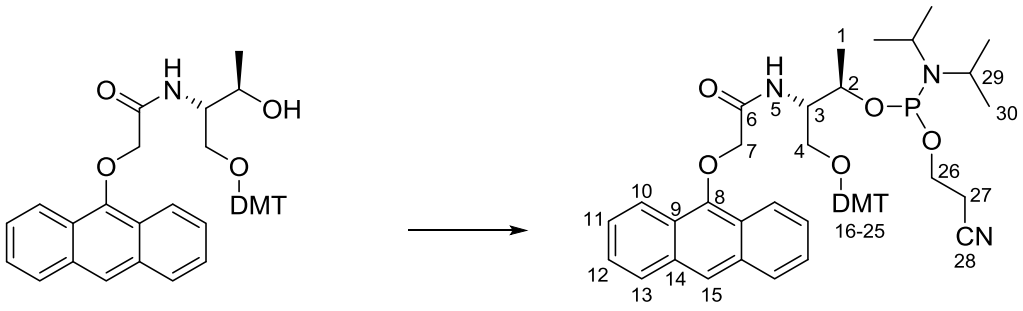

In a round bottomed flask, the DMT protected 2-(anthracen-9-yloxy)-N-((2S,3S)-1,3-dihydroxybutan-2-yl)acetamide (100 mg) was dissolved in dry DCM (5 mL) under an inert atmosphere. To this DIPEA (0.22 mL) was added. (i-Pr_2N)$PClO(CH_2)_2CN$ (0.054 mL) was added dropwise to the reaction mixture, the reaction was then left to stir for 2 hours. Once the reaction was complete, degassed ethyl acetate (5 mL) was added, the solution was then washed with degassed Na_2CO_3 (2M, 2 x 50 mL) then degassed brine (50 mL) before being dried over Na_2SO_4. The solution was filtered and dried under reduced pressure before being purified by column chromatography on activated alumina (EtAc: Hexane: TEA, 50:49:1) the compound was then bottled up and placed under argon until used on the DNA synthesiser (88 mg, 73%)

Rf ; 0.85; ^{1}HNMR (300 MHz, DMSO) δ 8.28 (1H, s, H_{15}) 8.13 (2H, d, J 8.7, H_{10}) 7.98 (2H, d, J 8.2, H_{13}) 7.35-7.48 (5H, m, H_5 H_{12} H_{23}) 7.26-7.37 (6H, m, H_{11} H_{18}) 7.09-7.26 (3H, m, H_{24} H_{25}) 6.72-6.80 (4H, m, H_{19}) 4.61 (2H, s, H_7) 4.15-4.37 (2H, m, H_3 H_2) 3.63 (6H, s, H_{21}) 3.40-3.81 (4H, m, H_{26} H_{29}) 3.27-3.38 (2H, m, H_4) 2.47-2.61 (2H, m, H_{27}) 1.09 (3H, d, J 3.1, H_1) 0.92 (12H, dd, J 20.0,7.29, H_{30}); ^{31}PNMR (120 MHz, MeCN) δ 146.1;

6.1.5 Thioctic acid phosphoramidite synthesis

6.1.5.1 5-(1,2-dithiolan-3-yl)-N-(2-hydroxyethyl)pentanamide (Compound 7)

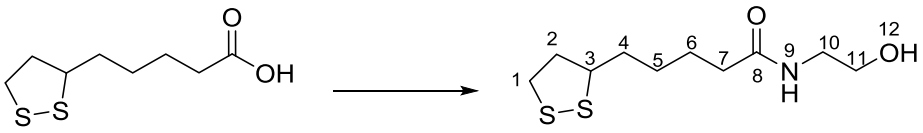

In a round bottomed flask, thioctic acid (0.71 g) and HOBt (0.46 g) were dissolved in dry DMF (10 mL) and stirred over ice. To this, EDC.HCl (0.66 g) was added and the mixture was stirred for 1 hour, still over ice. The solution was allowed to warm to room temperature for 1 hour. In a separate flask, 4-ethylmorpholine (0.39 g) and 2-aminoethan-1-ol (0.15 g) was dissolved in dry DMF (5 mL), this was then added to the thioctic acid containing solution and then allowed to stir overnight. The solution was washed with DCM: H_2O, the DCM was then removed under reduced pressure. The product was purified by column chromatography on silica (5% MeOH, $CHCl_3$) giving the product as a yellow solid (455 mg, 73%).

Rf = 0.41 in $CHCl_3$: 5% MeOH; ^{1}HNMR (300 MHz, $CDCl_3$) δ 6.57 (1H, s, H_9), 3.58-3.77 (2H, m, H_{11}), 3.45-3.56 (1H, m, H_3), 3.28-3.40 (2H, m, H_{10}), 3.20-2.97 (2H, m, H_1), 2.40 (1H, dq, J 12.6, 6.1, H_{2a}), 2.16 (2H, t, J 7.3, H_7), 1.85 (1H, dq, J 13.2, 6.7, H_{8b}), 1.52-1.72 (4H, m, H_4 H_6), 1.33-1.45 (2H, m, H_5); ^{13}CNMR (100 MHz, $CDCl_3$) δ 174.2 (C_8), 61.9 (C_{11}), 56.4 (C_3), 42.4 (C_{10}), 40.3 (C_2), 38.5 (C_1), 36.3 (C_7), 34.6 (C_4), 28.9 (C_5), 25.4 (C_6);

TOF-MS-ES$^+$ $[249.1]^+$

6.1.5.2 2-(5-(1,2-dithiolan-3-yl)pentanamido)ethyl (2-cyanoethyl) diisopropylphosphoramidite (Compound 8)

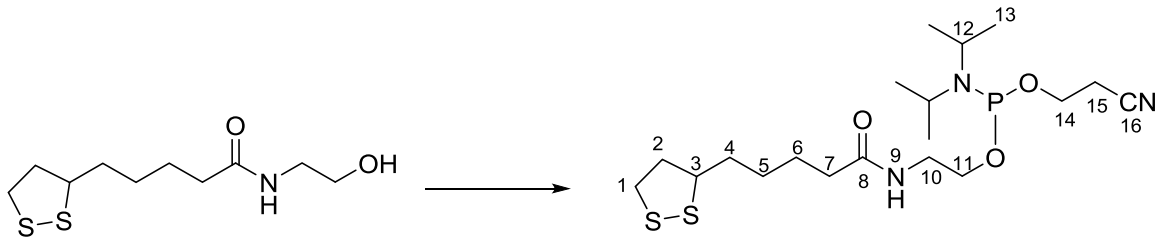

In a round bottomed flask, the 5-(1,2-dithiolan-3-yl)-N-(2-hydroxyethyl)pentanamide (125 mg) was dissolved in dry DCM (5 mL) under an inert atmosphere. To this DIPEA (0.716 mL) was added. (i-Pr_2N)$PClO(CH_2)_2CN$ (0.314 mL) was added dropwise to the reaction mixture, the reaction was then left to stir for 2 hours. Once the reaction was complete, degassed EtAc (5 mL) was added, the solution was then washed with degassed Na_2CO_3 (2 M, 2 x 50 mL) then degassed brine (50 mL) before being dried over Na_2SO_4. The solution was filtered and dried under reduced pressure before being purified by column chromatography on activated alumina (EtAc: Hexane: TEA, 50:49:1) giving a yield of 75%.

Rf ; 0.9; ^{1}HNMR (300 MHz, CD_3CN) δ 3.44-3.90 (7H, m, H_3 H_{11} H_{12} H_{14}) 3.34-3.44 (2H, m, H_{10}) 2.99-3.17 (2H, m, H_1) 2.60 (2H, t, J 6.2, H_{15}) 2.40 (1H, dtd, J 12.9,6.6,5.5, H_2) 2.13 (2H, t, J 7.5, H_7) 1.84 (1H, dq, J 12.7,7.0, H_2) 1.5-1.73 (4H, m, H_4 H_6) 1.33-1.47 (2H, m, H_5) 1.12 (12H, dd, J 6.9,4.6, H_{13}); ^{13}CNMR (100 MHz, CD_3CN) 173.0 (C_8), 117.8 (C_{16}), 62.5 (C_{11}), 58.9 (C_{14}), 56.9 (C_3), 54.6 (C_7), 43.3 (C_{12}), 40.6 (C_{10}), 38.8(C_2), 36.1(C_1), 34.8(C_4), 29.0(C_5), 25.6(C_6), 24.6 (C_{13}), 20.4 (C_{15}); ^{31}PNMR (120 MHz, CD_3CN) δ 148.0;

TOF-MS-ES$^+$ $[M+H]^+$ 450, $[M+Na]^+$ 472.

6.2 Gold Nanoparticle synthesis

6.2.1 13 nm gold nanoparticles

All glassware was soaked in aqua regia for at least 30 minutes prior to reaction, the glassware was then rinsed 10 times with deionised water and placed in an oven prior to use. In a 250 mL round bottomed flask fitted with a condenser, 100 mL of 2.75 mM citrate buffer (75:25 sodium citrate: citric acid) was heated until boiling, ensuring a vortex is formed by the vigorous stirring. After 15 minutes of boiling, 1.6 mg of Ethylenediaminetetraacetic acid (EDTA) was added to the solution. In a separate flask, 25 mL of $HAuCl_4.3H_2O$ (Sigma Aldrich) (8.5 mg) is placed in an oven to heat until 90°C. The solution of gold was then added rapidly to the centre of the vortex of the citrate buffer solution and allowed to boil for 20 minutes. After 20 minutes the heat is turned off, and the solution is allowed to cool to room temperature still with vigorous stirring.

SPR = 519 nm, number distribution = 12 nm (± 3 nm), intensity distribution = 21 nm (± 6 nm)

6.2.2 100 nm gold nanoparticles

The larger particles are grown by the particle seeding method starting with 13 nm particles, which are synthesised as described above (**6.2.1**). Initially stock solutions of the reactants were made up as: 5 mM $HAuCl_4.H_2O$ (100 mg in 50 mL deionised H_2O), 57 mM ascorbic acid (500 mg in 50 mL deionised H_2O) and 34 mM trisodium citrate dehydrate (500 mg in 50 mL deionised H_2O).

25 nm gold nanoparticles

A solution of 30 mL 13 nm AuNP (2 nM) was diluted to 40 mL with deionised water in a 250 mL three necked round bottomed flask. The solution was vigorously stirred. Two solutions were then made up using the stock solutions, solution A = 1 mM $HAuCl_4.H_2O$ (20 mL) solution B = 2.85 mM ascorbic acid and 1.7 mM trisodium citrate dehydrate (20 mL). Solution A and B were then added to the AuNP solution using a peristaltic pump over 45 mins. Once added, the AuNP solution was refluxed for 30 minutes and allowed to cool to room temperature.

Number distribution =22 nm (± 5 nm), intensity distribution = 31 nm (± 8 nm)

50 nm gold nanoparticles

A solution of 9 mL 25 nm AuNP (0.7 nM) was diluted to 40 mL with deionised water in a 250 mL three necked round bottomed flask. The solution was vigorously stirred. Two solutions were then made up using the stock solutions, solution A = 1 mM $HAuCl_4.H_2O$ (20 mL) solution B = 2.85 mM ascorbic acid and 1.7 mM trisodium citrate dehydrate (20 mL). Solution A and B were then added to the AuNP solution using a peristaltic pump over 45 mins. Once added, the AuNP solution was refluxed for 30 minutes and allowed to cool to room temperature, the solution was neutralised with 0.01 M NaOH.

Number distribution = 38 nm (± 9 nm), intensity distribution = 56 nm (± 16 nm)

100 nm gold nanoparticles

A solution of 40 mL 50 nm AuNP (80 pM) was placed in a 250 mL three necked round bottomed flask. The solution was vigorously stirred. Two solutions were then made up using the stock solutions, solution A = 4 mM $HAuCl_4.H_2O$ (20 mL) solution B = 11.4 mM ascorbic

acid and 3.4 mM trisodium citrate dehydrate (20 mL). Solution A and B were then added to the AuNP solution using a peristaltic pump over 45 mins. Once added, the AuNP solution was refluxed for 30 minutes and allowed to cool to room temperature.

SPR = 561 nm, number distribution = 68 nm (± 20 nm), intensity distribution = 105 nm (± 32 nm) (100%)

6.2.3 Characterising AuNP

6.2.3.1 Inductively Coupled Plasma Mass Spectrometry

The DNA/ruthenium coated AuNP were synthesised and purified. 3 mL of 1 nM coated AuNP was dissolved using 5% aqua regia. These samples were sent to Warwick University to be analysed by ICP-MS by Professor Lijiang Song.

6.2.3.2 Sizing

1 mL of 2 nM AuNP sample is placed into a disposable DT50012 cuvette (SARSTEDT) before sizing the particles on a Zetasizer NANO (Malvern). Each sample was run 12 times, repeating this 3 times and taking an average of the value.

6.2.3.3 Zeta Potential

800 µL of 2 nM AuNP sample is injected into a disposable DTS 1070 cuvette (Malvern) using a 1 mL syringe. The samples were then run on a Zetasizer NANO (Malvern). Each sample was run 30 times, repeating this 10 times and taking an average value.

6.2.3.4 Transmission Electron Microscopy

Using tweezers to hold the copper grid (3 mm, FORMVAR) in a clean and safe area, 20 µL of 2 nM sample of AuNP is pippeted onto the grid. The sample is left to settle for 20 minutes, after 20 minutes wick away excess using filter paper. The samples were then imaged using a JEOL 1200 Transmission Electron Microscope. Coated AuNP procedure

6.2.4 Coating AuNP procedures

6.2.4.1 Coating 13 nm AuNP with DNA

In an Eppendorf containing a magnetic stirrer, citrate coated AuNPs (13 nm, 3 nM) are made up in 10 mM pH 7.0 phosphate buffer. Thioctic acid modified DNA (0.99 μM) is added to the AuNPs and stirred for 2 minutes before the solution is sonicated for 20 seconds. The UV-vis spectrum of the particles is taken prior to purification. This process is repeated a further two times giving a final DNA concentration of 2.97 μM. The particles are passed through a Sephadex G-50 column (stored in 20% ethanol) with deionised water as eluent. A final UV-vis spectrum is taken to confirm concentration (explained in **7.1.3**), histogram sizing data in **7.5**.

Particle	SPR (nm)	Size: number distribution (nm)	Size: intensity distribution (nm)	Zeta potential (mV)
Citrate AuNP	519	12 (± 3)	21 (± 6) *100%*	-35 (± 10) *100%*
P.UM-AuNP	520	13 (± 4)	48 (± 34) *96%*	-32 (± 10) *57%* +7 (± 8) *42%*
P.AF-AuNP	522	14 (± 4)	48 (± 32) *96%*	-37 (± 12) *97%*
P.1L-AuNP	522	14 (± 4)	34 (± 17) *96%*	-23 (± 8) *99%*
P.1D-AuNP	522	14 (± 4)	30 (± 11) *96%*	-26 (± 7) *96%*
m.P.1L-AuNP	522	14 (± 3)	24 (± 12) *95%*	-37 (± 6) *96%*
l.P.1L-AuNP	522	15 (± 4)	39 (± 21) *97%*	-32 (± 8) *97%*
P.5L-AuNP	522	15 (± 4)	32 (± 16) *97%*	_

6.2.4.2 Coating 13 nm AuNP with DNA and RubpySS

In an Eppendorf containing a magnetic stirrer, citrate coated AuNPs (13 nm, 3 nM) are made up in 10 mM pH 7.0 phosphate buffer. Thioctic acid modified DNA (0.33 μM) is added to the AuNPs and stirred for 2 minutes before the solution is sonicated for 20 seconds. This process

is repeated a further two times giving a final DNA concentration of 0.98 μM. RubpySS (1.5 μM) probe is added to the particles and allowed to stir for 20 minutes. This process is repeated, giving a final RubpySS concentration of 3 μM. The particles are passed through a Sephadex G-50 column (stored in 20% ethanol) with deionised water as eluent. A final UV-vis spectrum is taken to confirm concentration (explained in **7.1.3**), histogram sizing data in **7.5**.

Particle	SPR (nm)	Size: number distribution (nm)	Size: intensity distribution (nm)
P.AF-AuNP-Ru	524	14 (± 4)	40 (± 19) *97%*
P.1L-AuNP-Ru	524	14 (± 4)	34 (± 17) *96%*
P.1D-AuNP-Ru	524	14 (± 4)	23 (± 9) *87%* 286 (± 97) *10%*
l.P.1L-AuNP-Ru	524	16 (± 5)	36 (± 6) *96%*
P.5L-AuNP-Ru	524	15 (± 4)	35 (± 16) *96%*

6.2.4.3 Coating 100 nm AuNP with P.1L

In an Eppendorf containing a magnetic stirrer, citrate coated AuNPs (100 nm, 40 pM) are made up in 10 mM pH 7.0 phosphate buffer. **P.1L** (0.73 μM) is added to the AuNPs and stirred for 2 minutes before the solution is sonicated for 20 seconds. The UV-vis spectrum of the particles is taken prior to purification. This process is repeated a further two times giving a final DNA concentration of 2.23 μM. The particles are then spun down to form a pellet at 13000 rpm for 90 seconds. The supernatant is removed, with care taken to not disturb the pellet. The particles are re-dispersed in deionised water.

SPR = 564 nm, number distribution = 69 nm ± 21 nm, intensity distribution = 105 nm ± 34 nm (100%), histogram sizing data in **7.5**.

6.2.4.4 Coating 100 nm AuNP with P.1L and RubpySS

In an Eppendorf containing a magnetic stirrer, citrate coated AuNPs (100 nm, 40 pM) are made up in 10 mM pH 7.0 phosphate buffer. **P.1L** (0.25 µM) is added to the AuNPs and stirred for 2 minutes before the solution is sonicated for 20 seconds. This process is repeated a further two times giving a final DNA concentration of 0.75 µM. RubpySS (1.13 µM) probe is added to the particles and allowed to stir for 20 minutes. This process is repeated, giving a final RubpySS concentration of 2.3 µM. The particles are then spun down to form a pellet at 13000 rpm for 90 seconds. The supernatant is removed, with care taken to not disturb the pellet. The particles are re-dispersed in deionised water.

SPR = 565 nm, number distribution = 73 nm ± 26 nm, intensity distribution = 106 ± 38 nm, histogram sizing data in **7.5**.

6.2.4.5 Coating 13 nm AuNP with siRNA

In an Eppendorf containing a magnetic stirrer, citrate coated AuNPs (13 nm, 3 nM) are made up in 10 mM pH 7.0 phosphate buffer. **siRNA.1** (0.99 µM) is added to the AuNPs and stirred for 2 minutes before the solution is sonicated for 20 seconds. The UV-vis spectrum of the particles is taken prior to purification. This process is repeated a further two times giving a final RNA concentration of 2.97 µM. The particles are passed through a Sephadex G-50 column (stored in 20% ethanol) with deionised water as eluent. A final UV-vis spectrum is taken to confirm concentration (explained in **7.1.3**). The particles are made up in 10 mM pH 7.0 phosphate buffer and 100 mM NaCl. To this solution **RNA.2** (1.2 µM) is added.

SPR = 522 nm, number distribution = 14 nm ± 3 nm, intensity distribution = 28 nm ± 17 nm, histogram sizing data in **7.5**.

6.2.4.6 Coating 13 nm AuNP with siRNA and RubpySS

In an Eppendorf containing a magnetic stirrer, citrate coated AuNPs (13 nm, 3 nM) are made up in 10 mM pH 7.0 phosphate buffer. **RNA.1** (0.33 μM) is added to the AuNPs and stirred for 2 minutes before the solution is sonicated for 20 seconds. The UV-vis spectrum of the particles is taken prior to purification. This process is repeated a further two times giving a final **RNA.1** concentration of 0.98 μM. **RubpySS** (1.5 μM) is added to the particles and stirred for 20 minutes. This process is repeated, giving a final RubpySS concentration of 3 μM. The particles are passed through a Sephadex G-50 column with deionised water as eluent. A final UV-vis spectrum is taken to confirm concentration (**7.1.3**). The particles are made up in 10 mM pH 7.0 phosphate buffer and 100 mM NaCl, to this **RNA.2** (0.4 μM) is added.

SPR = 524 nm, number distribution = 15 nm ± 3 nm, intensity distribution = 30 nm ± 15 nm, histogram sizing data in **7.5**.

6.2.4.7 Coating 100 nm AuNP with siRNA

In an Eppendorf containing a magnetic stirrer, citrate coated AuNPs (100 nm, 40 pM) are made up in 10 mM pH 7.0 phosphate buffer. **RNA.1** (0.73 μM) is added to the AuNPs and stirred for 2 minutes before the solution is sonicated for 20 seconds. The UV-vis spectrum of the particles is taken prior to purification. This process is repeated a further two times giving a final **RNA.1** concentration of 2.23 μM. The particles are then spun down to form a pellet at 13000 rpm for 90 seconds. The supernatant is removed, with care taken to not disturb the pellet. The particles are re-dispersed in deionised water, before making up in 10 mM pH 7.0 phosphate buffer and 100 mM NaCl. To this solution **RNA.2** (0.9 μM) is added.

SPR = 526 nm, number distribution = 71 nm (± 19 nm), intensity distribution = 159 nm (± 74 nm), histogram sizing data in **7.5**.

6.3 Biological Techniques

6.3.1 Reagents

6.3.1.1 Medium 199

To a bottle of Medium 199 (450 mL, GE Healthcare) was added Foetal Bovine Serum (50 mL, Gibco), Penicillin Streptomycin (2 mL, Gibco), L-glutamine (2 mM, Gibco), Heparin (1 mL) and brain extract (0.5 mL). The solution was mixed before passing through a filter (0.22 µm, Corning incorporated) into an autoclaved bottle. This solution was kept refrigerated and used within 6 months.

6.3.1.2 Dulbecco's Modified Eagle's Medium

To a bottle of Dulbecco's Modified Eagle's Medium (450 mL, Sigma life sciences) was added Foetal Bovine Serum (50 mL), Penicillin Streptomycin (2 mL) and L-glutamine (2mM). The solution was mixed before passing through a filter (0.22 µm) into an autoclaved bottle. This solution was kept refrigerated and used within 6 months.

6.3.1.3 Phosphate Buffered Saline (PBS)

For 1L 2.5 x PBS tablets (Sigma) dissolved in deionised water with vigorous stirring. The solution is then autoclaved.

6.3.1.4 0.1% Gelatin solution

0.1% gelatin (Fluka) by weight of gelatin in PBS, the solution is then autoclaved before use.

6.3.1.5 Radioimmunoprecipitation assay RIPA buffer

1:1 NP40 lysis buffer (2x conc): deionised water plus 1 % protease inhibitor.

6.3.1.6 Loading buffer

For 100 mL of 2x loading buffer (non-reducing): 5 mL 1 M Tris pH 7.0, 25 mL 20% SDS, 20 mL glycerol, 2 mg bromophenol blue, bring up the volume to 100 mL with deionised water.

6.3.1.7 Running buffer

For a 10 x solution: 30.2 g of Tris Base (Sigma), 187.6 g of glycine (Promega), 50 mL of 20% sodium dodecyl sulphate (SDS) top up solution to 1 L with deionised water.

6.3.1.8 Transfer buffer

For a 10 x solution: 30.2 g Tris Base, 144 g glycine, make up the solution to 1L with deionised water.

6.3.1.9 Phosphate Buffer Saline Tween-20 (PBS-T)

To 1 L of PBS solution add 0.1% by volume of Tween-20 (Sigma) with vigorous stirring.

6.3.1.10 10 % SDS Page gel

Resolving gel

4 mL deionised water, 3.3 mL Protogel (Geneflow), 2.6 mL Resolving buffer (1.5 M Tris base, 0.4% SDS, pH 8.8), 100 µL 10% Ammonium Persulfate (APS) (Sigma) mixed together in a falcon tube. 10 µL of tetramethylethylenediamine (TEMED) (Sigma) is added to the mixture and stirred, then the mixture is quickly poured into a gel cassette until ¾ full before adding a small amount of EtOH on top to ensure a flat top. The gel is allowed to set for 10 minutes.

Stacker gel

The excess ethanol is poured off the gel. 2.1 mL deionised water, 500 µL Protogel, 380 µL Stacking buffer (0.5 M Tris base, 0.4% SDS, pH 6.8), 30 µL 10% APS mixed together in a falcon tube. 3 µL of TEMED is added to the mixture and stirred, before quickly pouring the mixture on top of the set resolving gel, well combs are pushed into the top of the cassette and the gel allowed to set for 10 minutes. The gel is either used immediately or wrapped in damp tissue and clingfilm and kept at 4°C for up to 2 months.

6.3.2 Cell Splitting

Assuming working with 10 cm petri dish of cells, the media was removed and the cells washed with Phosphate Buffer Saline twice. The cells were then treated with tripsin (1.5 mL, 2x conc, (Gibco), after swirling the mixture to ensure it has covered all cells the dish is left for 10 minutes. After 10 minutes the dish is firmly tapped on the side to dislodge the cells, media (4.5 mL) is then added to the cells and the solution is pipetted up and down vigorously a number of times. The solution is pipetted into a 15 mL falcon tube and centrifuged at 1200 rpm for 5 minutes. The supernatant is removed; the pellet is then re-suspended in media with vigorous pipetting to break up the cells. 10 µL of the cell containing media is pipetted into a haemocytometer and the cells counted in each 4x4 grid and averaged to give a number of cells per 4x4 grid. Multiplying this value by 10^6 gives the number of cells present per mL, the required number of cells can then be seeded.

6.3.3 Imaging cells

Cells were plated onto 2.5 cm glass cover slips. Once treatment completed, the cells were washed 3 times with PBS. The cells were then covered with 4% paraformaldehyde (PFA) for 10 minutes, upon which the PFA is removed and the cells washed with PBS and then water. The cover slip containing the cells is then mounted onto the glass slide using Hydromount media (national diagnostics) before sealing the edges with clear nail varnish. The slides could be imaged after letting them dry at 4°C for 2 hours. Reflectance microscopy was done on a Leica SP2 inverted confocal microscope using a 100 x objective lens. λ_{ex} = 488 nm λ_{em} = 478-498 nm. Line average = 4 Slide average = 4.

6.3.4 Freezing / Defrosting cells

Assuming working with 10 cm petri dish of cells, the media was removed and the cells washed with Phosphate Buffer Saline twice. The cells were then treated with tripsin (1.5 mL, 2x conc, after swirling the mixture to ensure it has covered all cells the dish is left for 10 minutes. After 10 minutes the dish is firmly tapped on the side to dislodge the cells, media (4.5 mL) is then added to the cells and the solution is pipetted up and down vigorously a number of times. The solution is pipetted into a 15 mL falcon tube and centrifuged at 1200 rpm for 5 minutes. The supernatant is removed and the cells re-dispersed with a solution of 90% Foetal calf serum (FCS) and 10% DMSO (3 mL), the cells are placed into CRYO.S tubes (Greiner bio-one) then clearly labelled and placed in a -80°C freezer.

To bring out cells from the freezer, they are removed from the freezer and quickly defrosted by rubbing in hands. The solution is placed into a 15 mL Falcon tube and media added to this (4 mL), the cells are then centrifuged at 1200 rpm for 5 minutes, before removing the supernatant and re-dispersing in media (5 mL). The cells are then plated in a 10 cm plate, when they are confluent, they can be split and used for assays.

6.4 HUVEC isolation from umbilical chord

In a sterile fume hood, a metal dissection tray was lined with tissue and sprayed with 70% EtOH. Taking care, the cord was placed onto the dissection tray (6 inches of cord = cells for 1 T25 plate). The outside of the cord was wiped with tissue and examined for damage; any damaged areas were removed by cutting the cord cleanly at a right angle to the length of the cord. The cord was sprayed with 70% EtOH. The vein was identified at one end of the cord;

into this a sterile balloon canula was inserted, ensuring that the canula was inserted far enough so it was secure. The cord was attached to the canula tube using cable ties. PBS was then injected into the cord pushing through any clots out of the other end. Enough PBS was passed through until it came out clear, at least 20 mL was used. The cord was then flushed with 20 mL of air. The other end of the cord was then cannulated as stated above. Clamps were then attached to both ends but left open initially. A syringe filled with collagenase 1A (0.1 mg/mL) in M199 media (serum free) is attached to one end of the cord, and passed through until it filled the large balloon in the canula at the far end of the cord (the cord should be tilted upward to avoid any bubbles being trapped inside). The far end of the cord is clamped, before clamping the end near the syringe. The cord was then placed in an autoclave bag and incubated for 20 minutes at 37°C. Whilst waiting, the metal dissection tray should be cleaned and tissue replaced before again spraying with 70% EtOH.

The cord was carefully tipped out of the bag onto the newly cleaned tray ensuring the cable ties remain tight. PBS (20 mL) was passed through the cord collecting the contents in a 50 mL Falcon tube, then 20 mL of air was flushed though before another 10 mL of PBS finishing with a further 20 mL of PBS. Throughout flushing the cord, the syringe is held highest and the cord is tilted downwards towards the 50 mL Falcon tube.

The cells were spun down in the Falcon tube at 1200 rpm for 6 minutes. The supernatant was aspirated before re-dispersing the cells in M199 media. The cells were then plated onto a gelatin coated T25 flask; the media was changed after 2 hours and then again after a further 24 hours. Upon confluence, the cells can be used for assays.

6.5 Western Blot

6.5.1 siRNA transfection of HUVEC in 6 well plate

175000 HUVEC were plated onto a gelatin coated 6 well plate and allowed to grow overnight. After 24 hours, the cells were treated with siRNA duplexes. The siRNA duplexes (2.5 µL of 20 µM) were mixed with 167 µL of Opti-MEM™ (Gibco). In a separate Eppendorf, 3 µL of RNAiMAX lipofectamine (Invitrogen) is mixed with 27 µL of Opti-MEM™. Both of these mixtures were kept at room temperature for 10 minutes after which the RNAiMAX containing mixture was added to the other and incubated for 10 minutes at room temperature. The seeded cells were washed with PBS (2x). 800 µL of Opti-MEM™ is added to the cells before adding the 200 µL mix containing the siRNA duplex. The cells are incubated at 37 °C for 4 hours; the Opti-MEM™ is then removed and replaced with antibiotic free medium. The cells were then left for 48 hours in an incubator before performing the Western Blot assay.

6.5.2 AuNP-siRNA addition to HUVEC in 6 well plate

175000 HUVEC were plated onto a gelatin coated 6 well plate and allowed to grow overnight. After 24 hours, the cells were treated with siRNA duplexes. The siRNA-AuNP duplexes (100 µL of 2.5 nM) were mixed with 100 µL of Opti-MEM™ and kept at room temperature for 10 minutes. The seeded cells were washed with PBS (2x), then 800 µL of Opti-MEM™ is added to the cells before adding the 200 µL siRNA-AuNP containing mix. The cells are incubated at 37 °C for 4 hours; the Opti-MEM™ is aspirated off and replaced with antibiotic free medium. The cells were then left for 48 hours before performing the Western Blot assay.

6.5.3 Developing Western Blot

The supernatant was removed from the cells and the cells washed with PBS. The cells were then removed from the plate using a cell scraper and 100 mL PBS. The cells were spun down for 2 minutes at 13000 rpm and the supernatant was removed. The cells were re-dispersed in 50 µL of RIPA buffer (**6.3.1.5**) passing through a 50 µL needle (Terumo) to break up the cells. The cell/RIPA mixture was left on ice for 30 minutes. The cell/RIPA solution was then spun at 14000 rpm for 15 minutes at 4 °C in a refrigerated centrifuge. The supernatant was removed and kept; this supernatant could then be stored at -80 °C before being used in the next step.

Loading buffer (**6.3.1.6**) was added to the cell lysate and boiled for 2 minutes before being loaded to the gel. The samples were run on a 10 % SDS page gel (**6.3.1.10Error! Reference ource not found.**) using running buffer (**6.3.1.7**) to run the gel. The gel was run at 80 volts for 1 hour, then 140 volts for another hour.

The transfer membrane and all foam layers were soaked in transfer buffer (**6.3.1.8**) and loaded into the transfer module with the gel. The transfer module was filled with transfer buffer and run for 2 hours at 30 mV in a cold room.

The membrane is removed from the transfer module and washed 3 times with PBS-T for 5 minutes. The membrane is then blocked in a 10 % milk PBS-T solution for 2 hours. After washing the membrane again with PBS-T (3 x 5 minutes), the membrane is cut at a known position so that each protein of interest (CLEC-14A and Tubulin) can be treated with its own specific antibody. Each half of membrane is then treated with its own primary antibody for 2 hours, washed 5 x 5 minutes PBS-T, and treated with the secondary antibody for a further 2

hours. For CLEC-14A an anti-sheep primary antibody was used (Anti-CLEC14A, R & D Systems) at a dilution of 1 in 1000, followed by horseradish peroxidase (HRP) tagged anti sheep (Antisheep IgG HRP, R & D Systems) secondary antibody at a dilution of 1 in 5000. For Tubulin an anti-mouse primary antibody (Anti-Tubulin Mouse, Sigma) was used at a dilution of 1 in 2000, followed by HRP tagged anti mouse (Polyclonal Goat anti mouse Immunoglobulins HRP, Dako), at a dilution of 1 in 5000. After treating with the secondary antibody, the membranes are washed 5 x 5 minutes with PBS-T.

The membranes were soaked in a 1:1 mixture of Detection reagent 1 and 2 (GE Healthcare) for 30 seconds on each side of the membrane; excess solution was wicked off using a paper towel. The membranes were then developed using Amersham Hyperfilm™ ECL (GE Healthcare) and using a Film developer.

7 APPENDIX

7.1 Chapter 3

7.1.1 Calculating the concentration of 13 nm gold nanoparticles

Original Turkevich method

Mass of $HAuCl_4$ (49 % Au by assay) = 0.09889 g

Mass of Au = 0.49 × 0.09889 = 0.04846 g

Moles of Au = 0.04846 / 197 = 2.4597×10^{-4} moles

Concentration of Au = 2.4597×10^{-4} moles / 0.275 dm^3 = 8.944×10^{-4} M.

Estimated atomic radius of gold = 140 pm

Number of gold atoms per 13 nm nanoparticle = $(6.5 \times 10^{-9})^3 / (140 \times 10^{-12})^3$ = 106,802

(assuming the particles are perfectly spherical).

Concentration of 13 nm gold nanoparticles = 8.944×10^{-4} M / 100,000 = 8.944 nm ≈ **9 nM**.

Improved Turkevitch method

Mass of $HAuCl_4$ (49 % Au by assay) = 0.0085 g

Mass of Au = 0.49 × 0.0085 = 0.004165 g

Moles of Au = 0.004165 / 197 = 2.114×10^{-5} moles

Concentration of Au = 2.114×10^{-5} moles / 0.125 dm^3 = 1.6914×10^{-4} M.

Estimated atomic radius of gold = 140 pm

Number of gold atoms per 13 nm nanoparticle = $(6.5 \times 10^{-9})^3 / (140 \times 10^{-12})^3$ = 106,802

(assuming the particles are perfectly spherical).

Concentration of 13 nm gold nanoparticles = 1.6914×10^{-4} M / 106,802 = 1.584 nm ≈ **1.6 nm**

7.1.2 ICP-MS calculations

Example calculation for P.AF-AuNP

Au ppb convert to mg/L
= 1163/1000000
= 0.001163 mg/L of Au

Convert mg/L of Au to mg/L of AuNP
= 0.001163/78717 = 1.477 x 10^{-8} mg/L of AuNP

Convert mg/L of AuNP to concentration of AuNP
= 1.447 x 10^{-8} / 196.97
= 0.075 nM

Repeat for phosphorus

P ppb convert to mg/L
= 38.75/1000000
= 0.00003875 mg/L of P

Convert mg/L of P to concentration of P
= 0.00003875/ 31
= 1250 nM

16 P atoms in each strand of DNA, therefore conc of DNA is:
= 1250/16
= 78.125 nM

Therefore number of DNA strands per AuNP:
= 78.125/0.075
= 1042 DNA strands per AuNP

7.1.3 Tracking nanoparticle concentration

Initial concentration of nanoparticles after preparation is calculated as stated previously (section **7.1.1**). Concentration is then known through tracking dilution. Prior to Sephadex G-50 column purification, UV-vis absorption of particles is recorded, the maximum absorbance at SPR band is recorded. Once particles are passed through the column, the absorbance band of SPR for the newly purified particles is recorded. Comparing the ratio of the absorbance values before and after column, allows the level of dilution during purification to be calculated.

7.1.4 UV-vis absorption for varied length probes

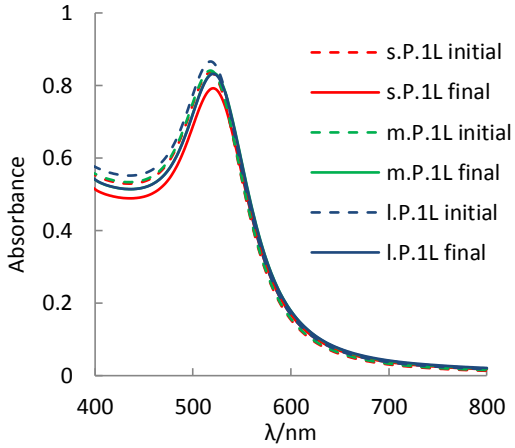

Appendix 7.1 Tracking binding of varied length 1L probes to AuNP using UV
*UV absorption of SPR band showing before and after addition of DNA strands with varying distance between anthracene and the AuNP. Black=**s.P.1L** Green = **m.P.1L**, Red = **l.P.1L**. Particles at 3 nM in deionised water and 10 mM pH 7.0 phosphate buffer.*

7.1.5 Anthracene signal strength on AuNP for varied length probes

The concentration for AuNP was assumed constant for each experiment, calculated using the method described above (section **7.1.3**). The number of probes per AuNP was then calculated by noting the amount of target added before anthracene signal plateau.

Appendix 7.2 Calculating signal strength per anthracene probe on AuNP for varied length anthracene probes.

Probe	Initial anthracene signal	Final anthracene signal	Calculated probes per AuNP	Initial ratio (signal/probe)	Final ratio (signal/probe)
P.1L	10921	21726	450	**24.3**	**48.3**
m.P.1L	15408	24219	525	**29.3**	**46.1**
l.P.1L	20247	31709	675	**30.0**	**47.0**

7.1.6 SPR track of DNA coating 100 nm AuNP

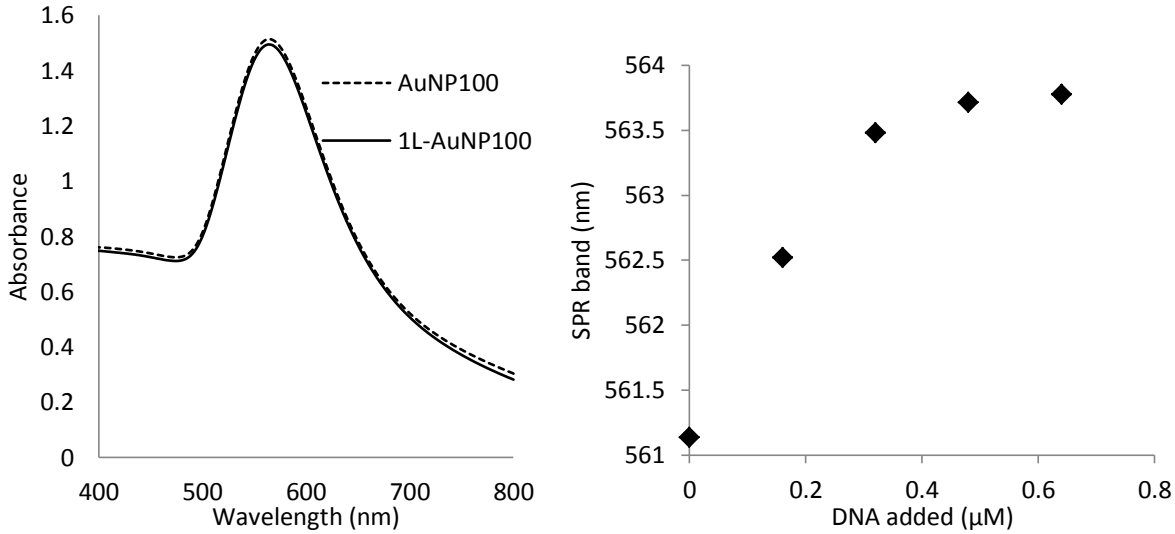

Appendix 7.3 UV-vis absorption spectrum of SPR band of 100 nm AuNP showing before and after addition of P.1L.
Particles at 40 pM in deionised water and 10 mM pH 7.0 phosphate buffer.

7.1.7 Brightfield images for AuNP uptake

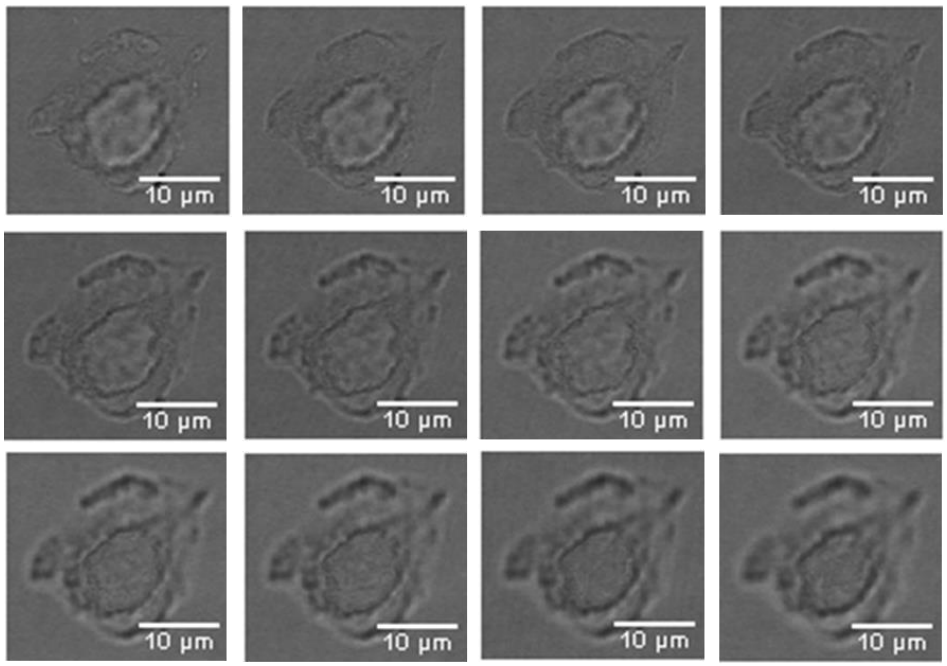

Appendix 7.4 Transmission microscopy images of 100 nm P.1L-AuNP treated CHO cells
Z-stack of transmission microscopy images showing slices of CHO cell treated with 4 pM P.1L-100 nm AuNP. Images taken after cells treated for 2 hours. Slices taken at 0.24 µM intervals.

7.2 Chapter 4

7.2.1 Percentage change in emission upon target addition for P.1L-AuNP-Ru and P.1D-AuNP-Ru

Appendix 7.5 Percentage emission change values of anthracene and ruthenium signal upon target hybridisation for P.1L-AuNP-Ru and P.1D-AuNP-Ru.
Percentage change in emission for anthracene (λ_{ex}=350 nm, λ_{em}=426 nm) and ruthenium (λ_{ex}=465 nm, λ_{em}=630 nm) probes after the addition of targets. Average of three separate AuNP preparation repeats.

	anthracene	ruthenium
P.1L-AuNP-Ru + DNA-T.1	-67	-18
P.1L-AuNP-Ru + DNA-T.2	65	-19
P.1D-AuNP-Ru + DNA-T.1	-72	-19
P.1D-AuNP-Ru + DNA-T.2	-63	-12
P.1L-AuNP-Ru + Random	-8	6
P.NA-AuNP-Ru + DNA-T.1	0	-14

7.2.2 P.1D-AuNP-Ru percentage change of ruthenium and anthracene

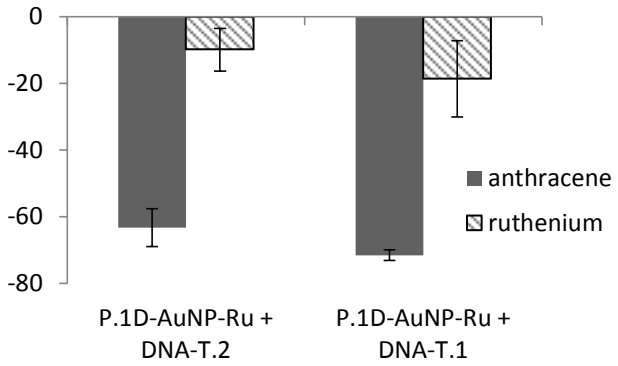

Appendix 7.6 Percentage emission change of anthracene and ruthenium signal upon target hybridisation for P.1D-AuNP-Ru

Bar chart showing percentage change in emission for anthracene (grey, 426 nm) and ruthenium (dashed line, 630 nm) probes after the addition of SNP targets, for the particles 1D-AuNP-Ru. Error bars indicate the standard deviation of three repeats using three different preps of probe coated AuNP.

7.2.3 T-test comparing difference in ruthenium emission for P.1L-AuNP and l.P-1L-AuNP

A t-test tests whether the null hypothesis of two data sets can be rejected. Here the null hypothesis is that the difference in ruthenium emission between the two data sets is not significant. If t Stat > t Critical two tail then the null hypothesis can be rejected, if not then it cannot be.

	1L-AuNP-Ru + DNA-T.1	*l.1L-AuNP-Ru + DNA-T.1*	*1L-AuNP-Ru + DNA-T.2*	*l.1L-AuNP-Ru + DNA-T.2*
Mean	-17.530	-12.905	-18.577	-23.241
Variance	106.973	55.674	137.776	152.001
t Stat	-0.76636		0.566091	
t Critical two-tail	2.446912		3.182446	

For neither target can the null hypothesis be rejected, therefore the difference in ruthenium emission observed for **1L-AuNP-Ru** and **l.1L-AuNP-Ru** cannot be considered significant.

7.2.4 Integrated emission response for P.1L-AuNP-Ru and l.P.1L-AuNP-Ru

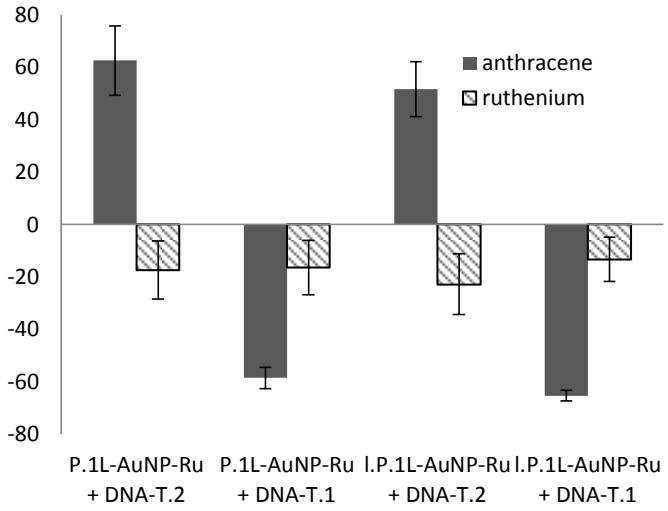

Appendix 7.7 Comparing anthracene and ruthenium emission response upon target addition for P.1L-AuNP-Ru and l.P.1L-AuNP integrating fluorescence response

*Chart showing the percentage change in emission for anthracene (λ_{ex} = 350 nm, λ_{em} = 370-550 nm) and ruthenium (λ_{ex} = 465 nm, λ_{em} = 580-800 nm) signals for the **P.1L-AuNP-Ru** (dark grey) and the **l.P.1L-AuNP-Ru** (dashed line) after the addition of the SNP targets: fully complementary **DNA-T.1** and single mismatch **DNA-T.2**. Error bars are the standard deviation of 3 repeats, each repeat is with a fresh preparation of particles. 2 nM AuNP in deionised water with 10 mM pH 7.0 phosphate buffer, 100 mM NaCl at room temperature.*

7.2.5 ICP-MS data for ruthenium coating of AuNP

Appendix 7.8 ICPMS values for ruthenium coating of AuNP co-coated with DNA

Data for DNA strands without any anthracene modification and DNA strands with 1L anthracene modification. Values given assume particles are 13 nm in size, containing 100082 gold atoms.

Sample	Ruthenium atoms per AuNP
P.1L-AuNP-Ru	**153**
P.1D-AuNP-Ru	**216**
l.P.1L-AuNP-Ru	**403**
P.NA-AuNP-Ru	**288**

7.2.6 Integrated emission for ratiometric sensing for P.5L-AuNP-Ru

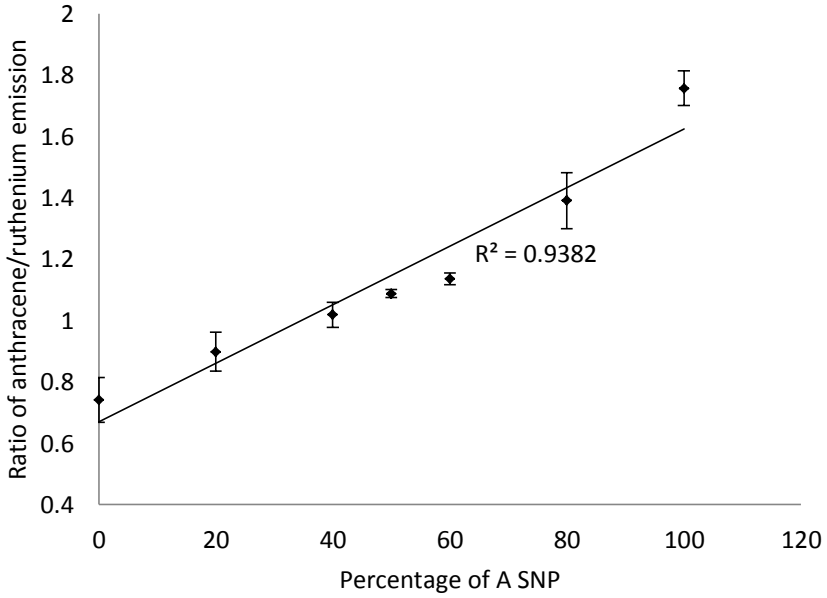

Appendix 7.9 Ratiometric response for P.5L-AuNP-Ru integrating anthracene and ruthenium signal
*Percentage variation in anthracene (λ_{ex} = 350 nm, λ_{em} = 370-550 nm) and ruthenium (λ_{ex} = 465 nm, λ_{em} = 580-800 nm) for **P.5L-AuNP-Ru** particles once probe is fully hybridised with target. Percentage of the targets containing A (**DNA-T.3**) or C (**DNA-T.4**) SNP variant on x-axis. Error bars are standard deviation of three repeats.2 nM AuNP in deionised water with 10 mM pH 7.0 phosphate buffer, 100 mM NaCl at room temperature.*

7.2.7 SPR track of DNA and RubpySS coating 100 nm AuNP

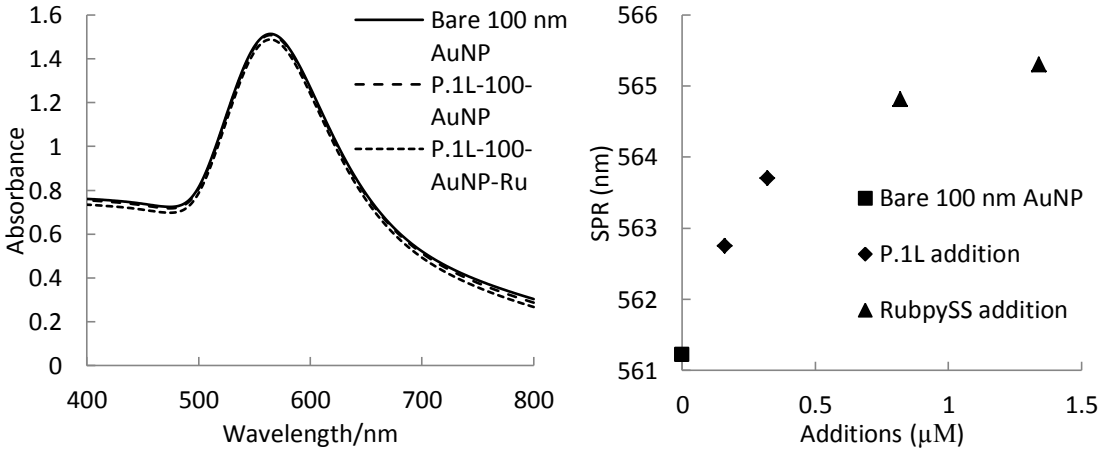

Appendix 7.10 UV-vis absorption spectrum of SPR band of 100 nm AuNP showing before and after addition of P.1L and RubpySS probes.
Particles at 40 pM in deionised water and 10 mM pH 7.0 phosphate buffer.

7.2.8 Brightfield images tracking uptake of 100 nm P.1L-AuNP-Ru

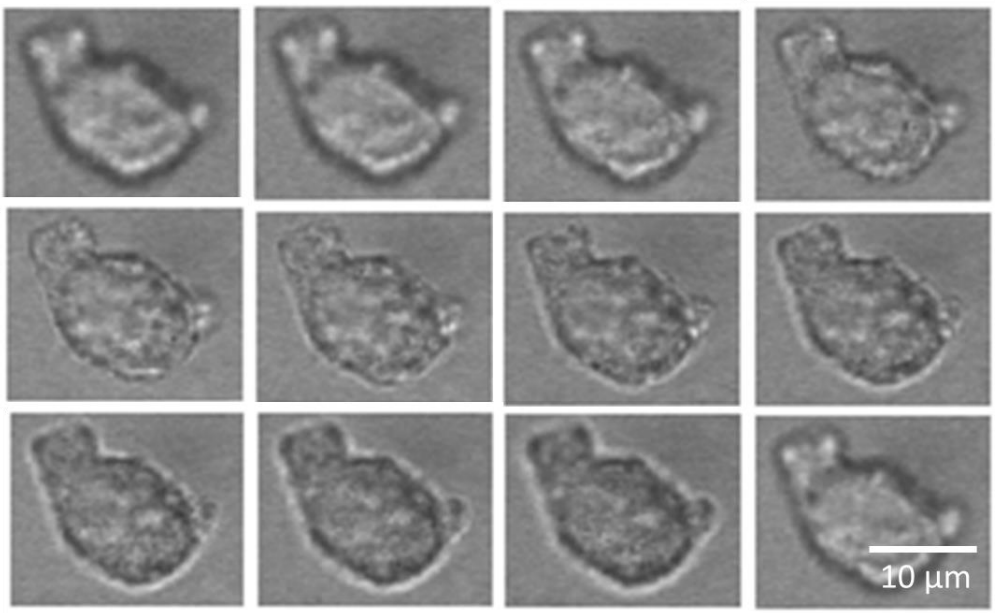

Appendix 7.11 Transmission microscopy images of uptake of 100 nm P.1L-AuNP-Ru by CHO cells
Z-stack of transmission microscopy images showing slices of CHO cell treated with 4 pM 100 nm ***P.1L-AuNP-Ru****. Images taken after cells treated for 2 hours. Slices taken at 0.45 µM intervals.*

7.3 NMR spectra

7.3.1 2,5-dioxopyrrolidin-1-yl 5-(1,2-dithiolan-3-yl)pentanoate (Compound 1)

^{1}HNMR

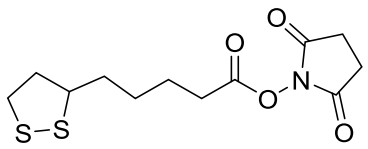

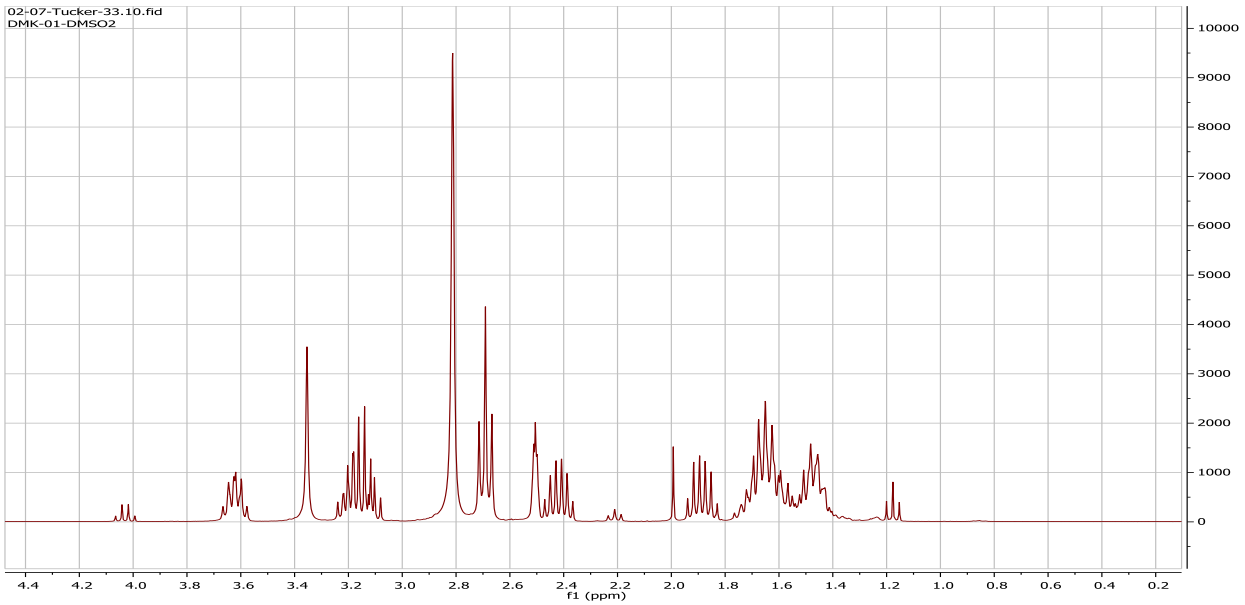

^{13}CNMR

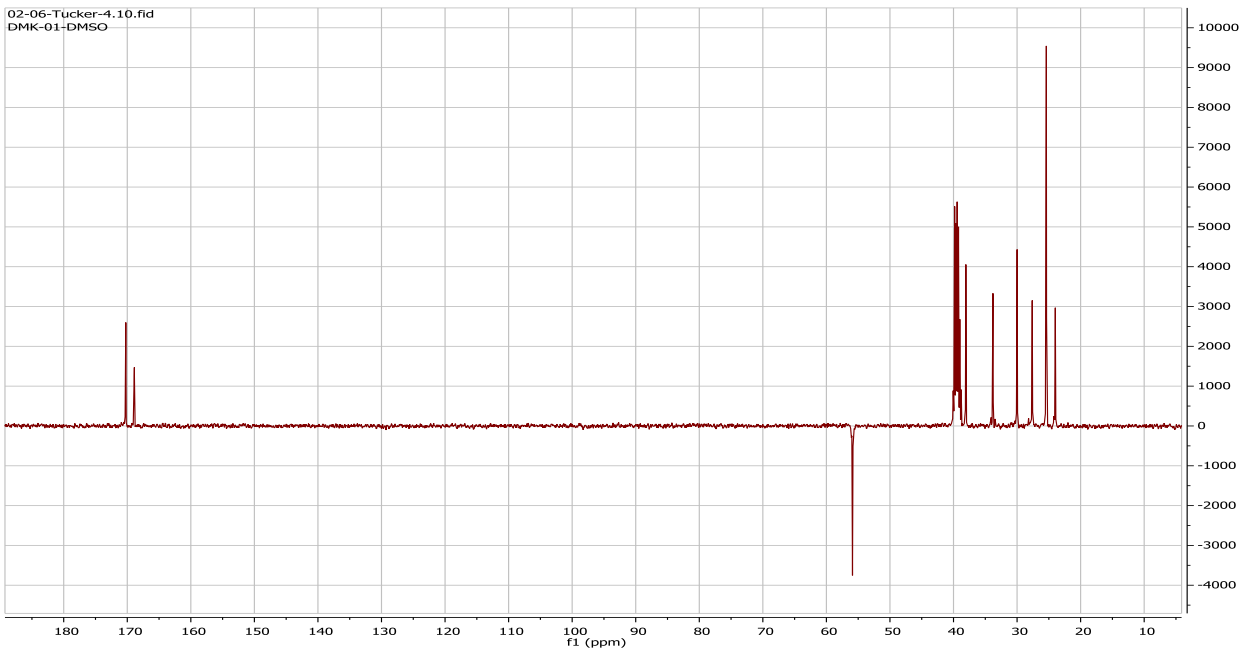

7.3.2 Synthesis of acetate (Compound 2)

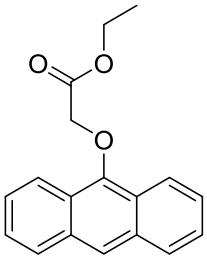

^{1}HNMR

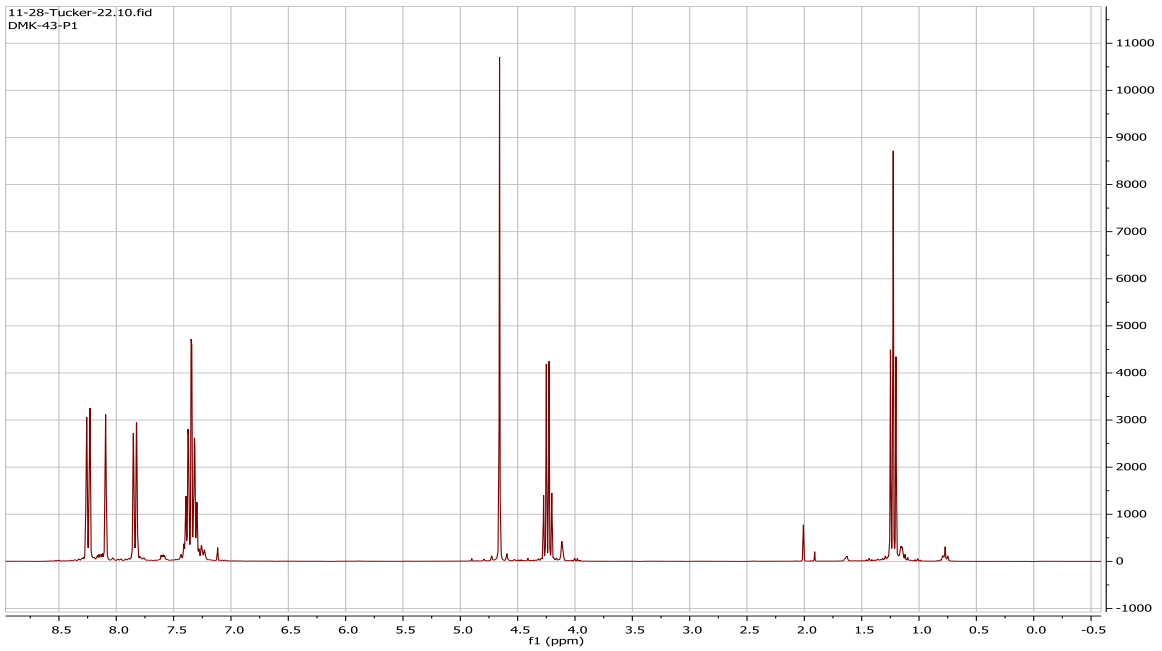

^{13}CNMR

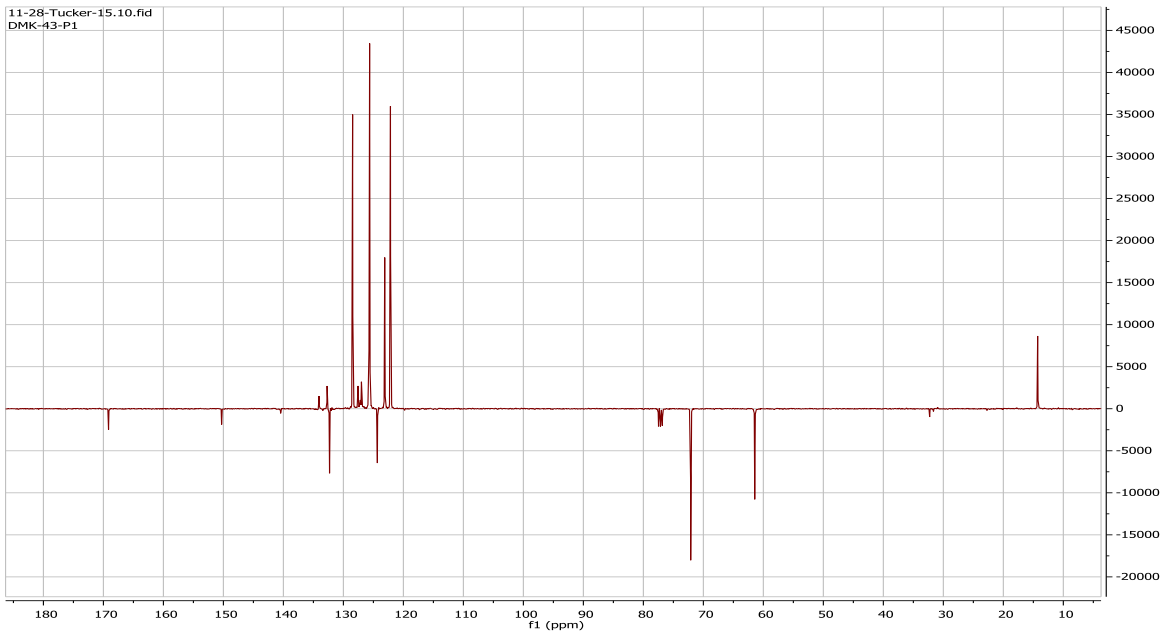

7.3.3 Synthesis of Carboxylic acid (Compound 3)

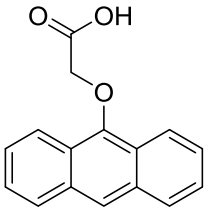

^{1}HNMR

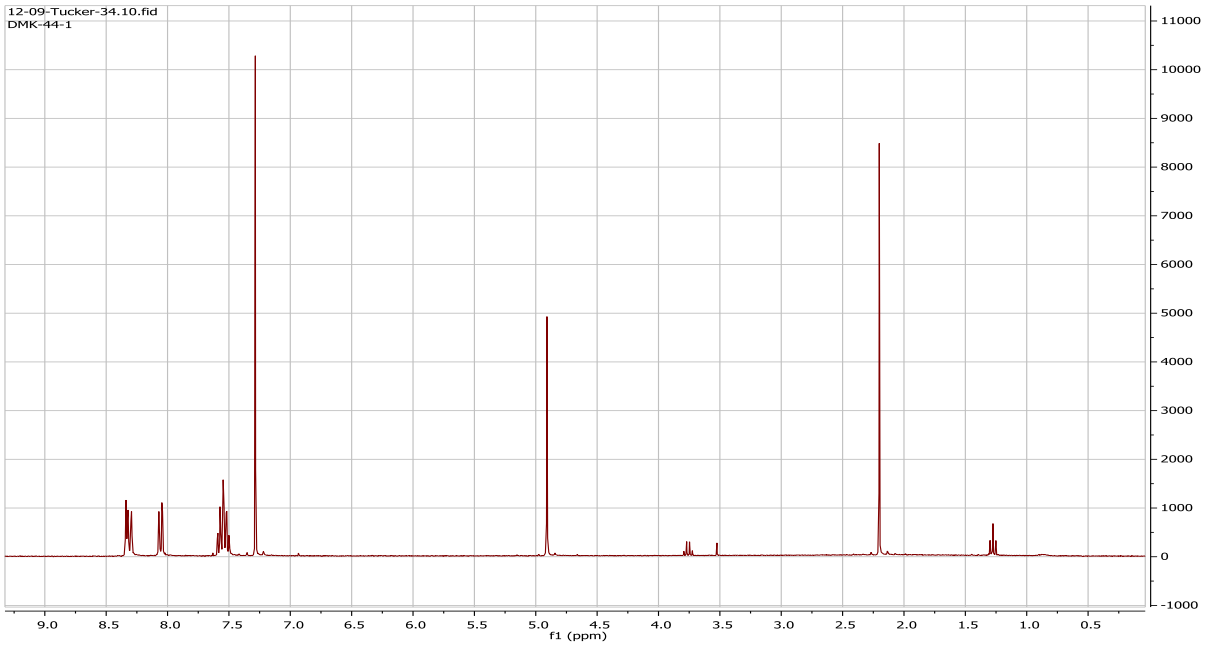

7.3.4 Synthesis with L-threoninol (Compound 4)

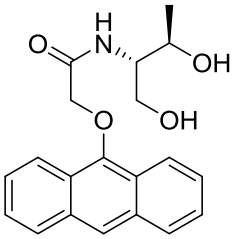

^{1}HNMR

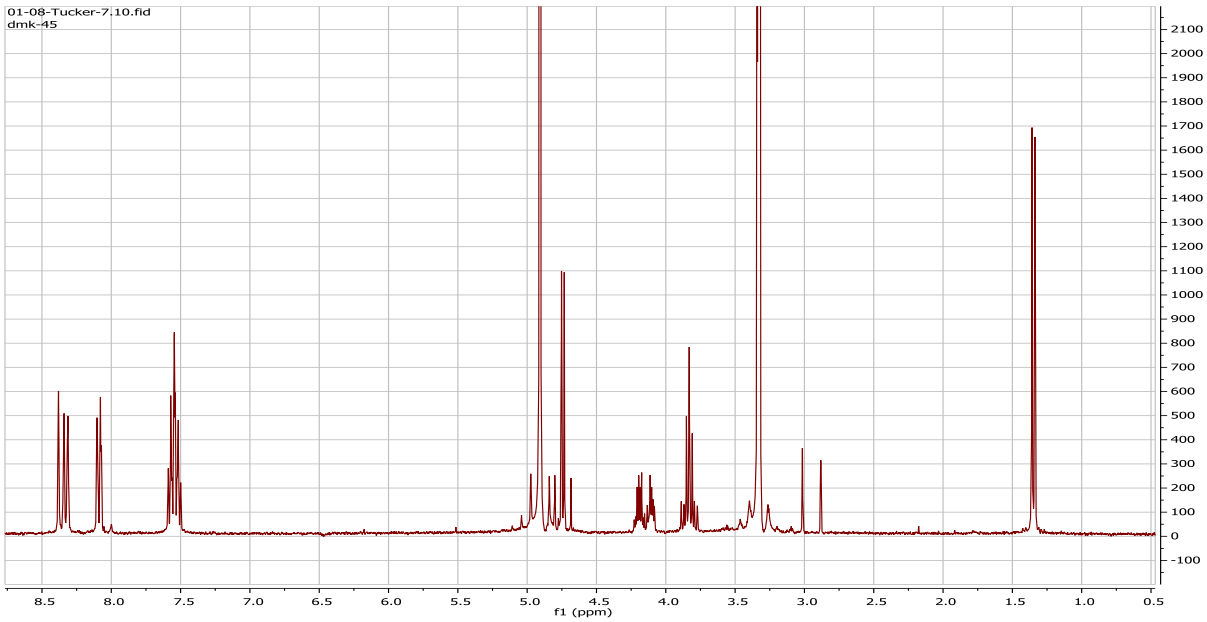

^{13}CNMR

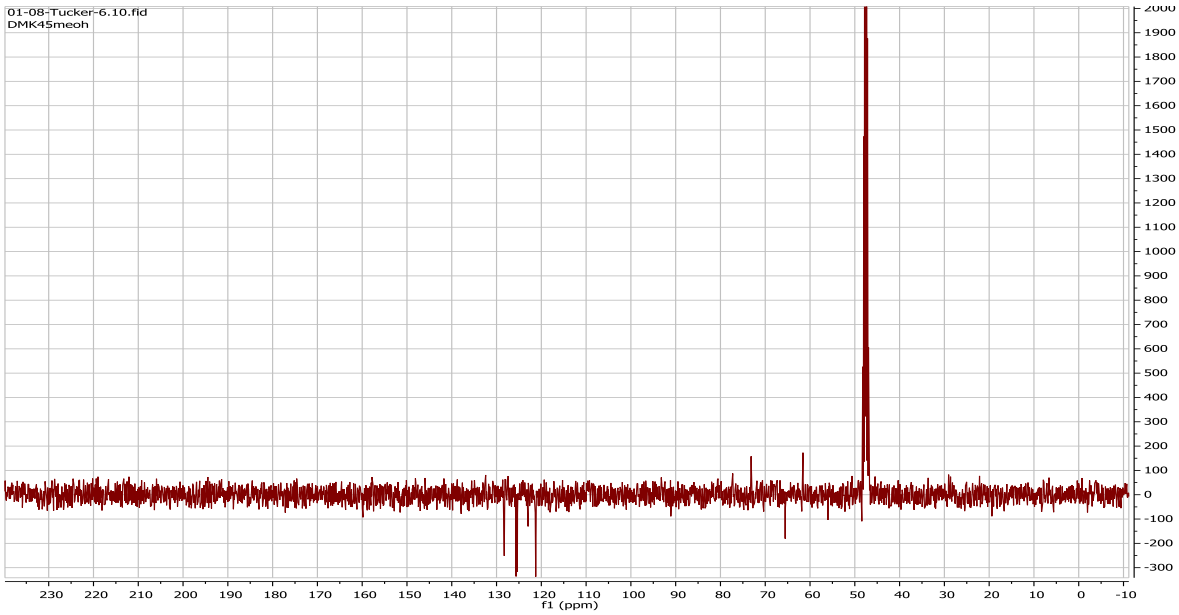

7.3.5 DMT protection of primary alcohol (Compound 5)

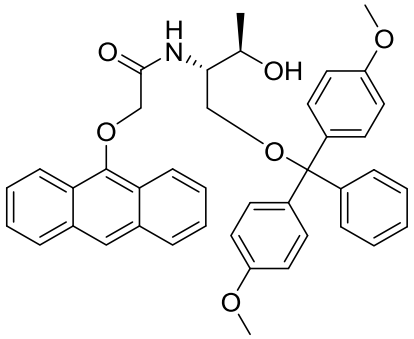

^{1}HNMR

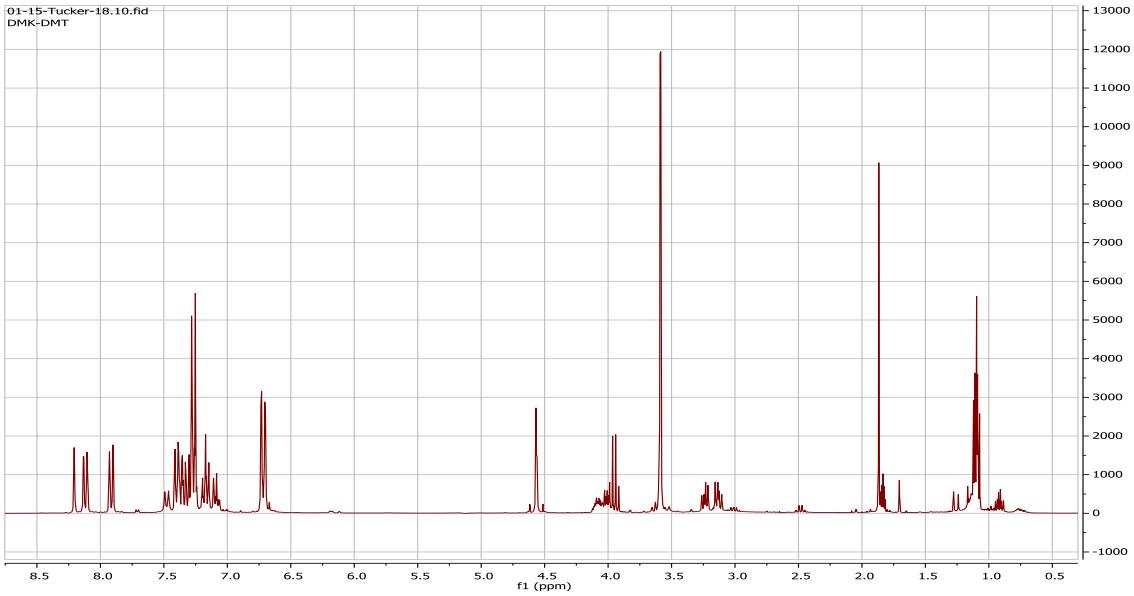

^{13}CNMR

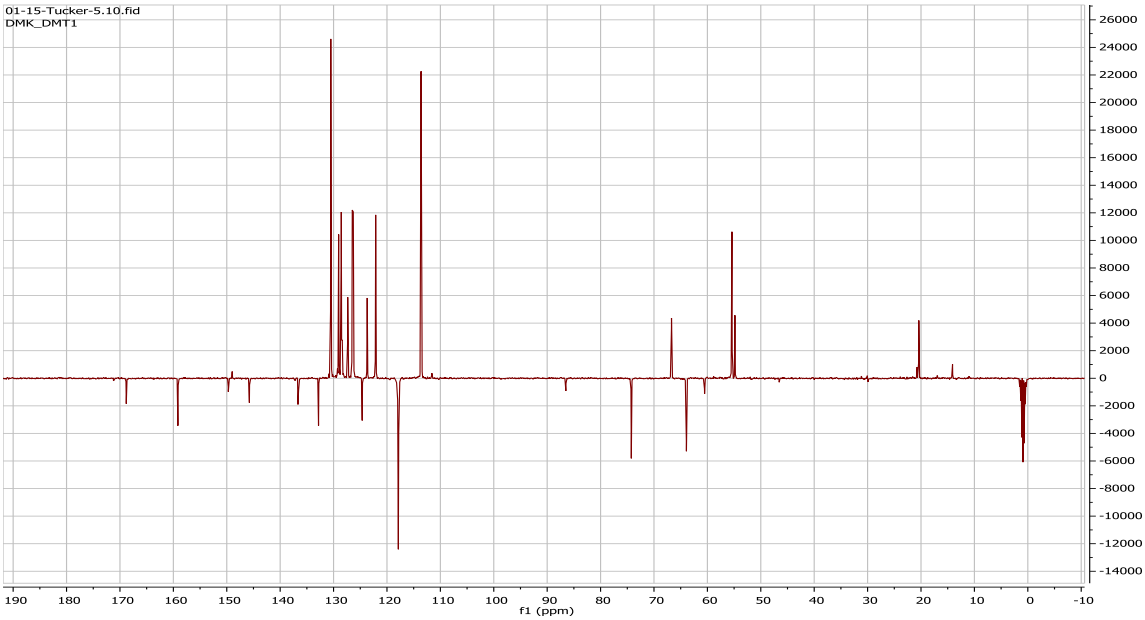

7.3.6 Reaction forming phosphoramidite (Compound 6)

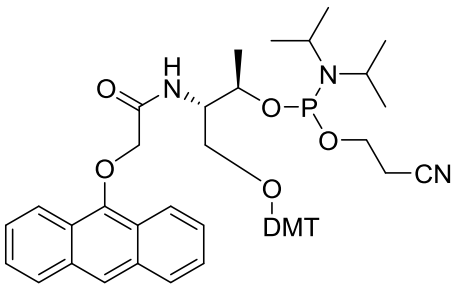

^{1}HNMR

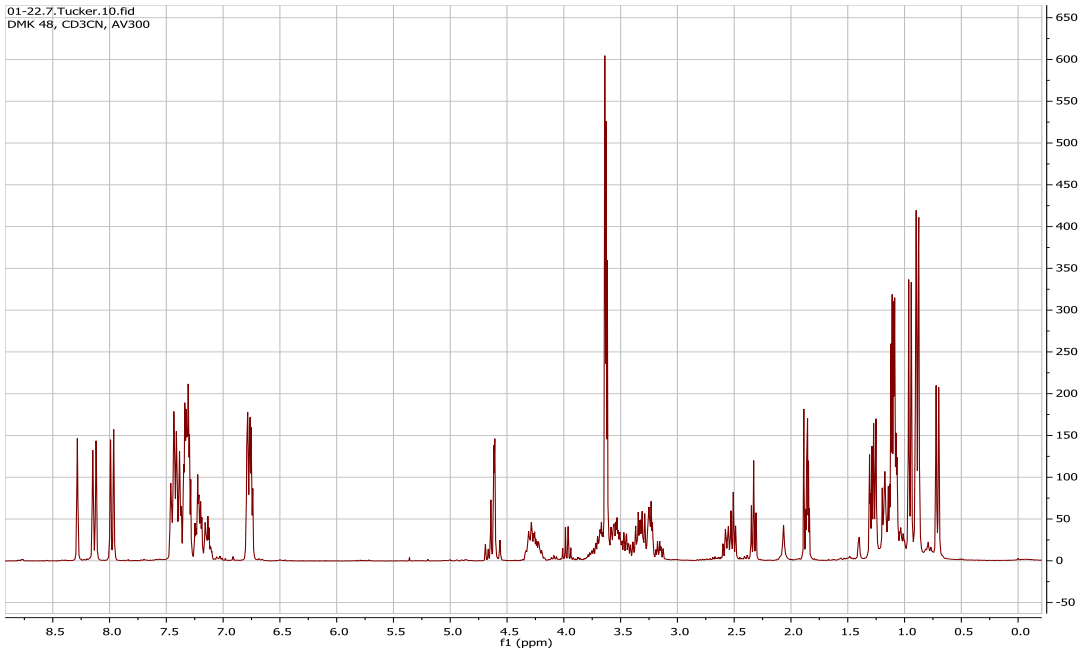

^{31}PNMR

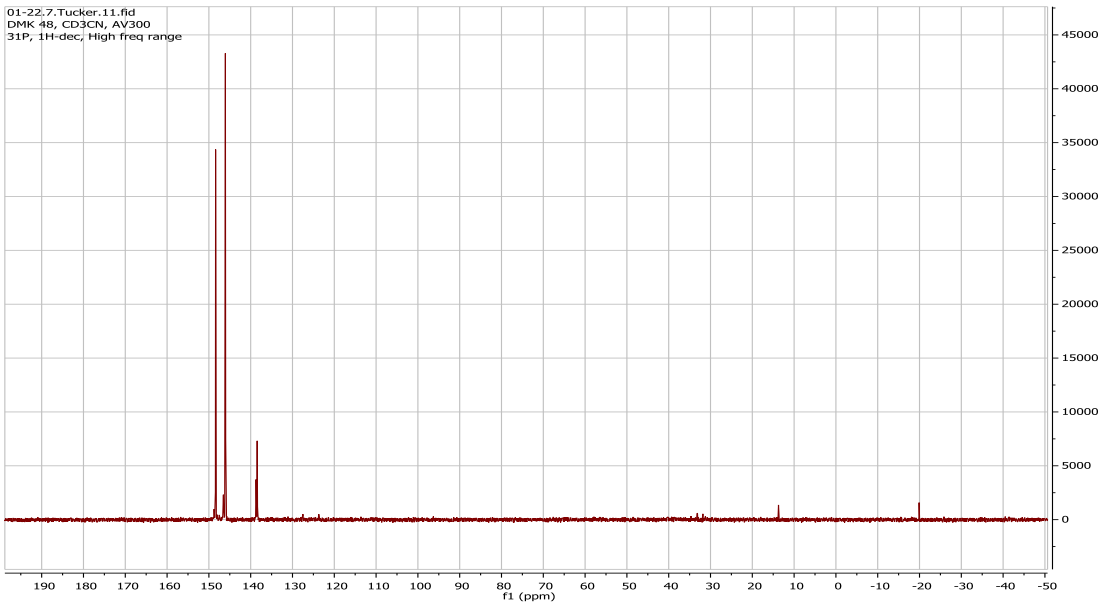

7.3.7 Compound 7 5-(1,2-dithiolan-3-yl)-N-(2-hydroxyethyl)pentanamide

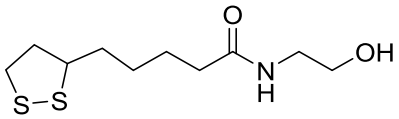

^{1}HNMR

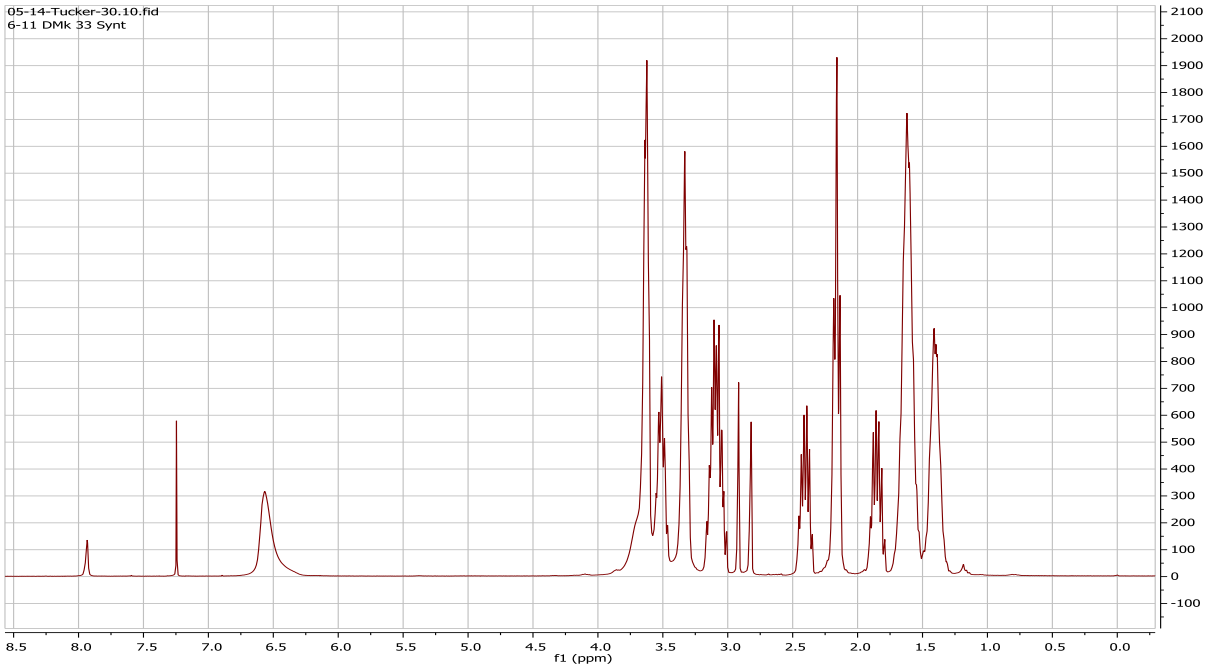

^{13}CNMR

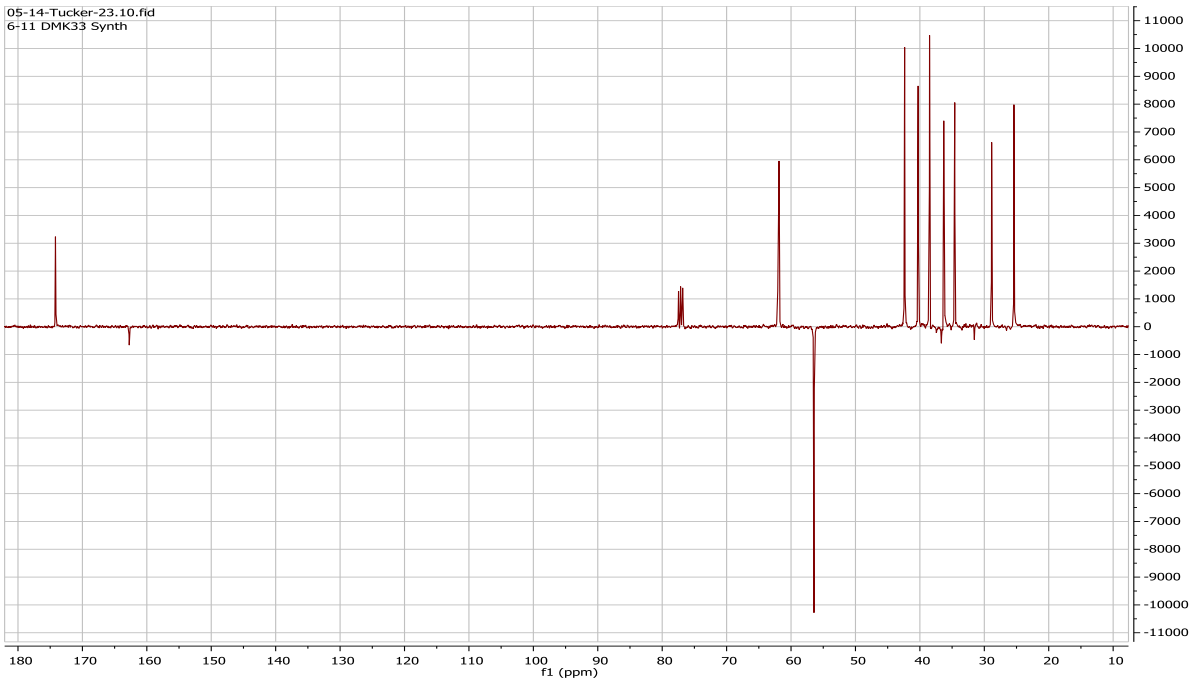

7.3.8 2-(5-(1,2-dithiolan-3-yl)pentanamido)ethyl (2-cyanoethyl) diisopropylphosphoramidite (Compound 8)

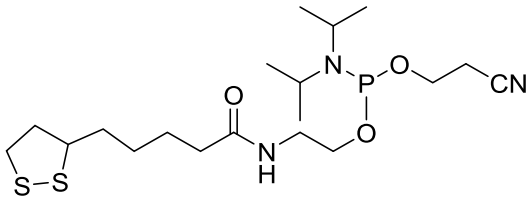

^{1}HNMR

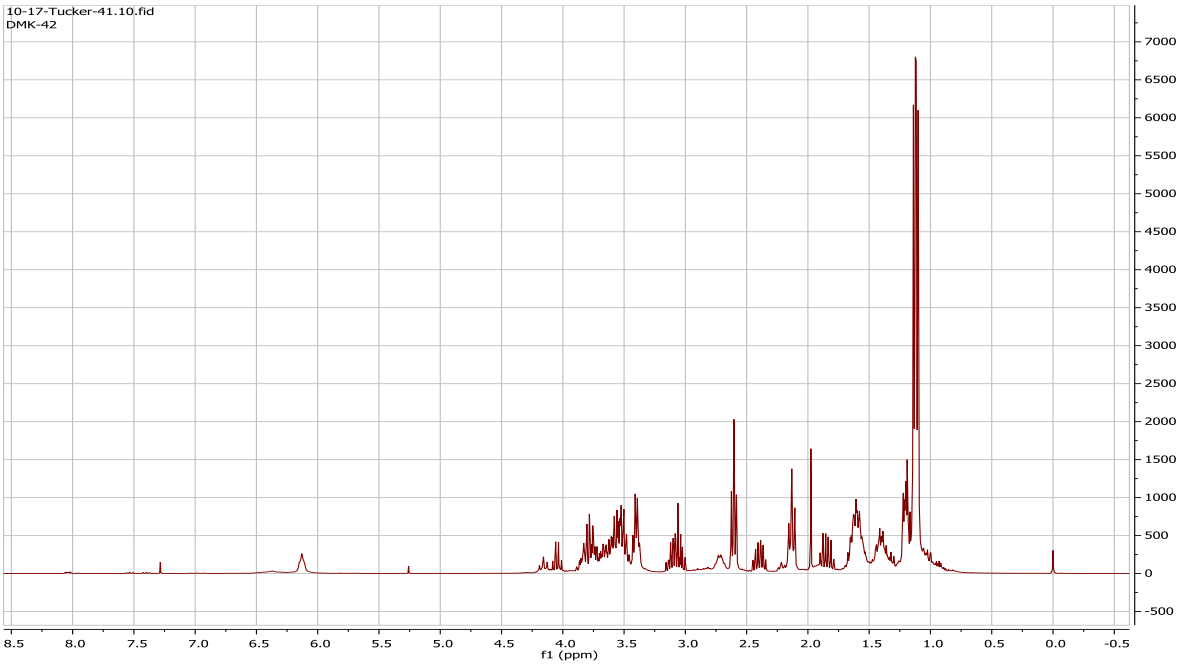

^{13}CNMR

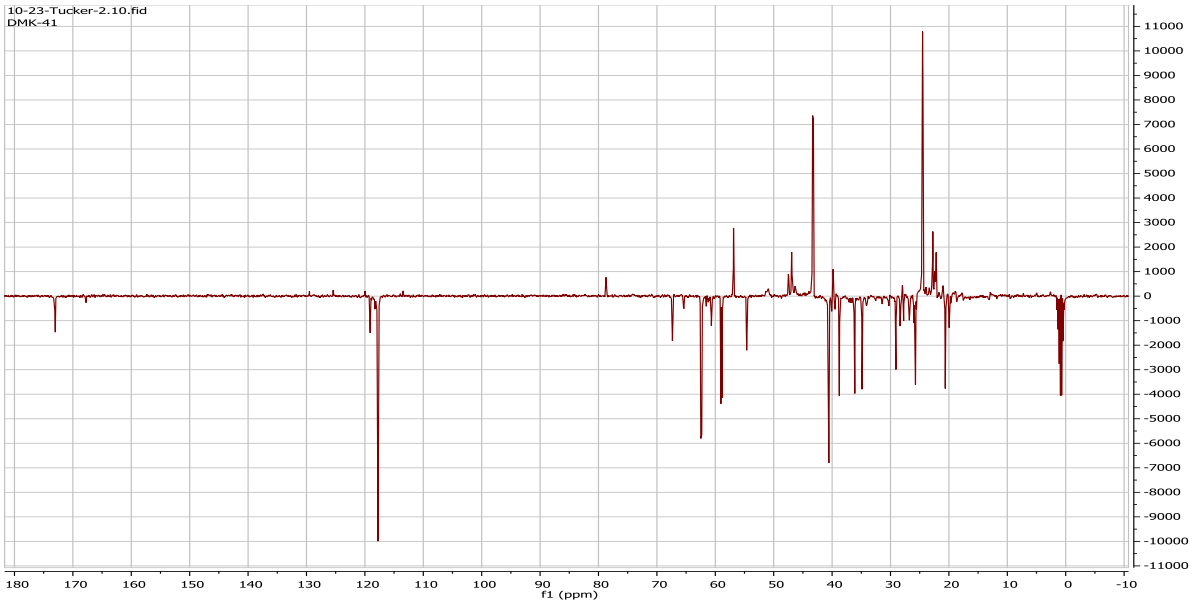

^{31}PNMR

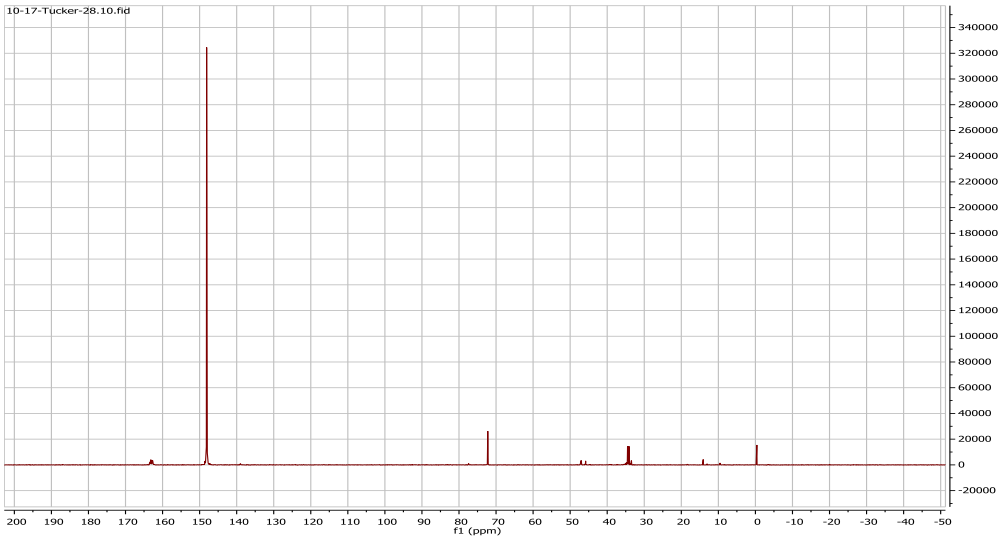

7.4 Using semi-prep HPLC to estimate reaction yield

Semi-prep HPLC of successful modification of DNA with thioctic acid analogue (**P.1L**). Analysing the integral of the peak at 40.4 minutes, estimated yield of the reaction is 77%. Peaks at 38.5 and 39.7 minutes are unsuccessful reactions.

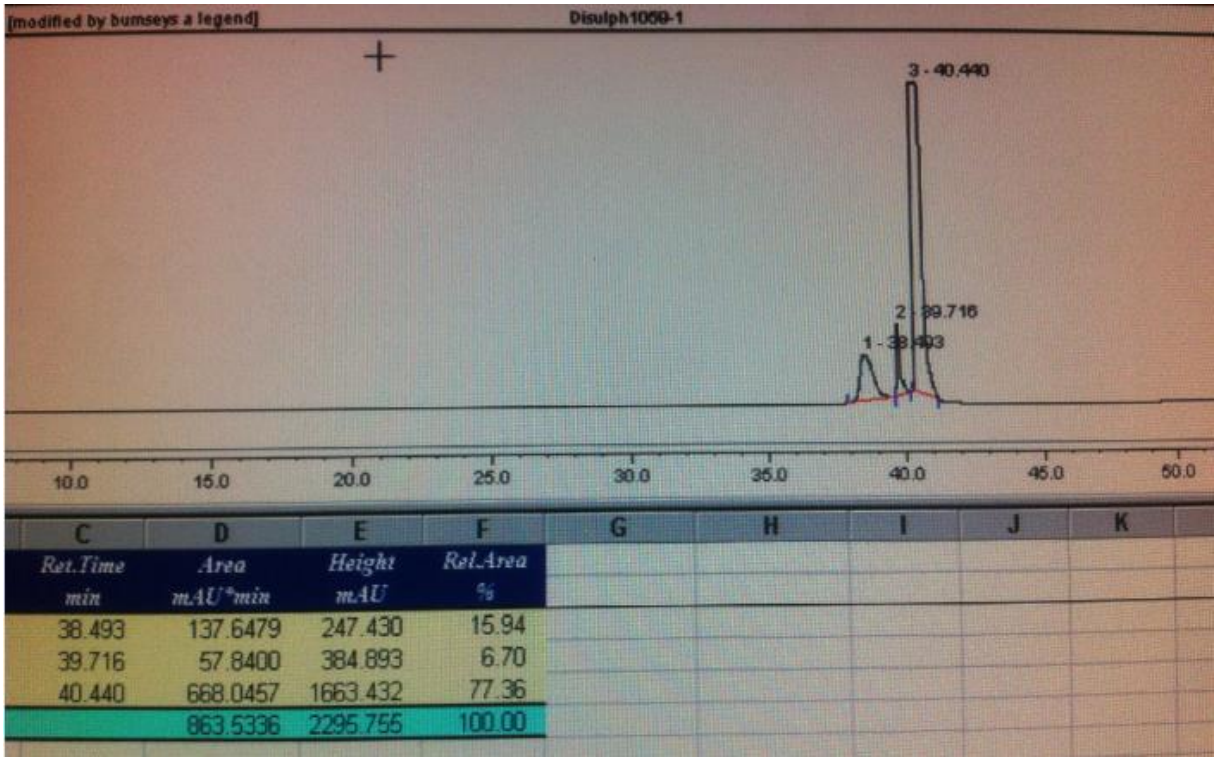

Ret.Time min	Area mAU*min	Height mAU	Rel.Area %
38.493	137.6479	247.430	15.94
39.716	57.8400	384.893	6.70
40.440	668.0457	1663.432	77.36
	863.5336	2295.755	100.00

7.5 DLS number distribution histogram

Bare AuNP (13 nm)

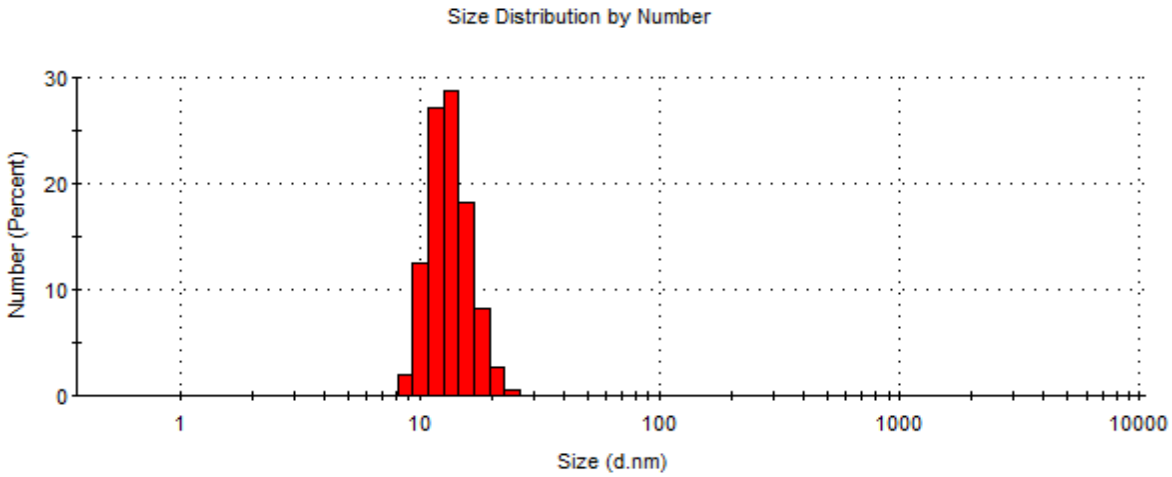

Bare AuNP (100 nm)

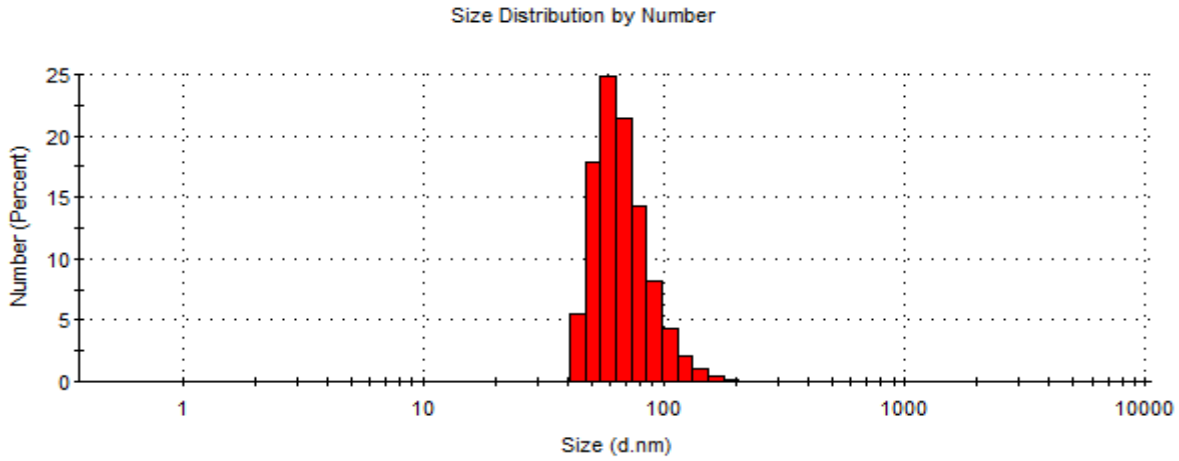

P.UM-AuNP (13 nm)

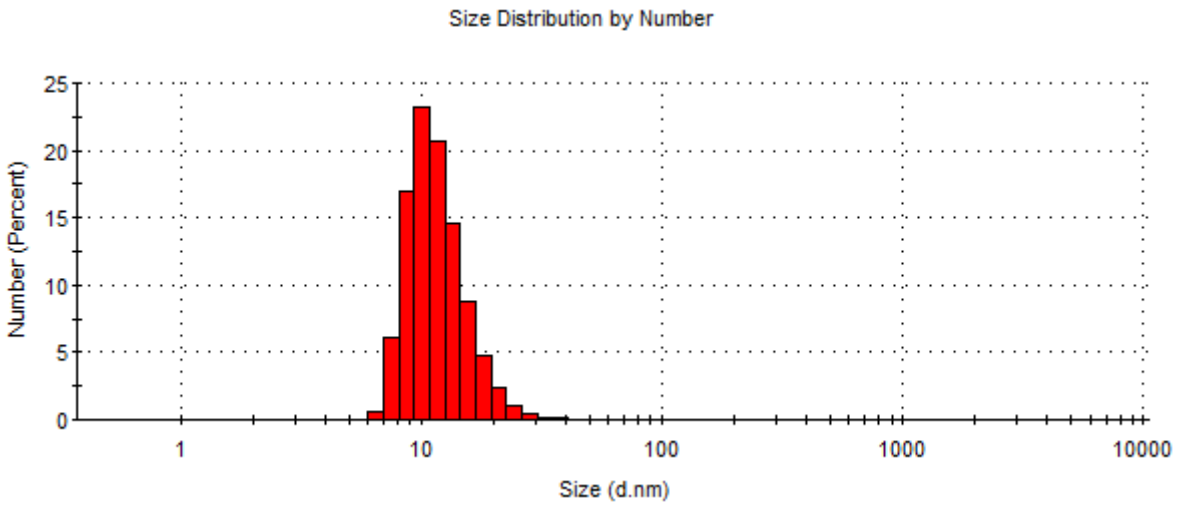

P.AF-AuNP (13 nm)

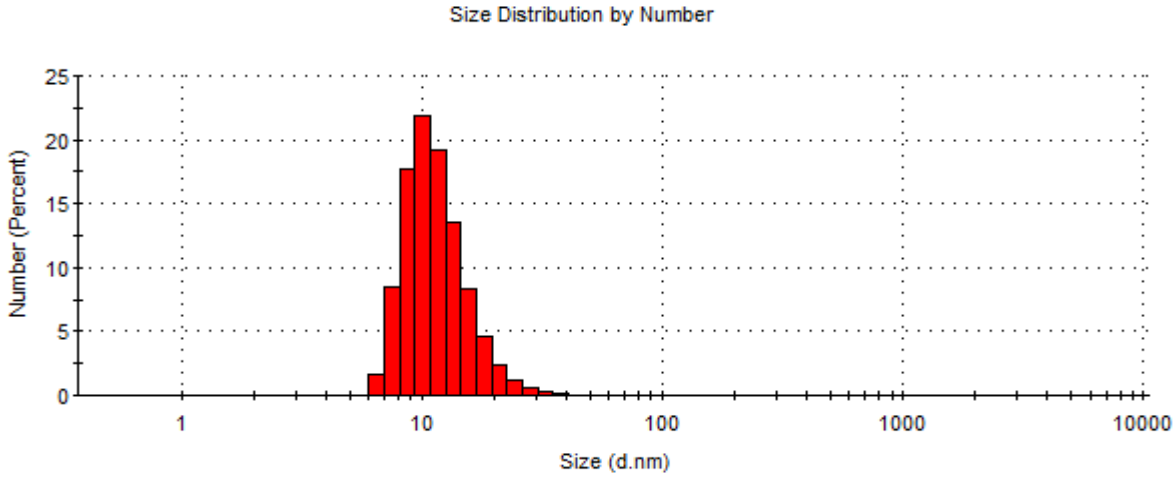

P.AF-AuNP-Ru (13 nm)

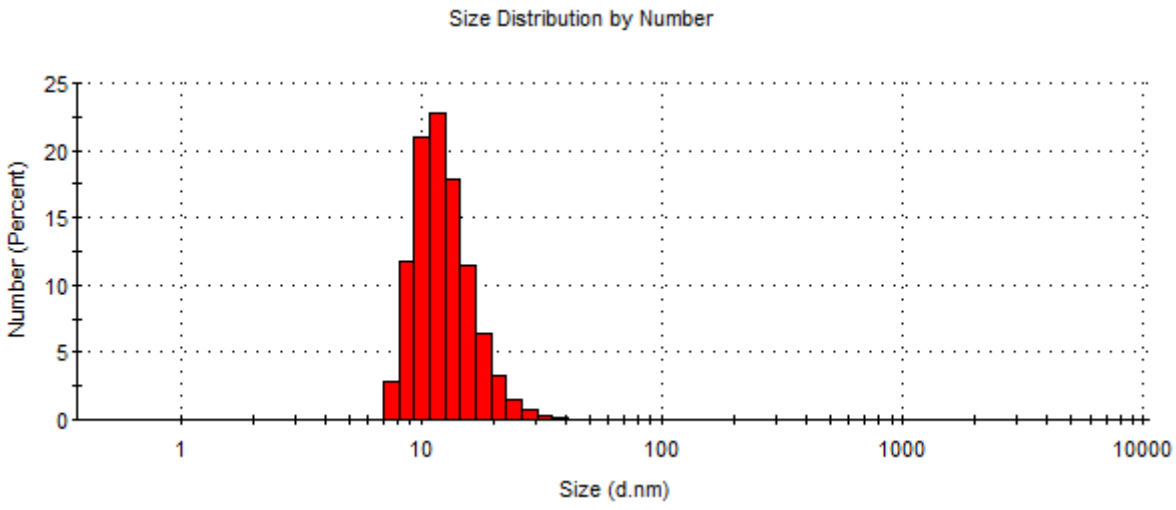

P.1L-AuNP (13 nm)

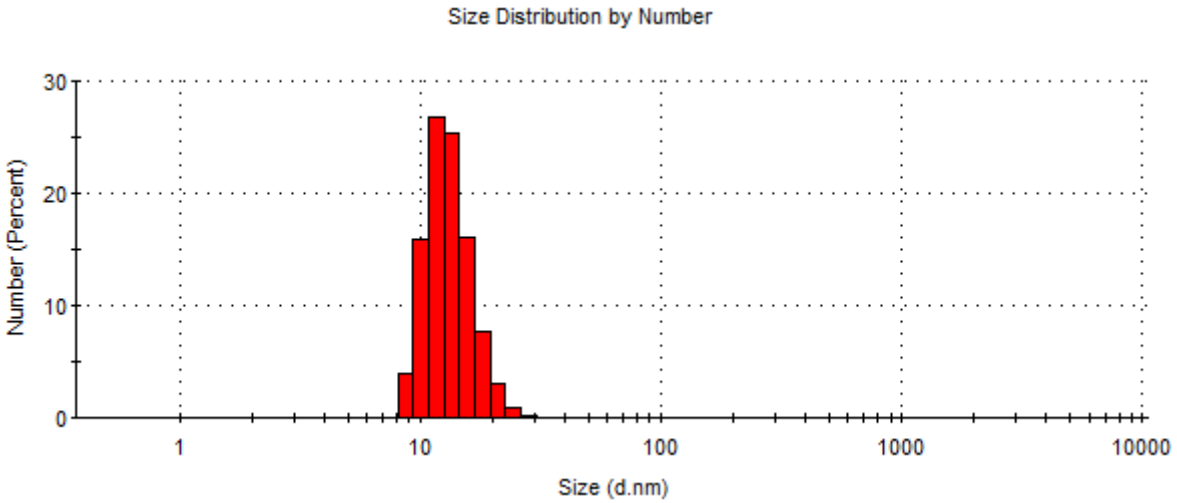

P.1L-AuNP (100 nm)

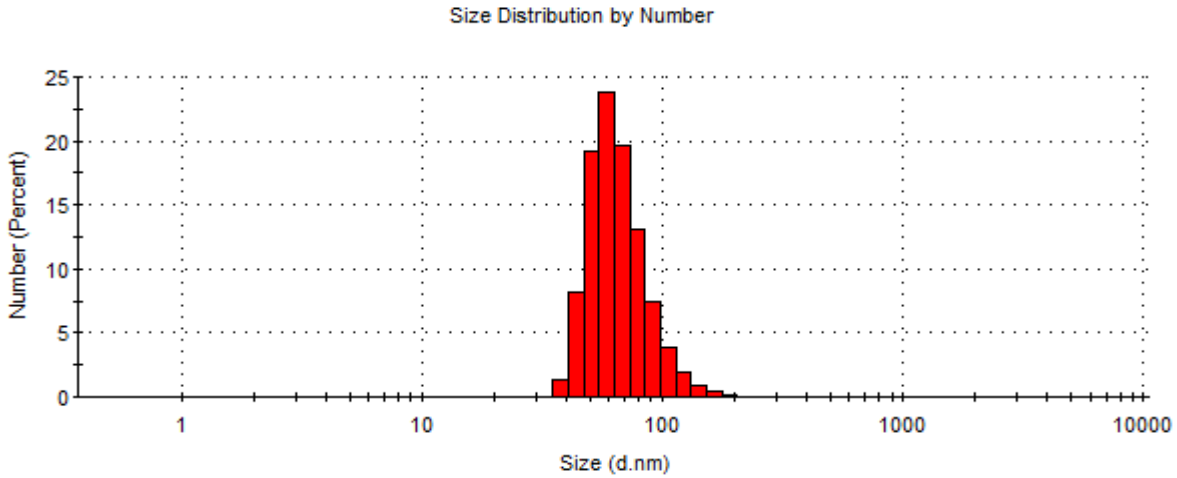

P.1L- AuNP-Ru (13 nm)

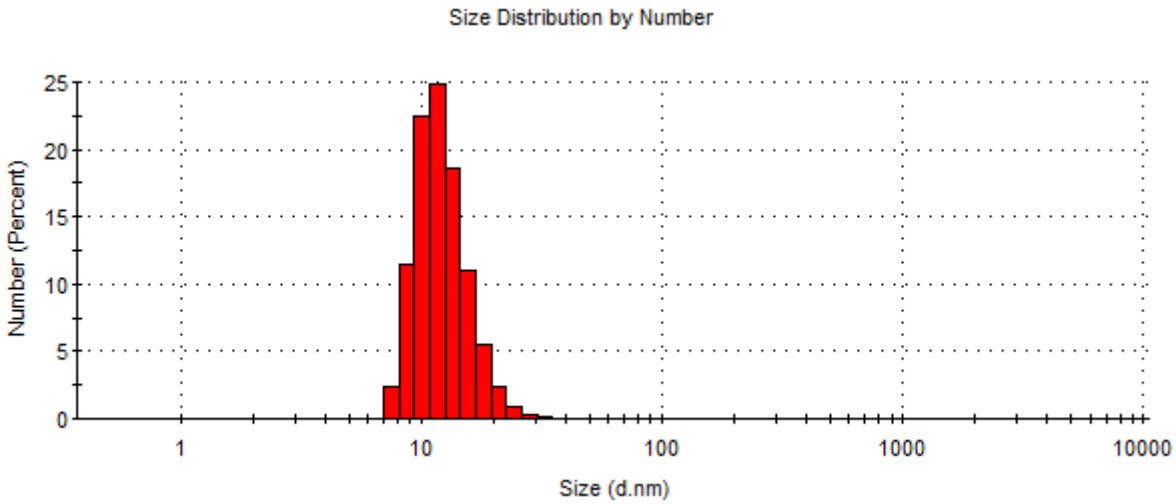

P.1L-AuNP-Ru (100 nm)

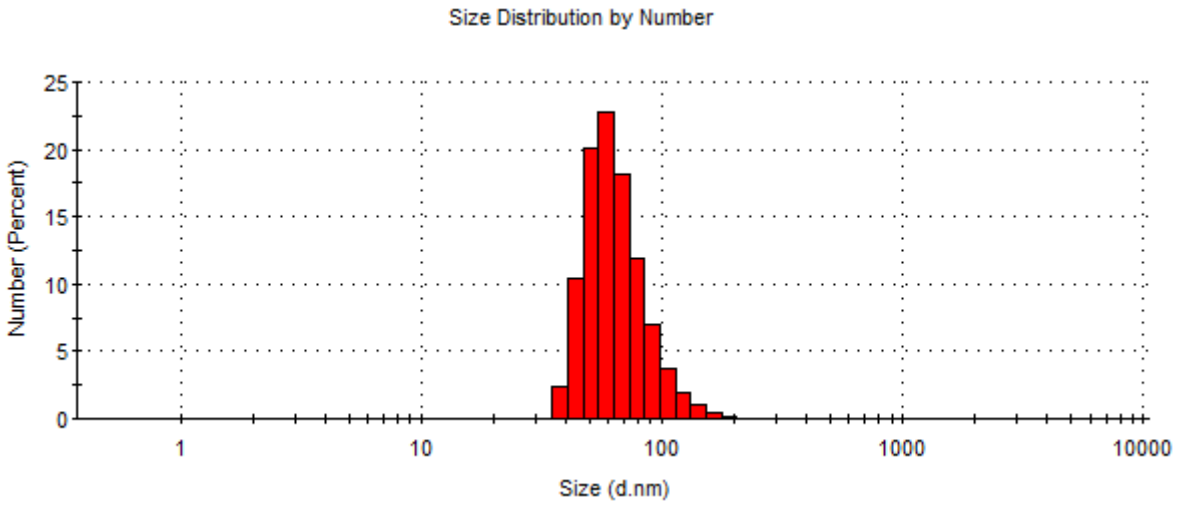

P.5L-AuNP (13 nm)

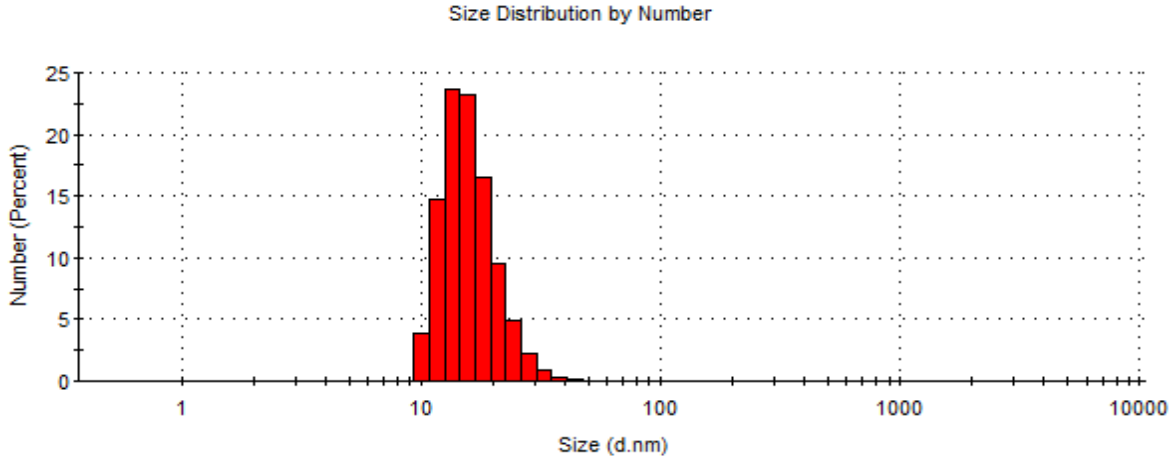

P.5L-AuNP-Ru (13 nm)

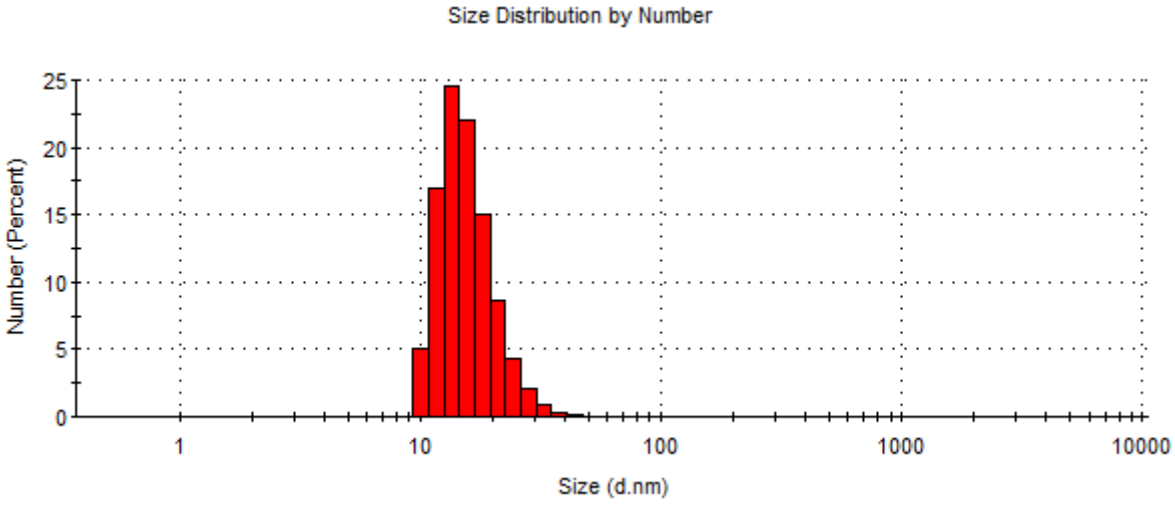

P.1D-AuNP (13 nm)

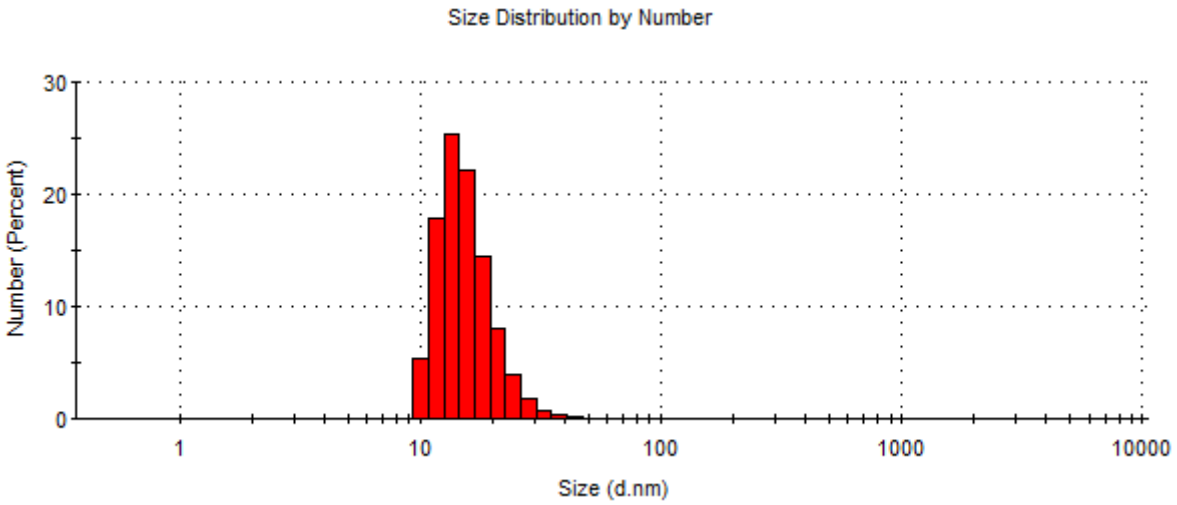

P.1D-AuNP-Ru (13 nm)

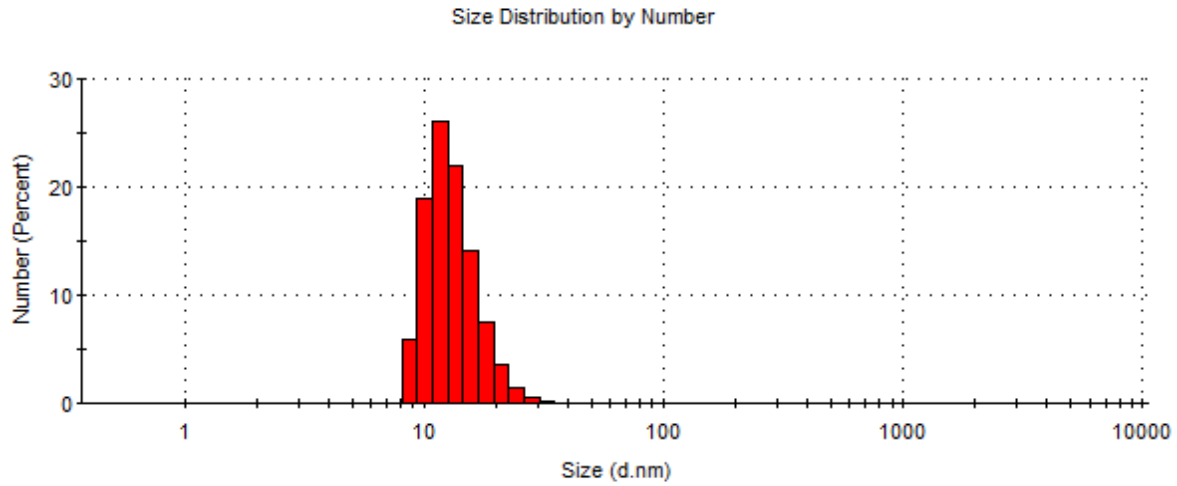

l.P.1L-AuNP (13 nm)

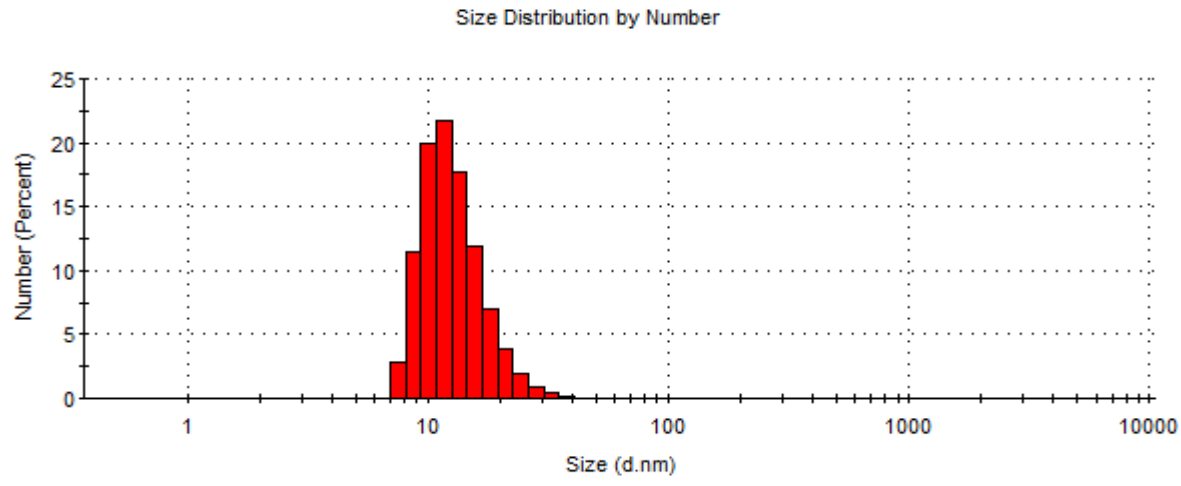

l.P.1L-AuNP-Ru (13 nm)

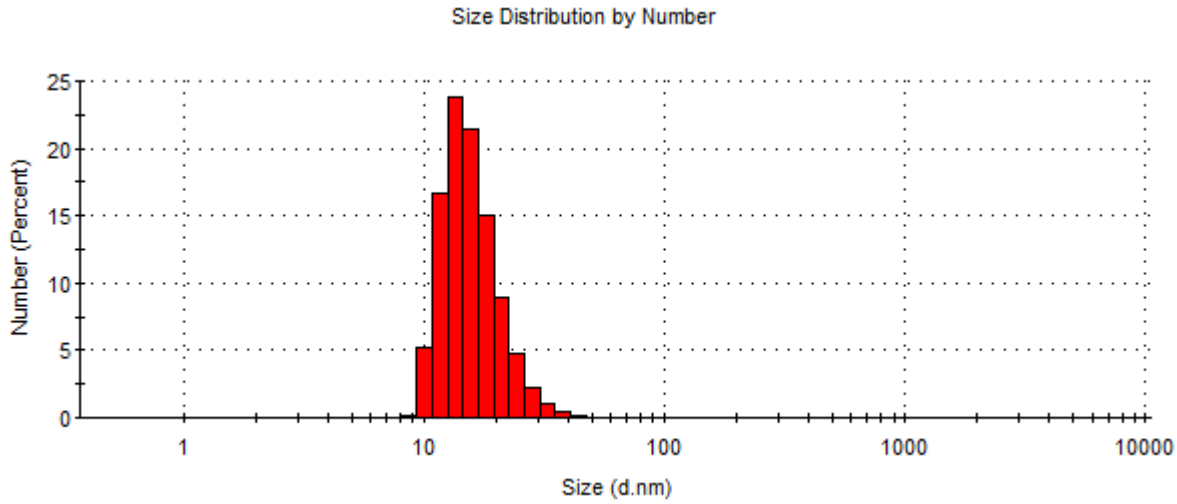

m.P.1L-AuNP

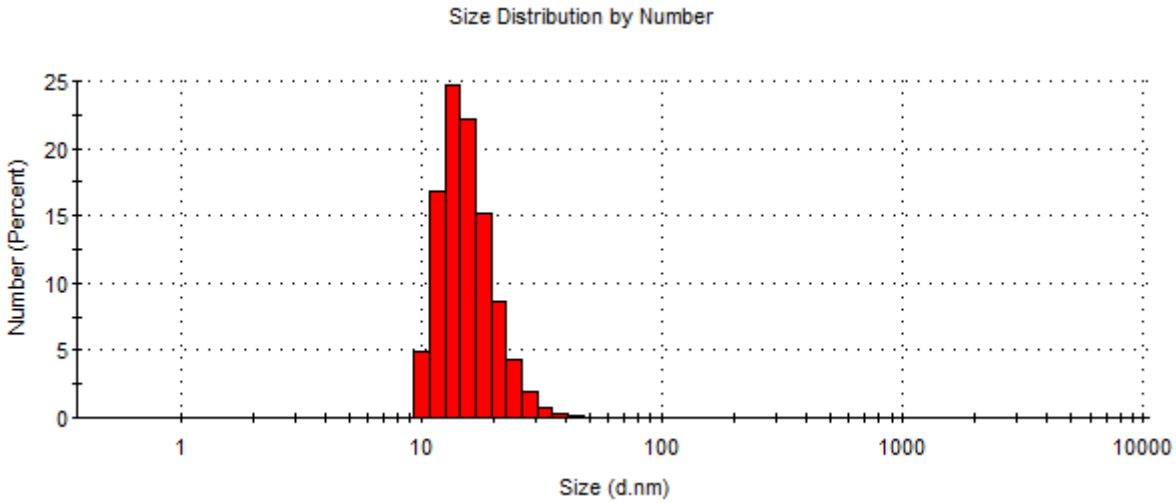

siRNA-AuNP (13 nm)

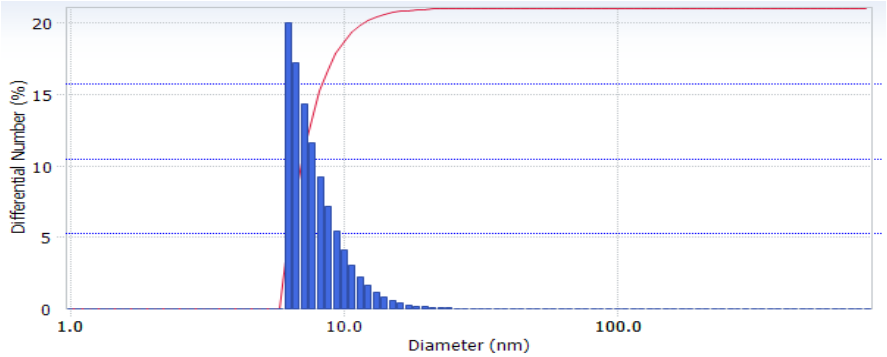

siRNA-AuNP-Ru (13 nm)

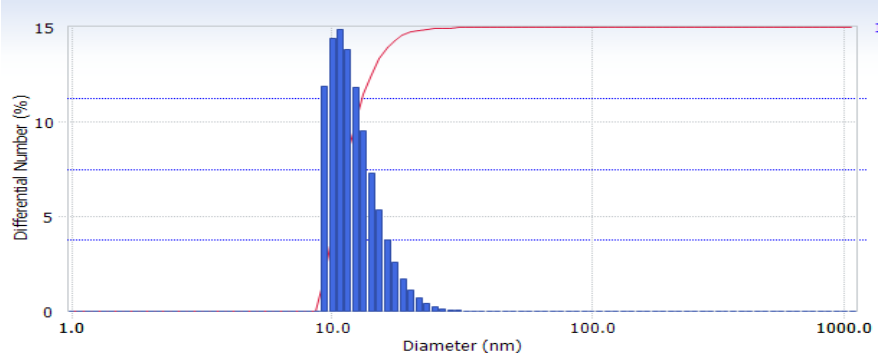

siRNA-AuNP (100 nm)